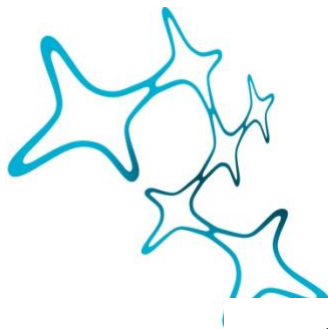# Probing neuronal (dys)function in motor cortex of ALS transgenic mice by *in vivo* two-photon calcium imaging

Wing Yin Vanessa Kan

Graduate School of Systemic Neuroscices

LMU Munich

Dissertation der Graduate School of Systemic Neurosciences
der Ludwig-Maximilians-Universität München

December 20th 2022

Table of Contents

List of Abbreviations

2PM	Two-photon microscopy
5-HT	Serotonin
AAV	Adeno-associated virus
Ach	Acetylcholine
AD	Alzheimer's Disease
ALS	Amyotrophic lateral sclerosis
AMPA	α-amino-3-hydroxy-5-methyl-4-isoxazole propionic acid
AQP4	Aquaporin-4
AR	Adrenoceptors
AUD	Auditory cortex
BF	Basal forebrain
BOLD	Blood-oxygen-level-dependent
C9ORF72	Chromosome 9 open reading frame 72
CaM	Calcium-binding messenger protein calmodulin
CC	Cortico-cortico
ChAT	Choline acetyltransferase
CICR	Calcium-induced calcium release
CNO	Clozapine N-oxide
CNS	Central nervous system
CSF	Cerebrospinal fluid
CSP	Cortical silent period
CStr	Cortico-striatal
CuN	Cuneate nucleus
DA	Dopamine
DPRs	Dipeptide repeat proteins
DR	Dorsal raphe
DREADDs	Designer Receptors Exclusively Activated by Designer Drugs
EAAT1	Excitatory amino acid transporters 1
EAAT2	Excitatory amino acid transporters 2
EMG	Electromyogram
EPSC	Excitatory postsynaptic current
ER	Endoplasmic reticulum
fALS	Familial amyotrophic lateral sclerosis
FC	Frontal cortex

fMRI	Functional magnetic resonance imaging
FRET	Fluorescence resonance energy transfer
FTD	Frontotemporal dementia
FUS	Fused in sarcoma
GABAA	γ-aminobutyric acid A
GECIs	Genetically-encoded calcium indicators
GFAP	Glial fibrillary acidic protein
GFP	Green fluorescent protein
GPCRs	G protein-coupled receptors
H-MRS	Proton magnetic resonance spectroscopy
H_2O	Water
HA	Histamine
HD	Huntington's disease
hM3Dq	Human M3 muscarinic receptor
ICF	Intracortical facilitation
INs	Interneurons
IPSC	Inhibitory postsynaptic current
IT	Intratelencephalic tract
K^+	Potassium ion
LC	Locus coeruleus
LMNs	Lower motor neurons
M1	Motor cortex
MEP	Motor evoked potential
MND	Motor neuron disease
MRI	Magnetic resonance imaging
MRS	Magnetic resonance spectroscopy
MS	Multiple sclerosis
NE	Norepinephrine
NMDAR	N-methyl-D-aspartate receptors
NMJ	Neuromuscular junction
OC	Orbital cortex
OPTN	Optineurin
PMT	Photomultiplier tube
PNF	Phosphorylated neurofilament
PNs	Pyramidal neurons
PT	Pyramidal tract

PV	Parvalbumin
RMT	Resting motor threshold
ROS	Reactive oxygen species
S1	Somatosensory cortex
sALS	Sporadic amyotrophic lateral sclerosis
SICI	Short interval intracortical inhibition
SOD1	Superoxide dismutase 1
SST	Somatostatin
TARDBP/TDP-43	TAR DNA-binding protein 43
tg	Transgenic
TH	Thalamus
TMN	Tuberomammillary nucleus
TMS	Transcranial magnetic stimulation
UHF	Ultra-high field
UMNs	Upper motor neurons
V1	Visual cortex
VAPB	Vesicle-associated membrane protein/synaptobrevin-associated membrane protein B
VGAT	Vesicular GABA transporter
VIP	Vasoactive intestinal peptide
VPL	Ventral posterolateral nucleus
VTA	Ventral tegmental area

Abstract

Amyotrophic Lateral Sclerosis (ALS) is a rare yet devasting neurodegenerative disease that involves the degeneration of upper and lower motor neurons. It is diagnosed in around every 2 out of 100,000 people. Upon diagnosis, patients typically die within 3 to 5 years from respiratory failure. As the current pathomechanistic insight yielded little success in developing effective treatment options or a cure, the aim of this thesis is to better understand one of the early features detected in ALS patients – cortical hyperexcitability, specifically its *source*. To this end, I performed *in vivo* calcium imaging in motor cortex (M1) of two mouse models of ALS, namely *Fus*$^{\Delta NLS/+}$ and SOD1^{G93A} mice. By imaging *Fus*$^{\Delta NLS/+}$ mice under anesthesia, I showed cortical hyperactivity at both 4 and 10 months. Together with collaborators, ultrastructural analysis and RNAseq of frontal cortex revealed deficits in inhibitory synapses, proposing compromised inhibition as the source of cortical hyperexcitability in *Fus*$^{\Delta NLS/+}$ mice. In SOD1^{G93A} mice, I first demonstrated partial coherence of activity under anesthesia and during wakefulness by imaging the same neurons in both conditions. The finding raised further questions of what neurons respond to (i.e. response properties) during wakefulness and whether excitability and activity changes are compensatory. To answer these questions, I performed *in vivo* two-photon calcium imaging in head-fixed, performing SOD1^{G93A} mice in a visual-flow feedback paradigm. I identified five unique clusters of neurons characterized by their average activity to locomotion during different conditions, namely neurons responsive to (i) running in general, (ii) running with feedback, (iii) running in darkness, (iv) all conditions and (v) quiet wakefulness. Of which, I detected an increased fraction of neurons that are more active during (iii) running in darkness in layer 2/3 and fewer neurons that are (v) spontaneously active. I identified further changes in locomotion-associated activity, specifically an increase in fraction of running-responsive cells (i.e. neurons with activity increases with locomotion) and a hyperresponsiveness to locomotion. These changes were only restricted to layer 2/3 at the

presymptomatic stage and was later detected in both layer 2/3 and 5. When neuronal activity is chemogenetically dampened in M1 layer 2/3, treated SOD1^{G93A} mice demonstrated a delay in symptom onset accompanied with improved motor behavior. Together, the findings presented in this thesis show compromised inhibition as the source of cortical hyperexcitability in *Fus*$^{\Delta NLS/+}$ mice and increased input from layer 2/3 in SOD1^{G93A} mice.

Zusammenfassung

Amyotrophe Lateralsklerose (ALS) ist eine seltene, aber verheerende neurodegenerative Erkrankung, bei der die oberen und unteren Motoneuronen degenerieren. Diese wird bei etwa 2 von 100.000 Menschen diagnostiziert. Nach der Diagnose sterben die Patienten in der Regel innerhalb von 3 bis 5 Jahren an respiratorischer Insuffizienz. Da die aktuellen pathomechanischen Erkenntnisse wenig Erfolg bei der Entwicklung wirksamer Behandlungsoptionen oder einer Heilung erbrachten, ist das Ziel dieser Arbeit eines der frühen Merkmale von ALS-Patienten besser zu verstehen – kortikale Übererregbarkeit, insbesondere dessen Ursprung. Zu diesem Zweck führte ich eine *In-vivo*-Bildgebung von Calcium im motorischen Kortex (M1) von zwei Mausmodellen von ALS durch, nämlich von Fus$^{\Delta NLS/+}$- und SOD1^{G93A}-Mäusen. Durch die Bildgebung von Fus$^{\Delta NLS/+}$-Mäusen unter Anästhesie zeigte sich sowohl nach 4 als auch nach 10 Monaten eine kortikale Hyperaktivität. Zusammen mit Kollaboratoren zeigten eine Ultrastrukturanalyse und RNAseq des frontalen Kortex Defizite in hemmenden Synapsen, was auf eine beeinträchtigte Hemmung als Quelle der kortikalen Übererregbarkeit bei Fus$^{\Delta NLS/+}$-Mäusen hindeutet. In SOD1^{G93A}-Mäusen demonstrierte ich zuerst eine teilweise Kohärenz der Aktivität unter Anästhesie und im Wachzustand, indem ich dieselben Neuronen in beiden Zuständen abbildete. Der Befund warf weitere Fragen auf, worauf Neuronen im Wachzustand reagieren (d. h. auf Reaktionseigenschaften) und ob Erregbarkeits- und Aktivitätsänderungen kompensatorisch sind. Um diese Fragen zu beantworten, habe ich in vivo eine Zwei-Photonen-Kalzium-Bildgebung in kopffixierten SOD1^{G93A}-Mäusen in einem Visual-Flow-Feedback-Paradigma durchgeführt. Ich identifizierte fünf einzigartige Cluster von Neuronen, die durch ihre durchschnittliche Aktivität zur Fortbewegung unter verschiedenen Bedingungen gekennzeichnet sind, nämlich Neuronen, die auf (i) Laufen im Allgemeinen, (ii) Laufen mit Feedback, (iii) Laufen in Dunkelheit, (iv) alle Bedingungen und (v) ruhiger Wachzustand reagieren. Davon habe ich in Schicht 2/3 einen

erhöhten Anteil an Neuronen festgestellt, die während (iii) im Dunkeln aktiver sind, und weniger Neuronen, die (v) spontan aktiv sind. Ich identifizierte weitere Veränderungen in der Fortbewegungs-assoziierten Aktivität, insbesondere eine Zunahme des Anteils an auf das Laufen ansprechenden Zellen (d. h. Neuronen, deren Aktivität mit der Fortbewegung zunimmt) und eine Hyperreaktivität auf Fortbewegung. Diese Veränderungen waren im präsymptomatischen Stadium nur auf Schicht 2/3 beschränkt und wurden später sowohl in Schicht 2/3 als auch in Schicht 5 nachgewiesen. Wenn die neuronale Aktivität in M1-Schicht 2/3 chemogenetisch gedämpft wird, zeigten behandelte SOD1^{G93A}-Mäuse einen verzögerten Symptombeginn, begleitet von verbessertem motorischen Verhalten. Die in dieser Dissertation vorgestellten Ergebnisse zeigen zusammen eine beeinträchtigte Hemmung als Quelle der kortikalen Übererregbarkeit bei Fus$^{\Delta NLS/+}$-Mäusen und einen erhöhten Input von Schicht 2/3 bei SOD1^{G93A}-Mäusen.

1. Introduction

The "Father of Neurology" Jean-Martin Charcot described the first cases of Amyotrophic Lateral Sclerosis (ALS) in the 1860s. Trained as a pathologist, Charcot recognized the important link between clinical symptoms and anatomical changes revealed in autopsies. Charcot and his colleagues identified lesions, associated with the degeneration of neurons and glial cells, in both the anterior and lateral horn of the spinal cord that would also extend to the medulla oblongata (Kumar et al., 2011). The site of lesion resulted in different clinical outcomes. Notably, lesions in the anterior horn led to paralysis and muscle atrophy, while that in the lateral horn resulted in progressive paralysis without muscle atrophy (Corcia & Meininger, 2019; Kumar et al., 2011). Thus, the disease was termed ALS, in which "amyotrophic" refers to the degeneration of nerves innervating the muscles, which results in muscle wasting; and "lateral sclerosis" refers to hardening of the anterior and lateral spinal cord column.

Distinctive from other motor neuron diseases, such as primary lateral sclerosis, in which only upper motor neurons (UMNs) are affected and progressive muscular atrophy, characterized by exclusive lower motor neuron (LMNs) degeneration, both upper and lower motor neurons are affected in ALS. ALS became more widely known in the 1930s when Lou Gehrig, an American professional baseball player, was diagnosed with the disease at the age of 36 and died two years later. Since then, the scientific community made huge progress in understanding the genetic and molecular mechanisms of motor neuron degeneration in ALS. However, the current pathomechanistic insight yielded little success in developing effective treatment options or a cure.

Cortical hyperexcitability is one of the early features detected in ALS patients. It was first described in the 1990s, and over the years, transcranial magnetic stimulation (TMS) and

functional magnetic resonance imaging (fMRI) studies in ALS patients provided insights into overall excitability and connectivity changes in the motor cortex. While cortical hyperexcitability can cause neurodegeneration, the source of the hyperexcitability remains unclear. Apart from UMNs in layer 5B, motor cortex comprises other neuronal cell types, excitatory or inhibitory and receives long-range inputs from other areas. In my thesis, I strove to gain insight into how and when various elements of the motor cortex circuitry are affected in the disease by *in vivo* two-photon calcium imaging in two transgenic mouse models of ALS.

1.1. Amyotrophic Lateral Sclerosis

Amyotrophic lateral sclerosis (ALS) is a progressive, fatal disease, characterized by the degeneration of upper motor neurons (UMNs) in cortex and lower motor neurons (LMNs) in spinal cord and brainstem, respectively. It is the most common form of motor neuron disease (MND) and the third most common neurodegenerative disease after Alzheimer's disease and Parkinson's disease (Shang et al., 2015).

Initial symptoms differ depending on the location of initial degeneration. Patients with limb onset are first affected by muscle weakness, cramps and twitching in their limbs (Hu et al., 1998; Turner et al., 2010), while patients with bulbar onset, in which degeneration is detected in the medulla oblongata, first present with symptoms in the face and neck region, such as problems with speech and swallowing (Shellikeri et al., 2017; Stegmann et al., 2020). Symptoms commonly manifest between the age of 51- 66 (Longinetti & Fang, 2019), and without a cure, diagnosed patients typically pass away within 3 to 5 years due to respiratory complications (Taylor et al., 2016).

Epidemiological studies report an incidence of 0.6 to 3.8 new cases per 100,000 people per year (Benjaminsen et al., 2018; Jun et al., 2019; Leighton et al., 2019; Longinetti & Fang, 2019;

Longinetti et al., 2018; Palese et al., 2019; Rose et al., 2019; Turgut et al., 2019; Zhou et al., 2018), and a prevalence between 4.1 to 8.4 per 100,000 people (Benjaminsen et al., 2018; Jun et al., 2019; Leighton et al., 2019; Longinetti & Fang, 2019; Longinetti et al., 2018; Nakken et al., 2018; Nelson et al., 2018; Palese et al., 2019; Rose et al., 2019; Turgut et al., 2019). Overall, there is a higher incidence and prevalence in (younger) males than in females, with differences in clinical features presented in sporadic ALS (sALS) and familial ALS (fALS) (McCombe & Henderson, 2010). The male-to-female ratio is as high as 2.9 (Longinetti & Fang, 2019; Luna et al., 2019). In addition to sex-specific differences, there is also evidence of geographic and ethnical differences (Logroscino & Piccininni, 2019), suggesting possible lifestyle and environmental risk factors. To be more specific, patients who previously worked as manual workers in labor-intensive industries reported higher exposure to sustained strenuous physical activity (Farrugia Wismayer et al., 2021; Lian et al., 2019), corroborating a study identifying exercise as a risk factor for ALS (Julian et al., 2021).

1.1.1. Currently known ALS-linked genetic mutations and proposed cell-autonomous disease mechanisms in ALS

The heterogeneity of symptoms, such as more pronounced social deficits versus motor deficits, in ALS is partly due to the underlying genetic mutations and the corresponding molecular pathology. Approximately 5 to 10% of ALS cases are familial ALS (fALS), based on a genetic mutation and the remaining are spell out, which occur sporadically. Over 30 mutations have been identified in fALS cases (Figure 1a). Depending on the racial and geographic background of fALS patients, mutations in the *chromosome 9 open reading frame 72 (C9ORF72)* gene accounts for 3 to 35 percent of fALS cases, with the majority of them in European populations (Mejzini et al., 2019; Zou et al., 2017) (Figure 1b). The second-most common mutation is in the *superoxide dismutase 1 (SOD1)* gene, which accounts for 15 to 30 percent of fALS cases

(Mejzini et al., 2019; Zou et al., 2017) (Figure 1). Mutations in *fused in sarcoma (FUS)* and *TAR DNA-binding protein 43 (TARDBP)* genes each account for around 2 to 7 percent of fALS cases (Mejzini et al., 2019; Zou et al., 2017) (Figure 1b). Other less commonly-known mutations are found in *ALS2, vesicle-associated membrane protein/synaptobrevin-associated membrane protein B (VAPB)* and *optineurin (OPTN)* (Coppedè, 2011; Teuling et al., 2007) (Figure 1A). Some ALS-causing genetic mutations can also cause frontotemporal dementia (FTD), characterized by symptoms, such as behavioral and personality changes as well as aphasia (Abrahams et al., 2004; Ferrari et al., 2011; Mackenzie & H. Feldman, 2005).
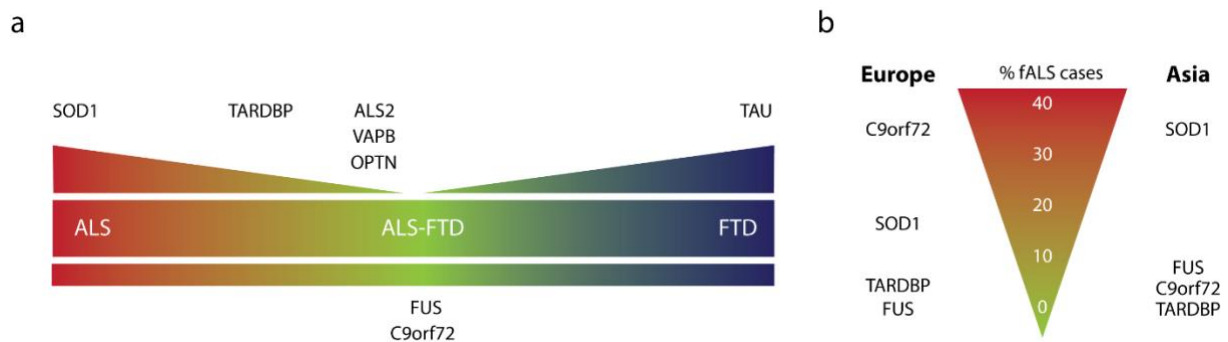
Figure 1. ALS-associated genetic mutations.
(a) Genetic mutations along the ALS-FTD spectrum. (b) Percentage of genetic mutations identified in European and Asian fALS patients. *Modified after (Ling et al., 2013), and adapted from data in (Zou et al., 2017) with permission.*

SOD1 was the first gene identified in fALS patients in 1993 (Rosen et al., 1993). *SOD1* encodes the protein superoxide dismutase, an enzyme responsible for breaking down free superoxide radicals. Over 185 mutations such as D90A and G93A have been identified in *SOD1*, which contribute to different clinical outcomes, disease progression and severity (Berdyński et al., 2022; Yamashita & Ando, 2015). Most of the variants are consequences of missense mutations, resulting in aggregation of the misfolded protein (misfolded-SOD1), as well as reduced and impaired protein function (Deng et al., 1993). Studies conducted in the SOD1[G93A] mouse model revealed that the G93A variant causes an overexpression of SOD1 in the cytoplasm and absence in the nucleus, resulting in higher oxidative DNA damage (Sau et al., 2007). Though no

developmental nor motor deficits were detected in SOD1 knockout mice, SOD1-deficient motor neurons were more susceptible to cell death after injury, indicating that SOD1 is essential for coping with physiologically stressful conditions (Reaume et al., 1996). In addition to fALS-SOD1 patients who present misfolded SOD1 (Da Cruz et al., 2017), non-native forms of the wild-type SOD1 protein have also been detected in other fALS forms (Forsberg et al., 2019; Mejzini et al., 2019) and sALS patients (Berdyński et al., 2022; Forsberg et al., 2010; Guareschi et al., 2012), indicating that misfolded SOD1 could be a common event in ALS.

Mutations in *TARDBP* (Sreedharan et al., 2008) and FUS (Blair et al., 2010; Vance et al., 2009) were identified in ALS patients in 2008 to 2009. *TARDBP* encodes a DNA/RNA – binding protein (TDP-43) that shuttles between the nucleus and cytoplasm to regulate gene expression and RNA processing (Buratti & Baralle, 2008; Kuo et al., 2009; Tollervey et al., 2011). Mutations cause a nuclear import deficit, resulting in cytoplasmic mislocalization of TDP-43 and subsequent nuclear depletion of TDP-43. However, even in the absence of *TARDBP* mutations, cytoplasmic inclusions of TDP-43 are also detected in over 95% of ALS patients (Majumder et al., 2018), though absent in those with *SOD1* and *FUS* mutations (Arai et al., 2006; Chen et al., 2018; Neumann et al., 2006).

Similar to TDP-43, FUS is an RNA binding protein involved in nucleocytoplasmic transport and is thus transported to the nucleus (Zinszner et al., 1997). Missense mutations in FUS cause cytoplasmic mislocalization of FUS, which has been shown to be toxic to the cells in FUS-associated ALS rodent models, resulting in phenotypes recapitulating a mild motor phenotype associated with more pronounced cognitive and social deficits also seen in humans (Arai et al., 2006; Scekic-Zahirovic et al., 2017; Scekic-Zahirovic et al., 2021; Sharma et al., 2016). Though both the complete knockout as well as the knock-in of mutant FUS resulted in cytoplasmic FUS mislocalization and led to perinatal death, only knock-in mice survived and displayed motor

neuron loss that could be rescued by the conditional expression of wild-type FUS, suggesting its role in neuronal death (Scekic-Zahirovic et al., 2016).

In 2011, the non-coding hexanucleotide repeat expansion (GGGGCC) in the *C9ORF72* gene was discovered. It is currently the most frequent gene mutation in ALS patients, who might have hundreds to thousands of copies of this repeat expansions (Smeyers et al., 2021). Under physiological conditions, *C9ORF72* comprises two non-coding and ten coding exons, producing three coding variants, which translate into a guanine nucleotide exchange factor, a protein that regulate Rab GTPases and downstream intracellular and vesicle-mediated transport (Iyer et al., 2018; Stenmark, 2009). The mutation results in both gain- and loss-of-function, namely the formation of toxic RNA foci that affect post-transcriptional RNA processing, and non-AUG initiated translation of five toxic dipeptide repeat proteins (DPRs) that induce double-strand DNA break, reduces *C9ORF72* gene expression (haploinsufficiency) (Barker et al., 2017; Donnelly et al., 2013; Niblock et al., 2016; Wang et al., 2021) (Mori et al., 2013; Nonaka et al., 2018). However, there is contradicting evidence of the role of *C9ORF72* mutations alone in causing motor neuron degeneration and motor deficits in *C9ORF72*-associated mouse models, and the effect could be dose-dependent (Koppers et al., 2015; Mordes et al., 2020; Shao et al., 2019; Verdone et al., 2022).

Like in most neurodegenerative diseases, intracellular protein aggregation is a key pathological hallmark of ALS, as a result of protein misfolding and/or cytosolic mislocalization (Blokhuis et al., 2013; Gunes et al., 2020; Tyzack et al., 2019). Protein aggregation is believed to trigger various cell-autonomous mechanisms (that is changes occurring within the affected neuron). Proposed molecular and cellular mechanisms underlying the degeneration in UMNs include (1) impaired DNA repair and genome instability (Higelin et al., 2018; Naumann et al., 2018; Polymenidou et al., 2012; Sun et al., 2020), (2) changes in RNA metabolism, which affects

RNA splicing and translation and mRNA transport (Butti & Patten, 2019; Polymenidou et al., 2012), (3) compromised protein homeostasis and protein aggregation (Blokhuis et al., 2013; Webster et al., 2017), (4) increased oxidative stress (Ikawa et al., 2015; Zimmerman et al., 2007), (5) mitochondrial dysfunctions (Cozzolino & Carrì, 2012; Zimmerman et al., 2007), (6) nucleocytoplasmic (Bitetto & Di Fonzo, 2020), (7) vesicular transport deficits (Burk & Pasterkamp, 2019; Sundaramoorthy et al., 2015), (8) changes in structure and dynamics of cytoskeleton and impaired axonal transport (Bilsland et al., 2010; Liu et al., 2022a; Marinković et al., 2012; Xiao et al., 2006) (Figure 2).
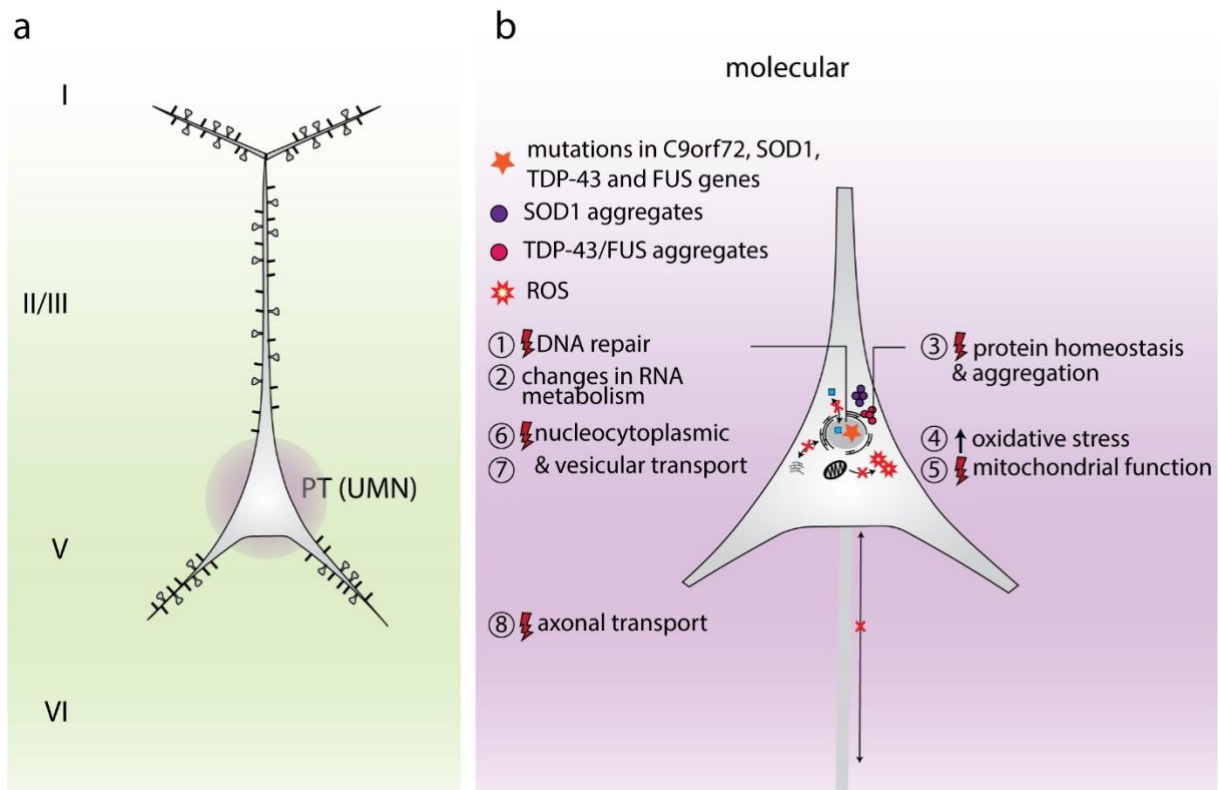
Figure 2. Cell-autonomous mechanisms of degeneration in ALS.
(a) Illustration of a pyramidal tract (PT, a.k.a. upper motor neuron (UMN)). (b) Mutations in C9orf72, SOD1, TDP-43 and FUS genes are found in the genome and aggregates consisting of either mutant SOD1, TDP-43 or FUS are detected in the cytoplasm. These changes include (1) deficits in DNA impair, (2) changes in RNA metabolism, (3) altered protein homeostasis and aggregation, (4) increased oxidative stress, (5) mitochondrial dysfunction, (6-7) impaired nucleocytoplasmic and vesicular transport and (8) impaired axonal transport. *Modified after (Bonafede & Mariotti, 2017) under the Creative Commons Attribution License.*

1.1.2. Current available treatment options for ALS

There are currently three FDA-approved drugs available to treat ALS, namely riluzole and edaravone and recently relyvrio. Riluzole is a glutamate antagonist that blocks glutamate release in pre-synaptic terminals as well as glutamate binding to N-methyl-D-aspartate receptors (NMDAR) on the post-synaptic neuron (Doble, 1996). Existing real-world data suggests that riluzole treated ALS patients have an extended lifespan of 6 to 21 months (Chen, 2020; Hinchcliffe & Smith, 2017; Miller et al., 2009; Turner et al., 2002), which exceeds the range of 2 to 3 months shown in clinical trials (Andrews et al., 2020; Bensimon et al., 1994). Edaravone is an antioxidant that scavenges excess reactive oxygen species (ROS), which cause neuronal degeneration and death (Cho & Shukla, 2020; Jami et al., 2015; Roh et al., 2011). Some treated patients, especially during the early phases of ALS, have demonstrated delayed motor function deterioration (Abe et al., 2017; Sawada, 2017). To maximize the benefits of the approved drugs, a combination of riluzole and edaravone is recommended at an early stage of ALS (Dash et al., 2018; Sawada, 2017).

With an increasing though still insufficient understanding of the pathophysiological mechanisms of ALS, most clinical trials halt at phase three. One of the recent FDA-approved treatments for ALS is AMX0035, a combination of two compounds, namely sodium phenylbutyrate and tauroursodeoxycholic acid ("Amylyx Pharmaceuticals Announces FDA Approval of RELYVRIO™ for the Treatment of ALS," 2022). AMX0035 prevents neuronal death by targeting ER stress and abnormal mitochondrial metabolism (Heo, 2022). Thus far, AMX0035 extended life expectancy by 6.5 months (Kiernan et al., 2021). For fALS patients, there are antisense oligonucleotides targeting specific mutated proteins which are either still at an early stage of development or were halted at later phases of the clinical trials, such as toferson for SOD1 (Miller et al., 2022; Mullard, 2021; Shaw et al., 2022), ION363 for FUS

(Korobeynikov et al., 2022) and FOCUS-C9 for C9ORF72 (Corcia et al., 2022; Liu et al., 2022b). Taken together, current treatment options extend the lifespan of ALS patients by a mere few months, but a cure is still far from reach; thus, this warrants a more thorough understanding of the disease at a deeper level.

1.1.3. Debated origin of ALS: the dying forward vs. dying backward hypotheses

Diverging symptoms presented in ALS patients as well as the pathology seen in upper (UMNs) and lower motor neurons (LMNs) led to the two main hypotheses explaining neuronal degeneration in ALS: the dying forward- and dying backward hypotheses

The dying forward hypothesis, also known as the corticofugal model, suggests that the pathology begins in upper motor neurons (UMNs) and propagates to lower motor neurons (LMNs) in the spinal cord via glutamate-mediated excitotoxicity. Evidence that supports this hypothesis includes cortical hyperexcitability, detected by means of transcranial magnetic stimulation (TMS) (Vucic et al., 2008) as well as the expression of TDP-43, in both UMNs and other corticofugal-projection neurons prior to the emergence of spinal (LMNs) and motor symptoms (Eisen, 2021; Eisen et al., 2017). Moreover, in pre-symptomatic rodent models of ALS, both structural and electrophysiological changes are detected in UMNs (Fogarty et al., 2016a; Fogarty et al., 2016c; Fogarty et al., 2015b; Jara et al., 2020). To test whether the observed cortical hyperexcitability in fact drives neurodegeneration, chronic neuronal activation was induced chemogenetically with Designer Receptors Exclusively Activated by Designer Drugs (DREADDs) in otherwise healthy, control mice. DREADDs target modified G protein-coupled receptors (GPCRs) — specifically the modified human M3 muscarinic receptor (hM3Dq) that can be activated by clozapine N-oxide (CNO). The chronically increased

neuronal activity results in cortical and spinal cytoplasmic mislocalization of TDP-43 and motor deficits (Haidar et al., 2021), further supporting the notion of a corticofugal spread.

On the contrary, the dying backward hypothesis proposes that degeneration begins at the neuromuscular junctions and triggers pathology in the LMNs in the spinal cord and subsequently affects UMNs in the cortex in a retrograde manner. Degenerative mechanisms in NMJs and LMNs include the lack of neurotrophic factors, modifications in the cytoskeleton structure in LMNs, mitochondrial dysfunction and increased oxidative stress, and glutamate-mediated excitotoxicity in LMNs (Dadon-Nachum et al., 2010; Ekestern, 2004). Evidence in favor of the dying backward hypothesis include (1) reduced retrograde uptake and transport of cargos like mitochondria, lysosomes and neurotrophic factors which could be detrimental to the health and function of neurons (Parkhouse et al., 2008; Ström et al., 2008) and (2) changes in synaptic transmission at the neuromuscular junction (NMJ) (Rocha et al., 2013).

1.1.4. Excitability changes in motor cortex of humans

Despite the controversial views on the origin of motor neuron neurodegeneration in ALS, one consistent finding in both cortex and spinal cord is excitability changes (Gunes et al., 2020). A compelling piece of evidence that supports the dying-forward hypothesis is the causal relationship between chronic cortical hyperexcitability and the recapitulation of TDP-43 pathology as well as motor symptoms established by Haidar et al. (Haidar et al., 2021). However, the molecular and cellular mechanisms underlying cortical hyperexcitability remain incompletely understood. The hyperexcitability detected in motor cortex of ALS patients and in transgenic mouse models (Dyer et al., 2021a; Fogarty et al., 2015a; Geevasinga et al., 2015; Kim et al., 2017; Menon et al., 2017; Menon et al., 2015; Nieto-Gonzalez et al., 2011; Pieri et al., 2009; Van den Bos et al., 2018; Vucic et al., 2009; Vucic et al., 2008; Vucic et al., 2021;

Zanette et al., 2002a; Zhang et al., 2016) could be a result of cell-autonomous changes of UMNs, such as lower threshold potential in UMNs, and/or altered circuit mechanisms, a.k.a. non-cell-autonomous, such as reduced inhibition, increased long-range inputs and changes in neuromodulation.

The excitability of human motor cortex (M1) is assessed by means of transcranial magnetic stimulation (TMS), a technique in which an electromagnetic stimulus is applied to the motor cortex, followed by the measurement of evoked potentials in the innervated muscle, such as the abductor pollicis brevis (Figure 3). Parameters that indicate hyperexcitability include decreased resting motor threshold (RMT), in which a stimulus of lower intensity can trigger the same response elicited by a stimulus of higher intensity; increased motor evoked potential (MEP), in which a stimulus of the same intensity leads to a bigger response compared to healthy controls; and decreased short interval intracortical inhibition (SICI) and a shorter cortical silent period (CSP), which reflects compromised intracortical inhibition involving GABAergic interneurons (Cengiz et al., 2019; Cengiz & Kuruoğlu, 2020; Menon et al., 2017; Shibuya et al., 2017; Van den Bos et al., 2018; Vucic et al., 2009; Zanette et al., 2002a; Ziemann et al., 1997); please see reviews (Gunes et al., 2022; Gunes et al., 2020) for more details. Thus, findings in both sALS and fALS patients argue for hyperexcitability in motor cortex as a result of both, increased excitation and deficits in inhibition (thus causing excitation/inhibition dysbalance), and the degree of excitability could be used to predict the progression of cognitive and behavioral symptoms (Agarwal, 2021). In addition to local excitation/inhibition balance, functional connectivity of M1 has also been measured in patients using functional magnetic resonance imaging (fMRI). fMRI detects changes in blood-oxygen-level-dependent (BOLD) signal, and thus measures brain activity. In ALS patients, increased functional connectivity across cortical areas was observed, which also was negatively correlated with motor function (Schulthess et al., 2016). Though these studies show cortical hyperexcitability and increased functional

connectivity, the technique employed do not have layer-specific nor cell type-specific resolution. Therefore, the *source* of cortical hyperexcitability remains unclear and hampers the development of effect treatment.
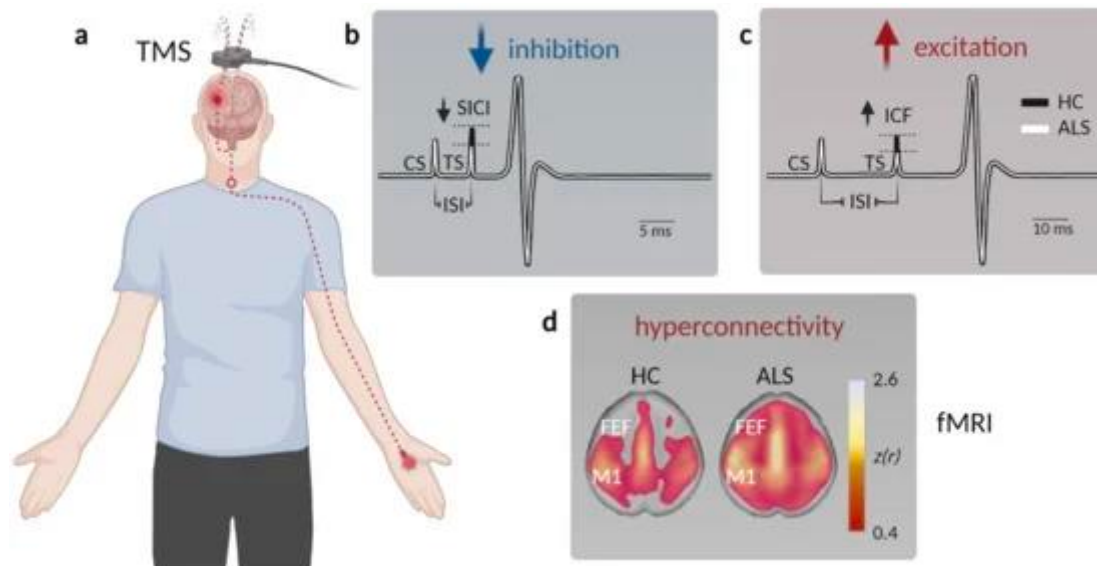
Figure 3. Measurement of hyperexcitability and hyperconnectivity in the motor cortex of ALS patients. (a) An electromagnetic coil is placed on top of the subject's scalp at motor cortex (M1), triggers an electric current in M1, "and the resulting evoked potential is measured at the innervated muscle". (b-c) Example illustration of the motor evoked potential (MEP) with a smaller amplitude in short interval intracortical inhibition (SICI) following the conditioned stimulus (CS) and test stimulus (TS) applied after a shorter interstimulus interval (ISI) (black: healthy controls (HC); white: ALS); and an increased intracortical facilitation (ICF) following a TS applied after a longer ISI. (d) Functional magnetic resonance imaging (fMRI) study in ALS patients with increased hyperconnectivity in frontal eye field (FEF) and M1. *Reprinted from (Gunes et al., 2022) under the Creative Commons Attribution License.*

1.1.5. Rodent models of ALS and excitability changes in motor cortex

To understand the underlying mechanisms and to dissect the temporal order of degenerative events, rodent models were generated. The most established model of ALS, namely the SOD1^{G93A} transgenic (tg) mouse model is based on the expression of the mutant human SOD1 discovered in ALS (Gurney et al., 1994; Tu et al., 1996). It recapitulates the cellular alterations and motor deficits typical of human patients. Similar to patients with SOD1 mutations, misfolded-SOD1 inclusions are also found in neurons in SOD1 tg mice (Commisso et al., 2018;

Genc et al., 2020; Sábado et al., 2014), as well as increased ER stress (Nishitoh et al., 2008), astrogliosis (Özdinler et al., 2011), and upper and lower motor neuron degeneration and death (Nishitoh et al., 2008; Özdinler et al., 2011). Behavioral deficits include hindlimb tremor, declined muscle strength and motor function, weight loss due to muscle wasting, and reduced life expectancy (Bennett et al., 2014; Kreilaus et al., 2020; Oliván et al., 2014; Wooley et al., 2005).

In addition to the SOD1^{G93A} mouse model, there are also models based on other known mutations, such as TDP-43 and FUS. Most of the TDP-43 mouse models are generated based on an overexpression of TDP-43 (Yang et al., 2022) – some using knock-in (Huang et al., 2020; Silva et al., 2019). The models do not fully recapitulate all symptoms described in ALS patients. For example, TDP-43^{Q331K} mice exhibited cellular changes like increased nuclear expression of TDP-43 in lower motor neurons and behavioral phenotypes though they lacked the cytoplasmic TDP-43 proteinopathy (Watkins et al., 2021).

To study the disease progression of FUS-associated ALS and FTD, various models have been developed based on either an overexpression (Mitchell et al., 2013), knock-out (Kino et al., 2015; Scekic-Zahirovic et al., 2016), or knock-in of mutated FUS, causing cytoplasmic mislocalization (Scekic-Zahirovic et al., 2016). Though the model described in Scekic-Zahirovic et al., 2016 does not display severe motor phenotypes like SOD1^{G93A} mice, they still display phenotypes such as the loss of LMN (Scekic-Zahirovic et al., 2016), increased spontaneous locomotion and disrupted social behavior (Scekic-Zahirovic et al., 2021).

To understand cellular mechanisms underlying cortical hyperexcitability seen in ALS patients, structural and electrophysiological alterations were assessed in mouse models such as SOD1^{G93A}, TDP-43^{Q331K} and TDP-43$^{\Delta NLS}$. Dendritic regression and spine loss were observed

in UMNs in pre-symptomatic SOD1^{G93A} (Commisso et al., 2018; Fogarty et al., 2016b; Fogarty et al., 2015a; Saba et al., 2016), TDP-43^{Q331K} (Fogarty et al., 2016a) and TDP-43$^{\Delta NLS}$ (Dyer et al., 2021b) tg mice (Figure 4a-b). To probe excitability of UMNs, whole-cell patch-clamp recordings can be performed in acute brain slices. In addition to an increased likelihood to fire, as reflected in a reduced rheobase (Kim et al., 2017; Pieri et al., 2009; Saba et al., 2016), there is also an increase in the frequency of post-synaptic excitatory currents in UMNs of SOD1^{G93A} mice (Fogarty et al., 2015a; Kim et al., 2017; Pieri et al., 2009; Saba et al., 2016) and TDP-43^{Q331K} (Fogarty et al., 2016a) (Figure 4b). However, the hyperexcitability did not translate into activity changes in wakefulness as probed by Kim et al. using *in vivo* two-photon calcium imaging (Kim et al., 2017) (Figure 4b). In addition, a decrease in the size and number of UMNs were also observed in both pre- and symptomatic SOD1^{G93A} mice, indicating somatic degeneration at an early stage (Gunes et al., 2020; Özdinler et al., 2011; Zang & Cheema, 2002) (Figure 4b).
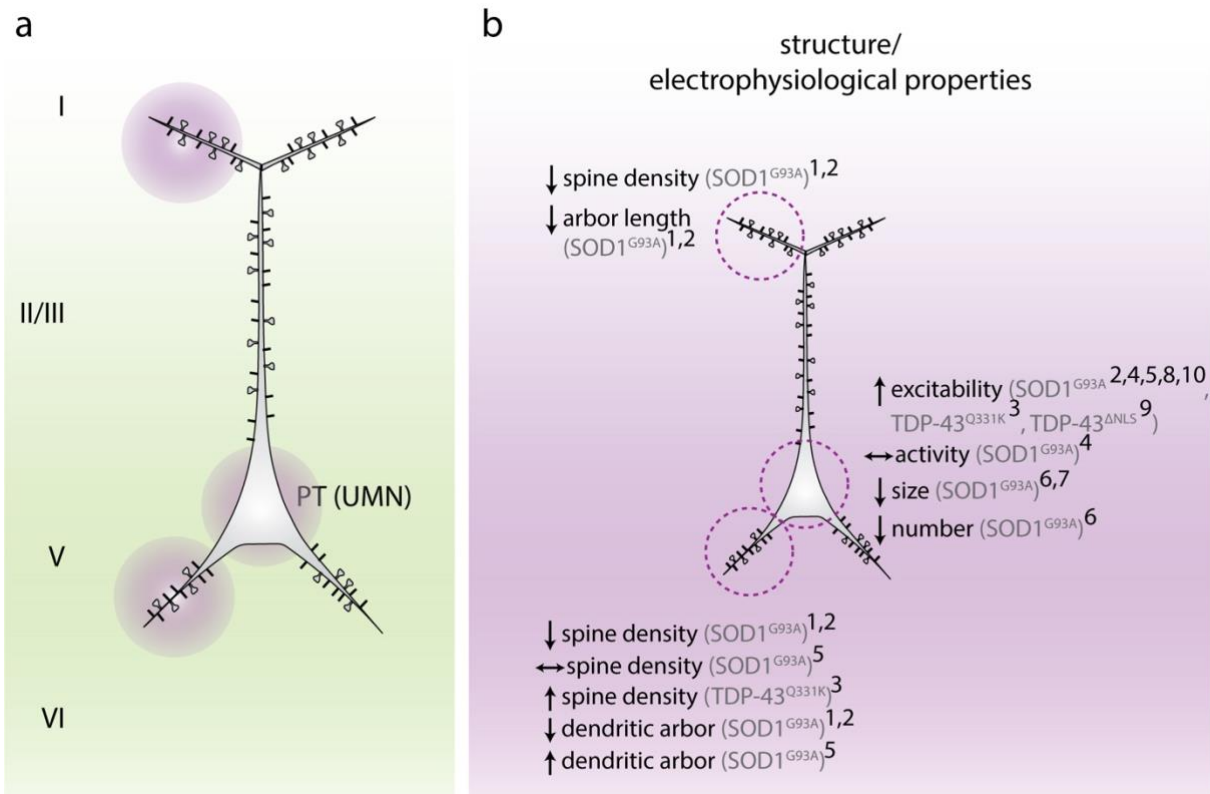
Figure 4. Changes in structural and electrophysiological properties of UMNs in ALS. (a) Illustration of a pyramidal tract (PT) neuron. **(b)** Alterations in spine density and arbor length of apical[1,2] and basal[1,2,3,5] dendrites of UMNs are accompanied by an overall reduction in size[6,7] and number[6]. In addition to structural changes, increased excitability is detected in UMNs of SOD1^{G93A} [2,4,5,8,10], TDP-43^{Q331K} [3] and TDP-43$^{\Delta NLS}$ [9] mice, with no changes in activity[4]. [1](Fogarty et al., 2016b), [2](Fogarty et al., 2015a), [3](Fogarty et al., 2016a), [4](Kim et al., 2017), [5](Saba et al., 2016), [6](Zang & Cheema, 2002), [7](Özdinler et al., 2011), [8](Gautam et al., 2016), [9](Dyer et al., 2021a), [10](Pieri et al., 2009). *Adapted from (Gunes et al., 2020) under the Creative Commons Attribution License.*

Our current knowledge of the pathophysiology of ALS gave rise to therapeutic options, which target glutamate and increased oxidative stress in motor neurons, that demonstrated limited benefits in patients. In rodent models, intrinsic excitability changes, as evidenced by both structural and electrophysiological changes, have been identified in UMNs. However, to unravel non-cell-autonomous mechanisms underlying neurodegeneration and most importantly, the *source* of cortical hyperexcitability, the role of other circuit elements in M1 have also been probed and will be discussed in chapter 1.2.

1.2. Motor cortex

To investigate the role of other circuit elements in M1 underlying cortical hyperexcitability in ALS, we first need to understand the function and role of each circuit element in M1 under physiological conditions. The motor system controls body movement and is composed of elements in both the central, such as motor cortex and spinal cord, and peripheral nervous system such as the neuromuscular junction. The primary motor cortex is crucial for motor learning and performing fine movements (Chen et al., 2015; Harrison et al., 2012; Heindorf et al., 2018; Komiyama et al., 2010; Makino et al., 2017). Components of the M1 microcircuitry will be outlined in the following section.

1.2.1. "No neuron is an island": components of a cortical microcircuit and the corresponding potential circuit mechanisms underlying cortical hyperexcitability in ALS

Glutamatergic, excitatory pyramidal neurons

The M1 microcircuitry is composed of glutamatergic pyramidal neurons (PNs), GABAergic interneurons, as well as supporting glial cells such as astrocytes, microglia and oligodendrocytes. PNs can further be classified based on their projections, with the two major subtypes being intratelencephalic (IT) and pyramidal-tract (PT) neurons (Shepherd, 2013). IT neurons are found in layer 2/3, 5, 6, and can be further categorized into cortico-cortical (CC; primarily in layer 2/3) and cortico-striatal (CStr; primarily in layer 5A, 5B and 6) neurons, which project transcallosally and to the striatum, respectively. PT neurons, on the other hand, are restricted to layer 5B and are also known as upper motor neurons (UMNs) or Betz cells in humans (Genç et al., 2017; Shepherd, 2013). They project to either the brainstem

(corticobulbar) or the spinal cord (corticospinal) and innervate the contralateral and subcortical regions (Shepherd, 2013). The strongest input to layer 5 neurons, including UMNs, is provided by layer 2/3 IT-PNs, followed by intralaminar input within layer 5, by CC and CStr PNs in layer 5A and UMNs in layer 5B (Anderson et al., 2010; Kiritani et al., 2012; Shepherd, 2013).
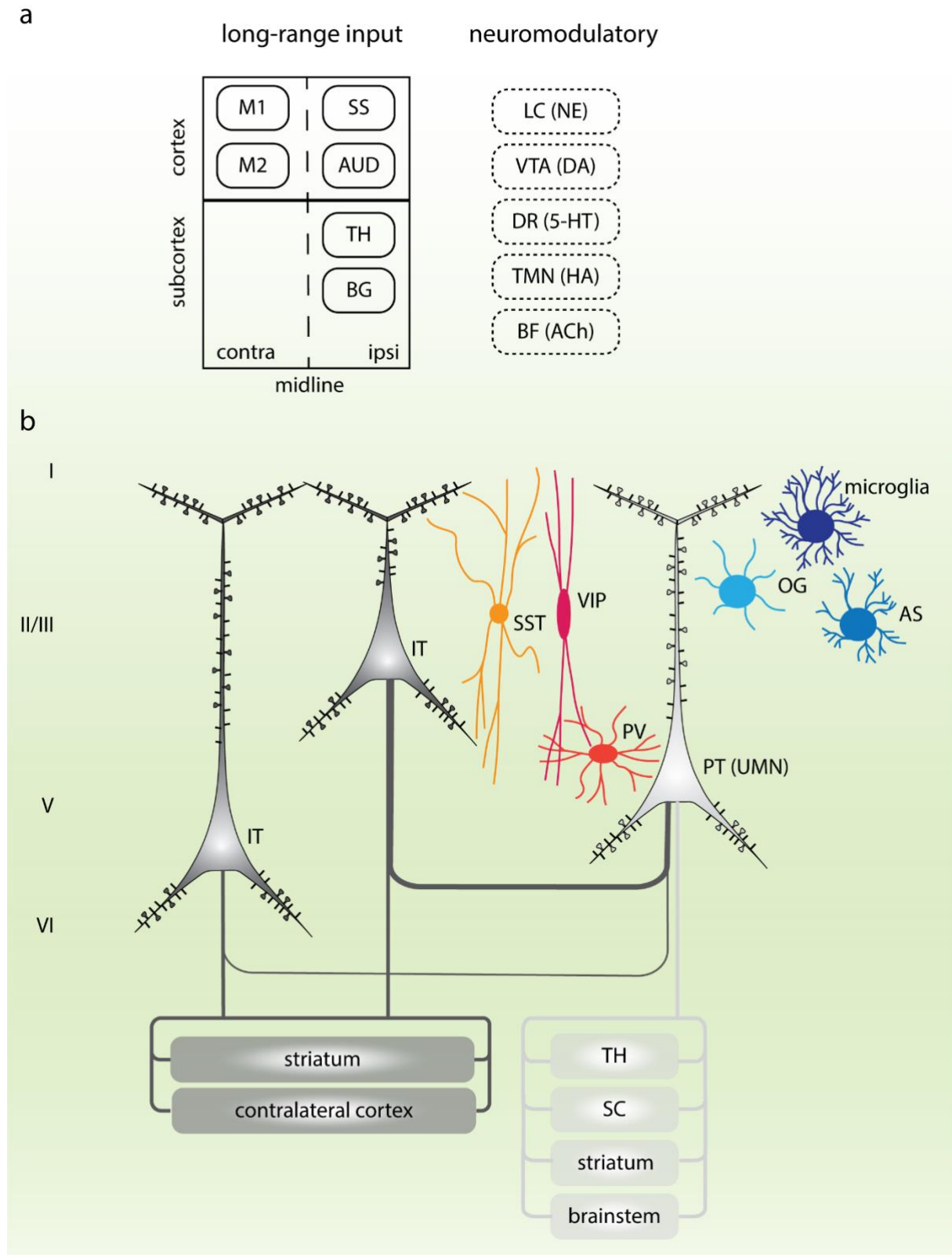
Figure 5. Input to, components and output of the M1 microcircuitry.
(a) Primary motor cortex (M1) receives long-range output from somatosensory cortex (SS), auditory cortex (AUD), thalamus (TH) and basal ganglia (BG), and contralateral M1 and secondary motor cortex (M2). The microcircuitry is fine-tuned by neuromodulation from locus coeruleus (LC), ventral tegmental area (VTA), dorsal raphe (DR), tuberomammillary nucleus (TMN) and basal forebrain (BF), releasing norepinephrine (NE), dopamine (DA), serotonin (5-HT), histamine (HA) and acetylcholine (Ach), respectively. (b) Locally, two major subtypes of pyramidal neurons can be found, namely intratelecephalic (IT) and pyramidal tract (PT). IT neurons are found throughout layers 2 to 6 while PT neurons, a.k.a. UMN, are restricted to layer 5B. UMNs receive the strongest input from layer 2/3 IT, followed by layer 5A IT (thickness reflects input strength). In addition to glutamatergic

pyramidal neurons, there are also GABAergic interneurons, namely parvalbumin (PV), somatostatin (SST) and vasoactive intestinal peptide (VIP); and supportive glial cells, namely microglia, oligodendrocytes (OG) and astrocytes (AS). Modified after *(Shepherd, 2013) and (Kubota et al., 2016) with permission.*

In ALS, in addition to the structural and electrophysiological changes of UMNs described above, there is also evidence of spine loss and decreased arbor length of layer 2/3 PNs (Fogarty et al., 2016b; Fogarty et al., 2015a; Gunes et al., 2020) and increased spontaneous synaptic excitation (Fogarty et al., 2015b; Saba et al., 2016), suggesting a more complex involvement of M1 circuit elements other than UMNs in neurodegeneration typical of ALS.

GABAergic, inhibitory interneurons

Within the microcircuit, excitation is regulated by inhibition termed excitation/inhibition balance. GABAergic interneurons (INs) constitute 10-20% of the cortical neuronal population (Beaulieu, 1993; Meyer et al., 2011; Morin & Beaulieu, 1994; Nigro et al., 2018; Swanson & Maffei, 2019), and they can be categorized based on their morphological and physical properties, postsynaptic targets and marker proteins expressed (Markram et al., 2004; Tremblay et al., 2016). The three largely non-overlapping IN classes are parvalbumin (PV) (40%), somatostatin (SST) (30%) and ionotropic serotonin receptor 5-HT3a (30%, and majority of them express vasoactive intestinal peptide (VIP)) expressing cells (Nigro et al., 2018; Rudy et al., 2011; Swanson & Maffei, 2019; Tremblay et al., 2016; Wood et al., 2017). PV are also known as fast-spiking neurons; the majority of which are basket cells, that provide strong inhibition on PNs by targeting their soma and proximal dendrites (Bartos & Elgueta, 2012; Safari et al., 2017; Veres et al., 2017). They constitute the largest fraction of INs, especially in layer 5 (Gonchar et al., 2008; Lee et al., 2010; Naka & Adesnik, 2016; Xu et al., 2010). SST INs are found throughout layer 2 to 6 though most abundant in layer 5 (Nigro et al., 2018; Scheyltjens & Arckens, 2016). They are mostly Martinotti cells with axons ascending to layer

1 to 3 as well as within layer 5, allowing them to target dendrites of PNs (Markram et al., 2004; Silberberg & Markram, 2007). VIP are found most abundantly in upper layers (layer 2/3) with dendritic arborization in layer 1 (Lee et al., 2010; Prönneke et al., 2015; Xu & Callaway, 2009). They are also found in layers 5 and 6, but with more elaborate dendrites, allowing them to be activated either locally or via long-range inputs (junior Apicella & Marchionni, 2022; Prönneke et al., 2015; Prönneke et al., 2020; Sohn et al., 2016). VIP regulate feedforward inhibition in the network by inhibiting INs (disinhibition) (junior Apicella & Marchionni, 2022; Krabbe et al., 2019; Lee et al., 2013; Yu et al., 2019). GABAergic INs are activated by glutamatergic input and their activity is also modulated by neuromodulatory inputs. Differential expression patterns of neuromodulatory receptors were also identified in PV, SST and VIP INs (Paul et al., 2017; Swanson & Maffei, 2019). For example, SST express a wider range of receptors to neuropeptides released from the hypothalamus such as orexin and oxytocin, while VIP express more G-protein coupled receptors (GPCRs) for neuromodulators like norepinephrine (NE), acetylcholine (Ach) and serotonin (5-HT) (Paul et al., 2017).

In the cortex of ALS transgenic rodents, though there are no detectable changes in the density of PV, SST and VIP INs (Clark et al., 2017; Özdinler et al., 2011; Zhang et al., 2016), excitability changes of INs appear to be disease-stage and mutation-specific. In SOD1^{G93A} mice, PV were first found to be hypoactive at the pre-symptomatic stage (Khademullah et al., 2020) and turned hyperexcitable at the early-symptomatic stage (Kim et al., 2017). On the contrary, reduced inhibition is a result of hyperexcitable SST and hypoactive PV in TDP-43^{A315T} mice (Zhang et al., 2016). Additionally, *in vivo* magnetic resonance spectroscopy (H-MRS) in both pre-symptomatic and symptomatic SOD1^{G93A} mice revealed a reduction in GABA levels (Lei et al., 2019). The differential functional deficits of IN subtypes in ALS thus warrant further scrutiny.

Long-range input and neuromodulation

In addition to local excitatory and inhibitory synaptic connections, M1 is innervated by neighboring cortical areas, such as the ipsilateral somatosensory cortex (S1) and the contralateral M1, and more distal regions such as the frontal cortex (FC), thalamus (TH), orbital cortex (OC) and auditory cortex (AUD) (Commisso et al., 2018; Geng et al., 2021; Luo et al., 2019; Takahashi et al., 2021). Layer-specifically, input from motor and sensory TH is primarily targeted at layer 5A, while neurons in FC and OC target deeper layers like 5B and 6 (Hooks et al., 2013). Increased excitatory input from S1 was reported in pre-symptomatic SOD1-G93A mice, followed by the contralateral M1, TH and AUD as the disease progresses (Commisso et al., 2018).

Information processing and motor function in M1 is further fine-tuned by neuromodulatory input. These inputs stem from the locus coeruleus (LC), the ventral tegmental area (VTA), the dorsal raphe (DR), the tuberomammillary nucleus (TMN) and the basal forebrain (BF), releasing norepinephrine (NE), dopamine (DA), serotonin (5-HT), histamine (HA) and acetylcholine (ACh), respectively (Brunet et al., 2020; Vitrac & Benoit-Marand, 2017). Together, monoaminergic systems regulate arousal, learning and motor output.

Briefly, NE input to layers 2 to 6 of M1 is associated with arousal, sensory processing and locomotion (Aston-Jones & Bloom, 1981; Aston-Jones et al., 2001; Aston-Jones & Waterhouse, 2016; Breton-Provencher & Sur, 2019; Carter et al., 2010; Janitzky et al., 2015). There are two main classes of adrenoceptors (AR) for NE, each with two to three subtypes, namely α1 and α2 and β1, β2 and β3. NE facilitates excitation and inhibition by binding to α1-AR and β-AR, respectively (Mouradian et al., 1991). DA, on the other hand, is involved in learning-induced plasticity and motor skill learning (Hosp et al., 2011; Vitrac et al., 2014). DA

innervates deeper layers of M1 and acts on two classes of G protein-coupled receptors (GPCRs), namely D1-type and D2-type receptors (Jaber et al., 1996), producing different effects on M1. Activation of D2-type receptors result in increased PN firing (Vitrac et al., 2014), while a synergistic activation of both D1- and D2-type receptors result in inhibition of PN activity (Awenowicz & Porter, 2002; Huda et al., 2001). Furthermore, 5-HT innervates layers 2 to 6 of M1 and is important for behavioral adaptation to the environment. 5-HT facilitates motor output by activation of $5-HT_{1A}$ receptors that inhibit GABAergic INs (Batsikadze et al., 2013; Jacobs & Fornal, 1997; Loubinoux et al., 2005; Puig et al., 2010). Moreover, HA modulates neuroinflammatory responses, circadian rhythm as well as circadian motor activity such as feeding and exploratory behaviors, in which higher levels of HA are detected during the active phase (Apolloni et al., 2017; Haas & Panula, 2003; Inzunza et al., 2000; Lozeva et al., 2000). Unlike the other neuromodulators, HA innerves all layers of M1, with the strongest input to layer 1. HA binds to four classes of receptors, namely H_1, H_2, H_3 and H_4, and acts on excitation of PNs by binding to H_1 and H_2 receptors. To regulate release of HA and other neuromodulatory inputs like NE, 5-HT and Ach, HA binds to H_3 receptors, which causes autoinhibition of neurons in TMN and inhibition of neurotransmitter release (Cheng et al., 2021; Ellender et al., 2011; Haas & Panula, 2003; Moreno-Delgado et al., 2020; Valle-Bautista et al., 2021; Yu et al., 2015; Zant et al., 2012). Finally, ACh refines information processing within the network (Kuo et al., 2007), by acting on two major classes of receptors, namely nicotinic and muscarinic receptors. Activation of nicotinic receptors causes excitation and that of muscarinic receptors can cause both excitation and inhibition (Ballinger et al., 2016).

Given the role of neuromodulatory input in motor learning, locomotion, sensory processing and behavioral adaptation in M1, deficits in these systems may be involved in the pathophysiology of ALS. Indeed, in ALS patients, there is evidence for deficits in dopaminergic (Borasio et al., 1998; Takahashi et al., 1993; Vogels et al., 2000) and serotonergic (Dupuis et al., 2010; Turner

et al., 2005) systems, while less is known about changes in NE. TDP-43 inclusions were identified in TMN and BF of some ALS patients (Cykowski et al., 2014), accompanied by deregulation of HA-associated gene expression in cortex of both ALS patients and mouse models (Apolloni et al., 2017). Since HA stimulates the release of NE, DA and 5-HT (Flik et al., 2015), HA was administered as a therapy to SOD1^{G93A} mice to counteract deficits in DA and 5-HT, and there was an improvement in survival, motor function as well as a reduced neuroinflammatory response and cell death (Apolloni et al., 2019). To summarize, complex interactions across cell types, long-range and neuromodulatory input regulate M1 function; hence,the M1 circuitry and function should be investigated to better understand the pathophysiology of ALS.

Glial cells

Glial cells comprise microglia, astrocytes and oligodendrocytes. They are supporting cells crucial for the maintenance and modulation of neuronal health and activity. In contrast to neurons, glial cells are electrically silent, and they lack axons and dendrites. Instead, they have more complex processes at the cell body, and they communicate with each other through intracellular calcium changes, gap junctions and signaling molecule release such as cytokines and trophic factors, and with neurons via neurotransmitter and signaling molecule release (Fields & Stevens-Graham, 2002; Hansson & Rönnbäck, 2003).

Microglia are primary immune cells and tissue resident macrophages (that is mononuclear phagocytes) of the central nervous system (CNS). They survey neurons, regulate neuronal plasticity and shape structure and function of neural circuits (Cserép et al., 2021; Salter & Beggs, 2014; Tremblay et al., 2010; Wake et al., 2013). Microglia become activated in response to neuronal damage and neuroinflammation, in which case the ramified morphology is altered

by the retraction of processes into an amoeboid shape (Fernández-Arjona et al., 2017; Heindl et al., 2018). Activated microglia release pro-inflammatory cytokines and opsonins (Butler et al., 2021) (Smith et al., 2012) and phagocytose damaged cells (Butler et al., 2021). In ALS, apart from transcriptomic changes with enriched gene expression in neuroinflammatory and synaptic-associated pathways (Dols-Icardo et al., 2020), microglia also showed reduced complexity in morphology in M1 (Migliarini et al., 2021), which might contribute to excessive phagocytosis and inflammation (Butler et al., 2021).

Another class of glial cells is oligodendrocytes. Oligodendrocytes form myelin sheaths that surround axons of neurons in the CNS for insulation and fast propagation of action potentials. In multiple sclerosis (MS), a neuroimmune disorder characterized by demyelination, oligodendrocyte dysfunction is linked to motor impairment (Grace et al., 2017; Pepper et al., 2018). Their role in ALS is not fully understood yet. In spinal cord of SOD1^{G93A} tg mice, enhanced proliferation of oligodendrocyte progenitor cells was detected, but these progenitor cells were functionally and developmentally compromised (Cho, 2013; Kang et al., 2013).

Finally, astrocytes are vital for the regulation of synaptic transmission of neurons by glutamate reuptake at the synaptic cleft (Mahmoud et al., 2019; Rothstein et al., 1996; Trotti et al., 1999), and thus play an important role in a microcircuitry (Ben Achour & Pascual, 2012; Fellin et al., 2006; Halassa & Haydon, 2010; Lyon & Allen, 2022). In ALS, both molecular, structural and functional deficits of astrocytes in rodent models and ALS patients have been identified. In particular, the sodium-dependent glutamate transporters excitatory amino acid transporters 1 and 2 (EAAT1 and EAAT2) in humans and GLT-1 and GLAST in rodents are crucial for glutamate clearance (Rothstein et al., 1996). EAATs remove glutamate from the synaptic cleft and the glutamate is recycled to the presynaptic cleft, but in ALS, downregulation of EAAT2 was detected in motor cortex and spinal cord of patients (Rothstein et al., 1995) and in rodent

models (Bendotti et al., 2008; Bruijn et al., 1997; Howland et al., 2002; Wilson et al., 2003). Additionally, though overexpression of EAAT2 delays symptom onset and motor neuron death, the degenerative pattern persists, suggesting that targeting excess glutamate as a treatment approach is ineffective, justifying for more circuit-based approaches. In addition to glutamate clearance, there is also evidence of impaired potassium ion (K^+) balance and water (H_2O) clearance through the upregulation of aquaporin-4 (AQP4) and downregulation of the inward-rectifying K^+ channel Kir4.1, respectively (Bataveljic et al., 2012; Dai et al., 2017), which could affect neuronal excitability and could thus contribute to hyperexcitability in MN (Djukic et al., 2007; Kelley et al., 2018; Wang et al., 2022).
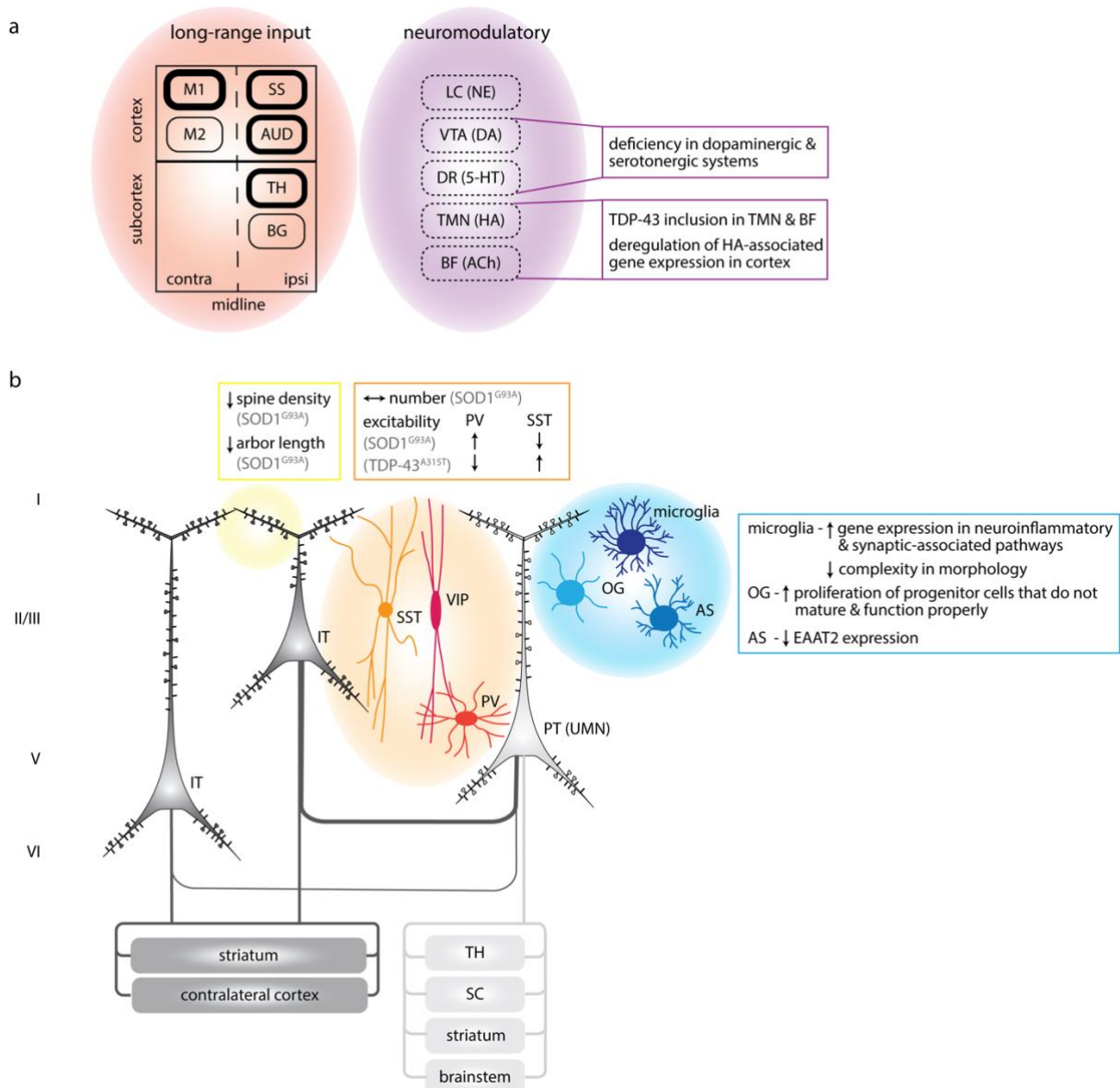
Figure 6. Non-cell autonomous mechanisms of degeneration in ALS.
(a) Increased long-range input from contralateral motor cortex (M1), somatosensory cortex (SS), auditory cortex (AUD) and thalamus (TH) (line thickness indicates increased input). Alterations in neuromodulation includes deficiency in dopaminergic and serotonergic systems, TDP-43 inclusions in both tuberomammillary nucleus (TMN) and basal forebrain (BF), and dysregulation of HA-associated gene expression in cortex. (b) Locally, decreased spine density and dendritic arbor length were detected in layer 2/3 pyramidal neurons (PNs) in SOD1^{G93A} transgenic (tg) mice. In terms of inhibition, no change was detected in the number of parvalbumin (PV), somatostatin (SST) and vasoactive intestinal peptide (VIP)-expressing neurons in SOD1^{G93A} tg mice, though opposing excitability changes were detected in two mouse models of ALS. While increased excitability in PV accompanied by decreased excitability in SST were detected in SOD1^{G93A} tg mice, hyperactive SST and hypoactive PV were observed in TDP-43^{A315T} tg mice. In addition, enhanced gene expression in neuroinflammatory and synaptic-associated pathways and reduced complexity in morphology were observe in microglia. There are also increased proliferation of oligodendrocyte progenitor cells that do not mature and function properly, and a reduction in excitatory amino acid transporter 2 (EAAT2) in astrocytes.

1.2.2. Glutamate-mediated excitotoxicity

Another molecular mechanism involved in the degeneration of motor neurons in ALS as well as of neurons in other neurodegenerative diseases is glutamate-mediated excitotoxicity, which proposes neurodegeneration as a result of excessive glutamatergic stimulation due to compromised glutamate reuptake and/or increased pre-synaptic release. Glutamate is the major excitatory neurotransmitter in the central nervous system (CNS). Under physiological conditions, glutamate is released from the pre-synaptic terminal and binds to glutamate receptors, such as N-methyl-D-aspartate (NMDA, α-amino-3-hydroxy-5-methyl-4-isoxazole propionic acid (AMPA) and Kainite receptors, on the postsynaptic neuron. The binding could cause a suprathreshold stimulus that results in an action potential in the postsynaptic neuron. The glutamate is taken up and removed from the synaptic cleft by Na^+-dependent excitatory amino acid transporters (EAATs) that are expressed in both neurons and astrocytes, and is recycled into the pre-synaptic neuron (O'Donovan et al., 2017). When glutamate is insufficiently cleared from the synaptic cleft, the build-up of glutamate can trigger excitotoxicity and eventually cell death.

In ALS, the main evidence arguing for glutamate-mediated excitotoxicity includes detection of elevated glutamate levels in the blood and cerebrospinal fluid (CSF) of ALS patients (Babu et al., 1998; Kostera-Pruszczyk et al., 2002; Rothstein et al., 1990) and impaired glutamate reuptake due to deficits in astrocytes as discussed above. However, there are a few contradicting studies that argue otherwise. Instead of elevated glutamate levels, reduced glutamate and glutamine levels were detected in fALS patients with the *SOD1* mutation (Wuolikainen et al., 2011). Researchers further tested the theory in rodent models by chronically blocking glutamate reuptake by targeting glutamate uptake transporters in the spinal cord (Tovar-y-Romo et al., 2009). Despite an increase in glutamate levels, there is no LMN loss nor motor deficits. Most

importantly, the link between increased glutamate levels and cortical hyperexcitability is not established.

Considering the many components of the M1 circuitry, there are many potential sources contributing to the development of cortical hyperexcitability. Therefore, the role of individual circuit elements in ALS pathophysiology needs to be investigated (Figure 7).
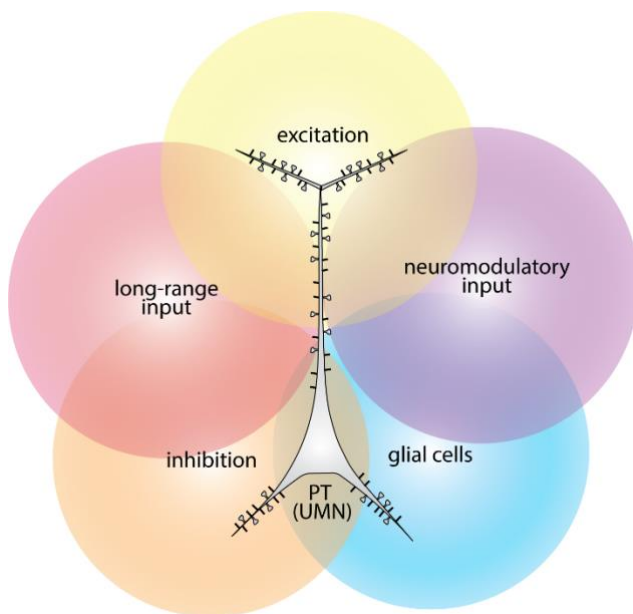

Figure 7. Interaction of proposed cell- and non-cell autonomous degenerative mechanisms in ALS. Cell-autonomous mechanisms affecting upper motor neurons (UMNs) in the center. Surrounding the UMNs are increased excitation (yellow), compromised inhibition (orange), glial cell dysfunction (blue), altered long-range (red) and neuromodulatory input (purple).

1.3. *In vivo* two-photon calcium imaging in awake, behaving rodents

Two-photon (calcium) imaging has been used in the past decade to investigate neuronal activity and dynamics in both anesthetized and awake mice in health and disease states (Blumenstock et al., 2021; Burgold et al., 2019; Eichhoff & Garaschuk, 2011; Korzhova et al., 2019; Liebscher et al., 2016; Scekic-Zahirovic et al., 2021). Furthermore, to dissect circuit mechanisms underlying processes such as sensory processing, memory formation and spatial navigation, different behavioral paradigms have been designed for awake, behaving mice.

1.3.1. Principles of two-photon microscopy

Unlike "classic" fluorescence microscopy such as widefield or confocal that are based on one high-energy photon, two-photon microscopy (2PM) uses two lower-energy infrared photons of a longer wavelength to excite a fluorophore (Svoboda & Yasuda, 2006). The two photons hit the target within femtoseconds and trigger a higher-energy electron transition, followed by the emission of light (Svoboda & Yasuda, 2006). The emitted light that passes through the objective is then amplified by a photomultiplier tube (PMT) unit. The objective as well as the medium in which the light passes through determine the dimensions of the field of view and how efficient light is transmitted (Svoboda & Yasuda, 2006). An example would be exciting the green fluorescent protein (GFP) used in many indicators at 910 nm in 2PM instead of 488 nm used in classic fluorescence microscopy. The near simultaneous absorption of the two photons results in a very narrow focal point, where the energy (laser light) is most focused, which means the highest photon density. As a result, there is less photodamage and phototoxicity to the entire sample, especially regions above and below the focal plane (Figure 8).
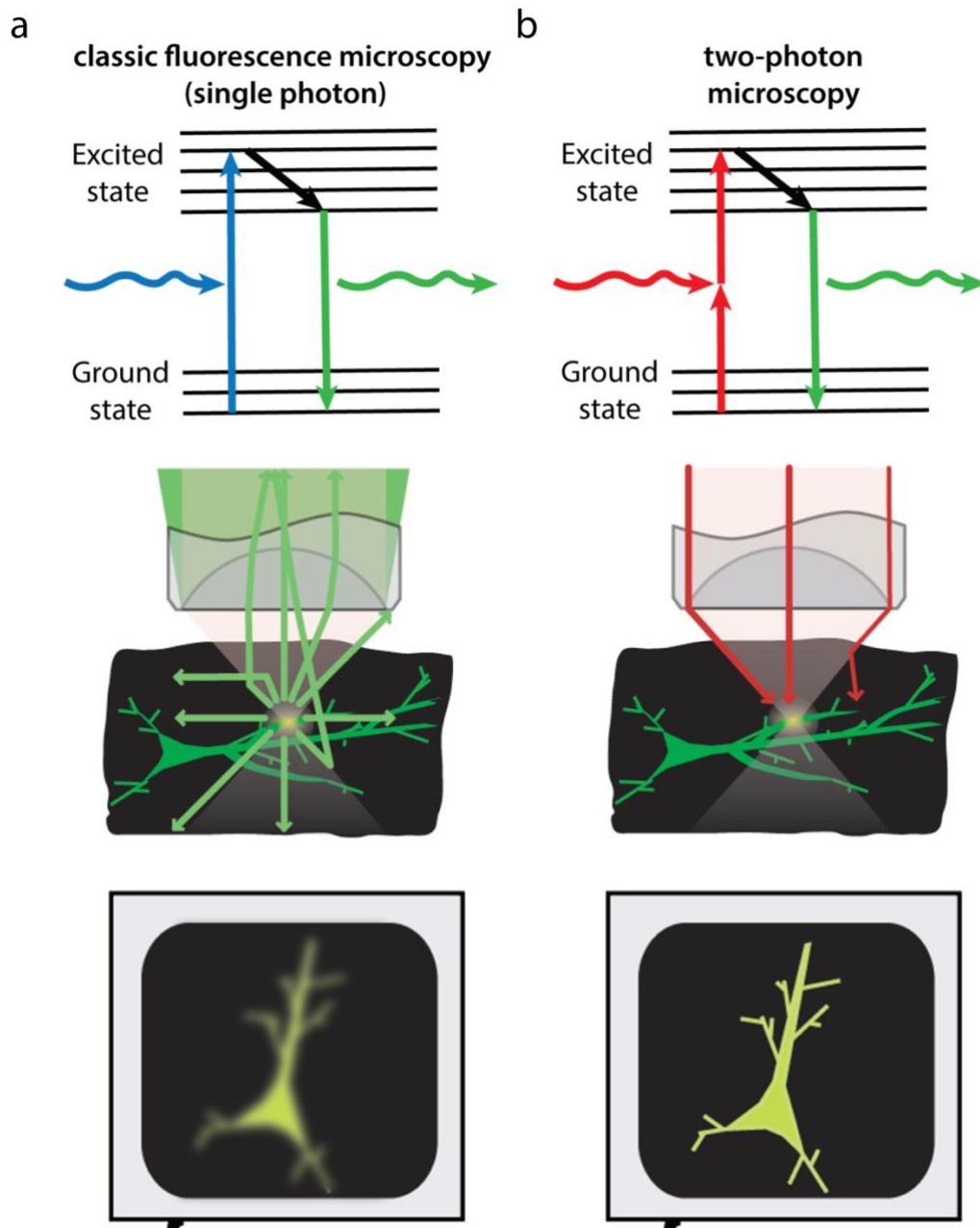
Figure 8. Advantages of two-photon microscopy over classic fluorescence microscopy. (a) Classic fluorescence (one-photon) microscopy uses a single high-energy photon (blue) instead of two equal lower-energy photons (red) at a higher wavelength in (b). While both scenarios result in the emission of the same wavelength (green), the near simultaneous absorption of two photons by the sample reduces light scattering, and thus produces a much clearer image. *Taken from Figure 1 of (Svoboda & Yasuda, 2006) with permission.*

1.3.2. Genetically encoded calcium indicators (GECIs) and its applications in dissecting neural circuits

To study neuronal activity, various techniques can be employed. Electrophysiological recordings assess the AP duration and frequency, input resistance and change in membrane potential of individual neurons or neuronal ensembles with high temporal resolution. However, the lack of visual control in these recordings limits this technique to the assessment of 'active' neurons. To optically measure neuronal activity at single-cell resolution, indicators were developed to detect fluctuations in voltage or intracellular calcium levels acting as a proxy for AP firing. Genetically encoded calcium indicators (GECIs) are one class of them.

GECIs are composed of the cytoplasmic calcium-binding messenger protein calmodulin (CaM), a CaM-binding domain and a fluorescent protein (Pologruto et al., 2004). An AP causes calcium influx in the neuron, and free calcium binds to CaM, causing conformational changes and thus the emission of fluorescence from the fluorophore. Changes in fluorescence in a cell that expresses a calcium indicator is commonly referred to as ΔF/F). Studies investigating neuronal activity with electrophysiology and two-photon calcium imaging simultaneously have demonstrated the correlation between spiking activity and ΔF/F (Ali & Kwan, 2019; Chen et al., 2013; Kerr et al., 2005; Kwan & Dan, 2012; Tian et al., 2009), supporting the use of calcium imaging as a proxy for neuronal activity. In addition to the soma, GECI can also be imaged in axons and boutons as correlates for presynaptic activity; and in dendrites as proxy for synaptic input, backpropagating and/or regenerative activity (Ali & Kwan, 2019) (Figure 9).

Upon an AP firing, voltage-gated sodium channels are activated, allowing an influx of positively charged sodium ions, followed by the opening of voltage-gated calcium channels and an influx of calcium ions. The influx of calcium ions into the cytosol comes from two sources,

first externally from the extracellular matrix, followed by internally primarily from the endoplasmic reticulum (ER) in a process known as calcium-induced calcium release (CICR) (Usachev & Thayer, 1997). Then, neurotransmitters are released into the synaptic cleft, which bind to dedicated receptors and activate post-synaptic neuron. Calcium is found in various compartments of a neuron, including the soma, axon and dendrites, and it has a low baseline concentration intracellularly and a high activity-driven change in concentration (Oh et al., 2019). Most importantly, calcium dynamics within a neuron are correlated with AP generation, neurotransmitter release (Augustine et al., 2003).

In addition to single fluorophore-based indicators described above, fluorescence resonance energy transfer (FRET)-based indicators employ two fluorophores that shift between baseline and excited states. FRET sensors are composed of a donor (baseline) and an acceptor (excited) fluorescent protein. The increase in "free" calcium binding to the sensor and causing a conformational change that reduces the distance between the two fluorescent proteins. The distance change causes a transfer of energy from the donor to the acceptor, and thus emitted fluorescence. These calcium sensors are advantageous over synthetic dyes as they allow for more even and specific labelling of intended structures.
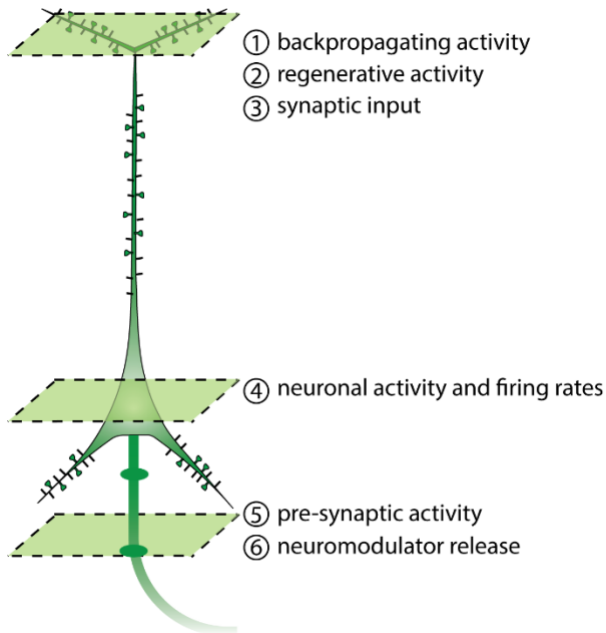
Figure 9. Applications of two-photon calcium imaging in different compartments of a neuron.
Genetically-encoded calcium indicators (GECIs) can be expressed in various compartments of a neuron. Imaging at the level of dendrites with spines provides information on (1) backpropagating activity, (2) regenerative activity and (3) synaptic input. At the level of the soma, calcium imaging is used to examine (4) neuronal activity and firing rates, and at the level of axons with boutons, calcium imaging reveals (5) pre-synaptic activity and (6) neuromodulator release.

GECIs differ with respect to dynamic range, sensitivity and kinetics, which pose advantages as well as limitations depending on the question one would like to answer. Dynamic range refers to the quotient of maximum fluorescent intensity divided by minimum fluorescent intensity (Imax/Imin). A wide spectrum of fluorophores is used in GECIs, ranging from blue to green to far-red, with most of them being green and red. The diversity allows simultaneous imaging of e.g. multiple cell populations. One of the most commonly used GECIs is GCaMP (latest version GCaMP8), based on the green fluorescent protein (GFP) (Nakai et al., 2001).

1.3.3. Sensory processing- and locomotion-related activity in rodent cortex

In vivo two-photon (2P) imaging and GECI are important tools to study neuronal population activity under physiological as well as under pathophysiological conditions. To gain insight into M1 microcircuit element function, it is relevant to study the response properties and activity levels of dedicated neuronal populations. Previous *in vivo* studies have revealed numerous features and response types in M1 (Dombeck et al., 2009; Peters et al., 2017). Functional

clusters of neurons with activity more correlated to movements such as locomotion and grooming have been identified, and activity of neurons within a functional cluster displays stronger correlation as they are more spatially clustered.

To better understand the activity of different neuronal populations in various brain areas, especially when performing a task, *in vivo* 2P calcium imaging has been performed in head-fixed and freely moving animals (Ahrens et al., 2013; Garner & Keller, 2022; Heindorf et al., 2018; Homann et al., 2017; Huber et al., 2012; Keller et al., 2012; Leinweber et al., 2017; Liu et al., 2021). Specifically, multi-projectional layer 5 PT and IT neurons have been shown to serve different functions based on the innervated area (Baker et al., 2018). For instance, layer 5 PT in M1 project to the medulla and to the thalamus and striatum to initiate movement on the contralateral side and to prepare for movement, respectively (Baker et al., 2018). Within M1, the inhibitory circuit has been shown to reshape the connectivity and activity among neurons during motor learning. In particular, SST inhibit the distal branches of the apical dendrites of layer 2/3 neurons, accompanied by a reduced inhibition of the soma by PV INs (Chen et al., 2015). Activity of layer 2/3 neurons also becomes more correlated and consistent over learning, whereas that of layer 5 remains unchanged over time with new distinct activity patterns generated for dissimilar movements, suggesting layer-specific role of M1 in motor learning and the complex circuit mechanisms within the cortex (Peters et al., 2017).

Sensory information such as visual input and tactile is processed in a timely manner and applied to shape and initiate (goal-directed) movement, in a process known as sensorimotor integration (Edwards et al., 2019; Wolpert et al., 1998). Sensorimotor integration can be divided into three levels: (1) cerebral cortex in which stimuli are identified and filtered; (2) subcortical areas that receive input from the cortex for motor command assembly, and (3) spinal cord relays the signal and executes the commands through muscle contraction (Velasques et al., 2013). In rodents,

whisker stimulation provides tactile information to the barrel cortex (part of the primary somatosensory cortex) regarding the environment and is highly correlated with locomotion (Arkley et al., 2014; Ayaz et al., 2019; Chakrabarti et al., 2021; Sofroniew et al., 2014). Interestingly, activity of neurons in the barrel cortex is more vigorously modulated by running than whisking alone (Ayaz et al., 2019). One of the sensorimotor circuits involves both the lemnisco-cortical and corticocortical pathways. These two pathways relay sensory information from the cuneate nucleus (CuN) in the medulla oblongata, through the ventral posterolateral nucleus (VPL) of thalamus (TH), to M1 (Yamawaki et al., 2021).

Furthermore, M1 is crucial for visually guided motion, and vice versa, visual information also determines and adjusts goal-directed movements. A disinhibition model has been proposed to underlie the locomotion associated gain in (visual) cortex (Pakan et al., 2016). PV INs mostly inhibit soma of PNs and directly control PN output, and they inhibit themselves (Deleuze et al., 2019; Szegedi et al., 2020); SST INs inhibit the apical dendrites of PNs, controlling distal input to PNs; and VIP INs inhibit both PV and SST and regulate PN activity through disinhibition (Figure 10). While response properties of neurons in visual cortex (V1) remain unchanged, locomotion enhances their response (Dadarlat & Stryker, 2017). Notably, while locomotion causes an increase in both excitatory and inhibitory neuronal activity in V1 (Ayaz et al., 2013; Ayaz et al., 2019; Niell & Stryker, 2010), it suppresses excitatory activity in auditory cortex (Schneider et al., 2014). However, there are also areas such as the superior colliculus with activity less modulated by locomotion (Savier et al., 2019). These studies suggest that locomotion modulates the activity of relevant sensory cortical areas.
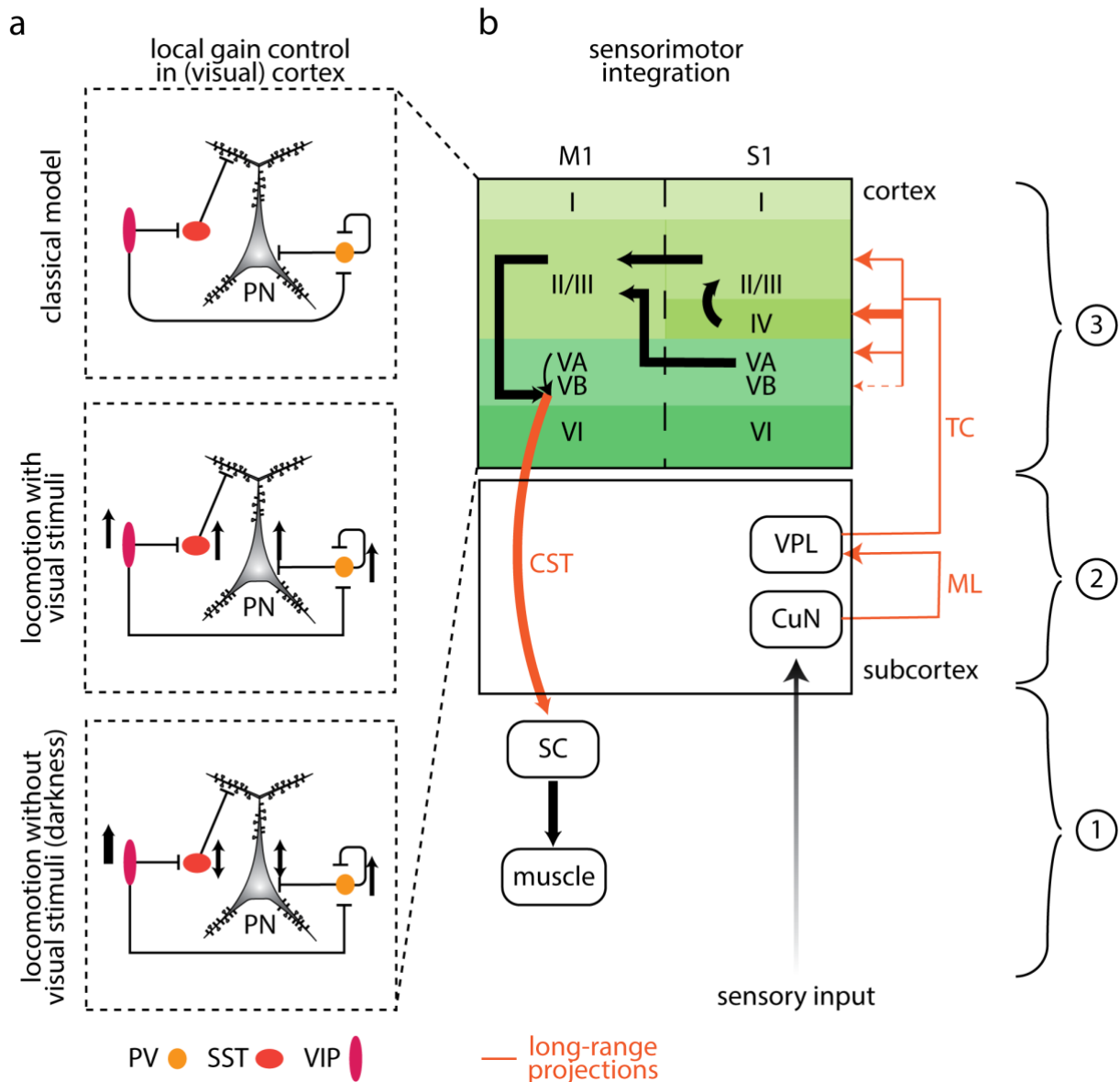
Figure 10. Circuit mechanisms of gain control of sensory input and sensorimotor integration.
(a) Local gain control in (visual) cortex. The classic disinhibition model poses that parvalbumin (PV) interneurons (INs) inhibit the soma of pyramidal neurons (PNs) and inhibiting themselves; SST inhibiting apical dendrites of PNs; and VIP inhibiting both PV and SST. During locomotion with visual stimuli, activity of both PNs and INs increases. However, in darkness, only activity of PV and VIP INs increases, while overall responses of PN and SST are unchanged with some activity increasing and some decreasing. (b) sensorimotor integration via the lemnisco-cortical and corticocortical pathways. Signal is relayed from the cuneate nucleus (CuN) to the ventral posterolateral nucleus (VPL) of the thalamus (TH) via the medial lemniscus (ML), then to the somatosensory cortex (S1) via the thalamocortical pathway (TC). Layer 4 of S1 receives the strongest input from VPL, followed by layer 2/3 and 5A. Layer 2/3 also receives additional input from layer 4 locally. Signal is then relayed to layer 2/3 in M1, which provides the strongest input to layer 5B. Layer 5B PNs (upper motor neurons; UMNs) then signals lower motor neurons (LMNs) in the spinal cord through the corticospinal tract (CST), then to the innervated muscle, in which the movement is generated. To summarize, sensorimotor integration can be divided into three levels, in ascending order, (1) muscle and spinal cord, (2) subcortex, and (3) cortex. *Adapted from (Pakan et al., 2016), (Busse, 2018) and (Yamawaki et al., 2021) under the Creative Commons Attribution License.*

Behavioral responses are associated with complex cell type specific interactions enabling information processing in M1 (Heindorf et al., 2018). While the effect of locomotion, in the presence or absence of visual stimuli, has been studied more extensively in the visual cortex (Busse, 2018; Dadarlat & Stryker, 2017; Erisken et al., 2014; Pakan et al., 2016), the impact on motor cortex remains unclear and thus warrants further scrutiny. Moreover, it is not known how individual neuronal circuit elements of M1 are affected in behaving ALS transgenic mice across disease stages, which is thus the objective of my thesis.

2. Aims and objectives

In humans as well as rodent models of ALS, cortical hyperexcitability has now been shown to be a key feature of ALS pathophysiology and to precede symptom onset in various ALS-linked genetic mutation carriers. However, the methods used such as electrophysiological recordings of layer V neurons and transcranial magnetic stimulation do not provide the layer-specific resolution to reveal the *source* of cortical hyperexcitability, hampering the development of effective therapies. Cortical excitability is regulated by several circuit elements, most of which are affected in ALS, highlighting the complexity of the disease and the need to study it at the circuit level.

Specifically, the objectives of this thesis were to address the following questions:

- Are activity levels of layer 2/3 and 5 neurons in primary motor cortex altered in ALS tg mice? If so, how?

- Are the activity changes detected under anesthesia also captured in wakefulness?

- Are response properties of layer 2/3 and layer 5 neurons altered in ALS?

- Which neuronal subtype in motor cortex is affected first in ALS mouse models?

- Can hyperexcitable neurons be targeted therapeutically to slow down or halt disease progression in ALS mouse models?
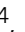
3. Results

The work of this doctoral thesis has resulted in a peer-reviewed publication in Nature Communications (see (Scekic-Zahirovic et al., 2021)) and a manuscript in preparation for submission (Kan et al.). In the following section, I will first outline the published work "Cytoplasmic FUS triggers early behavioral alterations linked to cortical neuronal hyperactivity and inhibitory synaptic defects", followed by the manuscript "A novel non-cell autonomous mechanism of cortical dysfunction in ALS".

Cytoplasmic FUS triggers early behavioral alterations linked to cortical

neuronal hyperactivity and inhibitory synaptic defects

Cytoplasmic FUS triggers early behavioral alterations linked to cortical neuronal hyperactivity and inhibitory synaptic defects

Jelena Scekic-Zahirovic[1,14], Inmaculada Sanjuan-Ruiz [1,14], Vanessa Kan[2,3], Salim Megat[1], Pierre De Rossi [4], Stéphane Dieterlé[1], Raphaelle Cassel[1,5], Marguerite Jamet[1], Pascal Kessler [6], Diana Wiesner[7,8], Laura Tzeplaeff[5], Valérie Demais[9], Sonu Sahadevan[4], Katharina M. Hembach [4], Hans-Peter Muller[7], Gina Picchiarelli[1], Nibha Mishra[10,11], Stefano Antonucci [7,8], Sylvie Dirrig-Grosch[1], Jan Kassubek [7], Volker Rasche [12], Albert Ludolph[7,8], Anne-Laurence Boutillier [5], Francesco Roselli [7,8], Magdalini Polymenidou [4], Clotilde Lagier-Tourenne [10,11], Sabine Liebscher [2,3,13,15✉] & Luc Dupuis [1,15✉]

Gene mutations causing cytoplasmic mislocalization of the RNA-binding protein FUS lead to severe forms of amyotrophic lateral sclerosis (ALS). Cytoplasmic accumulation of FUS is also observed in other diseases, with unknown consequences. Here, we show that cytoplasmic mislocalization of FUS drives behavioral abnormalities in knock-in mice, including locomotor hyperactivity and alterations in social interactions, in the absence of widespread neuronal loss. Mechanistically, we identified a progressive increase in neuronal activity in the frontal cortex of *Fus* knock-in mice in vivo, associated with altered synaptic gene expression. Synaptic ultrastructural and morphological defects were more pronounced in inhibitory than excitatory synapses and associated with increased synaptosomal levels of FUS and its RNA targets. Thus, cytoplasmic FUS triggers synaptic deficits, which is leading to increased neuronal activity in frontal cortex and causing related behavioral phenotypes. These results indicate that FUS mislocalization may trigger deleterious phenotypes beyond motor neuron impairment in ALS, likely relevant also for other neurodegenerative diseases characterized by FUS mislocalization.

[1] Université de Strasbourg, Inserm, Mécanismes centraux et périphériques de la neurodégénérescence, Strasbourg, France. [2] Institute of Clinical Neuroimmunology, Klinikum der Universität München, Ludwig-Maximilians-University Munich, Munich, Germany. [3] BioMedical Center, Medical Faculty, Ludwig-Maximilians-University Munich, Munich, Germany. [4] Department of Quantitative Biomedicine, University of Zurich, Zürich, Switzerland. [5] Université de Strasbourg, UMR 7364 CNRS, Laboratoire de Neurosciences Cognitives et Adaptatives (LNCA), Strasbourg, France. [6] Université de Strasbourg, Inserm, Unité mixte de service du CRBS, UMS 038, Strasbourg, France. [7] Department of Neurology, Ulm University, Ulm, Germany. [8] Deutsches Zentrum für Neurodegenerative Erkrankungen (DZNE), Ulm, Germany. [9] Plateforme Imagerie In Vitro, CNRS UPS-3156, NeuroPôle, Strasbourg, France. [10] Department of Neurology, The Sean M. Healey and AMG Center for ALS at Mass General, Massachusetts General Hospital, Harvard Medical School, Boston, MA, USA. [11] Broad Institute of Harvard University and MIT, Cambridge, MA, USA. [12] Ulm University Medical Center, Department of Internal Medicine II, Ulm, Germany. [13] Munich Cluster for Systems Neurology (SyNergy), Munich, Germany. [14] These authors contributed equally: Jelena Scekic-Zahirovic, Inmaculada Sanjuan-Ruiz. [15] These authors jointly supervised this work: Sabine Liebscher, Luc Dupuis. ✉email: sabine.liebscher@med.uni-muenchen.de; ldupuis@unistra.fr

Amyotrophic lateral sclerosis (ALS) is the major adult motor neuron disease, with onset usually in the 6th and 7th decade of life and death due to respiratory insufficiency and progressive paralysis typically occurring 3–5 years after onset of motor symptoms[1–3]. Mutations in the Fused in Sarcoma gene (FUS), encoding an RNA-binding protein from the FET family[4,5], are associated with the most severe forms of ALS[6,7], clinically presenting with a very early onset and rapid disease progression[8,9]. ALS associated mutations in FUS are clustered in the C-terminal region of the FUS protein that includes the atypical PY nuclear localization sequence, and is required for protein entry into the nucleus[6,7,10–12]. The severity of the disease correlates with the degree of impairment of FUS nuclear import[11,12], and the most severe cases of ALS known to date, are indeed caused by mutations leading to the complete truncation of the PY-NLS[8,9].

A number of clinical and pathological studies suggest that FUS mislocalization to the cytoplasm and subsequent aggregation could be relevant beyond the few ALS-FUS cases. First, FUS mutations, although rare in non-ALS cases, have been found in cases with frontotemporal dementia, either isolated[13,14] or as an initial presentation of ALS-FTD[15,16], as well as in patients with initial chorea[17], mental retardation[18], psychosis or dementia[19], and essential tremor[20]. In the absence of FUS mutations, FUS mislocalization[21], or aggregation[22,23] were found to be widespread in sporadic ALS. FUS pathology also defines a subset of cases with FTD (FTD-FUS) with prominent atrophy of the caudate putamen[24–26], concomitant pathology of other FET proteins, such as TAF15 and EWSR1[12,27–30] and frequent psychiatric symptoms[28]. FUS aggregates have also been observed in spinocerebellar ataxia and Huntington's disease[31,32]. While FUS mislocalization appears to be a common feature in neurodegenerative diseases, its pathological consequences have not been thoroughly studied beyond motor neuron degeneration.

Neurons with FUS pathology show decreased levels of FUS in the nucleus, that might compromise a number of processes dependent on proper FUS levels such as transcription and splicing regulation or DNA damage repair[4]. Interestingly, loss of FUS alters the splicing of multiple mRNAs relevant to neuronal function[33,34], such as MAPT, encoding the TAU protein, and alters the stability of mRNAs, encoding relevant synaptic proteins such as GluA1 and SynGAP1[35–39]. However, loss of nuclear FUS levels is very efficiently compensated for by autoregulatory mechanisms as well as by other FET proteins, and loss of nuclear FUS remains limited as opposed to loss of nuclear TDP-43, observed in TDP-43 pathology[40]. Indeed, heterozygous Fus knock-in mice, which carry one mutant allele leading to cytoplasmic and not nuclear localization of FUS, only show marginal loss of nuclear FUS due to compensatory overexpression[10,41]. Beyond nuclear loss of function, accumulation of cytoplasmic FUS was found to be a critical event in ALS-FUS in multiple studies in mouse models. For instance, cytoplasmic FUS is necessary to cause motor neuron degeneration in ALS-FUS[10,41–46] as heterozygous Fus knock-in mouse models develop mild, late onset muscle weakness and motor neuron degeneration, but not haploinsufficient Fus knockout mice[10,41,46]. To date, there are few studies investigating whether the accumulation of cytoplasmic FUS might lead to phenotypes beyond motor neuron degeneration. Interestingly, FUS is also found at synaptic and dendritic sites[38,47–51], and Sahadevan, Hembach et al.[52] identify synaptic mRNA targets for FUS that are critical for synaptic formation, function and maintenance.

Here, we show that a partial cytoplasmic mislocalization of FUS in heterozygous Fus knock-in mice is sufficient to drive a panel of behavioral abnormalities, including locomotor hyperactivity and alterations in social interactions, which preceded motor neuron degeneration. Behavioral deficits were accompanied by ventricle enlargement and atrophy of several subcortical structures in the absence of widespread neuronal loss in the cortex. Mechanistically, we could identify a progressive increase in neuronal activity in the frontal cortex of Fus knock-in mice in vivo. Furthermore, we observed a coordinated downregulation of multiple genes related to synaptic function in the frontal cortex throughout adulthood, which were confirmed by ultrastructural and morphological defects of synapses. These synaptic defects were more profound in inhibitory compared to excitatory synapses and accompanied by increased levels of FUS protein as well as of 3 of its RNA targets (Fus, Nrxn1, and Gabra1) in synaptosomes of heterozygous Fus knock-in mice. Thus, FUS cytoplasmic enrichment is sufficient to trigger synaptic deficits, leading to increased neuronal activity and behavioral phenotypes. These findings suggest that FUS mislocalization could trigger deleterious phenotypes beyond impaired motor function that could be relevant for both ALS-FUS but also for other neurodegenerative diseases based on FUS mislocalization.

Results

Spontaneous locomotor hyperactivity in $Fus^{\Delta NLS/+}$ mice. Since FUS mislocalization and aggregation are observed in patients with various neurodegenerative diseases, we hypothesized that partial FUS cytoplasmic mislocalization in $Fus^{\Delta NLS/+}$ mice could be sufficient to cause a number of behavioral phenotypes. Two independent cohorts of mice were analyzed at 4 months of age, before the appearance of motor impairment[41] and 10 months of age. Evaluation of basal motor activity in a familiar environment showed significantly increased locomotor activity in $Fus^{\Delta NLS/+}$ mice over the 3 consecutive days of observation (Fig. 1a, b). Interestingly, this hyperactivity was observed throughout the entire night in 4-months-old $Fus^{\Delta NLS/+}$ mice (Fig. 1a), but only during late night hours in older $Fus^{\Delta NLS/+}$ mice (Fig. 1b). In the open field, ambulatory distance, duration of ambulation, mean speed and preference for peripheral quadrants over central quadrants were similar in 10-months-old $Fus^{\Delta NLS/+}$ mice and wild-type littermates, indicating the absence of hyperactivity in a novel environment (Supplementary Fig. 1a, b). To further study potential anxiety-related phenotypes in $Fus^{\Delta NLS/+}$ mice, we used the dark/light box test, based on the preference of mice for dark compartments over illuminated places. In this test, 10-months-old $Fus^{\Delta NLS/+}$ mice and $Fus^{+/+}$ mice showed a similar latency to enter, similar frequency of transitions and similar duration to explore illuminated compartment (Supplementary Fig. 1c). Thus, $Fus^{\Delta NLS/+}$ mice are hyperactive, but do not show evidence of anxious behaviors, at least at the ages tested.

Mildly compromised consolidation of spatial memory in $Fus^{\Delta NLS/+}$ mice. To explore the possibility that behavioral phenotypes of $Fus^{\Delta NLS/+}$ mice included spatial memory defects, we performed the Morris water maze test. This task requires hippocampal function, at least during acquisition and memory formation, but relies on a proper cortico-hippocampal dialog for longer retention times or remote memory retrieval (Fig. 1c)[53]. At 10 months of age, $Fus^{\Delta NLS/+}$ mice performed similarly well to their $Fus^{+/+}$ littermates regarding the distance travelled and latency to find the hidden platform over training days (Fig. 1d, e). We then performed a probe trial 18 days after the last training and observed that, although both genotypes searched significantly in the target quadrant compared to nontarget areas, $Fus^{\Delta NLS/+}$ mice displayed a slightly decreased performance to retrieve memory at this timepoint (Fig. 1f). Furthermore, $Fus^{\Delta NLS/+}$ mice lost their previous memory significantly faster than wild-type
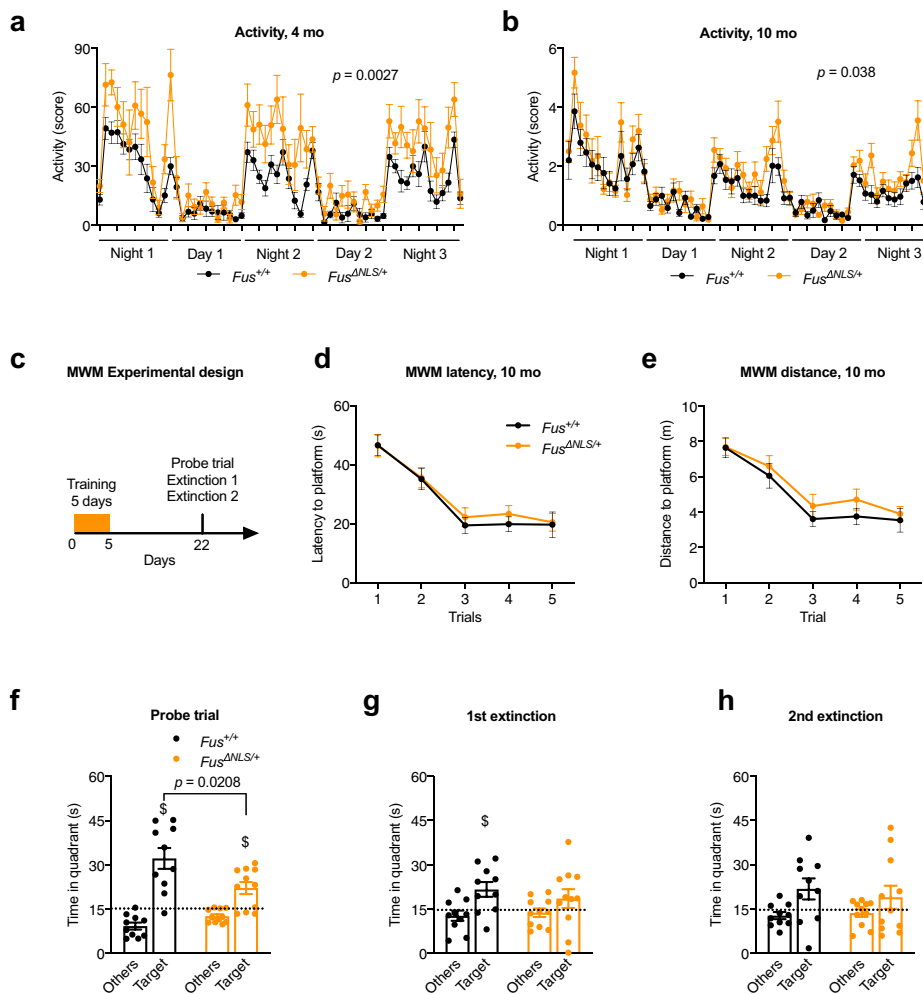
Fig. 1 $Fus^{\Delta NLS/+}$ mice display increased nocturnal spontaneous locomotor activity and cognitive defects. a, b Line graphs represent mice home cage activity–actimetry over three consecutive days at 4 months (**a**) and 10 months (**b**) of $Fus^{+/+}$ (black) and $Fus^{\Delta NLS/+}$ (orange) male mice $N = 11$ for $Fus^{+/+}$ and $N = 10$ for $Fus^{\Delta NLS/+}$ mice at 4 months and $N = 15$ for $Fus^{+/+}$ and $N = 14$ for $Fus^{\Delta NLS/+}$ mice at 10 months. Repeated measures Two-way ANOVA followed by Sidak for multiple comparisons, with time and genotype as variables. $P = 0.0027$ at 4 months and $p = 0.038$ at 10 months for genotype effect. Data are presented as mean ± SEM values of activity score per hour. **c** Schematic illustration of the Morris water maze (MWM) experimental strategy (paradigm). Mice were subjected to a five-day training period and tested for spatial memory retention in a probe trial (60 seconds) 18 days after the last acquisition. The probe trial was then followed by two extinction tests, performed at 2 h intervals. **d, e** Line graphs represent latency (in seconds) (**d**) and total distance swam (in meters) (**e**) to find the hidden platform during acquisition of 10-months-old $Fus^{+/+}$ (black) and $Fus^{\Delta NLS/+}$ (orange) male mice. Both genotypes improved similarly their performance between day 1 and 5. $N = 10$ for $Fus^{+/+}$ and $N = 11$ for $Fus^{\Delta NLS/+}$ mice. Data are presented as mean ± SEM values of four trials per day of training. A two-way repeated measure analysis of variance (ANOVA) (genotype * days) was conducted to determine the effect of genotype on learning over time. No significant effect of genotype is observed. **f** Bar graphs represent the time spent in the target quadrant (Target) and the average of the time spent in the other three quadrants (Others) during probe trial. Dashed line indicates chance level (15 seconds per quadrant; i.e., 25%). $N = 10$ for $Fus^{+/+}$ and $N = 11$ for $Fus^{\Delta NLS/+}$ mice. Data are presented as mean ± SEM. Both genotypes were significantly above random but $Fus^{\Delta NLS/+}$ mice performed significantly worse than $Fus^{+/+}$ littermates ($, $p < 0.01$, One sample t-test was used to compare to a chance level, Target quadrant: $p = 0.0008$ for $Fus^{+/+}$ and $p = 0.006$ for $Fus^{\Delta NLS/+}$). Genotype comparison was made using One-way ANOVA; F(1,19) = 6.33, $p = 0.0208$. **g, h** Bar graphs represent the time spent in quadrants (Target vs Others) during the first (**g**) and the second (**h**) extinction test ($, $p < 0.05$ vs chance levels). One-way ANOVA for genotype effect (F(1,19) = 0.56, $p = 0.46$) (**g**), (F(1,19) = 0.27, $p = 0.6$) (**h**) and One sample t-test was used to compare to a chance level, (Target quadrant: $p = 0.025$ for $Fus^{+/+}$ and $p = 0.22$ for $Fus^{\Delta NLS/+}$) (**g**), (Target quadrant: $p = 0.08$ for $Fus^{+/+}$ and $p = 0.09$ for $Fus^{\Delta NLS/+}$) (**h**). $N = 10$ for $Fus^{+/+}$ and $N = 11$ for $Fus^{\Delta NLS/+}$ mice, with same mice as panel **f**. Data are presented as mean ± SEM. Source data are provided as a Source Data file.

mice, as they were searching randomly in a first extinction test performed 2 h after the probe trial, while wild-type mice still showed a significant more directed searching behaviour and preferred the target area over others (Fig. 1g). This suggests that consolidation of long-term memory was mildly compromised in $Fus^{\Delta NLS/+}$ mice. Lastly, both genotypes did not distinguish the target over the other quadrants in a second extinction test (Fig. 1h). Altogether, these data show that $Fus^{\Delta NLS/+}$ mice were

able to learn but displayed impaired long-term memory in agreement with a dysfunction of cortical regions.

Social disinhibition in $Fus^{\Delta NLS/+}$ mice. Marked changes in personality and social behavior, such as social withdrawal or social disinhibition, obsessive-compulsive behaviors, euphoria or apathy are common in subjects with behavioral variant (bv)FTD, a disease with pronounced FUS mislocalization[54–56]. Social
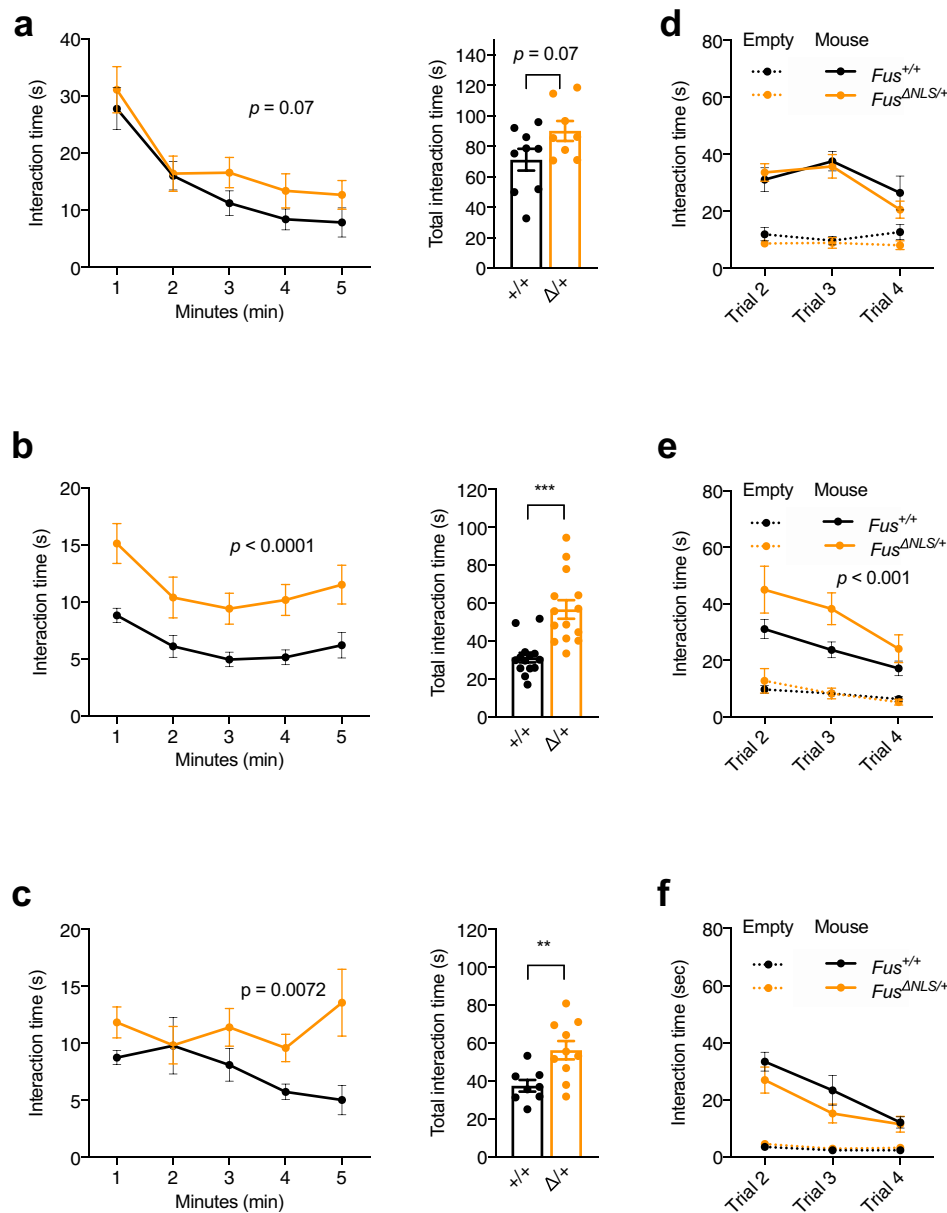
Fig. 2 Social behavior abnormalities in $Fus^{\Delta NLS/+}$ mice. a–c Line and bar graphs represent interaction time between resident (test) and intruder mice exclusively initiated by resident mouse in one-minute intervals (line graphs, on the left) or over the total time (bar graphs, on the right) during a 5 min resident-intruder test in home cage for 4 (**a**), 10 (**b**), and 22 (**c**) months-old $Fus^{+/+}$ (black) and $Fus^{\Delta NLS/+}$ (orange) male mice. Note that, young $Fus^{\Delta NLS/+}$ mice demonstrated a trend towards an increased social interest for intruder mouse (**a**) while older mice interacted with intruders significantly longer then $Fus^{+/+}$ (**b**, **c**) showing an age-dependent impairment of social behavior–disinhibition. All values are represented as mean ± SEM. At 4 months, $N = 9$ for $Fus^{+/+}$ and $N = 8$ for $Fus^{\Delta NLS/+}$ mice; At 10 months, $N = 14$ for $Fus^{+/+}$ and $N = 14$ for $Fus^{\Delta NLS/+}$ mice; At 22 months, $N = 8$ for $Fus^{+/+}$ and $N = 10$ for $Fus^{\Delta NLS/+}$ mice. Two-way repeated measures ANOVA followed by Sidak post-hoc test ($p = 0.07$ (4 months), $p < 0.001$ (10 months), and $p = 0.007$ (22 months) for genotype.effect); Two-sided Unpaired Student's t-test for total time $p = 0.07$ (4 months), $p < 0.001$ (10 months), and $p = 0.007$ (22 months)). **d**, **f** Line graphs represent sociability in the three-chamber test measured as interaction time with novel mice across three trials for $Fus^{+/+}$ (black) and $Fus^{\Delta NLS/+}$ (orange) male mice at 4 (**d**), 10 (**e**), and 22 (**f**) months of age. Time exploring an empty cage (object) across trials is represented as dashed lines. At 4 months, $N = 9$ for $Fus^{+/+}$ and $N = 8$ for $Fus^{\Delta NLS/+}$ mice; At 10 months, $N = 14$ for $Fus^{+/+}$ and $N = 14$ for $Fus^{\Delta NLS/+}$ mice; At 22 months, $N = 8$ for $Fus^{+/+}$ and $N = 9$ for $Fus^{\Delta NLS/+}$ mice. Data are presented as mean ± SEM. Three-way ANOVA with Newman Keuls post-hoc test for multiple comparisons, $p = $ ns (4 months), $p < 0.001$ (10 months) and $p = $ ns (22 months) for genotype effect). Source data are provided as a Source Data file.

deficits were also reported in progranulin haploinsufficient mice, a mouse model of FTD[57]. To determine whether $Fus^{\Delta NLS/+}$ mice have social behavioral deficits, we first performed the resident-intruder test specific for evaluating sociability in mice. Interestingly, 4-months-old $Fus^{\Delta NLS/+}$ mice showed a trend towards a

longer interaction with the intruder mouse as compared with $Fus^{+/+}$ mice ($p = 0.07$) (Fig. 2a), that was significant at 10 months of age (Fig. 2b) and persisted until 22 months of age (Fig. 2c). Aggressive behavior was only observed at 4 months of age, and not affected by the Fus genotype (attack duration:

13.0 ± 1.4 s in $Fus^{+/+}$ mice vs 11.6 ± 1.0 s in $Fus^{\Delta NLS/+}$ mice, $p = 0.88$ two-sided unpaired Student's t-test). To further characterize the social behavioral impairment, we used a modified version of the three-chamber social paradigm. After a first trial of habituation using an empty setup, a novel mouse is introduced in a side compartment. The interactions initiated by the test mouse with either the novel mouse or the empty cage was quantified. Of most relevance, across the three consecutive trials (Trial 2, 3, and 4), we observed that 10-months-old $Fus^{\Delta NLS/+}$ mice consistently interacted more with the novel mouse than $Fus^{+/+}$ mice, in line with social disinhibition (Fig. 2e). This was not observed at 4 or 22 months of age (Fig. 2d–f). Importantly, mice of both genotypes spent more time interacting with the novel mouse than with the empty cage, indicating that mice could recognize its conspecific. The interaction time gradually decreased in later trials, suggesting progressive loss of social interest in the novel mouse, while it became familiar (Fig. 2d–f). Similar findings of social disinhibition in both resident-intruder test and three-chamber paradigms as a novel environment exclude the possibility that the observed increased social interactions resulted from locomotor hyperactivity in the home cage. Importantly, the olfactory function of $Fus^{\Delta NLS/+}$ mice was preserved, since results showed no differences between genotypes at 22 months of age in the time spent sniffing filter paper, covered with either attractive scent (vanilla) or an aversive scent (2-methyl butyrate) (Supplementary Fig. 2). These findings together with absence of major motor phenotype at that age (Supplementary Fig. 1a, b) indicated that social behavior is specifically affected in $Fus^{\Delta NLS/+}$ mice. Taken altogether, behavioral analyses of $Fus^{\Delta NLS/+}$ mice uncovered locomotor hyperactivity, cognitive deficits, and altered memory consolidation as well as selective impairment in sociability.

Increased spontaneous neuronal activity in $Fus^{\Delta NLS/+}$ mice in vivo. As the behavioral changes observed are highly reminiscent of frontal lobe dysfunction, we next asked whether neuronal activity is altered within that brain area. We thus examined spontaneous neuronal activity using in vivo two-photon calcium imaging (Fig. 3a–c). We studied neurons in cortical layer II/III of the frontal cortex expressing the genetically encoded calcium indicator GCaMP (delivered through an AAV vector) in mice at the age of 4 and 10 months (Fig. 3b). Indeed, we observed a significant increase in spontaneous activity, which worsened with age. While in 4-month-old mice the fraction of active neurons did not differ between $Fus^{+/+}$ and $Fus^{\Delta NLS/+}$ mice (Fig. 3d), there was a decrease in transient amplitudes (Fig. 3e) and an increase in transient frequency (Fig. 3f) in $Fus^{\Delta NLS/+}$ mice. In 10-month-old animals, this increase in activity was already evident at the level of the fraction of active cells in $Fus^{\Delta NLS/+}$ (Fig. 3g). Moreover, we observed an increase in the transient amplitudes (Fig. 3h) and also in the transient frequency (Fig. 3i) in $Fus^{\Delta NLS/+}$ mice compared to their $Fus^{+/+}$ littermates. Taken together, our data demonstrate an age dependent, strong increase in neuronal activity in vivo within the upper layers of frontal cortex of $Fus^{\Delta NLS/+}$ mice.

$Fus^{\Delta NLS/+}$ mice show ventricle enlargement and atrophy of subcortical structures but preserved cortical neurons. We next sought to understand the structural basis of behavioral and electrophysiological abnormalities in $Fus^{\Delta NLS/+}$ mice by employing MR imaging. FLASH MRI datasets for $Fus^{\Delta NLS/+}$ mice and $Fus^{+/+}$ littermates were processed for volumetric quantification using an in-house developed script[58], aimed at registering the MRI images to a template derived from the Allen Brain Atlas reference and then at parcellating the cerebral structures into hierarchically arranged volumes of interest, which can be

interrogated for the volume of any region or group of regions (Fig. 4a, b). The overall intracranial volume (ICV) was comparable in $Fus^{\Delta NLS/+}$ and $Fus^{+/+}$ mice (Fig. 4c). However, upon normalization for the ICV, the volume of the brain parenchyma was significantly decreased in $Fus^{\Delta NLS/+}$ (by ~1.5%; average normalized volume was 98.52% for $Fus^{+/+}$ and 97.14% for $Fus^{\Delta NLS/+}$; Fig. 4d). Visual inspection of the MRI images revealed a substantial increase in the volume of lateral ventricles, which was confirmed by the registration algorithm and quantitated as an almost doubling of ventricular volumes (Fig. 4e). The ventriculomegaly was not associated with neocortical atrophy (Fig. 4f), but we identified a significant atrophy of the medial septum (Fig. 4g) and of the structures corresponding to the cortical subplate (including claustrum, endopiriform cortex and lateral, basomedial, basolateral, and posterior amygdalar nuclei; Fig. 4h). Only a nonsignificant trend for reduced volume was detected for hippocampus (9.06% for $Fus^{+/+}$ vs. 8.62% for $Fus^{\Delta NLS/+}$; $p = 0.15$; Two-sided Unpaired Student's t-test) and striatum (9.76% for $Fus^{+/+}$ vs. 9.89% for $Fus^{\Delta NLS/+}$; $p = 0.56$, Two-sided Unpaired Student's t-test). Interestingly, we also detected a significant degree of atrophy in the non-neocortical olfactory areas of the piriform cortex (2.48% for $Fus^{+/+}$ vs. 2.18% for $Fus^{\Delta NLS/+}$; $p = 0.0006$, Two-sided Unpaired Student's t-test). The lack of a prominent cortical atrophy phenotype was further confirmed by brain histology in $Fus^{\Delta NLS/+}$ mice at both 10 and 22 months of age. Cortical cytoarchitecture appeared preserved in $Fus^{\Delta NLS/+}$ mice, with normal lamination and no cortical thinning. The density of NeuN positive neurons in the frontal cortex was similar between $Fus^{\Delta NLS/+}$ mice and their wild-type littermates at 10 and 22 months of age (Fig. 4i, j).

Taken together, these data demonstrate a significant hydrocephalus ex vacuo in $Fus^{\Delta NLS/+}$, due to the atrophy of subcortical structures, such as the medial septum, several amygdalar nuclei, piriform areas, and tentatively the hippocampus.

Transcriptome of $Fus^{\Delta NLS/+}$ cortex points to defects in inhibitory neurotransmission and synapses. To understand the molecular basis of altered behavior in $Fus^{\Delta NLS/+}$ mice, we performed RNAseq on frontal cortex of 5- and 22-months-old $Fus^{\Delta NLS/+}$ mice and their wild-type littermates. Principal component analysis showed a clear separation between $Fus^{\Delta NLS/+}$ mice and their wild-type littermates at 22 months of age, while clustering was imperfect at 5 months of age, suggesting an exacerbation of the transcriptional differences between genotypes with age (Supplementary Fig. 3a).

Using a stringent analytical pipeline (FDR < 0.05), we did not identify differentially expressed genes between $Fus^{\Delta NLS/+}$ and $Fus^{+/+}$ mice at 5 and 22 months (Supplementary Fig. 3b). To ensure that the absence of differentially expressed genes was not due to the stringent calibration of p-values, we compared the 5-months and 22-months-old $Fus^{+/+}$ mice RNAseq datasets to probe age-related alterations. We were able to detect more than 2000 genes differentially expressed between 5- and 22-months-old wild-type mice, at a 5% false discovery rate, demonstrating that this approach can reliably detect changes in gene expression (Supplementary Fig. 3b).

To place gene expression changes in a systems-level framework, we performed weighted-gene coexpression network analysis (WGCNA) across all available $Fus^{\Delta NLS/+}$ and $Fus^{+/+}$ datasets, including 5 and 22-months RNAseq, as well as 1 and 6 months RNAseq datasets from Sahadevan et al.[52]. Potential batch effects were removed using a negative binomial regression model to estimate batch effects based on the count matrix[59] (Supplementary Fig. 3c) and allowed clustering between genotypes (Supplementary Fig. 3d). WGCNA analysis allowed us to
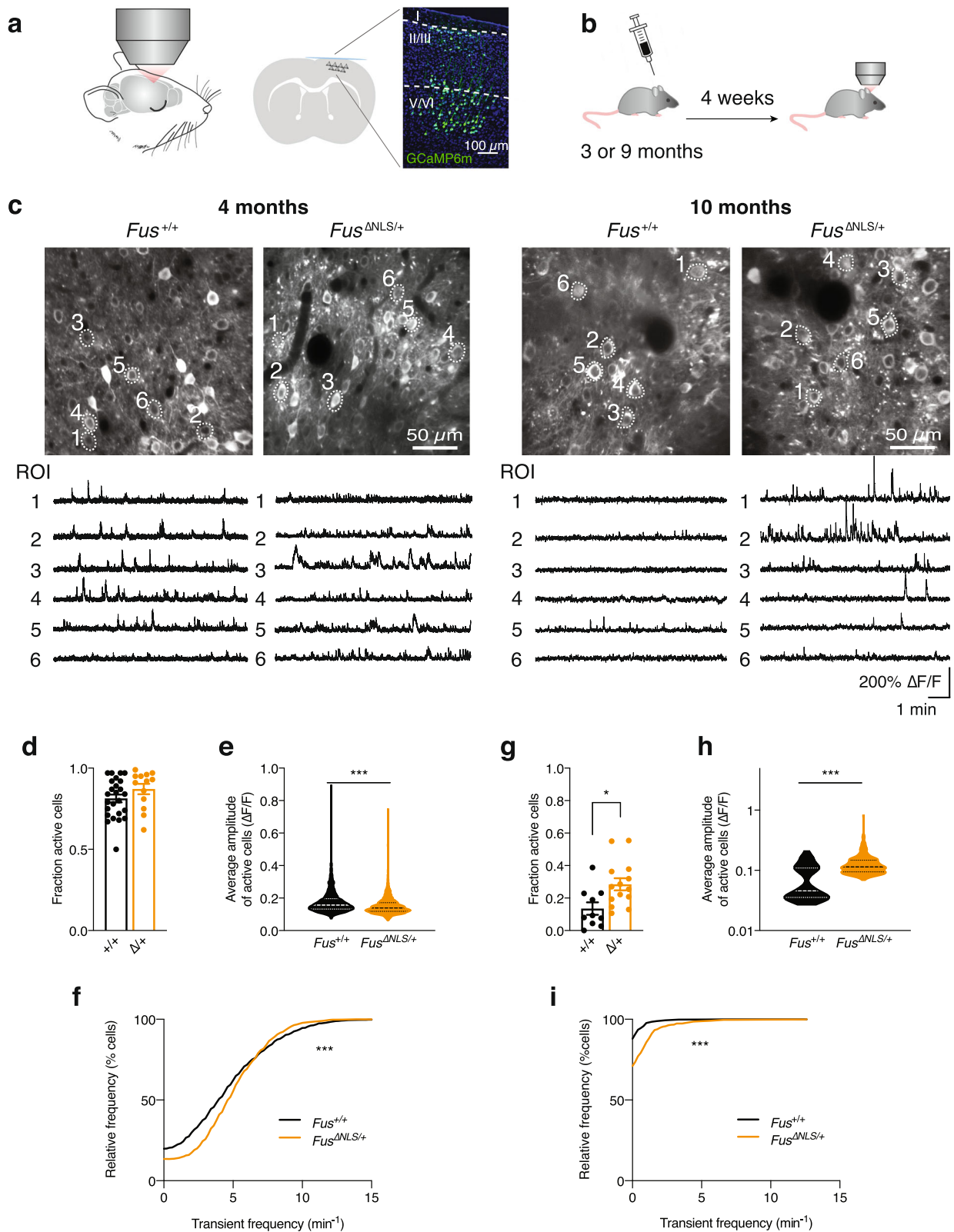
identify two mRNA modules significantly correlated with the genotype condition in cortex and labeled as turquoise and yellow modules according to the WGCNA conventions (Bonferroni-corrected $P < 0.05$; Fig. 5a, Supplementary Data 1). Cell-type enrichment analysis demonstrated that the turquoise module, but not the yellow module, was enriched in neuronally expressed

genes (Fig. 5b). Indeed, the Turquoise module, downregulated in $Fus^{\Delta NLS/+}$ mice (Fig. 5c–e), was enriched in genes related to synaptic physiology and development, most notably of GABAer-gic and glutamatergic synapses (Fig. 5d). Hub genes of the turquoise module included one GABA receptor encoding genes such as *Gabrb1*, one glutamate receptor gene (*Grid2*) and genes

Fig. 3 Assessment of neuronal activity in *Fus*$^{\Delta NLS/+}$ mice in vivo. a Neuronal activity was monitored in frontal cortex of anesthetized mice. Scheme of coronal section, indicating the expression of GCaMP6s in cortex assessed through a cranial window. Magnified view of imaged cortical area demonstrates neuronal expression of GCaMP (green) across all cortical layers. **b** Timeline of experiments. Male and female mice were injected with AAV9-syn-jGCaMP7s (at 3 months of age) or AAV2/1-hsyn-GCaMP6m (at 9 months of age) into frontal cortex and implanted with a cranial window. In vivo imaging began 4 weeks after implantation. **c** Representative examples (average projections) of field of views (FOV) imaged in *Fus*$^{+/+}$ and *Fus*$^{\Delta NLS/+}$ mice at 4 months ($N = 8$ *Fus*$^{+/+}$ mice and $N = 3$ *Fus*$^{\Delta NLS/+}$ mice, left) and at 10 months ($N = 5$ *Fus*$^{+/+}$ mice and $N = 6$ *Fus*$^{\Delta NLS/+}$ mice, right) are shown together with fluorescence calcium traces of selected regions of interest (ROIs). **d** The fraction of active cells per FOV was not affected in 4-month-old *Fus*$^{\Delta NLS/+}$ mice. $N = 13$ FOVs in 3 *Fus*$^{\Delta NLS/+}$ and $N = 25$ FOVs in 8 *Fus*$^{+/+}$ mice. Data are presented as mean ± SEM $p = 0.1627$, Two-sided Unpaired Student's t-test. **e, f** The calcium transient frequencies (**e**) were increased while the average transient amplitudes (**f**) were decreased in *Fus*$^{\Delta NLS/+}$ mice. $N = 1107$ ROIs in 3 *Fus*$^{\Delta NLS/+}$ and $N = 2264$ ROIs in 8 *Fus*$^{+/+}$, superimposed by the median (**e**). Kolmogorov–Smirnov test, ***$p < 0.0001$ for both panel **e** and **f**. **g–i** The fraction of active cells per FOV (**g**) as well as (**h**) the frequencies and (**i**) the average amplitudes of calcium transients of each ROI were increased in 10-month-old *Fus*$^{\Delta NLS/+}$ mice. Data are individual FOVs (**g**; $N = 14$ FOVs in 6 *Fus*$^{\Delta NLS/+}$ and $N = 10$ FOVs in 5 *Fus*$^{+/+}$ mice) or individual ROIs (**h, i**; $N = 855$ ROIs in 6 *Fus*$^{\Delta NLS/+}$ and $N = 631$ ROIs in 5 *Fus*$^{+/+}$ mice) superimposed by the mean ± SEM (**g**) or the median (**h, i**). panel **g:** Two-tailed Unpaired Student's t-test, *$p = 0.0126$; panel **h** and **i**: Kolmogorov–Smirnov test, ***$p < 0.0001$ for both panels. Source data are provided as a Source Data file.

tightly associated with synaptic development and autism (*Nrxn1, Lrfn5, Plcb1, Erc2, Frmpd4, Tanc2, Ctnnd2, Dmd*). Consistent with the known molecular function of FUS, the yellow module was enriched for genes related to RNA metabolism and processing and was progressively upregulated with age. Hub genes of this module comprise genes related to mRNA splicing (*Snrnp70, Ddx39b, Ilf3*), RNA transport (*Hnrnpl, Rbm3, Ipo4*), or RNA degradation (*Exosc10*) (Fig. 5f–h). Thus, transcriptome analysis points to the existence of synaptic defects in the frontal cortex of *Fus*$^{\Delta NLS/+}$ mice.

Synaptic defects in in *Fus*$^{\Delta NLS/+}$ mice. To independently validate potential synaptic defects in *Fus*$^{\Delta NLS/+}$ frontal cortex, we performed quantitative ultrastructural analysis of inhibitory (Fig. 6a) and excitatory (Fig. 6b) synapses in this brain region. Inhibitory synapses in layers II/III of the frontal cortex, identified by the presence of mitochondria on both sides of the synapse, showed major ultrastructural alterations in *Fus*$^{\Delta NLS/+}$ mice, with increased boutons sizes (Fig. 6c), longer active zones (Fig. 6d), prominently increased vesicle numbers (Fig. 6e), and increased distance of vesicles to the active zone as compared to wild-type synapses (Fig. 6f). Excitatory synapses, identified as asymmetrical, with a pronounced postsynaptic density, also showed ultrastructural alterations; however, in the opposite direction: excitatory synapses showed overall decreased bouton size, decreased length of the active zone, and decreased vesicle number in *Fus*$^{\Delta NLS/+}$ cortex (Fig. 6g–l). Importantly, ultrastructural alterations of excitatory synapses were less pronounced than those of inhibitory synapses.
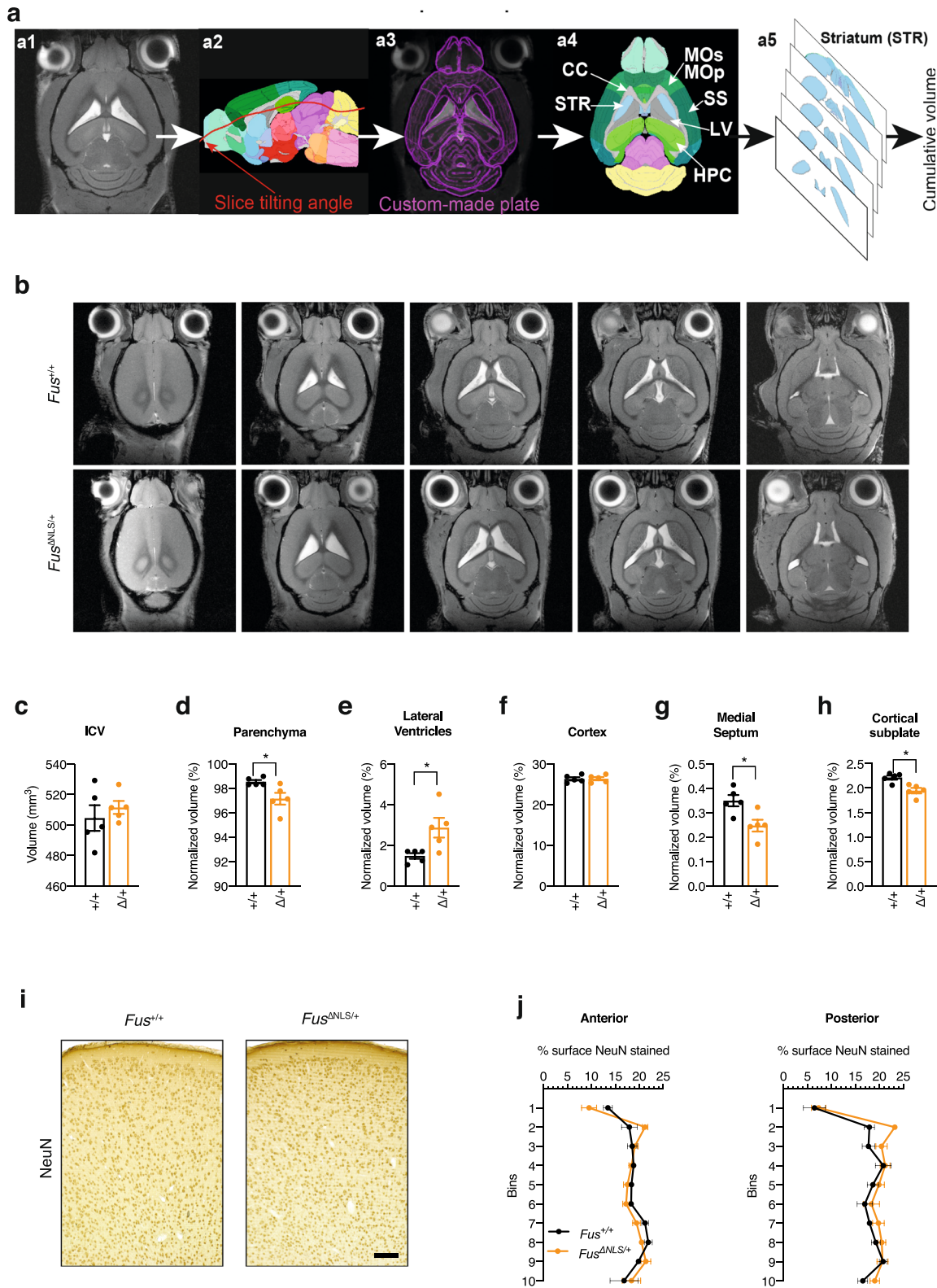
To further explore morphological changes occurring at inhibitory synapses, we quantified the density and the cluster size of three inhibitory synaptic markers: the GABA transporter VGAT localized at the presynaptic site[60] and two receptors specifically expressed at the postsynaptic site of all GABA monoaminergic synapses[61], the postsynaptic scaffold protein Gephyrin[62] and the GABA$_A$ receptor containing α3 subunit (GABA$_A$Rα3). Pictures were acquired in cortical layer 1 to allow imaging of inhibitory synapses located on the apical dendrites of pyramidal neurons[63]. Consistent with the observed ultrastructural abnormalities, a significant decrease in all markers for inhibitory synapses was identified (Fig. 6k, l). This decrease in density was associated with a decrease in the size of the clusters for VGAT, GABA$_A$Rα3, and Gephyrin (Fig. 6m), suggesting a functional impairment of the remaining synapses.

We then sought to determine whether these defects in inhibitory synapses were caused or associated with the loss of inhibitory neurons and focused on parvalbumin-positive (PV) interneurons as the largest group of inhibitory interneurons in the cortex. Using immunohistochemistry, we did not detect differences in the number of PV neurons in the frontal cortex of *Fus*$^{\Delta NLS/+}$ mice neither at 10 nor at 22 months of age (Supplementary Fig. 4a–c). As a result of the ΔNLS mutation, FUS would be expected to accumulate in the cytoplasm of PV neurons as previously shown in other cell types[10,41,49]. We thus performed double immunostaining for FUS and parvalbumin and determined the nuclear/cytoplasmic ratio selectively in PV neurons. As shown in Supplementary Fig. 4d, e, cytoplasmic FUS staining was increased in PV neurons of *Fus*$^{\Delta NLS/+}$ compared to *Fus*$^{+/+}$ mice. Intriguingly, FUS cytoplasmic staining increased with age in wild-type PV interneurons, but remained significantly lower than in *Fus*$^{\Delta NLS/+}$ neurons. Altogether, these results demonstrate the existence of defects in cortical *Fus*$^{\Delta NLS/+}$ synapses, affecting inhibitory synapses more prominently, which could underlie the observed neuronal hyperexcitability (Fig. 3).

Synaptic accumulation of FUS and its RNA targets in *Fus*$^{\Delta NLS/+}$ cortex. To determine whether the observed phenotypes could be linked to a disrupted function of FUS at the synapse, we performed synaptosomal fractionation of the frontal cortex from 5-months-old *Fus*$^{\Delta NLS/+}$ mice. Obtained fractions were enriched in the synaptophysin protein (Fig. 7a–c, and Source data for uncropped western blots) and depleted in the nuclear lncRNA *Malat* (Fig. 7d), consistent with synaptic enrichment. In synaptosomes of *Fus*$^{\Delta NLS/+}$ mice, we observed an almost ten-fold increase in FUS content compared to wild-type synaptosomes, while the total or cytoplasmic FUS contents only increased 2–3 times (Fig. 7a–d). This increased FUS content was mostly due to mutant FUS synaptosomal accumulation, since it was not observed when using an antibody targeting the NLS of FUS (and thus not the mutant FUS ΔNLS protein) (Fig. 7a–d). FUS is known to bind a number of mRNAs, including *Fus* mRNA itself, as well as mRNAs important for (inhibitory) synaptic function such as *Nrxn1* or *Gabra1*[34]. Consistently, we observed increased levels of these 3 mRNAs in synaptosomal fractions of *Fus*$^{\Delta NLS/+}$ mice (Fig. 7e). This enrichment was relatively selective as 3 mRNAs encoding genes from the Turquoise module showed distinct patterns of synaptosomal enrichment: *Gabrb1* and *Grid2*, but not *Ctnnd2*, mRNAs showed clear synaptosomal enrichment, but only *Gabrb1* mRNA showed slightly elevated levels in *Fus*$^{\Delta NLS/+}$ synaptosomes. Collectively, our data show that defects in synapses, which are more pronounced in inhibitory synapses, and are related to synaptic FUS accumulation, likely causing the increased spontaneous neuronal activity and subsequent widespread behavioral abnormalities in *Fus*$^{\Delta NLS/+}$ mice.

a

a1 a2 Slice tilting angle a3 Custom-made plate a4 Striatum (STR) a5

MOs/MOp, CC, STR, SS, LV, HPC

Cumulative volume

b

Fus^{+/+}

Fus[ΔNLS/+]

c ICV
d Parenchyma
e Lateral Ventricles
f Cortex
g Medial Septum
h Cortical subplate

i *Fus*^{+/+}   *Fus*[ΔNLS/+]

NeuN

j

Anterior
% surface NeuN stained

Posterior
% surface NeuN stained

Bins

Fus^{+/+}
Fus[ΔNLS/+]

Discussion

In this study, we show that knock-in mice with cytoplasmic accumulation of FUS display widespread behavioral alterations, beyond motor symptoms. We further determine that FUS mislocalization leads to increased spontaneous neuronal activity in the cortex, indicative of neuronal hyperexcitability, that is associated with structural and ultrastructural alterations of inhibitory synapses. Last, we show that the FUS mutation alters FUS synaptic content and modifies synaptic levels of a subset of its RNA targets, possibly underlying the observed phenotypes. The

Fig. 4 Structural and histological brain analysis of $Fus^{+/+}$ and $Fus^{\Delta NLS/+}$ mice. a Representation of the workflow used to determine volumes of corresponding brain structures from MRI slices per each mouse by the custom-made *Fiji* macro plugin (upper row). **b** Representative MRI slice images of $Fus^{+/+}$ (upper row) and $Fus^{\Delta NLS/+}$ (lower row) male mice. **c–h** Bar graph showing intracranial volume (ICV) (**c**), normalized volume of the brain parenchyma (**d**), of lateral ventricles (**e**), cortex (**f**), medial septum (**g**), and cortical subplate (**h**) in $Fus^{\Delta NLS/+}$ vs $Fus^{+/+}$ mice. For panels **c–h**, $N = 5$ for $Fus^{+/+}$ and $N = 5$ for $Fus^{\Delta NLS/+}$ mice. Data are presented as mean ± SEM. Two-tailed Unpaired Student's *t*-test, **c**: $p = 0.4838$; **d**: $p = 0.0249$; **e**: $p = 0.0249$; **f**: 0.9489; **g**: $p = 0.0151$; **h**: $p = 0.0051$. **i** Representative image of NeuN immunohistochemistry at 22 months of age in $Fus^{+/+}$ ($N = 3$ mice) or $Fus^{\Delta NLS/+}$ ($N = 5$) male mice in the anterior region of the M1/M2 cerebral cortex. Scale bar: 100 µm. **j** Distribution of NeuN+ neurons in $Fus^{+/+}$ (black) or $Fus^{\Delta NLS/+}$ (orange) male mice, in anterior and posterior regions of the M1/M2 cerebral cortex. $N = 3$ for $Fus^{+/+}$ and $N = 5$ for $Fus^{\Delta NLS/+}$ mice. Source data are provided as a Source Data file.

timelines of the different experimental studies are summarized in Supplementary Fig. 5.

The notion that FUS mislocalization is a widespread pathological event in sporadic ALS, but also in many other neurological diseases, prompted us to investigate the behavioral phenotype of $Fus^{\Delta NLS/+}$ mice. While motor defects can be detected as early as 6 months of age and motor neuron degeneration is not detected before 18–22 months of age, we observed an early spontaneous locomotor hyperactivity in $Fus^{\Delta NLS/+}$ mice. In addition, we observed various defects in executive functions, including impaired remote long-term memory, and abnormal social interactions. Hyperactivity and social and executive dysfunctions have been previously documented in other mouse models of ALS/FTD. As such the transgenic overexpression of mutant FUS can e.g., cause hyperactivity and cognitive deficits[64]. Similar abnormalities are also observed in TDP-43 knock-in mice[65], C9ORF72 BAC transgenic mice[66], or Chmp2b transgenic mice[67], suggesting that ALS mutations commonly lead to various behavioral alterations in mouse models, that are dominant over motor dysfunction. These phenotypes seen in mouse models nicely recapitulate widespread cognitive and executive dysfunction typical of ALS[68,69] and support the clinical overlap between ALS and FTD[70].

The deficits in executive functions and social behavior that we observe in $Fus^{\Delta NLS/+}$ mice are particularly relevant for FTD. Increased ventricular volume[71–73] as well as atrophy of subcortical structures[73,74] were found in FTD patients and presymptomatic mutation carriers, strengthening the analogy to $Fus^{\Delta NLS/+}$ mice. Pathology of FUS and other FET proteins (TAF15 and EWRS1) is a hallmark of a subset of FTD cases (FTD-FET cases). In FTD-FET cases, FUS pathology is associated with nuclear clearance of the FUS protein in neurons with FUS aggregates, although this nuclear clearance is not as pronounced as in cases with TDP-43 pathology[40]. Importantly, the FUS protein is accompanied by several other proteins in FTD-FET pathological aggregates, including TAF15 and EWSR1, two other FET proteins, as well as Transportin 1[12,27–30]. Thus, the disease in FTD-FET patients could be driven by several non-mutually exclusive mechanisms, including cytoplasmic accumulation and/or aggregation of FUS, nuclear clearance of FUS and/or aggregation of co-deposited pathological proteins. Previous studies indicate that complete loss of FUS could be sufficient to lead to FTD like symptoms in mice, and this was consistent with the role of FUS in controlling the splicing of mRNAs relevant to FTD, such as *MAPT*, encoding the TAU protein, or in the stability of mRNAs encoding relevant synaptic proteins such as GluA1 and SynGAP1[35–39]. In $Fus^{\Delta NLS/+}$ mice, there is, however, a limited loss of nuclear FUS immunoreactivity[10,41] and no obvious FUS aggregates, ruling out that these pathological events might play a major role in the observed behavioral alterations. The quasi-normal levels of FUS in the nucleus are explained by the existence of potent autoregulatory mechanisms, which are able to largely buffer the effect of the mutation on nuclear FUS levels. Mislocalization of either TAF15 or EWSR1 is also unable to account

for behavioral abnormalities as both of these proteins show normal localization in $Fus^{\Delta NLS/+}$ neurons, as well as ALS-FUS patients[30]. Together, our results show that FUS mislocalization alone is sufficient to trigger behavioral symptoms and suggest that this might be a major driver of disease pathophysiology in FTD-FET patients. Importantly, our findings do not exclude that at later stages of disease progression, loss of nuclear FUS function might occur as a result of collapsed autoregulatory mechanisms, thereby exacerbating neurological symptoms.

A major finding of this study is that $Fus^{\Delta NLS/+}$ mice develop morphological and ultrastructural synaptic defects. The combination of locomotor hyperactivity with social deficits, as observed in $Fus^{\Delta NLS/+}$ mice, is commonly observed in various mouse models with synaptic defects. For instance, mouse models of autism spectrum disorders, such as mice lacking the ProSAP/Shank proteins[75,76], display similar behavioral alterations. Our results point to a major defect in synapses, primarily affecting inhibitory synapses. This conclusion is supported by at least three main results: First, transcriptome analyses of the cerebral cortex show that genes related to synapses are affected. Second, the density of inhibitory synapses as well as the clusters size of three typical markers of inhibitory synapses (VGAT, GABA$_A$Ra3, and Gephyrin) are decreased. Third, inhibitory synapses are ultrastructurally abnormal, with increased size, increased number of vesicles and increased distance between vesicles and the active zone, which could be compensatory to their decreased density. Excitatory synapses were also abnormal, but their defects were minor compared to inhibitory synapses. Our data suggest that both the pre- and postsynaptic compartment of inhibitory synapses are affected by the *Fus* mutation. Indeed, the decrease in the density of Gephyrin positive puncta could reflect a disorganization of the postsynaptic density[77], potentially caused by decreased GABAR activity[78–80]. Decreased VGAT density, as well as increased bouton size or vesicle disorganization further suggest impairment of presynaptic GABAergic terminals. On its own, decreased VGAT density might reflect an overall reduction of inhibitory synapses throughout the cortical layers[81] and lead to impaired loading of GABA in the presynaptic vesicles[60]. Importantly, Sahadevan, Hembach and collaborators performed studies in $Fus^{\Delta NLS/+}$ mice at earlier ages and observed defects of inhibitory synapses, as early as 1 month of age, worsening at 6 months of age[52]. It is important to note that the disruption of inhibitory synapses can explain most of the detected behavioral and electrophysiological phenotypes observed in $Fus^{\Delta NLS/+}$ mice. Illustrating this, loss of *Gabra1*[82], or of *Gabra3*[83] are sufficient to lead to locomotor hyperactivity and the FUS target *Nrxn1* (encoding a key factor in the formation of GABAergic and glutamatergic synapses[84]), is critical in regulating locomotor activity and social behavior in mice[85,86]. Indeed, the deletion of all three neurexins from PV neurons is causing a decrease in the number of synapses of this neuronal type[87], in a manner similar to what is observed in $Fus^{\Delta NLS/+}$ mice.

Our current results do not allow to determine whether a specific subpopulation of inhibitory neurons would be more
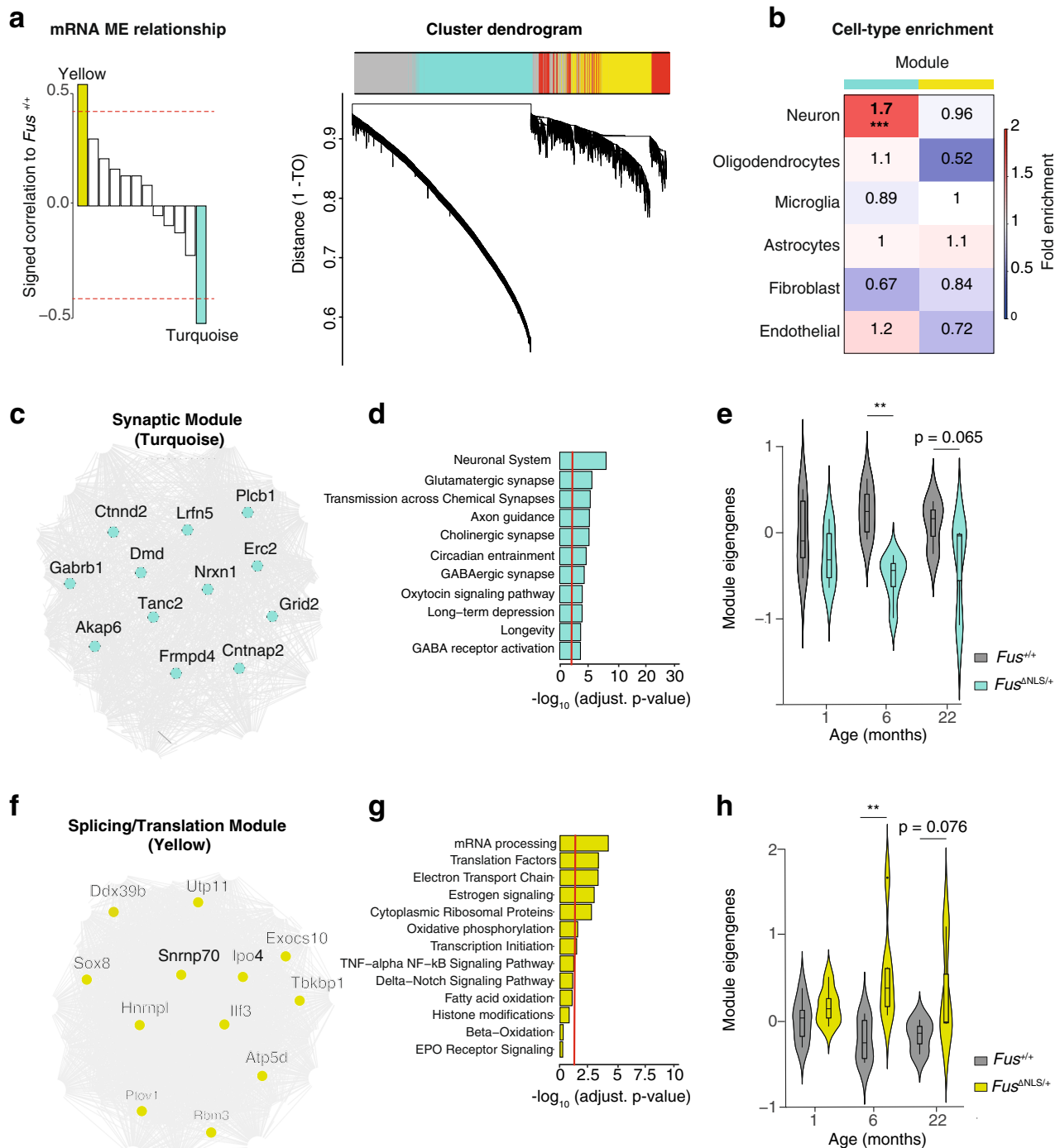
Fig. 5 mRNA coexpression network analysis pinpoints defects in inhibitory and excitatory synapses in *Fus*^ΔNLS/+ mice. a Signed association (Pearson correlation) of the mRNA MEs with transgenic condition. Modules with positive values indicate increased expression in transgenic mice; modules with negative values indicate decreased expression in transgenic mice. The red dotted lines indicate Bonferroni-corrected $P < 0.05$ for multiple comparisons ($n = 12$ modules, $n = 16$ mice per group). **b** Cell-type enrichment of modules (average $n = 200$ genes) using mouse genes in mRNA modules (Fisher's two-tailed exact test, ***FDR $= 2 \times 10^{-5}$). **c** Coexpression network plot of the synaptic (turquoise) module. The top 12 hub genes are indicated by name. **d** Gene ontology term enrichment of the synaptic module using 1791 synaptic module genes. **e** Trajectory of the synaptic module in the cortex of *Fus*^ΔNLS/+ mice across time. Boxplot show median and quartile distributions, the upper and lower lines representing the 75th and 25th percentiles, respectively. Two-way ANOVA, $F_{(1,24)} = 14.55$, $p = 0.0008$; $n = 4$–6 mice per group. **f** Coexpression network plot of the splicing/translation module. The top 12 hub genes are indicated by gene name. **g** GO term enrichment of the splicing/translation module using 1112 splicing/translation module genes. **h** Trajectory of the splicing/translation module in the cortex of *Fus*^ΔNLS/+ mice across time. Boxplot show median and quartile distributions, the upper and lower lines representing the 75th and 25th percentiles, respectively. Two-way ANOVA, $F_{(1,24)} = 11.92$, $p = 0.002$; $n = 4$–6 mice per group. The center line represents the median.
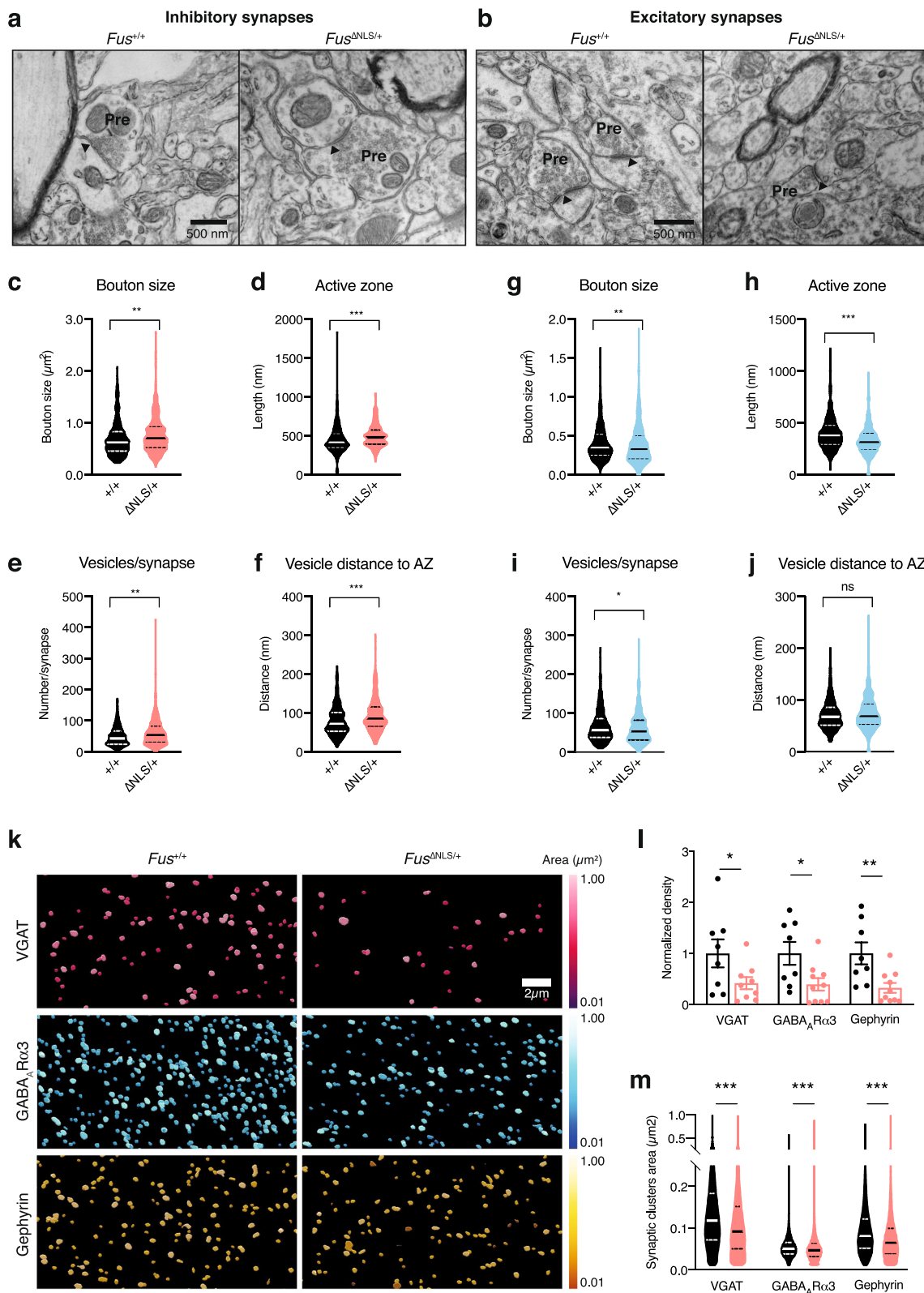
selectively affected in $Fus^{\Delta NLS/+}$ mice. PV interneurons are, however, a strong candidate according to the results of our studies, but also their involvement in TDP-43 knock-in mice[65], and in TDP-43 transgenic mice that display degeneration of hippocampal PV positive interneurons[88]. Functional impairment of PV interneurons might represent a unifying theme in ALS pathophysiology, as multiple electrophysiological studies demonstrate

hypoexcitability of PV neurons in SOD1 and TDP-43 transgenic mouse models of ALS[89–92]. Others, however, found PV interneurons to be unaltered presymptomatically and to turn hyperexcitable during the symptomatic phase in the same SOD1[G93A] mouse model[93]. In either case, those changes in PV excitability were always accompanied by hyperexcitability of layer V pyramidal neurons[89–91,93]. These findings in mouse models nicely

Fig. 6 Defects in synapses in 22-months-old $Fus^{\Delta NLS/+}$ mice. a, b Representative image of transmission electron microscopy in $Fus^{+/+}$ or $Fus^{\Delta NLS/+}$ layer II/III of the motor cortex at 22 months of age showing inhibitory synapses (**a**) (as containing ≥1 mitochondrion on each side of the synapse) and excitatory synapses (**b**). Pre: presynaptic compartment; active zone is shown with an arrowhead. $N = 4$ $Fus^{+/+}$ mice (1 male and 3 females), and $N = 4$ $Fus^{\Delta NLS/+}$ mice (1 male and 3 females) have been analyzed. **c–f** Violin plot showing the distribution of bouton sizes (**c**), the length of active zones (**d**), the number of vesicles per synapse (**e**), and the distance of individual vesicles to the active zone (**f**) in inhibitory synapses of $Fus^{+/+}$ (black) or $Fus^{\Delta NLS/+}$ (orange) mice. For panels **c–f**, $N = 379$ synapses from 1 male and 3 female $Fus^{+/+}$ mice and $N = 387$ synapses from 1 male and 3 female $Fus^{\Delta NLS/+}$ mice were analyzed. Kolmogorov–Smirnov test. **c**: $p = 0.0016$; **d**: $p < 0.0001$; **e**: $p = 0.0010$; **f**: $p < 0.0001$. **g–j** Violin plot showing the distribution of bouton size (**g**), the length of active zone (**h**), the number of vesicles per synapse (**i**), and the distance of individual vesicles to the active zone (**j**) in excitatory synapses of $Fus^{+/+}$ (black) or $Fus^{\Delta NLS/+}$ (cyan) mice. For panels **g–j**, $N = 463$ synapses from 1 male and 3 female $Fus^{+/+}$ mice and $N = 490$ synapses from 1 male and 3 female $Fus^{\Delta NLS/+}$ mice were analyzed. Kolmogorov–Smirnov test. **g**: $p = 0.0038$; **h**: $p < 0.0001$; **i**: $p = 0.0362$; **j**: $p = 0.2182$. **k** Representative images of GABAARα3, Gephyrin and VGAT intensity in 22-months male mice, coded by area size (Imaris). $N = 3$ $Fus^{+/+}$ mice and $N = 4$ $Fus^{\Delta NLS/+}$ mice have been analyzed. **l** Bar graphs representing the density analysis for VGAT, GABAARα3, and Gephyrin comparing $Fus^{+/+}$ vs $Fus^{\Delta NLS/+}$ mice. ($Fus^{+/+}$ vs $Fus^{\Delta NLS/+}$, Mann–Whitney test, VGAT, $p = 0.0464$; GABAARα3, $p = 0.0217$; Gephyrin, $p = 0.0043$). $N = 8$ FOVs from 3 $Fus^{+/+}$ mice and $N = 9$ FOVs from 4 $Fus^{\Delta NLS/+}$ mice were analyzed for VGAT; $N = 8$ FOVs from 3 $Fus^{+/+}$ mice and $N = 10$ FOVs from 4 $Fus^{\Delta NLS/+}$ mice were analyzed for GABAARα3 and Gephyrin. Data are presented as mean ± SEM. Mann–Whitney, One tailed, VGAT: $p = 0.0464$; GABAARα3: $p = 0.0217$; Gephyrin: $p = 0.0043$. **m** Violin plot representing the analysis of the clusters size for VGAT, GABAARα3, and Gephyrin comparing $Fus^{+/+}$ vs $Fus^{\Delta NLS/+}$ mice. $N = 142,416$ synapses from 3 $Fus^{+/+}$ mice and $N = 115,151$ synapses from 4 $Fus^{\Delta NLS/+}$ mice were analyzed for VGAT; $N = 202,302$ synapses from 3 $Fus^{+/+}$ mice and $N = 99,464$ synapses from 4 $Fus^{\Delta NLS/+}$ mice were analyzed for GABAARα3; $N = 169,036$ synapses from 3 $Fus^{+/+}$ mice and $N = 68,422$ synapses from 4 $Fus^{\Delta NLS/+}$ mice were analyzed for Gephyrin. Kolmogorov–Smirnov test. VGAT: $p < 0.0001$; GABAARα3: $p < 0.0001$; Gephyrin: $p < 0.0001$. Source data are provided as a Source Data file.

recapitulate human ALS pathology, in which cortical hyper-excitability is a frequent and, most importantly, early finding in familial and sporadic cases, including FUS mutation carriers[16,94]. In line with these findings, we also observed a pronounced increase in spontaneous neuronal activity in vivo, which is highly indicative of hyperexcitable pyramidal neurons. While we cannot rule out cell autonomous alterations affecting the intrinsic excitability of pyramidal neurons, our histological, ultrastructural, and transcriptomic data strongly argue for defective inhibitory neurotransmission by PV interneurons. In summary, our results, along with others, support the notion that dysfunction of cortical PV interneurons contribute to neural circuit defects in ALS and FTD. Importantly, while we observe molecular and structural defects in inhibitory neurons, we did not observe a loss of PV cell bodies in $Fus^{\Delta NLS/+}$ mice, suggesting that the major defect resembles a synaptopathy rather than frank neuronal loss, consistent with other studies[51]. Altogether, our results identify a role for FUS in regulating GABAergic synapse structure and function. Since other major classes of inhibitory interneurons[95] were not investigated, we cannot exclude that somatostatin positive (SST) or HTR3A expressing interneurons are also affected, although to a lesser extent than PV neurons. Furthermore, our work also shows that this *Fus* mutation alters glutamatergic synapses, as judged from both WGCNA analysis of RNAseq (Fig. 5) and electron microscopy (Fig. 7). This is consistent with results from Sahadevan, Hembach et al.[52] providing evidence that FUS is also critically involved in glutamatergic synaptogenesis, at least during development, and is in line with previous studies[96]. Further work is required to disentangle the causes and consequences of GABAergic and glutamatergic impairment, and their respective mechanisms.

How can mutant FUS regulate inhibitory synaptic structure? We observe that the loss of the FUS NLS leads to an increased level of the mutant protein in purified synaptosomes. These results are consistent with results from Sahadevan, Hembach et al., where the authors identified a number of FUS synaptic RNA targets, and a subset of these were also increased in synaptosomes of $Fus^{\Delta NLS/+}$ mice. Interestingly, in both studies, several FUS synaptic targets are not modified in $Fus^{\Delta NLS/+}$ synaptosomes, including some related to GABAergic neurons. Sahadevan, Hembach and collaborators further demonstrate that at least a subset of these FUS synaptic RNA targets show

increased stability in $Fus^{\Delta NLS/+}$ neurons. It seems thus reasonable to hypothesize that accumulation of synaptic FUS compromises synaptic homeostasis through altered stability of key synaptic RNAs, either through direct binding, or indirectly. This does not exclude additional mechanisms of toxicity for synaptic FUS, in particular effects on local synaptic translation[44,97], that could affect synaptic protein levels. Further work should focus on determining whether FUS might also regulate synaptic translation of specific proteins involved in inhibitory transmission, and whether rescuing synaptic defects in inhibitory neurons might translate into an efficient therapeutic strategy.

In summary, we show here that cytoplasmic accumulation of FUS leads to a major synaptopathy mainly in inhibitory neurons, that is accompanied by consistent behavioral and electrophysiological phenotypes. The identification of the mechanisms downstream of FUS' synaptic action might lead to efficient therapeutic strategies for FUS related neurodegenerative diseases.

Methods

Mouse models and behavioral analyses. Wild-type ($Fus^{+/+}$) and heterozygous ($Fus^{\Delta NLS/+}$) mice on a pure genetic background (C57BL/6 J), have been described previously[10], were bred and housed in the central animal facility of the Faculty of medicine of Strasbourg, with a regular 12-h light and dark cycle (light on at 7:00 am) under constant conditions (21 ± 1 °C; 60% humidity). Standard laboratory rodent food and water were available ad libitum throughout all experiments. Mice were genotyped by PCR of genomic DNA from tail biopsies using oligonucleotide primers (sequence provided in Supplementary Data 2)[10]. Mouse experiments were performed in compliance with all relevant ethical regulations for animal testing and researcher. All experiments were approved by local ethical committee from Strasbourg University (CREMEAS) under reference number AL/27/34/02/13 (behavior), by the Government of upper Bavaria (license number Az 55.2-1-54-2532-11-2016, two-photon microscopy) and by „Regierungspräsidium Tübingen" (animal license number 1431, MRI). Behavioral tests were done during the light phase (between 9 am and 5 pm) of their light/dark cycle except for indicated experiments. Until the mice reached the age when the behavioral tests were performed mice were group-housed. Once mice were single housed for the behavioral task they were kept individually for only a period necessary to finalize the set of behavioral experiments and in order to minimize possible negative effects of isolation, afterwards cohorts were sacrificed and processes for downstream analyses. Male mice of 4, 10, and 22 months of age were subjected to behavioral studies and data were analyzed blind to genotypes. The sex of the animals studied is indicated in each figure legend.

Spontaneous locomotor activity in the home cage–actimetry. Home cage activity was assessed according to previously published protocols[98]. Mice were placed individually in large transparent Makrolon cages ($42 \times 26 \times 15$ cm) adapted to the shelves of the testing device (eight cages/shelve). Two infrared light beams, passing through each cage, were targeted on two photocells, 2.5 cm above the cage floor
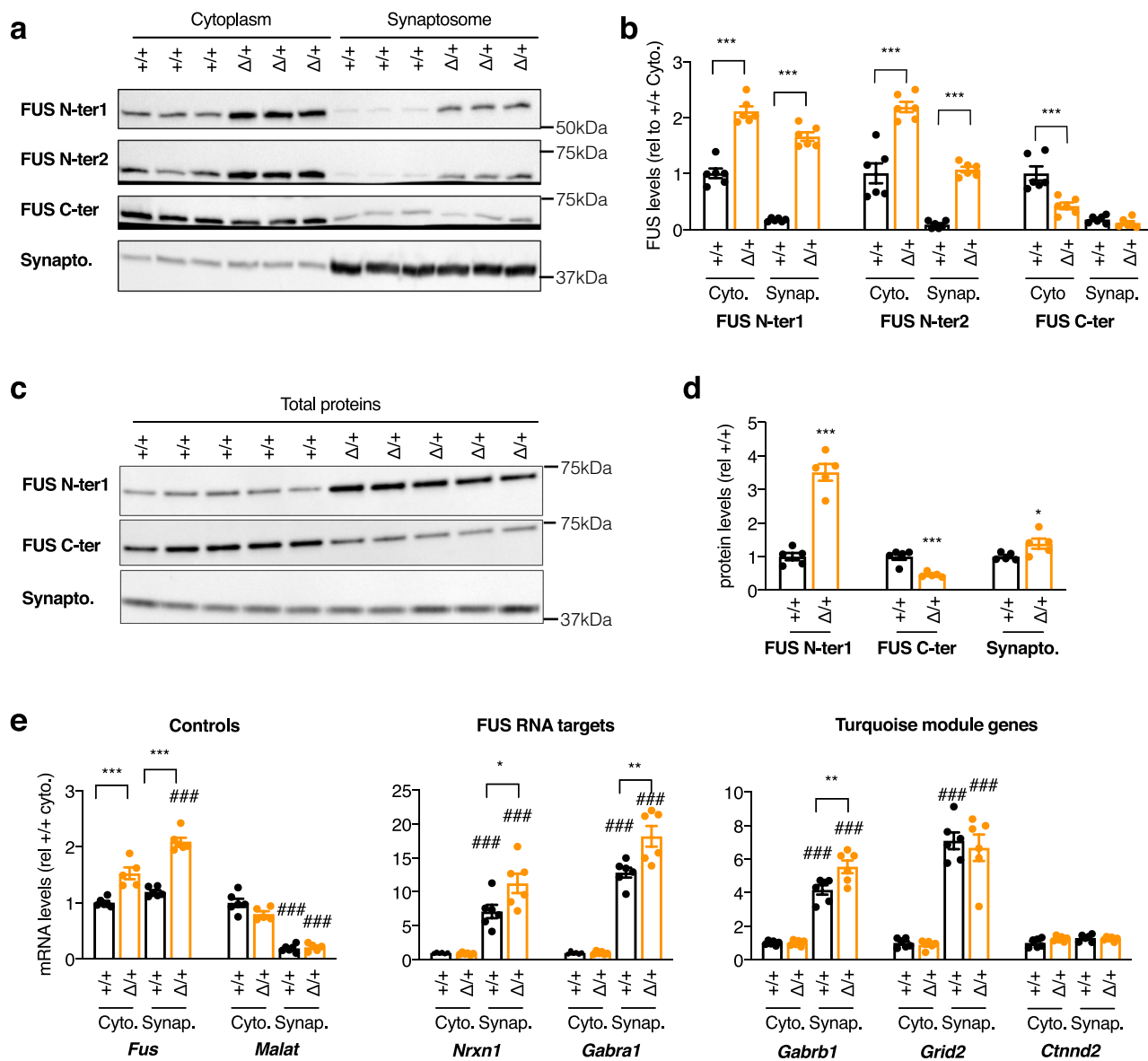
Fig. 7 FUS accumulates in synaptosomes of *Fus*^ΔNLS/+ mice and alters synaptosomal levels of a subset of its targets. a, b Representative western blot images (**a**) and respective quantifications (**b**) of cytoplasmic (**a**, left) or synaptosome (**a**, right) extracts from *Fus*^+/+ (+/+) or *Fus*^ΔNLS/+ (Δ/+) mice (4 months of age,) using two antibodies recognizing the N-terminal part of the FUS protein (FUS N-ter1 and FUS N-ter2), the C-terminal part of FUS (encoding the NLS, FUS C-ter) or synaptophysin protein to show enrichment in synaptic proteins in the synaptosome fraction. $N = 6$ *Fus*^+/+ mice and $N = 6$ *Fus*^ΔNLS/+ mice were analyzed. Data are presented as mean ± SEM. One-Way ANOVA with Tukey post-hoc test. ***$p < 0.0001$ Please note that the FUS western blots were run on independent gels, to avoid stripping and reprobing on the same membrane for the same protein. Each of these gels were controlled for equal loading using StainFree markers, that are provided in the source data. **c, d** Representative western blot images (**c**) and respective quantifications (**d**) of total extracts (**c**) from *Fus*^+/+ (+/+) or *Fus*^ΔNLS/+ (Δ/+) mice (4 months of age,) using the same antibodies as in panel **a**. $N = 5$ *Fus*^+/+ mice and $N = 5$ *Fus*^ΔNLS/+ mice were analyzed. Data are presented as mean ± SEM. Two-tailed Unpaired Student's *t*-test. N-ter1: $p < 0.0001$; C-ter: *p*-value: $p = 0.0006$; Synaptophysin: $p = 0.0411$. **e** mRNA levels of the indicated genes in RNAs extracted from cytoplasmic (Cyto.) or synaptosome (Synap.) extracts from *Fus*^+/+ (+/+) or *Fus*^ΔNLS/+ (Δ/+) frontal cortex from 4-months-old female mice as assessed using RT-qPCR. $N = 6$ *Fus*^+/+ mice and $N = 5$ *Fus*^ΔNLS/+ mice were analyzed. Data are presented as mean ± SEM. Genes are grouped by categories (controls, established FUS RNA targets, and genes belonging to the Turquoise module). All quantifications are presented relative to the +/+ cytoplasmic RNA levels set to 1. One-way ANOVA with Tukey post-hoc test. *Fus:* ***$p < 0.0001$ vs corresponding wild-type fraction; ###$p < 0.0001$ vs corresponding cytoplasmic fraction of the same genotype. *Malat:* ###$p = 0.0001$ vs corresponding cytoplasmic fraction of the same genotype. *Nrxn1* *$p = 0.0140$ vs corresponding wild-type fraction; ###$p < 0.0001$ vs corresponding cytoplasmic fraction of the same genotype. *Gabra1:* **$p = 0.0012$ vs corresponding wild-type fraction; ###$p < 0.0001$ vs corresponding cytoplasmic fraction of the same genotype. *Gabrb1:* **$p = 0.0029$ vs corresponding wild-type fraction; ###$p < 0.0001$ vs corresponding cytoplasmic fraction of the same genotype. *Grid2:* ###$p < 0.0001$ vs corresponding cytoplasmic fraction of the same genotype. *Ctnnd2:* no significant differences observed ($p > 0.05$). Source data are provided as a Source Data file.

level and 28 cm apart. The number of cage crossing was recorded automatically and was used to determine or score the spontaneous locomotor activity. The experiment began at 17.00 pm and after 2 h of habituation continued for 3 consecutive days for a complete 24 h nictemeral cycle (12 h dark and 12 h light).

Open field. The general exploratory locomotion and anxiety in a novel environment were tested during 15 min long sessions in the open field arena (72 × 72 × 36 cm) located in a test room and lit by a 600 lux for background lighting, according to published protocol[99]. The open maze was divided by lines into sixteen squares (18 × 18 cm). Each mouse was placed in the center of the arena and allowed to freely move while being video recorded. The recorded data were analyzed offline with EthoVision XT software system (Noldus Information Technology). The time spent in the center (four central quadrants) vs. the perimeter (12 peripheral quadrants) was used to measure anxiety, while the total distance traversed in the arena and average moving speed (mean velocity) was used to evaluate locomotor activity. For each mouse a movement heat map and trajectory tracking map that are representing a corresponding locomotor activity were made independently.

Dark/light box test. The light/dark box apparatus consisted of two Poly-Vinyl-Chloride (PVC) compartments of equal size (18.5 × 18.5 × 15 cm) one opaque and the other transparent, connected through an opaque tunnel (5 × 5.5 × 5 cm). The illumination of the transparent compartment was set at 400 lux. Each mouse was placed alone in the dark compartment and the mouse's behavior was recorded during 5 min with a video camcorder located ~150 cm above the center of the box. Test was conducted during the morning. The latency before the first transition into the light compartment, the number of transitions between the two compartments and the time spent in each compartment were tested to assess for anxiety level and exploratory behavior, as published previously[99].

Olfactory preference test. This test is designed to identify specific detection deficiencies and/or odor preference, namely the ability to sense attractive or aversive scents. After 30 min of habituation to empty cage with no bedding, each mouse was challenged with a filter paper embedded with two strong scents (vanilla and 2-methyl butyrate) or a neutral scent (water) was video recorded over 3 min. A 1-h pause in between the exposure to different scents was applied to each mouse using a procedure adapted from previously reported protocols[67,100]. The time the mouse spent sniffing the filter paper—the exploration time, is calculated post-hoc by an examiner blind to mouse genotype and condition. Those scents with the exploration time greater than water were designated as "attractive" while those with times less than water were termed "aversive".

Social interaction in the home cage (resident-intruder test). Social interaction was assessed in the home cage by a standard protocol[67,101]. Briefly, both resident and intruder mice were isolated and housed individually for 1 week before the task. After 30 min of habituation to the test room resident mouse was allowed to freely roam in his home cage without the cage top for 1 min. A novel male intruder mouse (nonlittermate of same background, same age, and similar weight) was then introduced in the opposite corner as the resident and allowed to interact for 5 min while videotaped. The total physical interaction, defined as the time during which the resident mouse actively explores the intruder was analyzed post-hoc. Only social activities, such as time spent investigating, grooming, following, sniffing etc. were quantified separately for each minute and for the whole time of the task and were differentiated from nonsocial/aggressive activities such as attacks, bites, and tail rattles.

Three-chamber social task. Specific social behaviors such as sociability and social recognition were analyzed by using three-chamber social task. The experimental procedure is adapted from Gascon E et al.[67]. The three-chamber box (59 × 39.5 × 21.5 cm) is made of transparent Plexiglas (Noldus Information Technology, Wageningen, The Netherlands) and is divided into three chambers (one middle and two side chambers) of equal size (18.5 × 39.5 cm) by the walls with a square opening (7 × 7 cm) that could be closed by a slide door. Each of the two side chambers contains a mobile wire cylinder shaped cage (20 × 10 cm diameter) that is made of transparent Plexiglas bars placed 6 mm apart. Cage is closed by the upper and lower lids.

Mice of both genotypes ($Fus^{+/+}$ and $Fus^{\Delta NLS/+}$) that are experimentally tested are referred to as the test mice and adult male unfamiliar mice of same background, age and weight used as the social stimulus are called novel mice. All mice were housed individually for 1 week before the test and were habituated to the testing room for at least 1 h before the start of behavioral tasks. One day prior to the testing, the novel mice were habituated to mobile wire cage for 5 min. The keeping of the novel mouse separated in a wire cage prevents aggressive and sexual activities, and in the same time ensures that any social interaction is initiated by the test mouse. Sessions were videotaped and visually analyzed post-hoc. The experimental procedure was carried out in four trials of 5 min each. After each trial, the mouse was returned to his home cage for 15 min. Trials were grouped into two consecutive parts.

Trial 1 (habituation): the test mouse was placed in the middle chamber and left to freely explore each of the three chambers: the empty middle or two sides' arenas containing the empty wire cages for 5 min.

Trials 2–4 (sociability, social recognition, social learning acquisition): the mouse was placed in the middle chamber, but an unfamiliar mouse (novel mouse) was placed into a wire cage in one of the side chambers (the wire cage in the other side-chamber remains empty). The test mouse had free access to all three chambers. The position of novel mouse and empty wired cage were alternated between trials. We quantified the time spent actively exploring a novel mouse or an empty cage by the test mouse as a social interaction time or an object exploration time, respectively. The longer time that test mouse spends in the close perimeter around the cage containing the novel mouse while actively interacting with it (staring, sniffing) compared to the empty cage—object, indicates social preference or social recognition as a result of the capability to differentiate a conspecific from an object. The motivation of the test mouse to spontaneously interact with novel mouse is considered as sociability which gradually decreased over trials as a result of social learning acquisition.

Water maze task. The water maze consisted of a circular pool (diameter 160 cm; height 60 cm) filled with water (21 ± 1 °C) made opaque by addition of a powdered milk (about 1.5 g/L). The habituation day consisted in one 4-trial session using a visible platform (diameter 11 cm, painted black, protruding 1 cm above the water surface and located in the South-East quadrant of the pool), starting randomly from each of the four cardinal points at the edge of the pool. During this habituation trial, a blue curtain surrounded the pool to prevent the use of distal cues and thus incidental encoding of spatial information. For the following days, the curtain was removed. Mice were given a 5-day training period (4 consecutive trials/day, maximum duration of a trial 60 seconds, inter-trial interval = 10–15 seconds) with a hidden platform located at a fixed position in the North-West quadrant. Animals were starting randomly from each of the four cardinal points at the edge of the pool and the sequence of the start points was randomized over days. Mice were tested for retention in a 18-days delay probe trial and two extinction tests: the first 2 h after probe trial and the second 2 h after the first. For the probe trial, the platform was removed; the mice were introduced in the pool from the North-East (a starting point never used during acquisition) and allowed a 60-seconds swimming time to explore the pool. Data were collected and computed by a video-tracking system (SMART; AnyMaze software). For the visible platform and training trials following parameters were used: the distance traveled and the latency time before reaching the platform and the average swimming speed. For the probe trial and extinction tests the time (in secondes) spent in the target quadrant (i.e., where the platform was located during acquisition) was analyzed[102].

Assessing neuronal activity by in vivo two-photon imaging

Cranial window implantation and virus injection. Mice of both sexes were implanted with a cranial window at 3 and 9 months of age (±10 days), respectively and received a stereotaxic injection of the genetically encoded calcium indicator (AAV2/1.hsyn.GCaMP6m.WPRE.SV40 diluted 1:6 in saline—10-month-old cohort or AAV9.syn.jGCaMP7s.WPRE diluted 1:6 in saline—4-month-old cohort (pGP-AAV-syn-jGCaMP7s-WPRE was a gift from Douglas Kim & GENIE Project, Addgene viral prep # 104487-AAV9; RRID:Addgene_104487)[103] into the primary motor cortex (M1)[104]. In brief, mice were first anesthetized with Fentanyl (0.05 mg/kg), Midazolam (5.0 mg/kg), and Metedomidin (0.5 mg/kg). A circular craniotomy with a 2 mm radius, centered at 1.7 mm lateral and 0.8 mm anterior to bregma, was performed, followed by the slow injection of a total of ~1 μl of the calcium indicator into three sites (~300 nl per site at 600 μm cortical depth). A 4 mm round glass coverslip (Warner Instruments) was placed over the cortex and sealed with UV-curable dental acrylic (Venus Diamond Flow, Heraeus Kulzer GmbH). A metal head bar was attached to the skull using dental acrylic (Paladur, Heraeus Kulzer GmbH), allowing for stable positioning during two-photon imaging.

Two-photon imaging in anesthetized mice. Four weeks following the cranial window implantation, in vivo two-photon imaging was performed within cortical layer II/III using a two-photon microscope (Hyperscope, Scientifica, equipped with an 8 kHz resonant scanner) at a frame rate of 30 Hz and a resolution of 512 × 512 pixels. Using a ×16 water-immersion objective (Nikon), stacks consisting of 15,000 frames (equivalent to ~8 min) were acquired, covering a field of view (FOV) of 300 × 300 μm. Light source was a Ti:Sapphire laser with a DeepSee pre-chirp unit (Spectra Physics MaiTai eHP)[104]. GCaMP was excited at 910 nm, with a laser power not exceeding 40 mW (typically 10–40 mW). In each mouse, two to five FOVs at cortical depths of 140–310 μm were imaged, yielding 2264 cells in $Fus^{+/+}$ (n = 25 experiments, 8 mice) and 1107 cells in $Fus^{\Delta NLS/+}$ (n = 13 experiments, 3 mice) at 4 months of age; and 631 cells in $Fus^{+/+}$ (n = 10 experiments, 5 mice) and 855 cells in $Fus^{\Delta NLS/+}$ mice (n = 14 experiments, 6 mice) at 10 months of age. During imaging, mice were anesthetized with 1.0–1.5 volume % isoflurane in pure O$_2$ at a flow rate of ~0.5 l/min, to maintain a respiratory rate in the range of 110–130 breaths per minute. Body temperature was maintained at 37 degrees using a physiological monitoring system (Harvard Apparatus).

Image processing and data analysis. All image analyses were performed in Matlab (Math Works) using custom-written routines[104]. In brief, full frame images were corrected for potential x and y brain displacement, and regions of interests (ROIs) were semi-automatically selected based on the maximum and mean projections of all frames. Fluorescence signals of all pixels within a selected ROI were averaged,

the intensity traces were low pass filtered at 10 Hz. Contamination from neuropil signals was accounted for using the following Eq. (1)[104],

$$\mathbf{F}_{ROI\_comp} = \mathbf{F}_{ROI} - 0.7 \times \mathbf{F}_{neuropil} + 0.7 \times median(\mathbf{F}_{neuropil}) \tag{1}$$

F_{ROI_comp} stands for neuropil-compensated fluorescence of the ROI, F_{ROI}, and $F_{neuropil}$ represent the initial fluorescence signal of the ROI and the signal from the neuropil, respectively. A neuron was defined as 'active' if it displayed at least one prominent calcium transient over 20 frames (corresponding to ~0.7 seconds). The overall difference in the fraction of active cells between 4- and 10-month-old mice could be due to both age as well as the usage of the more sensitive calcium indicator GCaMP7s[105]. To compare the impact of the indicator alone, we also investigated a control 4 m age cohort expressing GCaMP6m, in which case the fraction of active cells was 81% and not different from the average observed in the $Fus^{+/+}$ control cohort used here (ranksum test, $p = 0.87$, 7 experiments in 3 mice).

Histological techniques. Male mice were anesthetized with intraperitoneal injection of 100 mg/kg ketamine chlorhydrate (Imalgène 1000®, Merial) and 5 mg/kg xylazine (Rompun 2%®, Bayer), and then transcardially perfused with cold PFA 4% in 0.01 M phosphate buffered saline (PBS). After dissection, brains were post-fixed for 24 h and then included in agar 4% and serial cuts of 40 μm thick were made using vibratome (Leica Biosystems, S2000).

Peroxidase immunohistochemistry. For peroxidase immunohistochemistry, sections were incubated 10 min with H_2O_2 3%, rinsed with PBS 1× and incubated with blocking solution (8% Horse serum, 0.3% Bovine Serum Albumin, 0.3% Triton, PBS-0.02% Thimerosal). Sections were rinsed, and then incubated with anti-mouse NeuN or anti-mouse parvalbumin (Millipore, MAB377, 1:100 and Sigma, P3088, 1:1000, respectively) overnight at room temperature. The second day, sections were rinsed and incubated for 2 h at room temperature with biotinylated donkey anti-mouse antibody (Jackson, 715-067-003, 1:500). After sections were rinsed, they were incubated for 1 h in horseradish peroxidase ABC kit (Vectastain ABC kit, PK-6100, Vector Laboratories Inc.), rinsed and incubated with DAB (Sigma, D5905). The enzymatic reaction was stopped by adding PBS 1X, rinsed with water and sections were mounted with DPX mounting medium (Sigma, O6522).

Quantification. Images were quantified using a homemade ImageJ plugin. A Region Of Interest (ROI) was first defined by the user as the M1/M2 regions of the cerebral cortex as defined by the Paxinos Atlas[106] using the following coordinates: interaural 4.06 mm; Bregma 0.26 mm. For NeuN immunohistochemistry, a second, more anterior region of M1/M2 cortex was also quantified with the following coordinates: Interaural: 5.74 mm, Bregma: 1.94 mm.

In this region, a semi-automated segmentation led to the identification of the labelled structures (cells or nuclei). Finally, the plugin subdivided the previous ROI into 10 subregions and measured either the number of objects per subregion or the proportion of each subregion that is covered by labelled structures.

Immunofluorescence. Sections were rinsed with PBS 1X then incubated with blocking solution (8% Goat serum, 0.3% Bovine Serum Albumin, 0.3% Triton, PBS-0.02% Thimérosal) overnight at 4 °C in primary antibody: rabbit anti-FUS antibody (ProteinTech, 11570-1-AP, 1:100) and mouse anti-parvalbumin antibody (Sigma, P3088, 1:1000). After three rinses in PBS, sections were incubated for 2 h at room temperature with Hoechst (Sigma, B2261, 1/50.000) and secondary antibody: Goat anti-mouse Alexa-488 secondary antibody (Invitrogen, A11034, 1:500) and goat anti-mouse Alexa-647 secondary antibody (Invitrogen, A21245, 1:500). Finally sections were subsequently washed with PBS (3 × 10 min) and mounted in Aqua/polymount (Polysciences, 18606).

Images were acquired along the Z axis (Z stacking) using a Zeiss AxioImage.M2 microscope equipped with a Plan-Apochromat ×20/0.8 objective, high performance B/W camera (Orca Flash4, Hamamatsu) and run by the Zeiss Zen2 software. Images were quantified using the ImageJ freeware. First, the user defined ROIs corresponding to the cytoplasm and nucleus or several PV positive cells at several Z positions. Then a homemade macro was used to calculate the ratio, in the green channel, of the cytoplasm intensity divided by the nucleus one.

Electron microscopy. Mice from both sexes were used for electron microscopy. Mice were anesthetized by intraperitoneal injection of 100 mg/kg ketamine chlorhydrate and 5 mg/kg xylazine and transcardially perfused with glutaraldehyde (2.5% in 0.1 M cacodylate buffer at pH 7.4). Brains were dissected and immersed in the same fixative overnight. After three rinses in Cacodylate buffer (EMS, 11650), serial cuts of 80 μm thick were made with vibratome. Slides were then post-fixed in 1% osmium in Cacodylate buffer 1 h at room temperature. Finally, tissues were dehydrated in graded ethanol series and embedded in Embed 812 (EMS, 13940). The ultrathin sections (50 nm) were cut with an ultramicrotome (Leica, EM UC7), counterstained with uranyl acetate (1% (w/v) in 50% ethanol) and observed with a Hitachi 7500 transmission electron microscope (Hitachi High Technologies Corporation, Tokyo, Japan) equipped with an AMT Hamamatsu digital camera (Hamamatsu Photonics, Hamamatsu City, Japan). Analysis of electron micrographs was performed as follows: 100 inhibitory synapses located in layers II/III were imaged per animal. Inhibitory synapses were identified as containing at least one mitochondrion in each synaptic bouton. Synapses morphometry was analyzed using ImageJ freeware (National Institute of Health), where each synaptic boutons' area was manually drawn as previously described[107]. An automated plugin was used to drawn and measure the active zones' length, the number of synaptic vesicles within each bouton and the distance of each vesicle to the active zone, being as the beeline from the vesicle to the active zone. All images were acquired in layer II/III of the M1/M2 regions of the cerebral cortex as defined by the Paxinos Atlas[106] using the following coordinates: interaural 4.06 mm; Bregma 0.26 mm.

Synaptic density in brain sections. Male mice were anesthetized by CO_2 inhalation before perfusion with PBS containing 4% paraformaldehyde and 4% sucrose. Brains were harvested and post-fixed overnight in the same fixative and then stored at 4 °C in PBS containing 30% sucrose. Sixty micrometers thick coronal sections were cut on a cryostat and processed for free-floating immunofluorescence staining. Brain sections were incubated with the indicated primary antibodies (Rabbit GABAAalpha3 antibody Synaptic Systems, 1:500; Mouse Gephyrin antibody Synaptic Systems, 1:500, Guinea pig VGAT antibody, Synaptic Systems, 1/500) for 48 h at 4 °C followed by secondary antibodies (1:1000) for 24 h at 4 °C. The antibodies were diluted in 1× Tris Buffer Saline solution containing 10% donkey serum, 3% BSA, and 0.25% Triton-X100. Sections were then mounted on slides with Prolong Diamond (Life Technologies) before confocal microscopy.

Confocal images were acquired on a Leica SP8 Falcon microscope using ×63 (NA 1.4) with a zoom power of 3. Images were acquired at a 2048 × 2048 pixel image resolution, yielding a pixel size of 30.05 nm. To quantify the density of synaptic markers, images were acquired in the molecular layer 1/2 of the primary motor cortex area, using the same parameters for all genotypes. Images were acquired from top to bottom with a Z step size of 500 nm. Images were deconvoluted using Huygens Professional software (Scientific Volume Imaging). Images were then analyzed as described[108]. Briefly, stacks were analyzed using the built-in particle analysis function in Fiji[109]. The size of the particles was defined according to previously published studies[77,110]. To assess the number of clusters, images were thresholded (same threshold per marker and experiment), and a binary mask was generated. A low size threshold of 0.01 um diameter and high pass threshold of 1 um diameter were applied. Top and bottom stacks were removed from the analysis to only keep the 40 middle stacks. For the analysis, the number of clusters per 40 z stacks was summed and normalized by the volume imaged (75153.8 μm³). The density was normalized to the control group.

Structural MRI scans. Male mice were used for MRI studies. All data were acquired on a dedicated small bore animal scanner (Biospec 117/16, Bruker, Ettlingen, Germany) equipped with a cryogenically cooled two-element surface (MRI CryoProbeTM, Bruker BioSpec, Ettlingen, Germany) transmit/receive coil. Anatomical brain images were acquired in coronal slice orientation (30 slices) applying a gradient-echo (FLASH) sequence with acquisition parameters as: TE/TR 2.95/400 ms (TE = echo time, TR = repetition time), matrix 30 × 340 × 340, resolution 250 × 50 × 50 mm³).

Anatomical annotation of brain MRI images was performed in Fiji[58] using custom-written routines. In brief, in order to generate a plate corresponding to a single MRI cross section (Figure 4a1) a macro was run to reslice a stack of sagittal plates pursued via the Scalable Brain Atlas[111] according to a manually defined tilting angle by means of the Dynamic Reslice Fiji plugin (Figure 4a2). Custom-made plates were then registered onto the corresponding MRI slice by the manual denotation of the major, easily recognizable anatomical landmarks with the Big Warp plugin (Figure 4a3). The thresholding of the warped RGB plates (Figure 4a4) according to the brain structure color code resulted in parcellation of the MRI cross section into single regions. Due to the marked ventriculomegaly, for lateral ventricles and medial septum only, a loss of resolution in the custom plates was noticeable upon warping, therefore these areas along with the entire brain cross section (in order to include olfactory bulbs and cerebellum for the overall intracranial volume) were manually delineated. Finally, region volumes were determined following Cavalieri's principle, i.e., the measurement of the scaled cumulative area was multiplied by the slice increment (Figure 4a5). The volumetric analysis was blinded and evaluated by the same investigator. Code used for volumetric quantification of MRI scans is provided in Supplementary Software.

RNAseq. RNAseq on frontal cortex was performed as previously described[10,41]. Briefly, RNA from cortex of 22-months-old male $Fus^{\Delta NLS/+}$ mice and their control littermates were extracted with TRIzol (Invitrogen). RNA quality was measured using the Agilent Bioanalyzer system or RNA screenTape (Agilent technologies) according to the manufacturer's recommendations. Samples were processed using the Illumina TruSeq single Stranded mRNA Sample Preparation Kit according to manufacturer's protocol. Generated cDNA libraries were sequenced using an Illumina HiSeq 2000 sequencer with 4–5 biological replicates sequenced per condition using single read, 50 cycle runs. RNA from the cortex of 5-months-old male $Fus^{\Delta NLS/+}$ and control littermate mice was extracted, and libraries were generated using the Illumina TruSeq single Stranded mRNA Sample Preparation Kit. The cDNA libraries were sequenced on a HiSeq 4000 with three biological replicates per condition using single-end 50 bp read. Total reads sequenced varies from 35 to 45 million reads. Complete QC report will be made publicly available.

Raw reads were mapped to the mouse reference genome GRCm38 with STAR version 2.7.0[112] and default parameters using Ensembl gene annotations (version 87). Gene-level abundance estimates were estimated using the option–quantMode geneCount in STAR. We filtered the lowly expressed genes wherein each gene was required to have at least 15 counts across all samples and used both exonic and intronic reads. The filtered set of genes was used for the PCA plot and differential expression analysis. Differential gene expression analysis was performed with the ARMOR workflow[113] and a cut off FDR value of 0.05 was set in both datasets. RNA samples sequenced in the present study from 5–6-months-old mice ($n = 10$) were pooled to the samples from Sahadevan et al., 2020, ($n = 6$).

Weighted-gene coexpression network analysis. Coexpression network analysis was performed using a user-friendly R WGCNA library[114]. We wanted to investigate mouse brain coexpression networks that are disease specific in $Fus^{\Delta NLS/+}$ mice. Biweighted midcorrelations were calculated for all pairs of genes, and then a signed similarity matrix was created. In the signed network, the similarity between genes reflects the sign of the correlation of their expression profiles. The signed similarity matrix was then raised to the power β to emphasize strong correlations and reduce the emphasis of weak correlations on an exponential scale. The resulting adjacency matrix was then transformed into a topological overlap matrix as describe[115]. After scaling the network (consensus scaling quantile = 0.2), a threshold power of 5 was chosen (because it was the smallest threshold that resulted in a scale-free R^2 fit of 0.9) and the consensus network was created by calculating the component-wise minimum values for topological overlap. Using 1 − TOM (dissTOM) as the distance measure, genes were hierarchically clustered. Initial module assignments were determined using the blockwiseModules function as follows: blockwiseModules(datExpr, power = 5,TOMType = "signed", minModuleSize = 30, networkType = "signed",deepSplit = 2, reassignThreshold = 0, mergeCutHeight = 0.35, numericLabels = TRUE, pamRespectsDendro = FALSE, saveTOMs = TRUE, verbose = 3). The resulting modules or groups of coexpressed genes were used to calculate the MEs or the first principal component of the module. MEs were correlated with different biological and technical traits like transgenic condition and batch to find disease-specific modules. Module hubs were defined by calculating module membership (kME) values, which are the Pearson correlations between each gene and each ME. Genes with a kME < 0.7 were removed from the module. Network visualization was done with the igraph package in R. Module definitions from the network analysis were used to create synthetic eigengenes for the 1-month, 6 months and 22-months timepoint and were used to understand the trajectory of various modules across timepoints.

Enrichment analyses using single-cell experiment data. To reduce false positives, we used FDR-adjusted P-values for multiple hypergeometric test comparisons. For cell-type enrichment analysis, we used an already published single-cell mouse brain dataset[116]. Finally, genes in network modules were characterized using EnrichR (version 1.2.5)[117].

Synaptosomal enrichment followed by RT-qPCR and western blotting. Frontal cortex was removed from the brains of 4-months-old female mice by micro-dissection, as previously described[118], harvested, rapidly frozen in liquid nitrogen and stored at −80 °C until use. Synaptosomal fraction was isolated using Syn-PER Synaptic Protein Extraction kit (Thermo Scientific, 87793) according to manufacturer's instructions.

On synaptosomal preparations, RNA was extracted using TRIzol reagent (Sigma–Aldrich, 93289). 1 μg of RNA was reverse transcribed using iScript Ready-to-use cDNA supermix (Bio-Rad, 1708841). Quantitative PCR (qPCR) was performed using SsoAdvanced Universal SYBR Green Supermix (Bio-Rad, 172574) and quantified with Bio-Rad CFX Manager software. Gene expression was normalized by computing a normalization factor by Genorm software using three standard genes *Pol2*, *Tbp*, and *Actn* for nervous tissue. Primer sequences are provided in Supplementary Data 2.

For western blotting cytosolic and synaptosomal fractions were prepared using the same protocol, and protein concentration was quantitated using the BCA protein assay kit (Pierce). Fifteen micrograms of proteins were loaded into a gradient 4–20% SDS-PAGE gel (Bio-Rad, 5678094) and transferred on a 0.45 μm nitrocellulose membrane (Bio-Rad) using a semi-dry Transblot Turbo system (Bio-Rad). Membranes were saturated with 10% nonfat milk in PBS and then probed with the following primary antibodies: Anti-Synaptophysin (Abcam, ab14692, 1:1000), Anti-FUS N-ter1 (ProteinTech, 11570, 1:1000), Anti-FUS N-ter2 (Bethyl, A300-293A, 1:2000), and Anti-FUS C-ter (Bethyl, A300-294A, 1:2000) all diluted in 3% nonfat milk in PBS. Blots were washed and incubated with anti-Rabbit secondary antibody conjugated with HRP (P.A.R.I.S, BI2407, 1:5000) for 2 hours. Membranes were washed several times and analyzed with chemiluminescence using ECL Lumina Forte (Millipore, WBLUF0500) using the Chemidoc XRS Imager (Bio-Rad). Total proteins were detected with a stain-free gel capacity and normalized. Uncropped western blot images and stain-free images are provided in supplementary figures.

Statistics. If not stated otherwise, data are presented as mean ± standard error of the mean (SEM). Statistical analyses were performed using GraphPad Prism 8

(GraphPad, CA). Unpaired t-test was used for comparison between two groups, one-way or two-way analysis of the variance (ANOVA), followed by Tukey's multiple comparison post-hoc test and two-way repeated measures (RM) ANOVA, followed by Sidak multiple comparison post-hoc test were applied for three or more groups. Distributions were compared using the Kolmogorov–Smirnov (KS) test. Results were considered significant when $p < 0.05$.

Reporting summary. Further information on research design is available in the Nature Research Reporting Summary linked to this article.

References
1. Taylor, J. P., Brown, R. H. Jr. & Cleveland, D. W. Decoding ALS: from genes to mechanism. *Nature* **539**, 197–206 (2016).
2. Brown, R. H. Jr. & Al-Chalabi, A. Amyotrophic lateral sclerosis. *N. Engl. J. Med.* **377**, 162–172 (2017).
3. van Es, M. A. et al. Amyotrophic lateral sclerosis. *Lancet* **390**, 2084–2098 (2017).
4. Dormann, D. & Haass, C. TDP-43 and FUS: a nuclear affair. *Trends Neurosci.* **34**, 339–348 (2011).
5. Dormann, D. & Haass, C. Fused in sarcoma (FUS): an oncogene goes awry in neurodegeneration. *Mol. Cell Neurosci.* **56**, 475–486 (2013).
6. Kwiatkowski, T. J. Jr et al. Mutations in the FUS/TLS gene on chromosome 16 cause familial amyotrophic lateral sclerosis. *Science* **323**, 1205–1208 (2009).
7. Vance, C. et al. Mutations in FUS, an RNA processing protein, cause familial amyotrophic lateral sclerosis type 6. *Science* **323**, 1208–1211 (2009).
8. Waibel, S., Neumann, M., Rabe, M., Meyer, T. & Ludolph, A. C. Novel missense and truncating mutations in FUS/TLS in familial ALS. *Neurology* **75**, 815–817 (2010).
9. Waibel, S. et al. Truncating mutations in FUS/TLS give rise to a more aggressive ALS-phenotype than missense mutations: a clinico-genetic study in Germany. *Eur. J. Neurol.* **20**, 540–546 (2013).
10. Scekic-Zahirovic, J. et al. Toxic gain of function from mutant FUS protein is crucial to trigger cell autonomous motor neuron loss. *EMBO J.* **35**, 1077–1097 (2016).
11. Dormann, D. et al. ALS-associated fused in sarcoma (FUS) mutations disrupt Transportin-mediated nuclear import. *EMBO J.* **29**, 2841–2857 (2010).
12. Dormann, D. et al. Arginine methylation next to the PY-NLS modulates Transportin binding and nuclear import of FUS. *EMBO J.* **31**, 4258–4275 (2012).
13. Huey, E. D. et al. FUS and TDP43 genetic variability in FTD and CBS. *Neurobiol. Aging* **33**, 1016 e9–1016 17 (2012).
14. Van Langenhove, T. et al. Genetic contribution of FUS to frontotemporal lobar degeneration. *Neurology* **74**, 366–371 (2010).
15. Broustal, O. et al. FUS mutations in frontotemporal lobar degeneration with amyotrophic lateral sclerosis. *J. Alzheimers Dis.* **22**, 765–769 (2010).
16. Blair, I. P. et al. FUS mutations in amyotrophic lateral sclerosis: clinical, pathological, neurophysiological and genetic analysis. *J. Neurol. Neurosurg. Psychiatry* **81**, 639–645 (2010).
17. Flies, C. M. & Veldink, J. H. Chorea is a pleiotropic clinical feature of mutated fused-in-sarcoma in amyotrophic lateral sclerosis. *Amyotroph Lateral Scler Frontotemporal Degener* **21**, 309–311 (2020).
18. Yamashita, S. et al. Sporadic juvenile amyotrophic lateral sclerosis caused by mutant FUS/TLS: possible association of mental retardation with this mutation. *J. Neurol.* **259**, 1039–1044 (2012).
19. Yan, J. et al. Frameshift and novel mutations in FUS in familial amyotrophic lateral sclerosis and ALS/dementia. *Neurology* **75**, 807–814 (2010).
20. Merner, N. D. et al. Exome sequencing identifies FUS mutations as a cause of essential tremor. *Am. J. Hum. Genet.* **91**, 313–319 (2012).
21. Tyzack, G. E. et al. Widespread FUS mislocalization is a molecular hallmark of amyotrophic lateral sclerosis. *Brain* **142**, 2572–2580 (2019).

22. Deng, H. X. et al. FUS-immunoreactive inclusions are a common feature in sporadic and non-SOD1 familial amyotrophic lateral sclerosis. *Ann. Neurol.* **67**, 739–748 (2010).

23. Ikenaka, K. et al. Characteristic features of FUS inclusions in spinal motor neurons of sporadic amyotrophic lateral sclerosis. *J. Neuropathol. Exp. Neurol.* **79**, 370–377 (2020).

24. Snowden, J. S. et al. The most common type of FTLD-FUS (aFTLD-U) is associated with a distinct clinical form of frontotemporal dementia but is not related to mutations in the FUS gene. *Acta Neuropathol.* **122**, 99–110 (2011).

25. Seelaar, H. et al. Frequency of ubiquitin and FUS-positive, TDP-43-negative frontotemporal lobar degeneration. *J. Neurol.* **257**, 747–753 (2010).

26. Josephs, K. A. et al. Caudate atrophy on MRI is a characteristic feature of FTLD-FUS. *Eur. J. Neurol.* **17**, 969–975 (2010).

27. Suarez-Calvet, M. et al. Monomethylated and unmethylated FUS exhibit increased binding to Transportin and distinguish FTLD-FUS from ALS-FUS. *Acta Neuropathol.* **131**, 587–604 (2016).

28. Urwin, H. et al. FUS pathology defines the majority of tau- and TDP-43-negative frontotemporal lobar degeneration. *Acta Neuropathol.* **120**, 33–41 (2010).

29. Mackenzie, I. R. et al. Pathological heterogeneity in amyotrophic lateral sclerosis with FUS mutations: two distinct patterns correlating with disease severity and mutation. *Acta Neuropathol.* **122**, 87–98 (2011).

30. Neumann, M. et al. FET proteins TAF15 and EWS are selective markers that distinguish FTLD with FUS pathology from amyotrophic lateral sclerosis with FUS mutations. *Brain* **134**, 2595–2609 (2011).

31. Doi, H., Koyano, S., Suzuki, Y., Nukina, N. & Kuroiwa, Y. The RNA-binding protein FUS/TLS is a common aggregate-interacting protein in polyglutamine diseases. *Neurosci. Res.* **66**, 131–133 (2010).

32. Mori, S. et al. Expanded polyglutamine impairs normal nuclear distribution of fused in sarcoma and poly (rC)-binding protein 1 in Huntington's disease. *Neuropathology* **39**, 358–367 (2019).

33. Rogelj, B. et al. Widespread binding of FUS along nascent RNA regulates alternative splicing in the brain. *Sci. Rep.* **2**, 603 (2012).

34. Lagier-Tourenne, C. et al. Divergent roles of ALS-linked proteins FUS/TLS and TDP-43 intersect in processing long pre-mRNAs. *Nat. Neurosci.* **15**, 1488–1497 (2012).

35. Kino, Y. et al. FUS/TLS deficiency causes behavioral and pathological abnormalities distinct from amyotrophic lateral sclerosis. *Acta Neuropathol. Commun.* **3**, 24 (2015).

36. Orozco, D. et al. Loss of fused in sarcoma (FUS) promotes pathological Tau splicing. *EMBO Rep.* **13**, 759–764 (2012).

37. Ishigaki, S. et al. Altered Tau isoform ratio caused by loss of FUS and SFPQ function leads to FTLD-like phenotypes. *Cell Rep.* **18**, 1118–1131 (2017).

38. Yokoi, S. et al. 3'UTR length-dependent control of SynGAP isoform alpha2 mRNA by FUS and ELAV-like proteins promotes dendritic spine maturation and cognitive function. *Cell Rep.* **20**, 3071–3084 (2017).

39. Ishigaki, S. & Sobue, G. Importance of functional loss of FUS in FTLD/ALS. *Front. Mol. Biosci.* **5**, 44 (2018).

40. Neumann, M. & Mackenzie, I. R. A. Review: Neuropathology of non-tau frontotemporal lobar degeneration. *Neuropathol. Appl. Neurobiol.* **45**, 19–40 (2019).

41. Scekic-Zahirovic, J. et al. Motor neuron intrinsic and extrinsic mechanisms contribute to the pathogenesis of FUS-associated amyotrophic lateral sclerosis. *Acta Neuropathol.* **133**, 887–906 (2017).

42. Sun, S. et al. ALS-causative mutations in FUS/TLS confer gain- and loss-of-function by altered association with SMN and U1-snRNP. *Nat. Commun.* **6**, 6171 (2015).

43. Sun, S. et al. ALS-causative mutations in FUS/TLS confer gain and loss of function by altered association with SMN and U1-snRNP. *Nat. Commun.* **6**, 6171 (2015).

44. Lopez-Erauskin, J. et al. ALS/FTD-linked mutation in FUS suppresses intra-axonal protein synthesis and drives disease without nuclear loss-of-function of FUS. *Neuron* **100**, 816–830 e7 (2018).

45. Ling, S. C. et al. Overriding FUS autoregulation in mice triggers gain-of-toxic dysfunctions in RNA metabolism and autophagy-lysosome axis. *elife* **8**, e40811 (2019).

46. Devoy, A. et al. Humanized mutant FUS drives progressive motor neuron degeneration without aggregation in 'FUSDelta14' knockin mice. *Brain* **140**, 2797–2805 (2017).

47. So, E. et al. Mitochondrial abnormalities and disruption of the neuromuscular junction precede the clinical phenotype and motor neuron loss in hFUSWT transgenic mice. *Hum. Mol. Genet.* **27**, 463–474 (2018).

48. Schoen, M. et al. Super-resolution microscopy reveals presynaptic localization of the ALS/FTD related protein FUS in hippocampal neurons. *Front. Cell Neurosci.* **9**, 496 (2015).

49. Picchiarelli, G. et al. FUS-mediated regulation of acetylcholine receptor transcription at neuromuscular junctions is compromised in amyotrophic lateral sclerosis. *Nat. Neurosci.* **22**, 1793–1805 (2019).

50. Deshpande, D. et al. Synaptic FUS localization during motoneuron development and its accumulation in human ALS synapses. *Front. Cell Neurosci.* **13**, 256 (2019).

51. Sephton, C. F. et al. Activity-dependent FUS dysregulation disrupts synaptic homeostasis. *Proc. Natl Acad. Sci. USA* **111**, E4769–E4778 (2014).

52. Sahadevan, S. et al. Synaptic FUS accumulation triggers early misregulation of synaptic RNAs in a mouse model of ALS. https://doi.org/10.1038/s41467-021-23188-8. (2021).

53. Frankland, P. W. & Bontempi, B. The organization of recent and remote memories. *Nat. Rev. Neurosci.* **6**, 119–130 (2005).

54. Neary, D., Snowden, J. & Mann, D. Frontotemporal dementia. *Lancet Neurol.* **4**, 771–780 (2005).

55. Bang, J., Spina, S. & Miller, B. L. Frontotemporal dementia. *Lancet* **386**, 1672–1682 (2015).

56. Piguet, O., Hornberger, M., Mioshi, E. & Hodges, J. R. Behavioural-variant frontotemporal dementia: diagnosis, clinical staging, and management. *Lancet Neurol.* **10**, 162–172 (2011).

57. Roberson, E. D. Mouse models of frontotemporal dementia. *Ann. Neurol.* **72**, 837–849 (2012).

58. Schindelin, J. et al. Fiji: an open-source platform for biological-image analysis. *Nat. Methods* **9**, 676–682 (2012).

59. Zhang, Y., Parmigiani, G. & Johnson, W. E. ComBat-seq: batch effect adjustment for RNA-seq count data. *NAR Genom. Bioinform.* **2**, lqaa078 (2020).

60. Wojcik, S. M. et al. A shared vesicular carrier allows synaptic corelease of GABA and glycine. *Neuron* **50**, 575–587 (2006).

61. Fritschy, J. M. & Mohler, H. GABAA-receptor heterogeneity in the adult rat brain: differential regional and cellular distribution of seven major subunits. *J. Comp. Neurol.* **359**, 154–194 (1995).

62. Choii, G. & Ko, J. Gephyrin: a central GABAergic synapse organizer. *Exp. Mol. Med.* **47**, e158 (2015).

63. Kubota, Y., Karube, F., Nomura, M. & Kawaguchi, Y. The diversity of cortical inhibitory synapses. *Front. Neural Circuits* **10**, 27 (2016).

64. Shiihashi, G. et al. Dendritic homeostasis disruption in a novel frontotemporal dementia mouse model expressing cytoplasmic fused in sarcoma. *EBioMedicine* **24**, 102–115 (2017).

65. White, M. A. et al. TDP-43 gains function due to perturbed autoregulation in a Tardbp knock-in mouse model of ALS-FTD. *Nat. Neurosci.* **21**, 552–563 (2018).

66. Jiang, J. et al. Gain of toxicity from ALS/FTD-linked repeat expansions in C9ORF72 is alleviated by antisense oligonucleotides targeting GGGGCC-containing RNAs. *Neuron* **90**, 535–550 (2016).

67. Gascon, E. et al. Alterations in microRNA-124 and AMPA receptors contribute to social behavioral deficits in frontotemporal dementia. *Nat. Med.* **20**, 1444–1451 (2014).

68. Goldstein, L. H. & Abrahams, S. Changes in cognition and behaviour in amyotrophic lateral sclerosis: nature of impairment and implications for assessment. *Lancet Neurol.* **12**, 368–380 (2013).

69. Beeldman, E. et al. The cognitive profile of behavioural variant FTD and its similarities with ALS: a systematic review and meta-analysis. *J. Neurol. Neurosurg. Psychiatry* **89**, 995–1002 (2018).

70. Ling, S. C., Polymenidou, M. & Cleveland, D. W. Converging mechanisms in ALS and FTD: disrupted RNA and protein homeostasis. *Neuron* **79**, 416–438 (2013).

71. Tavares, T. P. et al. Ventricular volume expansion in presymptomatic genetic frontotemporal dementia. *Neurology* **93**, e1699–e1706 (2019).

72. Knopman, D. S. et al. Brain and ventricular volumetric changes in frontotemporal lobar degeneration over 1 year. *Neurology* **72**, 1843–1849 (2009).

73. Manera, A. L., Dadar, M., Collins, D. L., Ducharme, S. & Frontotemporal Lobar Degeneration Neuroimaging Initiative. Deformation based morphometry study of longitudinal MRI changes in behavioral variant frontotemporal dementia. *Neuroimage Clin.* **24**, 102079 (2019)..

74. Convery, R. S. et al. Basal forebrain atrophy in frontotemporal dementia. *Neuroimage Clin.* **26**, 102210 (2020).

75. Schmeisser, M. J. et al. Autistic-like behaviours and hyperactivity in mice lacking ProSAP1/Shank2. *Nature* **486**, 256–260 (2012).

76. Peixoto, R. T., Wang, W., Croney, D. M., Kozorovitskiy, Y. & Sabatini, B. L. Early hyperactivity and precocious maturation of corticostriatal circuits in Shank3B(-/-) mice. *Nat. Neurosci.* **19**, 716–724 (2016).

77. Craig, A. M., Banker, G., Chang, W., McGrath, M. E. & Serpinskaya, A. S. Clustering of gephyrin at GABAergic but not glutamatergic synapses in cultured rat hippocampal neurons. *J. Neurosci.* **16**, 3166–3177 (1996).

78. Dejanovic, B. et al. Palmitoylation of gephyrin controls receptor clustering and plasticity of GABAergic synapses. *PLoS Biol.* **12**, e1001908 (2014).

79. Tretter, V. et al. Molecular basis of the gamma-aminobutyric acid A receptor alpha3 subunit interaction with the clustering protein gephyrin. *J. Biol. Chem.* **286**, 37702–37711 (2011).

80. Mukherjee, J. et al. The residence time of GABA(A)Rs at inhibitory synapses is determined by direct binding of the receptor alpha1 subunit to gephyrin. *J. Neurosci.* **31**, 14677–14687 (2011).

81. Lin, T. W. et al. Regulation of synapse development by Vgat deletion from ErbB4-positive interneurons. *J. Neurosci.* **38**, 2533–2550 (2018).

82. Borghese, C. M. et al. An isoflurane- and alcohol-insensitive mutant GABA(A) receptor alpha(1) subunit with near-normal apparent affinity for GABA: characterization in heterologous systems and production of knockin mice. *J. Pharmacol. Exp. Ther.* **319**, 208–218 (2006).

83. Yee, B. K. et al. A schizophrenia-related sensorimotor deficit links alpha 3-containing GABAA receptors to a dopamine hyperfunction. *Proc. Natl Acad. Sci. USA* **102**, 17154–17159 (2005).

84. Graf, E. R., Zhang, X., Jin, S. X., Linhoff, M. W. & Craig, A. M. Neurexins induce differentiation of GABA and glutamate postsynaptic specializations via neuroligins. *Cell* **119**, 1013–1026 (2004).

85. Grayton, H. M., Missler, M., Collier, D. A. & Fernandes, C. Altered social behaviours in neurexin 1alpha knockout mice resemble core symptoms in neurodevelopmental disorders. *PLoS ONE* **8**, e67114 (2013).

86. Sudhof, T. C. Synaptic neurexin complexes: a molecular code for the logic of neural circuits. *Cell* **171**, 745–769 (2017).

87. Chen, L. Y., Jiang, M., Zhang, B., Gokce, O. & Sudhof, T. C. Conditional deletion of all neurexins defines diversity of essential synaptic organizer functions for neurexins. *Neuron* **94**, 611–625 e4 (2017).

88. Tsuiji, H. et al. TDP-43 accelerates age-dependent degeneration of interneurons. *Sci. Rep.* **7**, 14972 (2017).

89. Khademullah, C. S. et al. Cortical interneuron-mediated inhibition delays the onset of amyotrophic lateral sclerosis. *Brain* **143**, 800–810 (2020).

90. Zhang, W. et al. Hyperactive somatostatin interneurons contribute to excitotoxicity in neurodegenerative disorders. *Nat. Neurosci.* **19**, 557–559 (2016).

91. Clark, R. M., Brizuela, M., Blizzard, C. A. & Dickson, T. C. Reduced excitability and increased neurite complexity of cortical interneurons in a familial mouse model of amyotrophic lateral sclerosis. *Front. Cell Neurosci.* **12**, 328 (2018).

92. Gunes, Z. I., Kan, V. W. Y., Ye, X. & Liebscher, S. Exciting complexity: the role of motor circuit elements in ALS pathophysiology. *Front. Neurosci.* **14**, 573 (2020).

93. Kim, J. et al. Changes in the excitability of neocortical neurons in a mouse model of amyotrophic lateral sclerosis are not specific to corticospinal neurons and are modulated by advancing disease. *J. Neurosci.* **37**, 9037–9053 (2017).

94. Geevasinga, N., Menon, P., Ozdinler, P. H., Kiernan, M. C. & Vucic, S. Pathophysiological and diagnostic implications of cortical dysfunction in ALS. *Nat. Rev. Neurol.* **12**, 651–661 (2016).

95. Lim, L., Mi, D., Llorca, A. & Marin, O. Development and functional diversification of cortical interneurons. *Neuron* **100**, 294–313 (2018).

96. Udagawa, T. et al. FUS regulates AMPA receptor function and FTLD/ALS-associated behaviour via GluA1 mRNA stabilization. *Nat. Commun.* **6**, 7098 (2015).

97. Yasuda, K. et al. The RNA-binding protein Fus directs translation of localized mRNAs in APC-RNP granules. *J. Cell Biol.* **203**, 737–746 (2013).

98. Moreau, P. H., Cosquer, B., Jeltsch, H., Cassel, J. C. & Mathis, C. Neuroanatomical and behavioral effects of a novel version of the cholinergic immunotoxin mu p75-saporin in mice. *Hippocampus* **18**, 610–622 (2008).

99. Gould, T. D. *Mood and Anxiety Related Phenotypes in Mice* (Humana Press, 2009).

100. Witt, R. M., Galligan, M. M., Despinoy, J. R. & Segal, R. Olfactory behavioral testing in the adult mouse. *J. Vis. Exp.* **23**, 949 (2009).

101. Winslow, J. T. Mouse social recognition and preference. *Curr. Protoc. Neurosci.* 10.1002/0471142301.ns0816s22 (2003).

102. Cholvin, T. et al. Dorsal hippocampus and medial prefrontal cortex each contribute to the retrieval of a recent spatial memory in rats. *Brain Struct. Funct.* **221**, 91–102 (2016).

103. Chen, T. W. et al. Ultrasensitive fluorescent proteins for imaging neuronal activity. *Nature* **499**, 295–300 (2013).

104. Liebscher, S., Keller, G. B., Goltstein, P. M., Bonhoeffer, T. & Hubener, M. Selective persistence of sensorimotor mismatch signals in visual cortex of behaving Alzheimer's disease mice. *Curr. Biol.* **26**, 956–964 (2016).

105. Dana, H. et al. High-performance calcium sensors for imaging activity in neuronal populations and microcompartments. *Nat. Methods* **16**, 649–657 (2019).

106. Paxinos, G. & Franklin, K. B. J. *The Mouse Brain in Stereotaxic Coordinates* (Academic Press/Elsevier, 2001).

107. Dorgans, K. et al. Short-term plasticity at cerebellar granule cell to molecular layer interneuron synapses expands information processing. *elife* **8**, e41586 (2019).

108. De Rossi, P. et al. Aberrant accrual of BIN1 near Alzheimer's disease amyloid deposits in transgenic models. *Brain Pathol.* **29**, 485–501 (2019).

109. Rueden, C. T. et al. ImageJ2: ImageJ for the next generation of scientific image data. *BMC Bioinformatics* **18**, 529 (2017).

110. Specht, C. G. et al. Quantitative nanoscopy of inhibitory synapses: counting gephyrin molecules and receptor binding sites. *Neuron* **79**, 308–321 (2013).

111. Bakker, R., Tiesinga, P. & Kotter, R. The Scalable Brain Atlas: instant web-based access to public brain atlases and related content. *Neuroinformatics* **13**, 353–366 (2015).

112. Dobin, A. et al. STAR: ultrafast universal RNA-seq aligner. *Bioinformatics* **29**, 15–21 (2013).

113. Orjuela, S., Huang, R., Hembach, K. M., Robinson, M. D. & Soneson, C. ARMOR: An Automated Reproducible MOdular Workflow for Preprocessing and Differential Analysis of RNA-seq Data. *G3 (Bethesda)* **9**, 2089–2096 (2019).

114. Langfelder, P. & Horvath, S. WGCNA: an R package for weighted correlation network analysis. *BMC Bioinformatics* **9**, 559 (2008).

115. Li, A. & Horvath, S. Network neighborhood analysis with the multi-node topological overlap measure. *Bioinformatics* **23**, 222–231 (2007).

116. Ximerakis, M. et al. Single-cell transcriptomic profiling of the aging mouse brain. *Nat. Neurosci.* **22**, 1696–1708 (2019).

117. Kuleshov, M. V. et al. Enrichr: a comprehensive gene set enrichment analysis web server 2016 update. *Nucleic Acids Res.* **44**, W90–W97 (2016).

118. Spijker, S. in *Neuroproteomics* (ed. Li, K. W.) 23–26 (Humana Press, 2011).

Acknowledgements

Author contributions

J.S.Z. and I.S.R. performed behavioral analysis with help of R.C., L.T., and G.P. I.S.R. and J.S.Z. performed histology, imaging, and electron microscopy with help of P.D.R., M.J., P.K., V.D., and S.D.G. V.K. performed in vivo calcium imaging. S.M. performed RNAseq analysis, with the help of S.S., K.M.H., N.M., C.L.T., and M.P. D.W. performed and analyzed MRI with the help of J.S.Z., H.P.M., S.A., J.K., V.R., A.L., and F.R. S.D. performed synaptosomal extractions, western blotting and RT-qPCR with the help of I.S.R. and G.P. A.L., A.L.B., F.R., M.P., C.L.T., S.L., and L.D. secured funding. M.P., C.L.T., S.L., and L.D. designed and coordinated experiments. J.S.Z., I.S.R., S.L., and L.D. wrote the manuscript.

Funding

Competing interests

Additional information

Supplementary information The online version contains supplementary material available at https://doi.org/10.1038/s41467-021-23187-9.

Correspondence and requests for materials should be addressed to S.L. or L.D.

Peer review information *Nature Communications* thanks Abraham Acevedo-Arozena, Sami Barmada and the other, anonymous, reviewer(s) for their contribution to the peer review of this work. Peer reviewer reports are available.

Reprints and permission information is available at http://www.nature.com/reprints

Publisher's note Springer Nature remains neutral with regard to jurisdictional claims in published maps and institutional affiliations.

A novel non-cell autonomous mechanism of cortical dysfunction in ALS

A novel non-cell autonomous mechanism of cortical dysfunction in ALS

Vanessa W.Y. Kan[1,2,3], Evgeny Logunov[1,3], XiaoQian Ye[1,3], Monica Ziegler[1,3], Shenyi Jiang[1,3], Sabine Liebscher[1,3,4] #

#corresponding author

1 Institute of Clinical Neuroimmunology, Klinikum der Universität München, Ludwig-Maximilians-University Munich, Munich. Germany
2 Graduate School of Systemic Neurosciences, Ludwig-Maximilians-University Munich, Munich, Germany
3 BioMedical Center, Medical Faculty, Ludwig-Maximilians-University Munich, Munich, Germany
4 Munich Cluster for Systems Neurology (SyNergy), Munich, Germany

Correspondence:

Sabine LIEBSCHER, Institute of Clinical Neuroimmunology, Klinikum der Universität München, BioMedical Center, Grosshaderner Str. 9, 82152 Martinsried
e-mail: sabine.liebscher@med.uni-muenchen.de

Keywords: amyotrophic lateral sclerosis, *in vivo* two-photon calcium imaging, awake mice, anesthetized mice, motor cortex, microcircuit

Abstract

Amyotrophic lateral sclerosis (ALS) is a fatal neurological disease, characterized by the progressive degeneration of upper (UMN) and lower motor neurons (LMN). Cortical hyperexcitability is a commonly reported feature in ALS patients and rodent models of the disease, preceding overt motor symptoms and bearing the potency to trigger UMN and LMN degeneration. However, the pathomechanisms underlying cortical hyperexcitability remain unclear to date. Recent evidence argues for more complex, circuit level deficits exceeding cell autonomous UMN dysfunction and degeneration. To assess the spatiotemporal pattern and identify the main cellular drivers of cortical hyperexcitability, we here performed *in vivo* two-photon calcium imaging in motor cortex of anesthetized and in awake, behaving SOD1[G93A] transgenic (tg) mice. Employing a visuomotor feedback paradigm, we found both in cortical layer 2/3 (providing input to layer 5 and thus UMNs) as well as in layer 5 (harboring UMNs) a pronounced increase in the neuronal response to locomotion (hyperresponsiveness) and increased spontaneous activity levels in early symptomatic SOD1[G93A] tg mice, which were further associated with altered neuronal response cluster abundancies, overrepresenting locomotion-driven populations. Altered activity levels and response types severely compromised state-dependent coding space and thus feature encoding in primary motor cortex in SOD1[G93A] mice. Notably, hyperresponsiveness was already present in pre-symptomatic mice, but exclusively in layer 2/3 neurons, while layer 5 neurons, including UMN, were not affected yet. Chronic chemogenetic inhibition of pyramidal neurons in layer 2/3 indeed delayed symptom onset and disease progression. Together, our data argue for a novel cell - non autonomous mechanism based on hyperexcitable layer 2/3 pyramidal neurons, which chronically drive UMNs, thereby causing UMNs dysfunction and degeneration.

Introduction

Amyotrophic lateral sclerosis (ALS) is a devastating, still incurable neurodegenerative disease, characterized by the death of motor neurons in the brain and spinal cord, respectively (Kiernan et al., 2011). The underlying molecular and cellular mechanisms causing motor neuron death in ALS remain incompletely understood. A commonly observed feature, present in both sporadic (sALS) and familial ALS (fALS) cases, as well as in rodent models, is cortical hyperexcitability, typically assessed by means of transcranial magnetic stimulation (TMS) (Cengiz et al., 2019; Cengiz & Kuruoğlu, 2020; Menon et al., 2017; Menon et al., 2015; Shibuya et al., 2017; Siciliano et al., 1999; Turner et al., 2005; Van den Bos et al., 2018; Vucic et al., 2008; Zanette et al., 2002; Ziemann et al., 1997). Cortical hyperexcitability precedes overt motor symptoms in fALS patients (Menon et al., 2015; Vucic et al., 2008) and chemogenetically-driven chronic cortical hyperexcitability in healthy, WT mice seems sufficient to cause UMN and LMN pTDP43 pathology and degeneration (Haidar et al., 2021), thus emphasizing its cardinal relevance in ALS pathophysiology. However, the cellular and circuit mechanisms underlying 'hyperexcitability' of the primary motor cortex (M1) in ALS are poorly understood. Cell autonomous alterations of UMN were believed to be at the heart of this phenomenon, as UMNs display structural and functional changes in mice and men, such as reduced soma size (Genç et al., 2017; Özdinler et al., 2011; Zang & Cheema, 2002), dendritic regression accompanied by a reduction in apical and basal dendritic spine densities (Fogarty et al., 2016b; Genç et al., 2017) and hyperexcitability, indicated by an increase in maximum action potential frequency and changes in the spike frequency response to current injections (Kim et al., 2017).

Recent evidence, however, argues for at least a partial involvement of other motor cortex circuit elements. As such, TMS studies have already unraveled compromised inhibition in M1 of ALS patients, as evidence by an altered cortical silent period and short interval intracortical inhibition. Mouse models have further greatly helped to pinpoint cellular candidates, potentially involved in this process and identified hyperactive somatostatin (Sst) expressing interneurons in the TDP-43[A315T] mouse model (Zhang et al., 2016), while parvalbumin (PV) expressing interneurons in SOD1[G93A] mice were reported to be either hyperexcitable (Kim et al., 2017) or hypoexcitable (Khademullah et al., 2020). Alterations in interneuron excitability can cause an imbalance of the otherwise tightly regulated balance between excitation and inhibition (E/I) in M1 with the consequence of chronic excess stimulation of UMNs. Notably, interfering with the activity levels of these populations proves beneficial with respect to UMN health (Zhang et al., 2016) and even motor performance and survival of the mice (Khademullah et al., 2020), further emphasizing the therapeutic potential of circuit level interventions. In addition to defective inhibition there is

furthermore evidence for a 'surplus' excitation of UMN, reported as increase in excitatory synaptic transmission to UMNs in SOD[G93A] as well as in TDP-43[Q331K] mice (Fogarty et al., 2016a; Fogarty et al., 2015), associated either with reduced dendritic complexity and spine loss on both apical and basal dendrites of UMNs in SOD[G93A] mice (Fogarty et al., 2016b; Fogarty et al., 2015; Saba et al., 2016) or increased spine densities in TDP-43[Q331K] mice (Fogarty et al., 2016a) The sources of this excess synaptic input are not fully conclusive but tracing studies suggest it arises amongst others from somatosensory cortex (S1) and contralateral secondary motor cortex (M2) (Commisso et al., 2018).

The interpretation of findings from electrophysiological and histological studies, however, is complicated as it neither allows to draw direct conclusions regarding their function, such as response properties, within intact circuits nor does it reveal the nature of these alterations, that is whether these changes are cause or consequence and might in fact be (mal)adaptive or homeostatic. To fill this gap, we here performed *in vivo* two-photon calcium imaging of neurons in cortical layer 2/3 and layer 5 of M1 in SOD1[G93A] transgenic mice under anesthesia and in behaving mice, using a visuomotor feedback paradigm to probe locomotion –associated responses and sensorimotor integration, across different disease stages. We find a) increased spontaneous neuronal activity in M1 both under anesthesia and wakefulness, however, b) activity levels only partially persist across these states at the single cell level. At the population level we find two neural subspaces segregated by behavioral states, with c) a reduced distance between the two subspaces in SOD1[G93A] transgenic mice indicating a compromised coding space in M1. We also identified d) five distinct sensorimotor neuronal subtypes in M1 and detected e) increased locomotion-associated activity in both layer 2/3 and 5 neurons at the early symptomatic stage, which is however restricted f) to layer 2/3 neurons at the pre symptomatic stage. When neuronal activity is reduced chemogenetically chronically, we see g) a delayed symptom onset and improved motor behavior. Our data thus argue for a novel cell – non autonomous mechanism with hyperexcitable layer 2/3 pyramidal neurons, chronically driving UMNs and consequently UMNs dysfunction and degeneration.

Results

Early symptomatic SOD1[G93A] transgenic mice display increased neuronal activity in motor cortex under anesthesia and wakefulness

To assess the spatiotemporal pattern of functional alterations in M1 and to identify the main cellular drivers of cortical hyperexcitability in M1, we monitored neuronal activity at single cell

resolution by expressing the genetically encoded calcium indicator GCaMP6m in both neurons in cortical layer 2/3 and layer 5 in early-symptomatic (P90) SOD1[G93A] mice and the respective controls (Suppl. Fig. 1a,b). UMN affected in ALS represent a large proportion of layer 5 neurons, which in turn mainly receive input from neurons in layer 2/3. We first investigated the level of spontaneous activity in M1 by performing *in vivo* two-photon calcium imaging under light isoflurane anesthesia. We detected increased spontaneous activity levels (Suppl. Fig. 1c) accompanied with no changes in transient amplitude (Suppl. Fig. 1d) but increased synchronization in SOD1[G93A] mice (Suppl. Fig. 1e,f). We then asked whether the increase in spontaneous activity is also present in behaving mice and whether visuomotor integration might be affected in transgenic mice. Visuomotor integration requires coordination within a complex network to process and integrate sensory and motor signals, and impaired visuomotor integration would suggest brain network dysfunction underlying behavioral deficits. To this end, we imaged mice running head-fixed on an air-supported spherical treadmill, while navigating a virtual environment (VR) (Fig. 1a-c). The imaging paradigm consisted of a feedback session, in which running velocity was coupled to the visual flow generated by vertical black and white gratings presented on a toroidal screen, as well as a darkness session, during which visual input was omitted. Corroborating our findings under anesthesia, we detected an increase in activity in neurons in layer 2/3 and 5 during locomotion both in the feedback and the darkness session (Fig. 1d,e). During quiet wakefulness neuronal activity in layer 2/3 was not altered, while in layer 5 neurons we also observed a slight, yet significant increase in activity (Fig. 1d,e).

Partial coherence of activity levels under anesthesia and wakefulness

As we detected increased neuronal activity in both anesthetized and behaving mice, we wondered if activity levels would persist across brain states at the single cell level. To investigate that, we imaged the same set of neurons both under anesthesia as well as while mice were running head-fixed on a spherical treadmill (Fig. 2ab). When comparing the average neuronal activity under anesthesia and during wakefulness, we observed a broad distribution of activity types. A large proportion of neurons was exclusively active during one condition only, such as either under anesthesia (angle 90°) or during wakefulness (angle 0°). But overall the distribution did not differ between WT and SOD1[G93A] mice (Fig. 2c). We then investigated the change in activity from anesthesia to wakefulness for each neuron and found a less pronounced reduction in SOD1[G93A] mice, indicated by a rightward shift in the curve (Fig. 2d). To next address whether absolute activity levels determine the stability of the same, we next categorized neurons into three activity groups, namely low (0-0.25 transients/min), intermediate (0.25-3 transients/min) and high (>3 transients/min) neurons. Under both conditions, we found fewer intermediately active neurons

and a trend towards more highly active neurons in SOD1[G93A] mice (Fig. 2e). We next compared the 'stability' of activity categories between anesthesia and wakefulness (Fig. 2f). In both WT and SOD1[G93A] mice, we observed only a few highly active neurons that remained highly active, while the majority would turn intermediately active in awake mice (Fig. 2g). Interestingly, we found that a large proportion of low activity neurons remained in this category in SOD1[G93A] mice, while in WT mice a large part of 'low' neurons would become intermediately active during wakefulness (Fig. 2g). Together, this comparison highlights that activity levels under anesthesia only partially match those seen in awake mice and that anesthesia potentially unmasks higher excitability levels in SOD1[G93A] mice.

Coding space is compromised in M1 of SOD[G93A] mice

We next asked what neurons in M1 encode and whether these response properties would be altered in SOD mice. In an attempt to gain insight into information processing in M1, we recorded a number of behavioral parameters, such as locomotion, whisking, pupil width, and we applied short air puffs, to facilitate sensory input and arousal (Fig. 3a). The relationship between the activity within a given population of neurons and the corresponding behavior of an animal can be represented by a neural manifold, mapping the dimensionality-reduced single-neuron level activity to behavior states. To determine the strongest driver of neuronal activity in M1, we assessed the dimensionality and structure of the neuronal population activity by applying Principal Component Analysis (PCA)-based linear dimensionality reduction on our centered and z-scored ΔF/F traces and the associated behavioral parameters (Fig. 3b). A multi-dimensional structure of the population activity pattern was found in both WT and SOD1[G93A] mice, and together the first 3 principal components (PCs) explained ~30% of the variance (Fig. 3c). Linear regression was then applied to examine the encoding capacity of PC1 for the four behavioral parameters (Fig. 3d). Overall, there was a decrease in the coding capacity in SOD1[G93A] mice, which mainly affected the encoding of locomotion, as evidenced by a significantly lower variance explained by PC1 with regards to locomotion (Fig. 3d). Thus, we focused on locomotion-associated neuronal activity in the subsequent analyses. We next segregated our data into 2 behavioral states, namely running and quiet wakefulness and asked how well these 2 states would be encoded by the network. To address that question, we deployed PCA-based manifold analysis by mapping the multi-dimensional neuronal response pattern to 3 low-dimensional PCA space and identified two manifold subspaces as a function of velocity, one representing the subspace of quiet wakefulness and the other of locomotion (Fig. 3e). We observed a strong reduction in the coding space in SOD1[G93A] mice as seen in a shorter Euclidean distance within the subspace of quiet wakefulness and even more across subspaces of quiet wakefulness and running (Fig. 3f). We thus hypothesized

that compromised coding space of the investigated neuronal population, would also result in a less accurate representation of the actual behavior. To investigate that we decoded running velocity from neuronal activity by employing a random forest classifier (Fig. 3g) and indeed found a significantly lower coding accuracy of neuronal populations in layer 2/3 of SOD1^{G93A} mice (Fig. 3h).

Neuronal sensorimotor response types in M1

We next sought to gain insight into the response properties of individual neurons and aimed to identify groups displaying similar response patterns with regards to brain-states and sensorimotor integration. To this end, we computed the average activity level of each neuron during quiet wakefulness and running both during feedback sessions and during darkness and performed an unbiased clustering analysis. We discovered five unique neuronal response clusters: neurons that are primarily active during (1) running in general, (2) running with feedback, (3) running in darkness, (4) all conditions and (5) quiet wakefulness (Fig. 4a,b). We then quantified the abundancy of each cluster amongst our imaged neuronal populations in cortical layer 2/3 and 5 in WT and SOD mice and found an increase in the fraction of neurons belonging to cluster 3 (running in the darkness) in layer 2/3 neurons and a decrease in cluster 5 (active during quiescence) in both layer 2/3 and 5 neurons in SOD1^{G93A} mice (Fig. 4c). These data not only indicate that visuomotor integration does take place within M1 as locomotion-associated neuronal activity can either selectively occur with or without visual input as well as independently of it. Moreover, the data indicate that the surplus neuronal activity we observed in SOD1 mice results from a shift of neurons typically active during quiescence towards locomotion-associated neuronal activity.

Increased fraction of running-responsive neurons accompanied by hyperresponsiveness to locomotion in behaving early symptomatic SOD1^{G93A} mice

We thus next asked how locomotion- associated responses are altered in SOD1^{G93A} mice. We first characterized the running behavior per se in WT and SOD1^{G93A} mice. We found no difference in the fraction of time spent running during feedback and darkness sessions in layer 2/3 and layer 5 experiments (Suppl. Fig. 2a), as well as the velocity profile and the median running speed in WT and SOD1^{G93A} mice (Suppl. Fig. 2b-f).

We also quantified the fraction of running-responsive neurons, which are defined as neurons with increased activity during running epochs compared with stationary phases (Fig. 5a,b). In layer 2/3, we found an increase in neurons that are more active during running (Fig. 5c), accompanied by an increased fraction of running-responsiveness neurons (Fig. 5d) of SOD1[G93A] mice. Neuronal responses scaled with running speed and higher velocities caused more pronounced neuronal activity in SOD1[G93A] mice compared to non-transgenic controls (Fig. 5e,f). Among the layer 5 neurons we detected a similar change with more neurons displaying larger activity levels during locomotion in general (Fig. 5g), while no change in the fraction of running-responsive neurons was detected in SOD1[G93A] mice (Fig. 5h). However, locomotion-associated hyperresponsiveness was also detected in neurons in layer 5 (Fig. 5i-j).

Hyperresponsiveness to locomotion first detected in neurons in layer 2/3 of pre-symptomatic SOD1[G93A] mice

To assess the evolution and the sequence of events of these alterations in activity levels and response properties, we also investigated younger mice at the age of P60, corresponding to a presymptomatic stage in SOD1[G93A] mice (Fig. 6a). Indeed, at that presymptomatic stage we again detected more neurons tuned towards locomotion in layer 2/3 (Fig. 6b), accompanied by an increase in the fraction of running-responsive neurons (Fig. 6c). The tuning curves also revealed a clear hyperresponsiveness to locomotion in SOD1[G93A] mice, but surprisingly, only in layer 2/3 neurons (Fig. 6d,e). Neurons in layer 5, encompassing UMNs, in SOD1[G93A] mice were not affected at this early disease stage (Fig. 6f-i). As layer 2/3 neurons are the prime input source of layer 5 and thus also of UMN, our data argue for a novel cell-non autonomous mechanisms, based on hyperexcitable layer 2/3 neurons, which chronically excessively stimulate layer 5 neurons, including UMNs.

Dampening of activity in layer 2/3 delays symptom onset and improves behavioral deficits

Would the standard ALS treatment – Riluzole – reduce increased neuronal activity levels seen in M1 of SOD1[G93A] mice? To address that question, we treated SOD1[G93A] and their non-transgenic littermates with Riluzole provided through the drinking water over 7 days and recorded neuronal activity in anesthetized mice (Suppl. Fig. 3a). In WT mice, neuronal activity decreases only after 7 days of treatment (Suppl. Fig. 3b). On the contrary, in SOD1[G93A] mice neuronal activity decreases already after 2 days of treatment, while after 7 days neuronal activity was still lower than during the baseline, but gradually increased again, suggesting homeostatic mechanisms playing a role (Suppl. Fig. 3c).

As Riluzole inhibits glutamatergic signaling indiscriminately, with unknown consequences on interneurons as well as downstream homeostatic mechanisms, we next set out to more selectively chemogenetically inhibit only the identified neuronal population in layer 2/3 by expressing inhibitory DREADDs (G_i) in layer 2/3 neurons in pre-symptomatic mice and stimulating these Gi receptors through the application of their ligand clozapine-N-oxide (CNO) over the course of four weeks through the drinking water (Fig. 7a,b). We assessed the impact of this therapeutic strategy by regular scoring for disease symptoms and the measurement of motor performance in the Rotarod test. As hypothesized, we found that the symptom onset is delayed (Fig. 7c) and motor performance was increased (Fig. 7d) in DREADDs + CNO treated SOD1[G93A] mice. These findings thus argue for a pivotal role of neurons in layer 2/3 in driving cortical hyperexcitability in SOD1[G93A] and chronically driving UMNs in the motor cortex, which was shown to suffice to cause downstream TDP-43 pathology in UMN and LMN.

Discussion

To investigate circuit mechanisms underlying cortical hyperexcitability and subsequent neurodegeneration in ALS, we probed activity and response properties of neurons in M1 in SOD1[G93A] mice. We found that in early symptomatic SOD1[G93A] mice neurons in cortical layer 2/3 and 5 of M1 displayed increased spontaneous activity under anesthesia, which was only partially matched their activity levels during wakefulness. In behaving mice, we mainly observed a pronounced hyperresponsiveness to locomotion, causing a change in the composition of response type clusters and an overall compromised coding accuracy of the network. Hyperresponsiveness is detected both in layer 2/3 and 5 neurons at the early symptomatic stage, but is only present in layer 2/3 neurons at the pre-symptomatic stage when layer 5 neurons, including UMN are not affected yet, suggesting a top-down translaminar progression of the disease. Most importantly, we here show that selective chemogenetic inhibition of these layer 2/3 neurons provides a beneficial impact on disease onset and progression and could thus offer a novel therapeutic strategy.

Cortical hyperexcitability has been reported in both sALS and SOD1-fALS patients using transcranial magnetic stimulation (TMS) (Vucic et al., 2008), measuring parameters such as (reduced) resting motor threshold, (increase) intracortical facilitation and (decreased) short-interval intracortical inhibition, indicative of excitation/inhibition dysbalance (Gunes et al., 2020). In mouse models of ALS, whole-cell patch clamp recordings in both neuronal cultures as well as brain slice revealed reduced rheobase, meaning neurons are more likely to fire, and increased excitatory postsynaptic current (EPSC) accompanied by decreased inhibitory postsynaptic

current (IPSC), suggesting excitation/inhibition dysbalance (Gunes et al., 2020). In addition, proton magnetic resonance spectroscopy of the brain demonstrated changes in level of metabolites such as glutamate, GABA and glutamine (Foerster et al., 2012; Foerster et al., 2013; Lei et al., 2019). Most critically, chronic chemogenetic activation of neurons in M1 drives neurodegeneration in otherwise perfectly healthy WT mice (Haidar et al., 2021). These findings suggest a cortical origin of neurodegeneration and population-specific changes that together contribute to cortical hyperexcitability in ALS. However, the *exact* source of cortical hyperexcitability remains unclear.

To get an inkling into the cellular and circuit mechanisms we here performed chronic *in vivo* two-photon calcium imaging in the classical mouse model of the disease, namely SOD1^{G93A} mice. *In vivo* two-photon calcium imaging has been employed extensively by the neurodegenerative field (Blumenstock et al., 2021; Burgold et al., 2019; Busche, 2018; Liebscher et al., 2016; Takamura et al., 2021). Specifically, imaging in behaving mice enables us to probe functional response properties of neurons to stimuli such as locomotion and visual input, which goes beyond a simplistic determination of 'spontaneous' neuronal activity typically monitored under anesthesia. Locomotion is a particularly strong driver of neuronal activity, observed across various brain areas (Ayaz et al., 2013; Clancy et al., 2019). We also here do not only observe an increase of neuronal activity under anesthesia in SOD1^{G93A} mice, but for the first time can demonstrate that it is mainly the neuronal activity linked with locomotion that is strongly increased. Movement per se as well as locomotion were shown to drive a defined population of neurons in M1 (Heindorf et al., 2018; Peters et al., 2017). An earlier study, in which the impact of motor learning on neurons in M1 was characterized, reported three 'response' categories of neurons in M1, namely movement-active, quiescent-active and indiscriminately (spontaneously) active neurons (Peters et al., 2017). We here moreover found evidence that also visuomotor integration strongly determines response types in M1 and identified in addition two neuronal clusters in which locomotion-associated responses hinged on the absence or presence of visual input. These clusters however were differentially represented in neuronal populations in SOD1^{G93A} mice, with a shift towards locomotion-responsive neurons. What could cause this hyperresponsiveness to locomotion in SOD1^{G93A} mice? Locomotion-associated neuronal activity is triggered by neuromodulators such as norepinephrine and acetylcholine (Howe et al., 2019; Mitchell et al., 2006) and is tightly regulated by glutamatergic and GABAergic inputs (Galvan et al., 2006; Lindenbach et al., 2016). Locomotion causes an overall increase in cortical activity via a disinhibition circuit, which has been studied more extensively in the visual cortex (Fu et al., 2014; Pakan et al., 2016). Specifically, locomotion activates VIP interneurons through the release of acetylcholine, which then inhibits Sst and thereby disinhibiting pyramidal neurons (Fu et al., 2014; Pakan et al., 2016). Interestingly, the presence and absence of visual stimuli also has an

effect on this disinhibitory circuit. While locomotion combined with visual stimuli has a similar effect on pyramidal neurons as well as all 3 subtypes of interneurons, PV and VIP interneurons in visual cortex are more strongly activated in darkness (Pakan et al., 2016). Since we detected more pronounced changes in locomotion-associated neuronal activity in layer 5 in the presence of visual input, an involvement of interneurons in cortical hyperresponsiveness observed in SOD1[G93A] mice is possible. Indeed, electrophysiological recordings in brain slices of pre-symptomatic SOD1[G93A] mice revealed hypoexcitable PV and Sst accompanied by reduced inhibition in UMN (Clark et al., 2018; Jara et al., 2020; Khademullah et al., 2020; Kim et al., 2017). Chronic chemogenetic activation of PV interneurons showed a delay in symptom onset and improvement in motor function. While it was more beneficial to intervene at an earlier stage, the disease outcome was similar (Khademullah et al., 2020), supporting non-cell-autonomous degenerative mechanisms underlying neurodegeneration in ALS. However, to determine the precise involvement of each interneuronal population in the course of ALS, imaging studies in the respective cre-driver lines should be conducted. Interestingly, along the course of the disease progression in SOD1[G93A] mice, hyperresponsiveness to locomotion was first detected in layer 2/3 of M1, already at the pre-symptomatic stage, when no change in UMN responsiveness is detectable yet.

Our data corroborate previous reports showing that indeed layer 2/3 pyramidal cells in SOD1[G93A] mice are hyperexcitable at an early disease stage and the level of increased excitability strongly outnumbered the ones seen on UMN (Kim et al., 2017). Moreover, previous studies have also shown that UMN receive excess glutamatergic input, the source of which however could not be determined back then (Fogarty et al., 2016b). As layer 2/3 pyramidal neurons (PNs) provide the main input to layer 5 PNs it is conceivable and now confirmed by our data that this excess glutamatergic input is provided by hyperexcitable layer 2/3 PN (Anderson et al., 2010; Kiritani et al., 2012; Shepherd, 2013). Alternative cellular sources could however also be PN in other cortical areas, which were shown to establish aberrant connections with UMNs (Commisso et al., 2018). The observed functional changes are also paralleled by structural changes seen in layer 2/3 neurons, namely reduced apical spine density (Fogarty et al., 2016b). The apical spine loss seen in layer 2/3 PNs could be a compensatory mechanism to increased long-range input (Bhatt et al., 2009; Runge et al., 2020), and thus explain the hyperactivity and hyperresponsiveness detected in layer 2/3 of pre symptomatic SOD1[G93A] mice. Together, our data thus argue for a non-cell-autonomous mechanism critically involved in the development of cortical hyperexcitability and subsequently causing neurodegeneration in ALS.

Can cortical hyperexcitability be targeted therapeutically? The current treatment options for ALS, especially Riluzole, have been proven ineffective in three mouse models of ALS (Hogg et al., 2018;

Wright et al., 2021). Riluzole is a glutamate antagonist that blocks glutamatergic (excitatory) neurotransmission by preventing the release of glutamic acid (Doble, 1996) as well as exerting postsynaptic anti-glutamatergic effects (Kim et al., 2007). Though Riluzole has been shown to modulate the release of glutamate (Lamanauskas & Nistri, 2008), existing studies did not account for the effect of neural adaptation/homeostatis and plasticity in the cortex (Bernacchia, 2014; Bharmauria et al., 2022). This is further supported by excitability changes seen in various populations of neurons during different stages of ALS (Kim et al., 2017). Therefore, to better understand the effect of chronic administration of Riluzole on neuronal populations in M1, we imaged neuronal activity in motor cortex under anesthesia. Our data demonstrate that Riluzole decreases elevated neuronal activity levels within 2days, but that homeostatic mechanism are likely at play as after 7d of treatment an increase in activity could be detected again. As Riluzole indiscriminately inhibits glutamatergic signaling it also remains open what the impact on inhibitory interneurons is, which are of vital importance in the regulation of neuronal activity levels. These adaptive mechanisms could explain the very limited beneficial effect of Riluzole in the treatment of ALS and should prompt further investigations to identify altered application regimes to minimize the same.

In an attempt to more selectively only inhibit the identified population of layer 2/3 PNs, we employed a chemogenetic approach. Indeed, chronic inhibition of layer 2/3 PN during the pre-symptomatic stage over 30 days proves beneficial with respect to disease onset and progression, which outperforms Riluzole treatment in SOD1^{G93A} mice (Hogg et al., 2018). Our findings thus suggest that early and selective intervention could potentially "correct" alterations of circuit elements.

Lastly, what remains obscure is the link to typical hallmarks of the disease, which in the SOD1^{G93A} mouse model is the accumulation of misfolded-SOD1, against which antibodies have been generated as a treatment option (Maier et al., 2018). The burden of misfolded-SOD1 accumulation on neurons is layer- and population-specific. Misfolded-SOD1 expression is most abundant in M1 layer 5 of SOD1^{G93A} mice already at the pre-symptomatic stage (Commisso et al., 2018; Genc et al., 2020). Surprisingly, misfolded-SOD1 accumulation in layer 2/3 and 5 neurons of somatosensory (S1) and auditory (AUD) cortices in pre-symptomatic SOD1^{G93A} mice did not trigger changes in spine density despite increased connectivity from these neurons to M1 (Commisso et al., 2018). These data suggest that misfolded-SOD1 accumulation alone does not drive neurodegeneration.

To summarize, our study revealed hyperexcitable layer 2/3 pyramidal neurons as a key driver of cortical hyperexcitability in SOD1^{G93A} mice driving the downstream degeneration of UMN and

LMN, a process which is therapeutically amenable. Our findings thus suggest a novel non-cell-autonomous mechanism underlying cortical dysfunction in ALS.

Main Figures
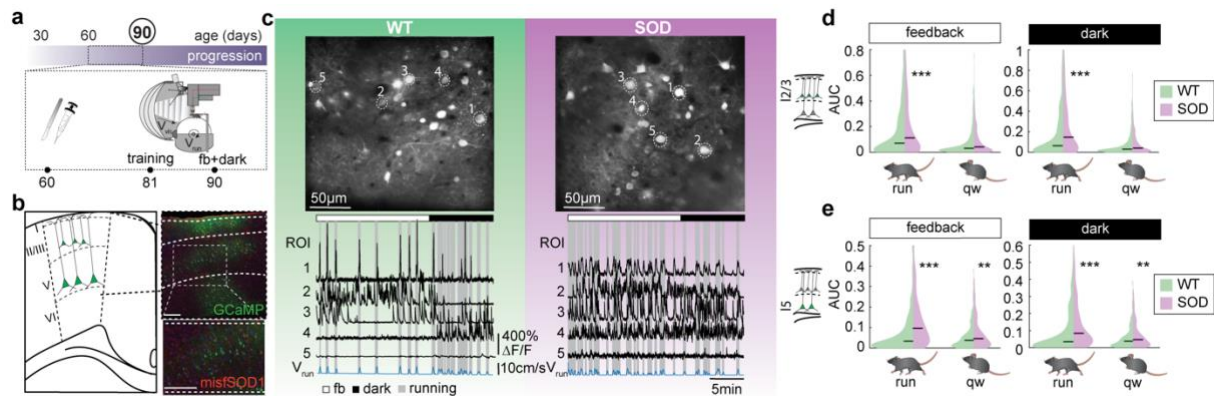
Fig. 1. *In vivo* **two-photon calcium imaging in motor cortex of behaving mice.**

(**a**) Experimental timeline. (**b**) Schematic of the targeted and imaged neuronal populations, i.e. neurons in layer 2/3 and 5 of motor cortex (M1). Immunohistological image of M1 of a SOD1[G93A] mouse (neurotrace (blue), GCaMP6m-expressing neurons (green), misfolded-SOD1 (red)). Cortical layers are delineated in (left) black and (right) white dashed lines. (**c**) Representative field of view (FOV) and the corresponding calcium traces of selected regions of interest (ROI, capturing neuronal somata) along with the running speed (V_{run}) in blue. (**d**) Neuronal activity (area under curve (AUC)/minute) during running and quiet wakefulness (qw) during visual feedback (fb) (run: $p = 0.00021$; qw: $p = 0.81$, Wilcoxon Rank Sum test,) and in darkness (dark) in layer 2/3 (run: $p < 10^{-8}$; qw: $p = 0.81$, Wilcoxon Rank Sum test, fb: WT: 875 neurons, 9 mice; SOD1[G93A]: 684 neurons, 8 mice; dark: WT: 789 neurons, 9 mice, SOD1[G93A]: 599 neurons, 8 mice, bold line represents median). (**e**) Same as in (d), but in layer 5 (fb: run: $p < 10^{-14}$; qw: $p = 0.009$; darkness: run: $p < 10^{-10}$; qw: $p = 0.009$, Wilcoxon Rank Sum test, fb: WT: 434 neurons, 6 mice, SOD1[G93A]: 390 neurons, 4 mice; dark: WT: 406 neurons, 6 mice, SOD1[G93A] : 353 neurons, 4 mice). Scale bar (b) 100μm, (c) 50μm, **$p < 0.01$, ***$p < 0.001$. Created with BioRender.com.
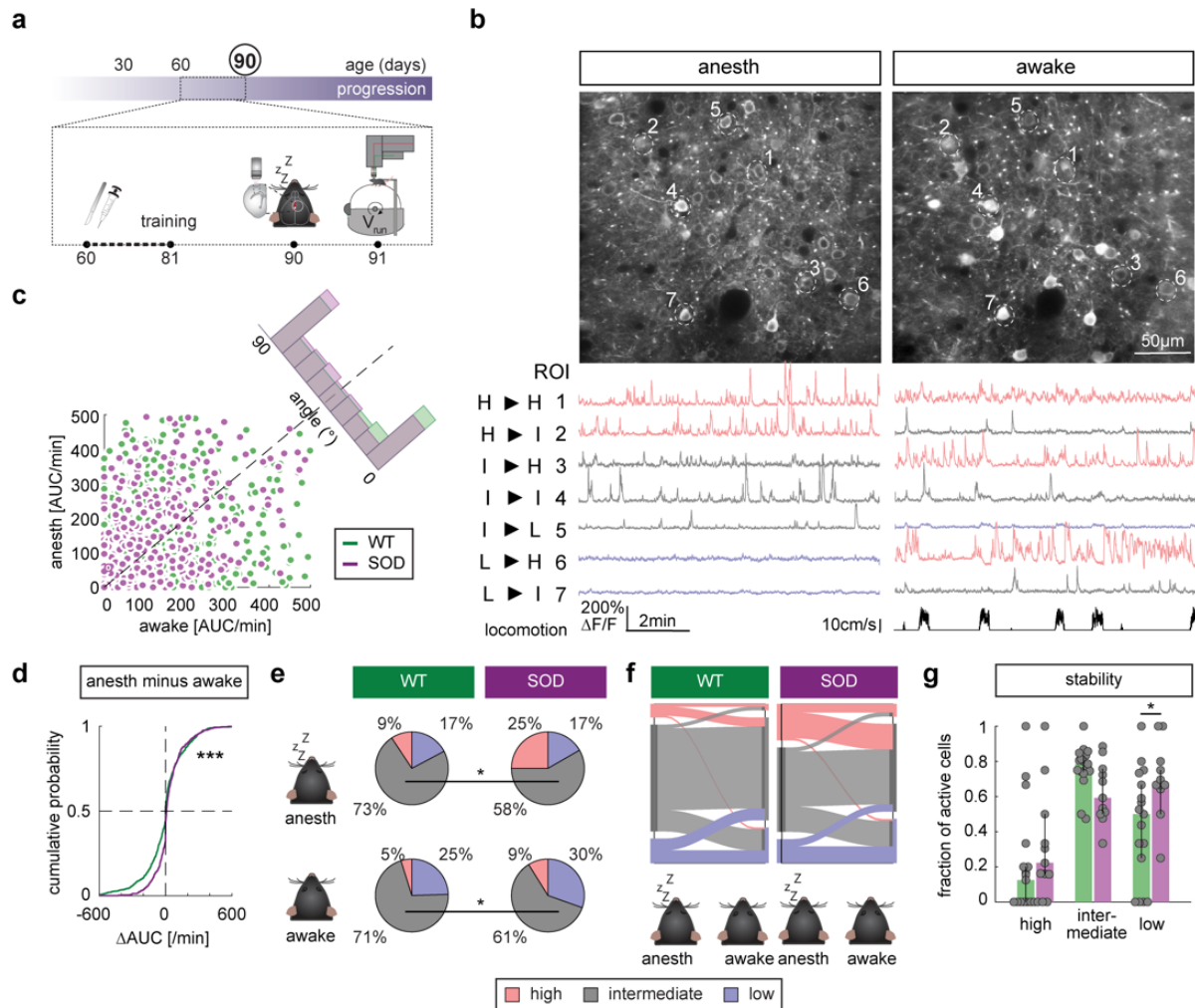
Fig. 2. Comparison of activity levels under anesthesia and during wakefulness in early symptomatic SOD1[G93A] mice.

(**a**) Experimental timeline of *in vivo* two-photon calcium imaging in mice under anesthesia and in wakefulness, illustrating stereotaxic injections of AAV2/1.syn.jGCaMP7s and window implantation at P60 and subsequent in vivo imaging under anesthesia and in wakefulness 4 weeks after. (**b**) Representative example field of view (FOV, average projection of 20,000 frames) and activity traces of selected ROIs under anesthesia and wakefulness (locomotion, black). Neurons are categorized by their activity into high (H, red, > 3 trans/min), intermediate (I, gray, 0.25 – 3 trans/min) and low (L, blue, < 0.25 trans/min). (**c**) Neuronal activity (area under the curve (AUC)/min), of the same neurons under anesthesia and during wakefulness, along with a histogram showing the distribution of angles formed between the x axis and a line formed by each data point and the origin *(p=* 0.68, two-sample Kolmogorov-Smirnov test). (**d**) Cumulative distribution of the change in activity from anesthesia to wakefulness (AUC anesth minus AUC awake, $p < 10^{-5}$, two-sample Kolmogorov-Smirnov test). (**e**) Fraction of all neurons in each activity category under anesthesia (high: *p=* 0.20, intermediate: *p=* 0.036; low: *p=* 0.91) and during wakefulness (high: p= 0.13, intermediate: p= 0.016; low: p= 0.09, all Wilcoxon Rank Sum test). (**f**) Alluvial plot showing of fractions of activity categories and their change during wakefulness. (g) Comparison of the fraction of neurons that remain in the same activity category during wakefulness and under anesthesia (Data are median $\pm$ 95%CI ; high: $p = 0.15$, intermediate: $p = 0.051$; low: *p=* 0.036, Wilcoxon Rank Sum test). Data in c-f (WT: 893 neurons, 5 mice, SOD1[G93A] : 575 neurons, 3 mice), in g (WT: 17 FOVs, 5 mice, SOD1[G93A]: 11 FOVs, 3 mice). *$p < 0.05$, **$p < 0.01$, ***$p < 0.001$. Created with BioRender.com.
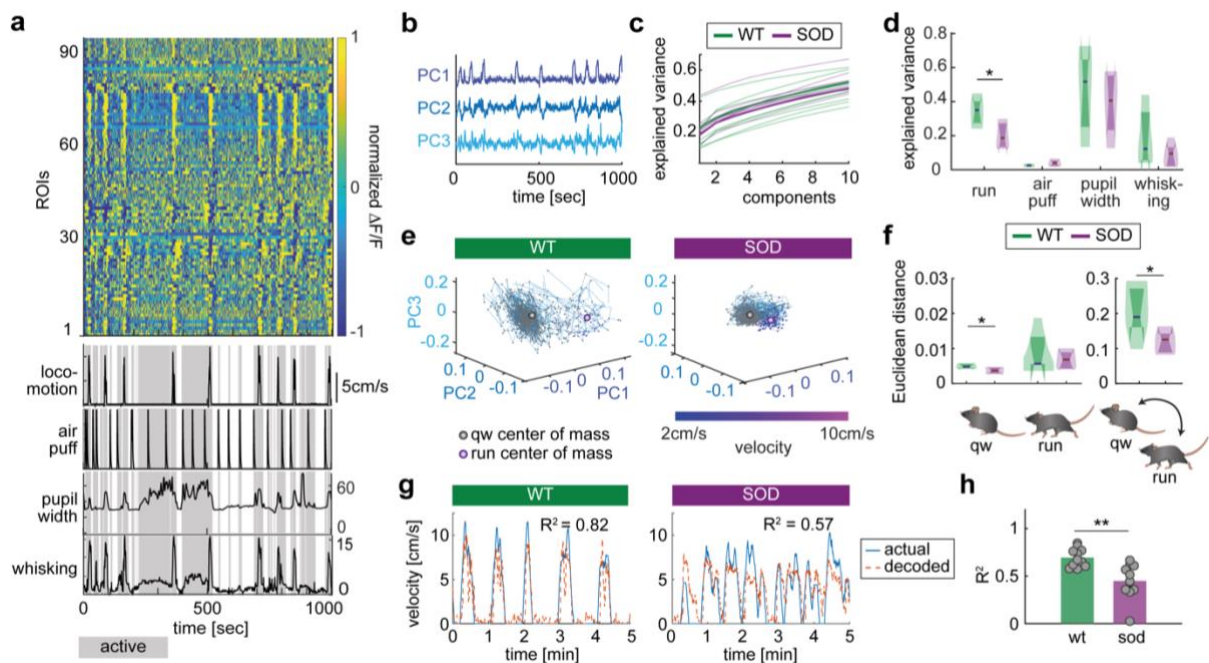
Fig. 3. Compromised state-dependent coding space in M1 of early-symptomatic SOD1^{G93A} mice.

(**a**) Representative input matrix of the centered and z-scored neuronal activity traces (ΔF/F) acquired during the feedback session, and the corresponding behavioral traces denoting locomotion, air puff, pupil width and whisking. Grey area represents the 'active phase', which corresponds to the detection 'activity' in any of the parameters measured. (**b**) Time series of the principal components (PC) 1, PC2 and PC3 from the representative example shown in (a). (**c**) Cumulative total variance explained by the principal component analysis (PCA) (p = 0.6, Wilcoxon rank sum test, WT: 15 FOVs, 10 mice; SOD1^{G93A}: 18 FOVs, 15 mice). (**d**) Explained variance of the measured behavioral parameters represented by PC1 (running p = 0.019, air puff p = 0.083, pupil width p = 0.8, whisking p = 0.24, all Wilcoxon rank sum test). (**e**) Example manifold structure of running (run) and quiet wakefulness (qw) in WT (left) and SOD1^{G93A} mice (right). Grey hollow circles indicate epochs of qw. Purple filled circles represent running epochs (color codes for running speed). Blue lines denote the trajectory. (**f**) Change in Euclidean distance within manifold associated with running, quiet wakefulness, or between the two states of layer 2/3 neurons in M1 in (within qw subspace p = 0.02, within running subspace p = 0.39, between qw – running subspaces p = 0.023, Wilcoxon rank sum test, WT: 9 FOVs, 6 mice, SOD1^{G93A} 7 FOVs, 6 mice). (**g**) Representative example of actual and decoded running velocity using the Random Forest decoder in WT (left) and SOD (right) mice. (**h**) Decoding accuracy (data are mean ± SEM; each dot represents an experiment; p = 0.0013, Student's t-test, WT: 11 FOVs, 7 mice; SOD1^{G93A}: 10 FOVs, 6 mice). *p < 0.05, **p < 0.01, ***p < 0.001. Created with BioRender.com.
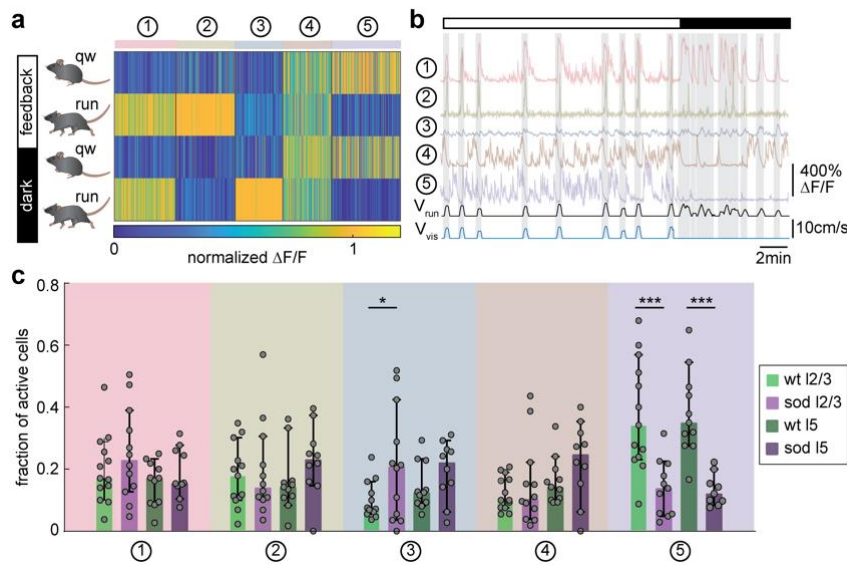
Fig. 4. Distinct neuronal sensorimotor activity clusters in M1.

(**a**) Heat map of average neuronal activity during running (run) and quiet wakefulness (qw) during feedback and darkness sessions of 5 identified sensorimotor response type clusters (cluster 1: 1241 neurons, cluster 2: 1195 neurons, cluster 3: 960 neurons, cluster 4: 985 neurons, cluster 5: 1392 neurons; all neurons from WT and SOD1 P60 and P90 mice pooled). (**b**) Representative example traces of each neuronal cluster, as well as the corresponding behavioral parameters (locomotion (V_{run}), black; visual flow (V_{vis}), blue; running epochs, light grey area). (**c**) Fraction of active neurons per cluster and cortical layer in early symptomatic mice (cluster 1 layer 2/3 (l2/3): $p = 0.51$, cluster 1 layer 5 (l5): $p = 0.48$, cluster 2 l2/3: $p = 0.65$, cluster 2 l5: $p = 0.13$, cluster 3 l2/3: $p = 0.039$, cluster 3 l5: $p = 0.22$, cluster 4 l2/3: $p = 0.77$, cluster 4 l5: $p = 0.21$, cluster 5 l2/3: $p = 0.0004$, cluster 5 l5: $p = 0.0002$, Wilcoxon Rank Sum test; N= 13 layer 2/3 (l2/3) FOVs in 9 WT mice, N= 12 l2/3 FOVs in 8 SOD1[G93A] mice, N= 11 layer 5 (l5) FOVs in 6 WT mice and 10 l5 FOVs in 4 SOD1[G93A] mice. Data are median $\pm$ 95%CI. *$p < 0.05$, ***$p < 0.001$. Created with BioRender.com.
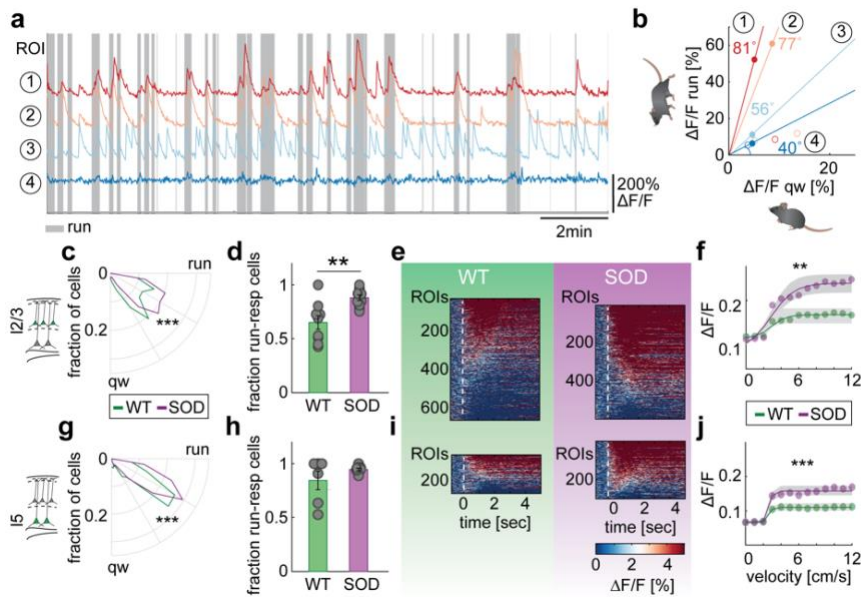
Fig. 5. Locomotion-associated hyperresponsiveness in layer 2/3 and 5 neurons of early symptomatic SOD1[G93A] mice.

(**a**) Example calcium traces of ROIs and their (**b**) corresponding angle denoting the median activity during running (run) and quiet wakefulness (qw). (**c**) Angle distribution in WT and SOD1[G93A] neurons in layer 2/3 ($p < 10^{-12}$, Kolmogorov-Smirnov test, WT: 635 neurons, 6 mice; SOD1[G93A]: 594 neurons, 8 mice). (d) Fraction of running-responsive neurons ($p = 0.0027$, Student's t-test, WT: 9 FOVs, 6 mice; SOD1[G93A]: 10 FOVs, 8 mice). (**e**) Heat maps of neuronal activity upon running onset (white dashed line), from -1s to 5s in layer 2/3 active neurons. (f) Neuronal activity as a function of instantaneous running velocity in layer 2/3 neurons (p (genotype)= 0.0024, Two-Way ANOVA for Unbalanced Design, WT: 9 FOVs, 6 mice; SOD1[G93A]: 10 FOVs, 8 mice). (**g**) Same as (c) but for layer 5 neurons ($p = 3.8 \times 10^{-4}$, Kolmogorov-Smirnov test, WT: 202 neurons, 4 mice; SOD1[G93A] : 301 neurons, 4 mice). (**h**) Same as (d) but for layer 5 neurons ($p = 0.2$, Student's t-test, WT: 6 FOVs, 4 mice; SOD1[G93A] : 8 FOVs, 4 mice). (i) Same as in (e) but for layer 5 neurons. (j) Same as (f) but for layer 5 neurons (p (genotype) $< 10^{-9}$, Two-Way ANOVA for Unbalanced Design, WT: 6 FOVs, 4 mice; SOD1[G93A] : 8 FOVs, 4 mice). Data are mean $\pm$ SEM (d,h), data are median $\pm$ 95% CI (f,j). *$p < 0.05$, **$p < 0.01$, ***$p < 0.001$. Created with BioRender.com.
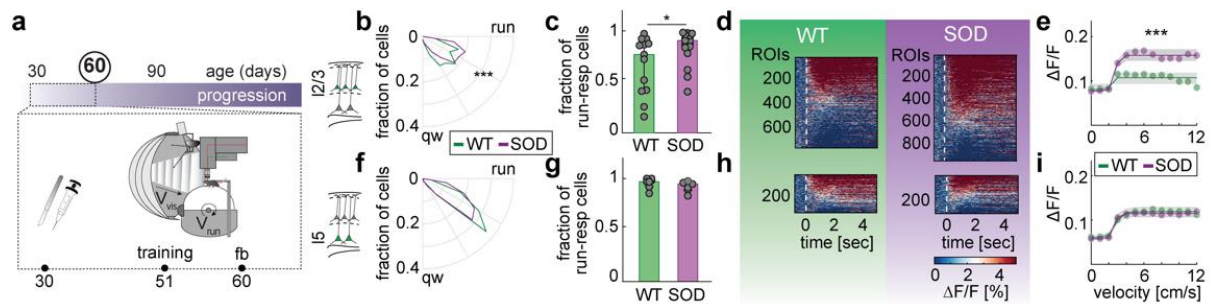
Fig. 6. Locomotion-associated hyperresponsiveness is exclusively present in M1 layer 2/3 neurons in pre-symptomatic SOD1[G93A] mice.

(a) Experimental timeline. (b) Distribution of angles between median activity during running and quiet wakefulness for neurons in layer 2/3 in WT and SOD1[G93A] ($p < 10^{-10}$, Kolmogorov-Smirnov test, WT: 744 neurons, 9 mice; SOD1[G93A]: 943 neurons, 10 mice. (c) Fraction of running-responsive neurons ($p = 0.049$, Wilcoxon rank sum test, WT: 13 FOVs, 9 mice; SOD1[G93A]: 17 FOVs, 10 mice). (d) Heat maps depicting neuronal activity upon running onset (white dashed line) of active neurons layer 2/3. (e) Neuronal activity as a function of instantaneous running velocity of neurons in layer 2/3 (p (genotype) $< 10^{-7}$, Two-Way ANOVA for Unbalanced Design, WT: 13 FOVs, 9 mice; SOD1[G93A]: 17 FOVs, 10 mice). (f) Same as (b) but for neurons in layer 5 ($p = 0.073$, Kolmogorov-Smirnov test, WT: 313 neurons, 5 mice; SOD1[G93A]: 313 neurons, 4 mice). (g) Same as (c) but for neurons in layer 5 ($p = 0.12$, Wilcoxon rank sum test, WT: 7 FOVs, 5 mice; SOD1[G93A]: 7 FOVs, 4 mice). (h) Same as (d) but for neurons in layer 5. (i) Same as (e) but for neurons in layer 5 (p (genotype) $= 0.61$, Two-Way ANOVA for Unbalanced Design, WT: 7 FOVs, 5 mice; SOD1[G93A]: 7 FOVs, 4 mice). Data are median $\pm$ 95% CI (c,e,g,i). *$p < 0.05$, ***$p < 0.001$. Created with BioRender.com.
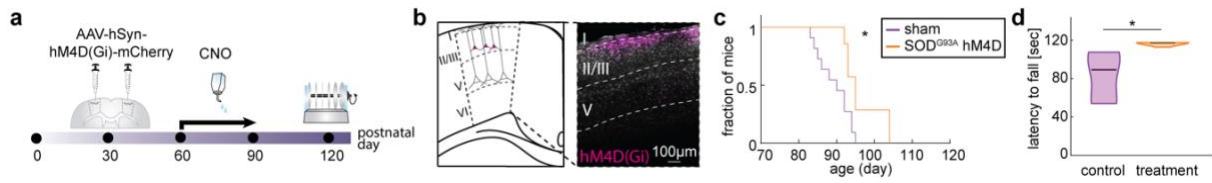
Fig. 7. Chemogenetic inhibition of neurons in layer 2/3 during the pre-symptomatic stage delays symptom onset and improves motor function in SOD1[G93A] mice.

(a) Timeline of experiment. (b) Schematic of the targeted population of neurons in layer 2/3 of M1. Fluorescent image of a histological section in M1 (neurons pseudo-colored in gray using neurotrace, mCherry-expressing neurons in magenta). Cortical layers are delineated in black (left) and white (right) dashed lines. (c) Symptom onset in mCherry SOD [G93A] sham and hM4D-mCherry SOD1[G93A] mice ($p = 0.01$, Log-rank (Mantel-Cox) test, SOD [G93A] sham: 11 mice, SOD [G93A] hM4D: 7 mice. (d) Latency to fall from the rod during the rotarod test ($p = 0.036$, Wilcoxon rank sum test, line indicates median, SOD [G93A] sham= 5, SOD [G93A] hM4D: 3 mice). *$p < 0.05$.

Suppl. Fig.
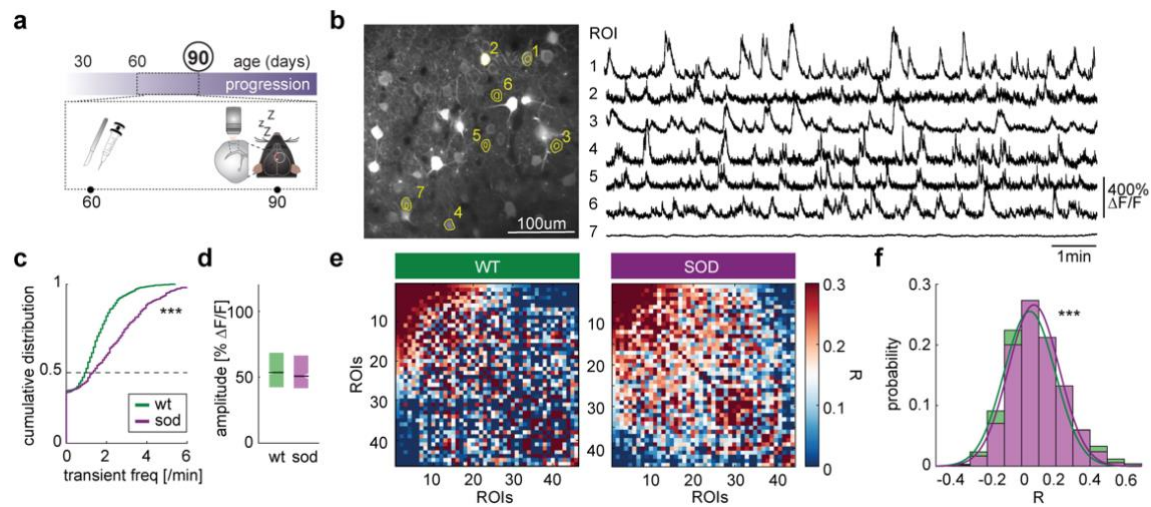
Suppl. Fig. 1. Increased neuronal activity levels in M1 of early symptomatic SOD1[G93A] transgenic mice under anesthesia.

(a) Scheme of two-photon calcium imaging in anesthetized animals. (b) Representative example of calcium traces from selected regions of interests (ROIs) in a field of view (FOV) imaged in layer 2/3 of a SOD1[G93A] transgenic mouse. (c) Increased transient frequency in SOD1[G93A] mice ($p < 10^{-18}$, Kolmogorov-Smirnov test). (d) Transient amplitude ($p = 0.19$, Kolmogorov-Smirnov test, WT: 1296 neurons, 6 mice; SOD1[G93A] : 591 neurons, 4 mice (c,d)). (e) Example correlogram illustrating pairwise activity correlations (Pearson's correlation coefficients, R) in WT (left) and SOD (right). (f) Histogram of pairwise activity correlations superimposed by gaussian fits of early symptomatic SOD1[G93A] mice. ($p < 10^{-16}$, Kolmogorov-Smirnov test, WT: 18878 pairwise comparisons, 6 mice, SOD1[G93A] : 7789 pairwise comparisons, 4 mice). ***$p < 0.001$
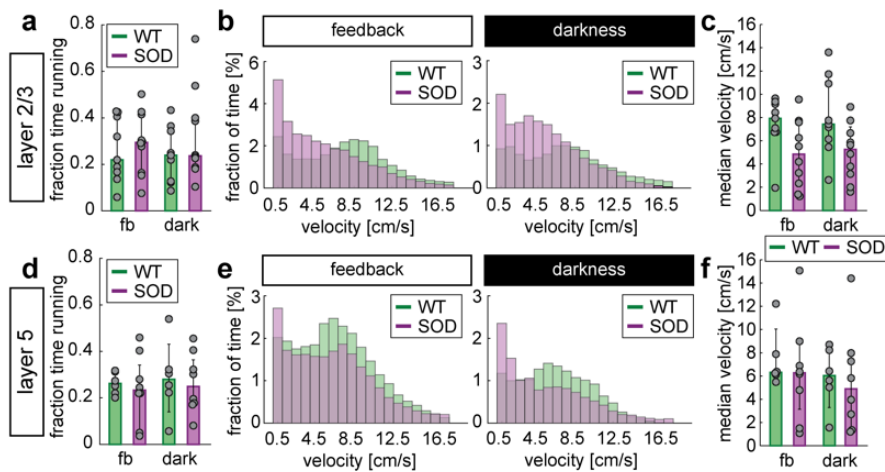
Suppl. Fig. 2. Running profiles of WT and SOD1^G93A transgenic mice.

(a) Fraction of time spent running in layer 2/3 experiments during feedback (fb) and darkness (dark) sessions. (fb: $p = 0.7$; dark: $p = 0.5$, Wilcoxon rank sum test, WT: 9 FOVs, 6 mice; SOD1^G93A: 10 FOVs, 8 mice). (b) Proportional velocity distribution in layer 2/3 experiments during feedback (left) and darkness (right) sessions (fb: $p = 0.77$; dark: $p = 0.57$, Kolmogorov-Smirnov test, WT: 9 FOVs, 6 mice; SOD1^G93A : 10 FOVs, 8 mice). (c) Median speed during running epochs in layer 2/3 experiments during feedback and darkness sessions (fb: $p = 0.053$; dark: $p = 0.053$, Wilcoxon rank sum test, WT: 9 FOVs, 6 mice; SOD1^G93A : 10 FOVs, 8 mice). (d) Same as (a) but for layer 5 experiments (fb: $p = 0.66$; dark: $p = 0.85$, Wilcoxon rank sum test; WT: 6 FOVs, 4 mice; SOD1^G93A : 8 FOVs, 4 mice). (e) Same as (b) but for layer 5 experiments (fb: $p = 0.059$; dark: $p = 0.13$, Kolmogorov-Smirnov test, WT: 6 FOVs, 4 mice; SOD1^G93A : 8 FOVs, 4 mice). (f) Same as (c) but for layer 5 experiments (fb: $p = 0.66$; dark: $p= 0.57$, Wilcoxon rank sum test, WT: 6 FOVs, 4 mice, SOD1^G93A: 8 FOVs, 4 mice. Data are median $\pm$ 95% CI (a,c,d,e).
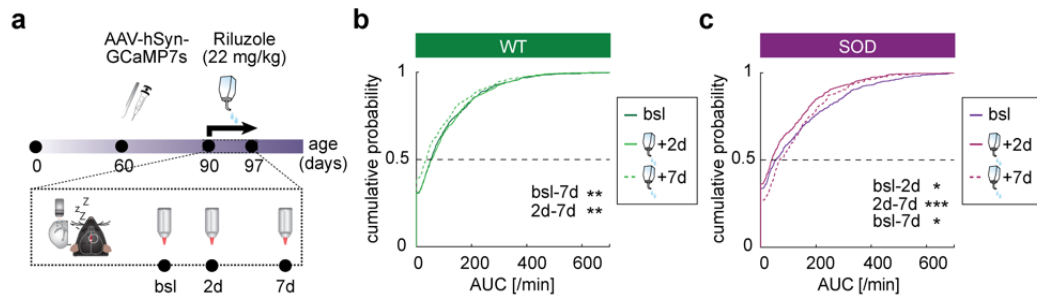
Suppl. Fig. 3. Effect of Riluzole on neuronal activity in motor cortex.

(**a**) Illustration of the experiment and imaging timeline. (**b**) Neuronal activity (area under the curve (AUC)) in WT mice at baseline (bsl; dark green), 2 days (2d; green) and 7 days (7d; dashed green) of chronic Riluzole treatment (bsl-2d: p = 0.83; 2d-7d: p = 0.004; bsl-7d: p = 0.006, Kolmogorov-Smirnov test, bsl: 1494 neurons, 13 FOVs, 4 mice; 2d: 1249 neurons, 11 FOVs, 3 mice; 7d: 955 neurons, 8 FOVs, 3 mice. (**c**) Neuronal activity levels in SOD1[G93A] transgenic mice (bsl; dark purple; 2d; magenta; 7d; dashed magenta, bsl-2d: p = 0.01; 2d-7d: p = 0.0008; bsl-7d: p = 0.003, Kolmogorov-Smirnov test; bsl: 929 neurons, 11 FOVs, 3 mice; 2d: 929 neurons, 11 FOVs, 3 mice; 7d: 366 neurons, 4 FOVs, 1 mouse. *p < 0.05, **p < 0.01, ***p < 0.001.

Material and Methods

Animals

All animal experiments were conducted in accordance with protocols approved by Regierung von Oberbayern, Munich, Germany. B6.Cg-Tg(SOD1*G93A)1Gur/J mice were obtained from the Jackson Laboratory, maintained on a C57Bl6/J background and housed with up to four littermates of the same sex with a regular 12-hour light and dark cycle at our Core Facility. For the pre-symptomatic cohort (P60), 10 WT mice (all female) and 10 SOD1^{G93A} mice (all female) were used for analyses. For the early-symptomatic cohort (P90), 9 WT mice (8 females and 1 male) and 8 SOD1^{G93A} mice (8 females) were used for analyses.

Surgery

Animals received a craniotomy with stereotactic cortical injections and a subsequent window implantation at P30 and P60 for pre-symptomatic (P60) and early-symptomatic (P90) cohorts, respectively, as previously described (Liebscher et al., 2016; Scekic-Zahirovic et al., 2021). Briefly, prior to the craniotomy and cortical injections, mice were given analgesia (Metacam, 1mg/kg, orally) 30 minutes before an intraperitoneal injection of Fentanyl (0.05 mg/kg), Midazolam (5.0 mg/kg), and Metedomidin (0.5 mg/kg). Eyes were covered with Bepanthen® creme at all times. Xylocain Gel 2% was applied prior to removing the skin of the head, exposing the skull and then on the exposed periost. A circular craniotomy (2mm in radius) was performed with a centre at 1.7mm lateral from the midline and 0.8mm anterior of bregma. A total of 1µl AAV2/1.Syn.GCaMP6m.WPRE.SV40 (addgene, diluted 1:6 in saline) or AAV9.Syn.jGCaMP7s.WPRE (addgene, diluted 1:10 in saline) was slowly injected at three sites (~300nl per site) at a cortical depth ~600µm to target both neurons in layer 2/3 and 5 of primary motor cortex (M1). Stereotactic coordinates of the injection sites were determined based on the anatomical definition of M1 defined by The Mouse Brain in Stereotaxic Coordinates (3rd Edition by Franklin & Paxinos): (1) 1.5mm lateral, (2) 1.7mm lateral and 0.8mm anterior, (3) 2.0mm lateral and 1.6mm anterior to bregma. A 4mm glass coverslip (Warner Instruments) was placed over the cortex and sealed with UV durable dental acrylic (Venus Diamond Flow, Heraeus Kulzer GmbH), followed by the attachment of a metal head bar to the skull with dental acrylic (Paladur, Heraeus Kulzer GmbH), allowing for stable repositioning of the mouse's head underneath the objective. Post-op analgesia (Metacam; 1mg/kg) was administered 12, 24, 48 and 72 hours after surgery. Mice were handled regularly and three weeks following implantation, mice were trained to run head-fixed on a floating treadmill.

For mice that received Riluzole, surgery was performed at P60, as described above. Riluzole (22mg/kg) was administered through drinking water to mimic dosage received by ALS patients (Hogg et al., 2018) daily for 7 days.

For mice that received l2/3 activity dampening treatment, surgery was performed at P30. 300ul of AAV2.hSyn.hM4D(Gi).mCherry (Addgene viral prep # 50475-AAV2, diluted with saline in 1:6) was injected bilaterally at a cortical depth ~100 μm in the following sites to target layer 2/3 of the entire motor cortex: (1) 2.4mm lateral and 1.8mm anterior, (2) 1.1mm lateral and 1.8mm anterior, (3) 1.6mm lateral and 1.1mm anterior to bregma, and (4) 2.4mm lateral and (5) 1.1mm lateral at bregma. Clozapine N-oxide (CNO) was administered daily from P61 to P90 via drinking water (0.04mg/ml in 24ml water with 2% sucrose every 48h for a cage of 2 animals).

In vivo two-photon calcium imaging in anesthetized mice

In anesthetized mice, isoflurane was delivered to the mouse in pure oxygen at a flow rate of ~0.8-1.0L/min. Mice were first given 3vol % isoflurane for ~3 minutes, followed by 1.5% for ~15 minutes and 1.25% for 30 minutes prior to imaging. Breathing rate and body temperature were monitored and maintained in the range of 110-130 breaths per minute and at 37 degrees, respectively, using a physiological monitoring system (Harvard Apparatus). Using a 16x water-immersion objective (Nikon), image series of 20,000 frames (amounting to ~11 minutes) with a field of view of 300 x 300 μm and a resolution of 512 x 512 pixels were acquired within layer 2/3 at a cortical depth of 200-300 μm.

In vivo two-photon calcium imaging in awake behaving head-fixed mice

Four weeks following the cranial window implantation, trained mice were head-fixed and imaged on a two-photon microscope (Hyperscope, Scientifica), equipped with an 8kHz resonant scanner, at frame rates of 30Hz. GCaMP was excited at 910nm with a Ti:Sapphire laser with a DeepSee pre-chirp unit (Spectra Physics MaiTai eHP) and detected by two photomultiplier tubes (Hyperscope, Scentifica) within 500 to 650nm (with 525/50nm and 620/60nm band-pass filters), as described previously (Liebscher et al., 2016; Scekic-Zahirovic et al., 2021). Using a 16x water-immersion objective (Nikon), image series of 15.000 frames (corresponding to ~8 minutes) with a field of view of 300 x 300 μm and a resolution of 512x512 pixels were acquired in both layer 2/3 and 5 at a cortical depth of 200-300 μm and beyond 550 μm, respectively.

Visual flow feedback paradigm

In awake behaving mice, a toroidal screen consisting of curved metal bars and white cardstock was placed in front of the head-fixed mouse. Visual flow of vertical gratings with equal spacing was projected onto a spherical screen (projector: Samsung, SP-F10M) and was coupled to (closed loop, or feedback) the mouse's running velocity. The imaging series consists of two different conditions, (1) feedback (30,000 frames), and (2) darkness (no visual input, 15,000 frames).

Running speed and pupil tracking

In all imaging experiments, running velocity was tracked using an optical mouse sensor (Logitech, G500s Laser Gaming Mouse) and pupil position of the mouse's right eye was recorded with a video camera (The Imaging Source, DMK 22BUC03, USB 2.0 monochrome industrial camera) by custom scripts in LabVIEW (National Instruments). The velocity and pupil size recordings were processed offline using custom scripts in MATLAB (MathWorks).

Post-processing of two-photon calcium imaging data

All imaging recordings were processed and analyzed using custom scripts in MATLAB (Mathworks) as described previously (Liebscher et al., 2016; Scekic-Zahirovic et al., 2021). Briefly, images were corrected for brain displacement due to locomotion and region of interests (ROIs) (corresponding to neuronal somata) were selected based on the mean fluorescent intensity and maximum change projections. Raw activity traces of each neuron are derived from the mean fluorescent intensity of all pixels within a ROI and were low pass filtered at 10Hz. Contamination from neuropil signals, either locally from neurites adjacent to the ROIs or globally from increased fluorescence in a larger area was taken into account using the following equation:

$$F_{ROI\_comp} = F_{ROI} - 0.7 \times F_{neuropil}$$

F_{ROI_comp}, F_{ROI} and $F_{neuropil}$ represents neuropil-compensated fluorescent signal, initial fluorescence signal of the ROI, and signal from the neuropil, respectively. Relative changes in fluorescence ($\Delta F/F$) were computed by dividing F_{ROI_comp} by the median of the "noise band" (baseline). The "noise band" was derived from the standard deviation of the activity trace (which was Fourier transformation with high pass filter at 0 and a low pass filter at 10) divided by the median of activity trace minus 1. The $\Delta F/F$ trace was further filtered (Fourier transformation with high pass filter at 0 and a low pass filter at 0.5) and subtracted by 1. In experiments conducted with

GCaMP6m, a neuron was considered active if there was at least one prominent calcium transient spanning 30 frames (equivalent to 1 second). For experiments conducted with jGCaMP7s, a neuron was considered active if there was at least one prominent calcium transient spanning 40 frames (equivalent to 1.33 seconds). To assess mean activity at each state (i.e. run or quiet wakefulness) , a thresholded trace, in which ΔF/F values smaller than 2x the standard deviation of the "noise band" were set to 0, was used.

Data analysis

Comparing neuronal activity levels under anesthesia and during wakefulness

Neuronal activity, measured as area under curve (AUC), was calculated for the same neurons under anesthesia and in wakefulness using the thresholded activity (at baseline + 2 x standard deviation of the filtered ΔF/F). To compare the change in activity, the following equation was used:

$$\Delta act = act_{anesth} - act_{awake}$$

Neurons were classified according to their activity levels, namely low (0-0.25 transients/min), intermediate (0.25-3 transients/min) and high (>3 transients/min).

k-means clustering of neurons

Only experiments with at least two clear running epochs (i.e. a minimum of 1 sec running within 1.2 seconds) during feedback and two clear running epochs during darkness and with a minimum of 1/8 of the time spent stationary were used for analyses. ΔF/F traces of active neurons were thresholded (2 x standard deviation of the filtered ΔF/F) for *k*-means clustering. The number of clusters was heuristically set to 5. The mean activity during running and stationary epochs was calculated for each neuron in both feedback and darkness sessions, and normalized to the maximum ΔF/F. The normalized ΔF/F values were then used for clustering. K-means clustering was performed using the kmeans function with the squared Euclidean distance as the distance metric in Matlab.

Definition of running-responsive neurons and fraction per FOV

We included experiments with at least three clear running epochs (i.e. a minimum of 1 sec running within 1.2 seconds) and two clear stationary epochs (i.e. a minimum of 1 sec stationary within 1.2

seconds) during feedback and two clear running epochs and one stationary epoch during darkness; as well as 1/8 of the total time spent stationary. To determine running-responsive neurons, we compared their mean activity during locomotion and stationary epochs in the actual data and compared it to a scrambled date set. To this end, we generated binarized running traces, which were randomly circularly shifting by at least 1500 frames (equivalent to 0.83 seconds) 10,000 times to decouple behavior from neuronal activity. For each iteration, we computed an angle between the x-axis and a line formed by the coordinates of the mean activity during the 'scrambled' running and stationary epochs with the [0,0] coordinates (Fig. 5b) using the atan2d function in Matlab:

$$\theta = tan(x, y)$$

where x = mean ΔF/F during stationary *and* y = mean ΔF/F during running.

The 5th percentile of values generated from the scrambled data was set as the threshold for each neuron, and only neurons with an angle greater than the threshold were considered running-responsive (i.e. neurons with higher activity during running phases). The fraction of running-responsive neurons was calculated within each FOV.

Neuronal activity dimensionality and manifold analysis

Principal component analysis (PCA) (PCA, Matlab) was implemented to reduce the dimensionality of the centered and z-scored neuronal activity traces (ΔF/F), acquired during the feedback session (Kato et al, 2015; Lanore et al, 2021). First, n principal components (PCs) and the variance of the original input matrix explained by the respective PCs were derived. To evaluate the strength of correlation between the neuronal population response and the corresponding behavior, linear regression (fitlm, Matlab) was applied to PC1 and the 4 behavioral parameters measured, namely locomotion, an applied air puff, pupil dilation and whisking. To make it comparable between FOVs, neuronal activity recordings were only taken into account when at least one of the four behavioral parameters mentioned above was considered active. In addition, to examine and visualize the structure of the behavior-associated neuronal population response patterns, manifold analysis based on PCA was employed. High-dimensional population response trajectories were mapped into lower three-dimensional PCA space. The manifold subspace was color-coded as a function of velocity, forming two subspaces, one corresponding to quiet wakefulness and the other to locomotion. The center of mass of the respective subspaces was calculated as the mean of the coordinates within each subspace. The Euclidean distance within each subspace was computed as

the mean length of each circle, representing the variance of subspace, to the center of mass. The Euclidean distance across subspaces was computed as distance between the center of mass in each subspace.

Neural decoding

To decode velocity from neuronal activity in M1, we applied a supervised machine learning algorithm based on Random Forest Regression (Huber et al., 2012; Liebscher et al., 2016). In Matlab, treebagger was used with the following parameters: number of trees = 150; method = 'regression'. Experiments from both feedback and darkness sessions were used to train the model separately. The model was trained four times using different parts for training and decoding, and the mean R^2 was computed for each experiment. 2/3 of the data (20,000 frames for feedback, equivalent to ~11 minutes; 10,000 frames for darkness, equivalent to ~5.5 minutes) was used for training and the remaining 1/3 (10,000 frames for feedback, equivalent to ~6 minutes, and 5,000 frames for darkness, equivalent to ~3 minutes) was used to validate the prediction. The chosen beginning of the data used for training was circularly shifted by 5000 frames for feedback and 3750 frames for darkness (that is the total number of frames per session/4) each time, such that a different training and testing sets were used.

Population response to locomotion

Both the velocity and the neuronal calcium traces were downsampled to 6Hz, and for each point in time an average ΔF/F value per ROI was computed and associated with its corresponding instantaneous running velocity.

Behavioral analyses

Measurement of symptom onset

Animals were scored daily with a SOD-score system (0-7) to measure disease progression. A score of 1 signifies symptom onset. Based on deficits detected in the hindlimbs and the rearing behavior in SOD1-G93A tg mice (Hayworth & Gonzalez-Lima, 2009), the SOD-scoring system consists of four parameters that assess these phenotypes. These are hindlimb tremor (0-1), hindlimb extension (0-2), tail elevation (0-2) and rearing (0-2). The first two parameters are measured by lifting the mouse by the tail. Once a tremor is detected in the hindlimbs, a score of 1 is assigned to hindlimb tremor. Upon tail suspension, a score of 0, 1 and 2 is assigned to full extension, partial

extension, and no extension (contracture) of the hindlimbs, respectively. The last two parameters are measured by observing the mouse in a cage for 5 minutes. As the mouse is moving the position of its tail is assessed: if the tail elevates to the level of the head or higher, a score of 0 is assigned. If the tail falls to the ground or the distal section of the tail falls below the level of the head, at least twice, when it is walking, a score of 1 is assigned. If the tail fails to elevate or the distal part of the tail touches the ground the entire time of observation, a score of 2 is assigned. Rearing behavior in a new environment: A score of 0 is given if the mouse displays rearing behavior at least twice within the 5 minutes of observation with full extension of the hindlimbs. A score of 1 is given for partial extension of hindlimbs. A score of 2 is given when no rearing is observed.

Rotarod

Rotarod testing was performed at the symptomatic stage (P120). Prior to the experiment, mice were handled at least every three days during the behavioral experimental phase (twice a week minimum). They were accustomed to the setup by training on the rod at constant speed (5 rpm) until they managed to stay on it for at least a minute. The test was then conducted on two consecutive days, with 4 trials per day and a 5-minute break between trials in acceleration mode (5-40 rpm within 5 min).

Statistics

Data was tested for normality using the Lilliefors test in Matlab. Normally distributed data was probed for significance by the Student's unpaired *t*-test, while the Wilcoxon rank sum test was used for non-normally distributed data, unless otherwise specified. Mean ± standard error of the mean (SEM) was plotted for normally distributed data, and median + 95% confidence interval (CI) for non-normally distributed data, unless otherwise specified. To test significance of the data distribution, either a two-sample Kolmogorov-Smirnov test or two-way ANOVA on binned data was used. For the sensorimotor clusters and behavioral analyses related to chemogenetic inhibition of layer 2/3 activity, statistics were performed in prism. First, data was tested for normality using D'Agostino-Pearson omnibus test, followed by outlier detection with Grubb's test (alpha=0.1). All tests reject the null hypothesis at the 5% significance level.

Author contributions

V.K. and E.L. performed *in vivo* two-photon calcium imaging. E.L. and L.Z. performed behavioral experiments. E.L., L.Z. and S.J. performed histology, immunohistochemistry and confocal imaging. X.Y. performed the manifold analysis. V.K. performed behavioral analysis. V.K. and S.L. designed and coordinated experiments, as well as wrote the manuscript.

References

Anderson, C. T., Sheets, P. L., Kiritani, T., & Shepherd, G. M. (2010). Sublayer-specific microcircuits of corticospinal and corticostriatal neurons in motor cortex. *Nature neuroscience*, *13*(6), 739.

Ayaz, A., Saleem, A. B., Schölvinck, M. L., & Carandini, M. (2013). Locomotion controls spatial integration in mouse visual cortex. *Current Biology*, *23*(10), 890-894.

Bernacchia, A. (2014). The interplay of plasticity and adaptation in neural circuits: a generative model. *Frontiers in Synaptic Neuroscience*, *6*, 26.

Bharmauria, V., Ouelhazi, A., Lussiez, R., & Molotchnikoff, S. (2022). Adaptation-induced plasticity in the sensory cortex. *Journal of Neurophysiology*, *128*(4), 946-962.

Bhatt, D. H., Zhang, S., & Gan, W.-B. (2009). Dendritic spine dynamics. *Annual review of physiology*, *71*, 261-282.

Blumenstock, S., Sun, F., Klaus, C., Marinković, P., Sgobio, C., Paeger, L., Liebscher, S., & Herms, J. (2021). Cortical circuit dysfunction in a mouse model of alpha-synucleinopathy in vivo. *Brain communications*, *3*(4), fcab273.

Burgold, J., Schulz-Trieglaff, E. K., Voelkl, K., Gutierrez-Angel, S., Bader, J. M., Hosp, F., Mann, M., Arzberger, T., Klein, R., Liebscher, S., & Dudanova, I. (2019). Cortical circuit alterations precede motor impairments in Huntington's disease mice. *Sci Rep*, *9*(1), 6634. https://doi.org/10.1038/s41598-019-43024-w

Busche, M. A. (2018). In vivo two-photon calcium imaging of hippocampal neurons in Alzheimer mouse models. In *Biomarkers for Alzheimer's Disease Drug Development* (pp. 341-351). Springer.

Cengiz, B., Fidanci, H., Kiyak Keceli, Y., Baltaci, H., & KuruoGlu, R. (2019). Impaired short- and long-latency afferent inhibition in amyotrophic lateral sclerosis. *Muscle Nerve*, *59*(6), 699-704. https://doi.org/10.1002/mus.26464

Cengiz, B., & Kuruoğlu, R. (2020). A new parameter to discriminate amyotrophic lateral sclerosis patients from healthy participants by motor cortical excitability changes. *Muscle & Nerve*, *61*(3), 354-362.

Clancy, K. B., Orsolic, I., & Mrsic-Flogel, T. D. (2019). Locomotion-dependent remapping of distributed cortical networks. *Nature neuroscience*, *22*(5), 778-786.

Clark, R. M., Brizuela, M., Blizzard, C. A., & Dickson, T. C. (2018). Reduced Excitability and Increased Neurite Complexity of Cortical Interneurons in a Familial Mouse Model of Amyotrophic Lateral Sclerosis. *Frontiers in cellular neuroscience*, *12*, 328. https://doi.org/10.3389/fncel.2018.00328

Commisso, B., Ding, L., Varadi, K., Gorges, M., Bayer, D., Boeckers, T. M., Ludolph, A. C., Kassubek, J., Müller, O. J., & Roselli, F. (2018). Stage-dependent remodeling of projections to motor cortex in ALS mouse model revealed by a new variant retrograde-AAV9. *Elife*, *7*, e36892. https://doi.org/10.7554/eLife.36892

Doble, A. (1996). The pharmacology and mechanism of action of riluzole. *Neurology*, *47*(6 Suppl 4), 233S-241S.

Foerster, B. R., Callaghan, B. C., Petrou, M., Edden, R. A., Chenevert, T. L., & Feldman, E. L. (2012). Decreased motor cortex gamma-aminobutyric acid in amyotrophic lateral sclerosis. *Neurology*, *78*(20), 1596-1600. https://doi.org/10.1212/WNL.0b013e3182563b57

Foerster, B. R., Pomper, M. G., Callaghan, B. C., Petrou, M., Edden, R. A., Mohamed, M. A., Welsh, R. C., Carlos, R. C., Barker, P. B., & Feldman, E. L. (2013). An imbalance between excitatory and inhibitory neurotransmitters in amyotrophic lateral sclerosis revealed by use of 3-T proton magnetic resonance spectroscopy. *JAMA Neurol*, *70*(8), 1009-1016. https://doi.org/10.1001/jamaneurol.2013.234

Fogarty, M. J., Klenowski, P. M., Lee, J. D., Drieberg-Thompson, J. R., Bartlett, S. E., Ngo, S. T., Hilliard, M. A., Bellingham, M. C., & Noakes, P. G. (2016a). Cortical synaptic and dendritic spine abnormalities in a presymptomatic TDP-43 model of amyotrophic lateral sclerosis. *Sci Rep*, *6*, 37968. https://doi.org/10.1038/srep37968

Fogarty, M. J., Mu, E. W., Noakes, P. G., Lavidis, N. A., & Bellingham, M. C. (2016b). Marked changes in dendritic structure and spine density precede significant neuronal death in vulnerable cortical

pyramidal neuron populations in the SOD1(G93A) mouse model of amyotrophic lateral sclerosis. *Acta Neuropathol Commun*, *4*(1), 77. https://doi.org/10.1186/s40478-016-0347-y

Fogarty, M. J., Noakes, P. G., & Bellingham, M. C. (2015). Motor cortex layer V pyramidal neurons exhibit dendritic regression, spine loss, and increased synaptic excitation in the presymptomatic hSOD1(G93A) mouse model of amyotrophic lateral sclerosis. *J Neurosci*, *35*(2), 643-647. https://doi.org/10.1523/jneurosci.3483-14.2015

Fu, Y., Tucciarone, J. M., Espinosa, J. S., Sheng, N., Darcy, D. P., Nicoll, R. A., Huang, Z. J., & Stryker, M. P. (2014). A cortical circuit for gain control by behavioral state. *Cell*, *156*(6), 1139-1152.

Galvan, A., Kuwajima, M., & Smith, Y. (2006). Glutamate and GABA receptors and transporters in the basal ganglia: what does their subsynaptic localization reveal about their function? *Neuroscience*, *143*(2), 351-375.

Genc, B., Gozutok, O., Kocak, N., & Ozdinler, P. H. (2020). The timing and extent of motor neuron vulnerability in ALS correlates with accumulation of misfolded SOD1 protein in the cortex and in the spinal cord. *Cells*, *9*(2), 502.

Genç, B., Jara, J. H., Lagrimas, A. K., Pytel, P., Roos, R. P., Mesulam, M., Geula, C., Bigio, E. H., & Özdinler, P. H. (2017). Apical dendrite degeneration, a novel cellular pathology for Betz cells in ALS. *Scientific reports*, *7*(1), 1-10.

Gunes, Z. I., Kan, V. W. Y., Ye, X., & Liebscher, S. (2020). Exciting Complexity: The Role of Motor Circuit Elements in ALS Pathophysiology. *Front Neurosci*, *14*, 573. https://doi.org/10.3389/fnins.2020.00573

Haidar, M., Viden, A., Cuic, B., Wang, T., Rosier, M., Tomas, D., Mills, S. A., Govier-Cole, A., Djouma, E., Luikinga, S., Rytova, V., Barton, S. K., Gonsalvez, D. G., Palmer, L. M., McLean, C., Kiernan, M. C., Vucic, S., & Turner, B. J. (2021). Cortical hyperexcitability drives dying forward ALS symptoms and pathology in mice. *bioRxiv*, 2021.2008.2013.456320. https://doi.org/10.1101/2021.08.13.456320

Hayworth, C., & Gonzalez-Lima, F. (2009). Pre-symptomatic detection of chronic motor deficits and genotype prediction in congenic B6. SOD1G93A ALS mouse model. *Neuroscience*, *164*(3), 975-985.

Heindorf, M., Arber, S., & Keller, G. B. (2018). Mouse motor cortex coordinates the behavioral response to unpredicted sensory feedback. *Neuron*, *99*(5), 1040-1054. e1045.

Hogg, M. C., Halang, L., Woods, I., Coughlan, K. S., & Prehn, J. H. (2018). Riluzole does not improve lifespan or motor function in three ALS mouse models. *Amyotrophic Lateral Sclerosis and Frontotemporal Degeneration*, *19*(5-6), 438-445.

Howe, M., Ridouh, I., Mascaro, A. L. A., Larios, A., Azcorra, M., & Dombeck, D. A. (2019). Coordination of rapid cholinergic and dopaminergic signaling in striatum during spontaneous movement. *Elife*, *8*, e44903.

Huber, D., Gutnisky, D. A., Peron, S., O'connor, D. H., Wiegert, J. S., Tian, L., Oertner, T. G., Looger, L. L., & Svoboda, K. (2012). Multiple dynamic representations in the motor cortex during sensorimotor learning. *Nature*, *484*(7395), 473-478.

Jara, J. H., Sheets, P. L., Nigro, M. J., Perić, M., Brooks, C., Heller, D. B., Martina, M., Andjus, P. R., & Ozdinler, P. H. (2020). The electrophysiological determinants of corticospinal motor neuron vulnerability in ALS. *Frontiers in molecular neuroscience*, *13*, 73.

Khademullah, C. S., Aqrabawi, A. J., Place, K. M., Dargaei, Z., Liang, X., Pressey, J. C., Bedard, S., Yang, J. W., Garand, D., & Keramidis, I. (2020). Cortical interneuron-mediated inhibition delays the onset of amyotrophic lateral sclerosis. *Brain*, *143*(3), 800-810.

Kiernan, M. C., Vucic, S., Cheah, B. C., Turner, M. R., Eisen, A., Hardiman, O., Burrell, J. R., & Zoing, M. C. (2011). Amyotrophic lateral sclerosis. *The Lancet*, *377*(9769), 942-955. https://doi.org/10.1016/S0140-6736(10)61156-7

Kim, J.-E., Kim, D.-S., Kwak, S.-E., Choi, H.-C., Song, H.-K., Choi, S.-Y., Kwon, O.-S., Kim, Y.-I., & Kang, T.-C. (2007). Anti-glutamatergic effect of riluzole: comparison with valproic acid. *Neuroscience*, *147*(1), 136-145.

Kim, J., Hughes, E. G., Shetty, A. S., Arlotta, P., Goff, L. A., Bergles, D. E., & Brown, S. P. (2017). Changes in the Excitability of Neocortical Neurons in a Mouse Model of Amyotrophic Lateral Sclerosis Are Not Specific to Corticospinal Neurons and Are Modulated by Advancing Disease. *J Neurosci*, *37*(37), 9037-9053. https://doi.org/10.1523/jneurosci.0811-17.2017

Kiritani, T., Wickersham, I. R., Seung, H. S., & Shepherd, G. M. (2012). Hierarchical connectivity and connection-specific dynamics in the corticospinal–corticostriatal microcircuit in mouse motor cortex. *Journal of Neuroscience*, *32*(14), 4992-5001.

Lamanauskas, N., & Nistri, A. (2008). Riluzole blocks persistent Na+ and Ca2+ currents and modulates release of glutamate via presynaptic NMDA receptors on neonatal rat hypoglossal motoneurons in vitro. *European Journal of Neuroscience*, *27*(10), 2501-2514.

Lei, H., Dirren, E., Poitry-Yamate, C., Schneider, B. L., Gruetter, R., & Aebischer, P. (2019). Evolution of the neurochemical profiles in the G93A-SOD1 mouse model of amyotrophic lateral sclerosis. *Journal of cerebral blood flow and metabolism : official journal of the International Society of Cerebral Blood Flow and Metabolism*, *39*(7), 1283–1298. https://doi.org/10.1177/0271678x18756499

Liebscher, S., Keller, G. B., Goltstein, P. M., Bonhoeffer, T., & Hubener, M. (2016). Selective Persistence of Sensorimotor Mismatch Signals in Visual Cortex of Behaving Alzheimer's Disease Mice. *Curr Biol*, *26*(7), 956-964. https://doi.org/10.1016/j.cub.2016.01.070

Lindenbach, D., Conti, M. M., Ostock, C. Y., George, J. A., Goldenberg, A. A., Melikhov-Sosin, M., Nuss, E. E., & Bishop, C. (2016). The role of primary motor cortex (M1) glutamate and GABA signaling in l-DOPA-induced dyskinesia in Parkinsonian rats. *Journal of Neuroscience*, *36*(38), 9873-9887.

Maier, M., Welt, T., Wirth, F., Montrasio, F., Preisig, D., McAfoose, J., Vieira, F. G., Kulic, L., Späni, C., & Stehle, T. (2018). A human-derived antibody targets misfolded SOD1 and ameliorates motor symptoms in mouse models of amyotrophic lateral sclerosis. *Science translational medicine*, *10*(470), eaah3924.

Menon, P., Geevasinga, N., van den Bos, M., Yiannikas, C., Kiernan, M. C., & Vucic, S. (2017). Cortical hyperexcitability and disease spread in amyotrophic lateral sclerosis. *Eur J Neurol*, *24*(6), 816-824. https://doi.org/10.1111/ene.13295

Menon, P., Kiernan, M. C., & Vucic, S. (2015). Cortical hyperexcitability precedes lower motor neuron dysfunction in ALS. *Clinical neurophysiology : official journal of the International Federation of Clinical Neurophysiology*, *126*(4), 803–809. https://doi.org/10.1016/j.clinph.2014.04.023

Mitchell, H. A., Ahern, T. H., Liles, L. C., Javors, M. A., & Weinshenker, D. (2006). The effects of norepinephrine transporter inactivation on locomotor activity in mice. *Biological psychiatry*, *60*(10), 1046-1052.

Özdinler, P. H., Benn, S., Yamamoto, T. H., Güzel, M., Brown, R. H., & Macklis, J. D. (2011). Corticospinal motor neurons and related subcerebral projection neurons undergo early and specific neurodegeneration in hSOD1G93A transgenic ALS mice. *Journal of Neuroscience*, *31*(11), 4166-4177.

Pakan, J. M., Lowe, S. C., Dylda, E., Keemink, S. W., Currie, S. P., Coutts, C. A., & Rochefort, N. L. (2016). Behavioral-state modulation of inhibition is context-dependent and cell type specific in mouse visual cortex. *Elife*, *5*.

Peters, A. J., Lee, J., Hedrick, N. G., O'Neil, K., & Komiyama, T. (2017). Reorganization of corticospinal output during motor learning. *Nature neuroscience*, *20*(8), 1133-1141.

Runge, K., Cardoso, C., & De Chevigny, A. (2020). Dendritic spine plasticity: function and mechanisms. *Frontiers in Synaptic Neuroscience*, *12*, 36.

Saba, L., Viscomi, M., Caioli, S., Pignataro, A., Bisicchia, E., Pieri, M., Molinari, M., Ammassari-Teule, M., & Zona, C. (2016). Altered functionality, morphology, and vesicular glutamate transporter expression of cortical motor neurons from a presymptomatic mouse model of amyotrophic lateral sclerosis. *Cerebral cortex*, *26*(4), 1512-1528.

Scekic-Zahirovic, J., Sanjuan-Ruiz, I., Kan, V., Megat, S., De Rossi, P., Dieterle, S., Cassel, R., Jamet, M., Kessler, P., Wiesner, D., Tzeplaeff, L., Demais, V., Sahadevan, S., Hembach, K. M., Muller, H. P., Picchiarelli, G., Mishra, N., Antonucci, S., Dirrig-Grosch, S., . . . Dupuis, L. (2021). Cytoplasmic

FUS triggers early behavioral alterations linked to cortical neuronal hyperactivity and inhibitory synaptic defects. *Nat Commun*, *12*(1), 3028. https://doi.org/10.1038/s41467-021-23187-9

Shepherd, G. M. (2013). Corticostriatal connectivity and its role in disease. *Nature Reviews Neuroscience*, *14*(4), 278-291.

Shibuya, K., Simon, N. G., Geevasinga, N., Menon, P., Howells, J., Park, S. B., Huynh, W., Noto, Y.-i., Vucic, S., & Kiernan, M. C. (2017). The evolution of motor cortical dysfunction in amyotrophic lateral sclerosis. *Clinical Neurophysiology*, *128*(6), 1075-1082.

Siciliano, G., Manca, M. L., Sagliocco, L., Pastorini, E., Pellegrinetti, A., Sartucci, F., Sabatini, A., & Murri, L. (1999). Cortical silent period in patients with amyotrophic lateral sclerosis. *Journal of the neurological sciences*, *169*(1-2), 93-97.

Takamura, R., Mizuta, K., Sekine, Y., Islam, T., Saito, T., Sato, M., Ohkura, M., Nakai, J., Ohshima, T., & Saido, T. C. (2021). Modality-Specific impairment of hippocampal CA1 neurons of Alzheimer's disease model mice. *Journal of Neuroscience*, *41*(24), 5315-5329.

Turner, M. R., Osei-Lah, A. D., Hammers, A., Al-Chalabi, A., Shaw, C. E., Andersen, P. M., Brooks, D. J., Leigh, P. N., & Mills, K. R. (2005). Abnormal cortical excitability in sporadic but not homozygous D90A SOD1 ALS. *J Neurol Neurosurg Psychiatry*, *76*(9), 1279-1285. https://doi.org/10.1136/jnnp.2004.054429

Van den Bos, M. A., Higashihara, M., Geevasinga, N., Menon, P., Kiernan, M. C., & Vucic, S. (2018). Imbalance of cortical facilitatory and inhibitory circuits underlies hyperexcitability in ALS. *Neurology*, *91*(18), e1669-e1676.

Vucic, S., Nicholson, G. A., & Kiernan, M. C. (2008). Cortical hyperexcitability may precede the onset of familial amyotrophic lateral sclerosis. *Brain*, *131*(Pt 6), 1540-1550. https://doi.org/10.1093/brain/awn071

Wright, A. L., Della Gatta, P. A., Le, S., Berning, B. A., Mehta, P., Jacobs, K. R., Gul, H., San Gil, R., Hedl, T. J., & Riddell, W. R. (2021). Riluzole does not ameliorate disease caused by cytoplasmic TDP-43 in a mouse model of amyotrophic lateral sclerosis. *European Journal of Neuroscience*, *54*(6), 6237-6255.

Zanette, G., Tamburin, S., Manganotti, P., Refatti, N., Forgione, A., & Rizzuto, N. (2002). Changes in motor cortex inhibition over time in patients with amyotrophic lateral sclerosis. *J Neurol*, *249*(12), 1723-1728. https://doi.org/10.1007/s00415-002-0926-7

Zang, D. W., & Cheema, S. (2002). Degeneration of corticospinal and bulbospinal systems in the superoxide dismutase 1G93A G1H transgenic mouse model of familial amyotrophic lateral sclerosis. *Neuroscience letters*, *332*(2), 99-102.

Zhang, W., Zhang, L., Liang, B., Schroeder, D., Zhang, Z. W., Cox, G. A., Li, Y., & Lin, D. T. (2016). Hyperactive somatostatin interneurons contribute to excitotoxicity in neurodegenerative disorders. *Nat Neurosci*, *19*(4), 557-559. https://doi.org/10.1038/nn.4257

Ziemann, U., Winter, M., Reimers, C. D., Reimers, K., Tergau, F., & Paulus, W. (1997). Impaired motor cortex inhibition in patients with amyotrophic lateral sclerosis: evidence from paired transcranial magnetic stimulation. *Neurology*, *49*(5), 1292-1298.

4. Discussion

In this doctoral thesis, I investigated neuronal activity in motor cortex of two transgenic mouse models of ALS, and could identify, cellular *sources* contributing to cortical hyperexcitability typical of ALS. The findings of my thesis are shared in one published (Scekic-Zahirovic et al., 2021) and one unpublished (Kan et al.) manuscript.

4.1 Investigating cortical functional impairment in neurodegenerative diseases by *in vivo* two-photon calcium imaging

Glutamate excitotoxicity, that is the toxic impact of excess glutamatergic stimulation mainly on neurons, has been proposed to be involved in various neurodegenerative diseases (Armada-Moreira et al., 2020; Lewerenz & Maher, 2015). Effects of corresponding treatment options such as Riluzole and Memantine, targeting glutamate excitotoxicity in Amyotrophic Lateral Sclerosis (ALS) and Alzheimer's Disease (AD), respectively, have been shown to be limited (Esposito et al., 2013; Obrenovitch, 1998). This is likely due to our lack of insight at the molecular, cellular and circuit level and potential homeostatic mechanisms, which could mitigate long-term beneficial effects of anti-glutamatergic treatments. In ALS, glutamate-mediated excitotoxicity has been linked to upper and lower motor neuron degeneration (Armada-Moreira et al., 2020; Rothstein, 1995; Van Den Bosch et al., 2006), but the underlying mechanisms driving glutamate excess in neurodegenerative diseases and ALS in particular remain incompletely understood. One common feature shared by various forms of ALS that might likely be linked to excitotoxicity is cortical hyperexcitability (Bae et al., 2013). Classically, cortical hyperexcitability is measured by transcranial magnetic stimulation (TMS) studies in which the motor cortex is stimulated through electromagnetic induction and simultaneously motor evoked potentials (MEP) of the innervated muscle are recorded.

Parameters that reflect increased excitation and reduced inhibition in motor cortex, include reduced resting motor threshold (RMT), increased intracortical facilitation (ICF), reduced short-interval intracortical inhibition (SICI) and shortened cortical silent period (CSP) (Cengiz et al., 2019; Cengiz & Kuruoğlu, 2020; Menon et al., 2017; Menon et al., 2015; Shibuya et al., 2017; Siciliano et al., 1999; Van den Bos et al., 2018; Vucic et al., 2009; Vucic et al., 2008; Zanette et al., 2002a). Though TMS studies demonstrated cortical hyperexcitability as a result of the combined increase in excitation and reduced inhibition, these findings do not allow any conclusions on the cellular or circuit *source* of cortical hyperexcitability.

Our work in two mouse models of ALS revealed both a) a hyperactivity of neurons in motor cortex in Fus$^{\Delta NLS/+}$ mice that is likely caused by defects in (inhibitory) synapses (Scekic-Zahirovic et al., 2021) and b) neuronal hyperresponsiveness to locomotion in SOD1^{G93A} mice that originates in upstream layer 2/3 (Kan et al.). More specifically, in the first paper (Scekic-Zahirovic et al., 2021), I assessed neuronal activity in motor cortex of Fus$^{\Delta NLS/+}$ mice at the age of 4-month-old and 10-month- thus prior to the development of overt neuromuscular deficits - under isoflurane anesthesia. Using *in vivo* two-photon calcium imaging, I showed that there is an increase in the fraction of active cells at 10 months and an increase in transient frequency at both 4 months and 10 months, suggesting neuronal hyperactivity in motor cortex. To identify the mechanisms of neuronal hyperexcitability, we, together with our collaborators, identified synaptic deficits, most prominently of inhibitory synapses, which could explain the observed aberrant neuronal activity and behavioral alterations in the presence of cytoplasmic FUS mislocalization. Specifically, RNAseq of frontal cortex from 5-month and 22-month old Fus$^{\Delta NLS/+}$ mice showed that genes related to physiology and development of GABAergic and glutamatergic synapses were downregulated, accompanied with more pronounced ultrastructural changes in inhibitory synapses. To further investigate alterations identified in inhibitory synapses, synaptosomal fractionation of 5-month-old frontal cortex revealed FUS accumulation in mRNAs crucial for synaptic function, especially in inhibitory synapses. Taken

together, Scekic-Zahirovic et al. showed hyperactivity in motor cortex and abnormal changes in social and motor behavior, most likely due to more pronounced defects in inhibitory synapses that are related to FUS accumulation in the synapses.

In the second manuscript (Kan et al.), I first show that there are also hyperactive neurons in M1 of early-symptomatic SOD1^{G93A} mice, which display increased synchrony when conducting in vivo two-photon calcium imaging under isoflurane anesthesia. However, little is known about how these neurons behave during wakefulness. Anesthesia can have various effects on diverse neuronal cell types, which are also dose-dependent (Hao et al., 2020). It is thus possible that anesthesia can dampen neuronal activity in general but it could also unmask changes in neuronal excitability, as it is known that the inhibitory drive is higher during wakefulness (Niethard et al., 2016; Poulet & Crochet, 2019). Moreover, alterations in excitability or activity can be compensatory in response to i.e. reduced synaptic input (Joseph & Turrigiano, 2017; Turrigiano, 2011; Turrigiano, 2008). Together, it is thus not clear whether altered neuronal activity identified under anesthesia would persist during wakefulness (Pan et al., 2018; Zanette et al., 2002b). Changes in brain states do not only occur through the induction of anesthesia, but can occur with behavior, such as locomotion (Poulet & Crochet, 2019). To thus be able to interpret neuronal activity levels during wakefulness one also needs to take into account behavioral changes and sensory stimulation. I thus imaged the same neurons in behaving mice in a visual-flow feedback paradigm. I show that there is a partial coherence in the activity levels under anesthesia and during wakefulness (i.e. neurons that are more active under anesthesia might be less active in wakefulness, and vice versa). This means activity and response properties of neurons are mediated by behavioral changes and sensory stimulation, which is crucial to studying cortical dysfunction in neurodegenerative diseases. Specifically, I found less activity change from anesthesia to wakefulness in SOD1^{G93A} mice (i.e. more activity during wakefulness), accompanied with a higher proportion of less active neurons remaining in the

same activity category during wakefulness. The partial activity coherence could potentially unmask higher excitability levels in M1 of SOD1^{G93A} mice. When characterizing locomotion-associated activity, we surprisingly revealed an increase in neuronal activity only in layer 2/3 during the pre-symptomatic stage, which is later seen in both layer 2/3 and 5 in early-symptomatic mice. Notably, pyramidal neurons in cortical layer 2/3 are the prime input source of layer 5 neurons, which also encompass upper motor neurons. We thus conclude that cortical hyperexcitability at least in part is based on cortical layer 2/3 hyperexcitability and that UMN receive excessive glutamatergic stimulation from upstream layer 2/3 neurons, proposing a strong non-cell autonomous component in the development of cortical hyperexcitability, UMN dysfunction and subsequent degeneration.

4.2 Sensorimotor integration in M1

Previous work has already highlighted that different neuronal populations amongst the corticospinal neurons exist in M1, which can be separated by their responsiveness to defined behavioral features. Identified populations are (limb) movement-responsive, indiscriminately – active, quiescence – active neurons (Peters et al., 2017), but also more specifically neurons responsive to touch (sensory input) or motor output (whisking, licking (Huber et al., 2012)). I now add to this knowledge by demonstrating that visual input is also determining responses in M1. As such, I found neurons whose activity related to locomotion was modified by the presence or absence of visual input, arguing for visuomotor integration taking place in M1 (Kan et al.). Visuomotor integration has thus far been mainly studied in visual cortex, demonstrating that locomotion can increase the gain to visual input by differentially modifying interneuronal subtypes (Busse, 2018; Pakan et al., 2016; Yamawaki et al., 2021). I identified five distinct neuronal populations characterized by their average activity to locomotion during different conditions, namely neurons responsive to (i) running in general, (ii) running with feedback, (iii)

running in darkness, (iv) all conditions and (v) quiet wakefulness. These neuronal subtypes occur at different frequencies in SOD1^{G93A} mice. I detected an increase in the fraction of neurons that are more active during running in darkness in layer 2/3 and fewer neurons that are spontaneously active (that is active during quiescence). As interneurons have previously been shown to play a vital role in visuomotor integration in visual cortex (Busse, 2018; Dadarlat & Stryker, 2017; Erisken et al., 2014; Pakan et al., 2016), it is possible that their involvement in the cortical dysfunction in ALS can explain the differences detected in SOD1^{G93A} mice. In ALS, there is evidence of hypoactive PV and hyperactive SST (Khademullah et al., 2020; Zhang et al., 2016) interneurons, both of which could also modify the response of pyramidal neurons to locomotion in the absence or presence of visual input. Hyperactive SST would inhibit PV, which are also found to be hypoactive in ALS, and thus releasing inhibition on UMN (Zhang et al., 2016).

4.3 The role of non-cell-autonomous mechanisms underlying neurodegeneration in ALS

The variability seen in presented symptoms, site of onset, extent of involvement from upper and lower motor neurons and progression rate in ALS, suggest possible diverging circuit mechanisms that underlie neurodegeneration. The diversity is already evident at the level of the dominantly involved protein. While in other neurodegenerative diseases, such as AD and Huntington's disease (HD), one central protein, namely amyloid-beta (Ab) for AD and huntingtin for HD, contributes to the abnormal aggregation in the brain (Ross & Poirier, 2004), in ALS several proteins, namely TDP-43, SOD1 and FUS have been shown to accumulate and aggregate within the cytoplasm of cells (Blokhuis et al., 2013). These differences could also result in different disease pathology and thus therapeutic approaches.

Despite the different pathways underlying protein aggregation and the resulting pathology in ALS, cortical hyperexcitability remains a consistent finding in ALS patients (TMS studies that included both fALS and sALS patients), which can be caused by deficits in numerous circuit elements, which include different neuronal populations, such as PNs and INs, and neuromodulators.

4.3.1. Structural and functional changes in the major source of input to UMN: layer 2/3

Our study revealed cortical layer- and disease stage-specific changes in SOD1^{G93A} tg mice. More precisely, increased locomotion-associated neuronal activity was first detected in layer 2/3 of pre-symptomatic mice, which was later identified in both layer 2/3 and 5 of early-symptomatic mice. Pathology (i.e. expression of phosphorylated neurofilament (PNF) in PN and glial fibrillary acidic protein (GFAP) in astrocytes) and structural changes (i.e. apical spine loss and dendritic regression) in layer 2/3 PNs were detected in both post-mortem motor cortex tissue of ALS patients (Sasaki & Maruyama, 1994), as well as in SOD1^{G93A} tg mice (Fogarty et al., 2016b). Dendrites are the main site of excitatory input to the PNs and their arborization pattern determines the synaptic input field of the dendrite (Arikkath, 2012; Spruston, 2008). In addition to perisomatic excitatory input, both layer 2/3 and 5 PNs receive long-range cortical and thalamic input onto distal apical dendrites in layer 1, while layer 2/3 PNs also receive input onto basal dendrites below the soma (Hooks et al., 2013; Rubio-Garrido et al., 2009). Dendritic spine density and dendritic arborization are critical determinants of synaptic input and network connectivity and play are role for neuronal plasticity (Arikkath, 2012; Chen et al., 2011; Citri & Malenka, 2008; Dao Duc et al., 2015; Jia et al., 2010).

In addition, there are layer-specific differences in spine density and dynamics during development as well as motor and sensory-related experiences (Tjia et al., 2017). For instance, spine density and dynamics of layer 2/3 PNs are higher than that of layer 5 neurons and motor skill learning and neonatal sensory deprivation result in higher spine dynamics in layer 5 PNs, arguing for layer-specific connectivity changes (Tjia et al., 2017). The changes seen in spine dynamics during motor learning coincide with the dynamic activity changes seen in layer 5 and stable activity pattern in layer 2/3 (Peters et al., 2017; Steffens et al., 2021), which is in line with the notion that synaptic activity regulates spine dynamics (Bloodgood & Sabatini, 2005; van Zundert et al., 2008). Therefore, spine loss on apical dendrites of layer 2/3 PNs of SOD1[G93A] mice could be a result of homeostatic structural plasticity in response to increased (long-range) input, such as ipsilateral somatosensory cortex and thalamus, detected in early-symptomatic SOD1[G93A] tg mice (Commisso et al., 2018) and evidenced by the increased excitatory postsynaptic current (EPSC) of layer 5 PNs (Fogarty et al., 2015a).

Another explanation for increased activity in layer 2/3 is compromised inhibition, namely inhibitory synaptic defects and excitability changes in interneurons (discussed above). Inhibitory synapses can be found on various parts of a neuron, namely the soma, dendrites, spines and axons, and axo-somatic synapses exert the strongest inhibition on the post-synaptic neuron (Kubota et al., 2016). γ-aminobutyric acid A (GABAA) receptors are known to mediate fast inhibitory transmission (Miyazaki et al., 2021). Despite the increased EPSC detected (discussed above), there are no compensatory increase in the inhibitory postsynaptic current (IPSC) (Fogarty et al., 2016a; Fogarty et al., 2015b). Additionally, inhibitory synaptic defects were detected in layer 2/3 of *Fus*[ΔNLS/+] mice using various techniques (Sahadevan et al., 2021; Scekic-Zahirovic et al., 2021). These changes include the downregulation of genes associated with physiology and development of synapses, ultrastructural deficits in inhibitory synapses, enhanced cytoplasmic mislocalization of FUS in PV INs and increased FUS accumulation in

synaptosomes (Sahadevan et al., 2021; Scekic-Zahirovic et al., 2021). In particular, the downregulation of gene and protein expression of inhibitory synaptic markers in the pre-synapse, namely vesicular GABA transporter (VGAT), and on the post-synapse, namely Gephyrin and GABAA receptors, suggest that both pyramidal and interneurons are affected (Scekic-Zahirovic et al., 2021).

In ALS patients, transcriptomic studies revealed dysregulated gene expression involved in pathways such as synaptic vesicle cycle and endoplasmic reticulum protein processing are found in excitatory neurons across layer 2 to 6 in ALS patients (Pineda et al., 2021). More importantly, there is a higher expression of synaptic genes in upper layer PNs while deeper layer PNs have a higher expression of genes involved in pathways such as protein folding and degradation (Limone et al., 2021). The molecular, structural and functional changes detected in layer 2/3 PNs at the pre-symptomatic stage further strengthen the argument that anomalies are detected upstream of layer 5 and that changes might be layer specific.

In summary, our data together with existing findings argue for increased input onto layer 5 neurons, including UMN, resulting from both increased excitation and compromised inhibition, causing neuronal dysfunction in ALS. This notion is further strengthened by Haidar et al. (Haidar et al., 2021), in which cortical hyperexcitability induced by chronic chemogenetic activation of motor cortex resulted in both cortical, spinal and motor TDP pathology and motor symptoms typical of ALS (Haidar et al., 2021). While it is evident that cortical hyperexcitability drives neuronal degeneration such as the formation of protein aggregates and cell death, the function of neurons and network integrity in M1 during the course of ALS remain unknown. Our study reveals functional impairments, namely hyperactivity under anesthesia and hyperresponsiveness to locomotion, in both layer 2/3 and 5 of M1, in which changes were first detected in layer 2/3 during the pre-symptomatic changes.

4.3.2. Circuit mechanisms underlying locomotion-associated hyperresponsiveness in ALS

In addition to local excitation and inhibition, neuromodulators such as norepinephrine (NE), dopamine (DA) and acetylcholine (ACh) are known to modulate locomotion-driven neuronal activity (Drenan et al., 2010; Howe et al., 2019; Mitchell et al., 2006). Decreased NE levels reduce spontaneous locomotion, with the exception that reduced levels of both NE and DA increases spontaneous locomotion in tg mice (Mitchell et al., 2006). Moreover, ACh release peaks at the transition between stationary and movement initiation, while DA levels increases during locomotion (Howe et al., 2019). These studies show that complex neuromodulatory input regulates locomotion and each system might play a different role. Though little is known about NE changes in ALS, positron emission tomography and single photon emission computed tomography in ALS patients as well as neurochemical studies in SOD1^{G93A} mice revealed deficits in the dopaminergic (Borasio et al., 1998; Takahashi et al., 1993) and cholinergic (Crochemore et al., 2005) system. These deficits involve the downregulation of cholinergic enzyme choline acetyltransferase (ChAT), that could explain the increased spontaneous locomotor activity seen in *Fus*$^{\Delta NLS/+}$ mice. The increased spontaneous locomotor activity could be a result of reduction of NE and DA and an increase in ACh.

Given that locomotion is modulated by local and long-range inputs, hyperresponsiveness to locomotion could be explained by deficits in connectivity between M1 and other brain regions. Responsiveness of a neuron refers to the increase in activity associated with the stimuli, which in this case is locomotion. Indeed, decreased functional connectivity is observed between sensorimotor cortex (S1) and cerebellum in ALS patients (Barry et al., 2021), suggesting impaired information processing and relay of motor signal. The reduced connectivity could dampen feedforward inhibition from the cerebellum to M1 (Nashef et al., 2022), and along with

the increased long-range input from areas such as S1 and contralateral M1 to M1 (Commisso et al., 2018), there could be an overall increase in excitation and reduced inhibition. The increased long-range input from certain areas to M1, as well as the hyperresponsiveness in M1 could be a compensatory mechanism towards the connectivity deficits among other areas (Bettus et al., 2009; Skouras et al., 2019).

4.4. Proposed mechanism of neurodegeneration in M1 of ALS

Taken together, studies conducted in ALS patients as well as in rodent models of ALS using various techniques, demonstrate that cortical hyperexcitability is a result of increased excitation and compromised inhibition. Sources of increased excitation onto layer 5 pyramidal neurons/UMN likely comprise both local, from layer 2/3, as well as long-range synaptic inputs; while compromised inhibition could be a result of deficits in formation and function of inhibitory synapses, altered response properties of INs, and changes in receptor density in pre- and/or post-synaptic neuron. Moreover, the increased fraction of locomotion-responsive neurons and the hyperresponsiveness during locomotion would support the hypothesis of degeneration in a use-dependent manner (Julian et al., 2021).

Though our studies revealed structural as well as functional impairments in motor cortex of ALS tg mice, to establish causal relationships among increased input from layer 2/3 to 5, compromised inhibition and UMN degeneration in ALS, further studies are warranted. To this end, we performed chemogenetic (Roth, 2016) dampening of neuronal activity in layer 2/3 of M1 in SOD1^{G93A} mice at the pre-symptomatic stages. The intervention resulted in a delay in disease onset (measured by motor deficits) and improvement in motor performance (i.e. increased latency in rotarod). Moreover, to understand the inhibitiory circuit mechanisms underlying locomotion with and without visual input, IN response to both conditions can be probed in cre-driver mouse lines of the respective INs using *in vivo* two-photon calcium

imaging. To better understand the changes in neuromodulators such as NE and ACh during locomotion in cortex, genetically encoded fluorescent sensors for the specific neuromodulators can be employed (Feng et al., 2019; Jing et al., 2018).

4.5. Considerations towards early diagnostic and treatment option development for ALS

Structural and functional neuronal impairments are intimately linked to compromised neuronal health. Not only are they at the heart of the symptoms of a CNS disorder, but they have also been causally linked to the degenerative process. The development of genetically encoded fluorescent sensors and imaging tools have enabled us to probe activity and response properties of neurons in behaving mice, revealing functional deficits in layer 2/3 and 5 PNs of motor cortex in ALS. In particular, hyperresponsiveness detected in layer 2/3 at the pre-symptomatic stage could be an early diagnostic marker for ALS patients. ALS is currently diagnosed based on patient history and tests such as electromyogram (EMG) of muscles, magnetic resonance imaging (MRI) of the brain and spinal cord and nerve conduction study ("Amyotrophic Lateral Sclerosis (ALS) Fact Sheet," 2013). Ultra-high field (UHF) MRI and magnetic resonance spectroscopy (MRS) can be employed to measure layer-specific structure, function and population-specific activity, in which task-modulated changes in layer 2/3 would be detected in ALS patients. In addition to diagnosis, activity changes in layer 2/3 and the possible associated mechanisms should be considered when developing treatment options.

Riluzole, one of the FDA-approved treatment for ALS, has been shown to exert transient effects in modulating cortical hyperexcitability in patients (Geevasinga et al., 2016) and no improvement in motor function in mouse models of ALS (Hogg et al., 2018). In our study, we showed that after an initial reduction in neuronal activity, the same gradually returned to reach

almost baseline levels after 7 days of treatment in SOD1^{G93A} tg mice (Kan et al.). The evidence favors the notion that neural homeostasis is present in ALS, which overwrites the anti-glutamatergic effect of riluzole, a finding which should be considered in future treatment options. In addition, the impact of riluzole on individual circuit elements, such as PNs and INs, remains unclear, and thus warrants further study. On the other hand, chronic activation of PV IN has been performed in SOD1^{G93A} tg mice and delayed motor symptom onset, especially when the treatment was administered during the pre-symptomatic stage (Khademullah et al., 2020), which reinforce the need for an earlier diagnosis. Along with antisense oligonucleotides that target specific mutations, circuit manipulation to normalize cortical hyperexcitability should be considered. Adeno-associated virus (AAV) gene therapy (Au et al., 2021; Maurya et al., 2022) can be used to deliver for instance designer receptors exclusively activated by designer drugs (DREADDS), which can be activated with spatial and temporal precision (Rao et al., 2019). More importantly, these studies should be performed chronically, for at least 30 days like in (Khademullah et al., 2020) and Kan et al., to investigate the potential involvement of adaptation in the effectiveness of the treatment.

5. Concluding Remarks and Future Direction

Taken together the findings of the two manuscripts, I demonstrated *sources* of cortical dysfunction in M1 of both $Fus^{\Delta NLS/+}$ and SOD1^{G93A} mice. In $Fus^{\Delta NLS/+}$ tg mice, cortical dysfunction stems from compromised inhibition most likely due to defects in inhibitory synapses that are related to FUS accumulation in the synapses. To probe the casual relationship between compromised inhibition and cortical hyperactivity, some follow-up experiments include (i) only introducing cytoplasmic mislocalization of FUS in interneurons and (ii) rescuing interneurons by not introducing the $FUS^{\Delta NLS}$ transgene.

On the other hand, in SOD1^{G93A} mice, I first revealed the partial coherence of activity of the same neurons under anesthesia and during wakefulness, emphasizing the importance of investigating neuronal activity and cortical dysfunction during wakefulness. More importantly, I found increase in locomotion-associated activity restricted to layer II/III at the presymptomatic stage that is later detected in both layer II/III and V at the early symptomatic stage. To probe the effect of reduced input from layer II/III to V in M1, we chemogenetically dampened neuronal activity in M1 layer 2/3 at the presymptomatic stage using DREADDs. Given the improved motor phenotype (i.e. improved latency in rotarod) and delayed disease onset observed in SOD1^{G93A} mice, some follow-up questions include (i) the effect of manipulating activity of a given population on M1, both at the level of synapses, with other cell types in M1 and connectivity with other brain regions; (ii) whether the treatment halts or reverses neurodegeneration by e.g. reduced expression level of protein markers such as misfolded-SOD1 as the behavioral phenotype improved. More studies that focus on how transcriptomic changes are translated into changes in neuronal activity and response properties as well as behavior should be conducted to better understand the potential homeostatic effects that each manipulation or treatment attempt causes.

The findings of the doctoral thesis provided further insights into potential early detection of the ALS as well as therapeutic treatment, specifically considering the involvement of circuit mechanisms when developing more effective treatment options.

References

Abe, K., Aoki, M., Tsuji, S., Itoyama, Y., Sobue, G., Togo, M., Hamada, C., Tanaka, M., Akimoto, M., & Nakamura, K. (2017). Safety and efficacy of edaravone in well defined patients with amyotrophic lateral sclerosis: a randomised, double-blind, placebo-controlled trial. *The Lancet Neurology*, *16*(7), 505-512.

Abrahams, S., Goldstein, L. H., Simmons, A., Brammer, M., Williams, S. C., Giampietro, V., & Leigh, P. N. (2004). Word retrieval in amyotrophic lateral sclerosis: a functional magnetic resonance imaging study. *Brain*, *127*(7), 1507-1517.

Agarwal, S., Highton-Williamson, E., Caga, J., Howells, J., Dharmadasa, T., Matamala, J., Ma, Y., Shibuya, K., Hodges, J., Ahmed, R., Vucic, S. and Kiernan, M. (2021). Motor cortical excitability predicts cognitive phenotypes in amyotrophic lateral sclerosis. *Scientific reports*, *11*(1). https://doi.org/https://doi.org/10.1038/s41598-021-81612-x

Ahrens, M. B., Huang, K.-H., Narayan, S., Mensh, B. D., & Engert, F. (2013). Two-photon calcium imaging during fictive navigation in virtual environments. *Frontiers in neural circuits*, *7*, 104.

Ali, F., & Kwan, A. C. (2019). Interpreting in vivo calcium signals from neuronal cell bodies, axons, and dendrites: a review. *Neurophotonics*, *7*(1), 011402.

Amylyx Pharmaceuticals Announces FDA Approval of RELYVRIO™ for the Treatment of ALS. (2022). https://www.amylyx.com/media/amylyx-pharmaceuticals-announces-fda-approval-of-relyvriotm-for-the-treatment-of-als

Amyotrophic Lateral Sclerosis (ALS) Fact Sheet. (2013). *NIH National Institute of Neurological Disorders and Stroke*.

Anderson, C. T., Sheets, P. L., Kiritani, T., & Shepherd, G. M. (2010). Sublayer-specific microcircuits of corticospinal and corticostriatal neurons in motor cortex. *Nature neuroscience*, *13*(6), 739.

Andrews, J. A., Jackson, C. E., Heiman-Patterson, T. D., Bettica, P., Brooks, B. R., & Pioro, E. P. (2020). Real-world evidence of riluzole effectiveness in treating amyotrophic lateral sclerosis. *Amyotrophic Lateral Sclerosis and Frontotemporal Degeneration*, *21*(7-8), 509-518.

Apolloni, S., Amadio, S., Fabbrizio, P., Morello, G., Spampinato, A. G., Latagliata, E. C., Salvatori, I., Proietti, D., Ferri, A., & Madaro, L. (2019). Histaminergic transmission slows progression of amyotrophic lateral sclerosis. *Journal of cachexia, sarcopenia and muscle*, *10*(4), 872-893.

Apolloni, S., Fabbrizio, P., Amadio, S., Napoli, G., Verdile, V., Morello, G., Iemmolo, R., Aronica, E., Cavallaro, S., & Volonté, C. (2017). Histamine regulates the inflammatory profile of SOD1-G93A microglia and the histaminergic system is dysregulated in amyotrophic lateral sclerosis. *Frontiers in Immunology*, *8*, 1689.

Arai, T., Hasegawa, M., Akiyama, H., Ikeda, K., Nonaka, T., Mori, H., Mann, D., Tsuchiya, K., Yoshida, M., & Hashizume, Y. (2006). TDP-43 is a component of ubiquitin-positive tau-negative inclusions in frontotemporal lobar degeneration and amyotrophic lateral sclerosis. *Biochemical and biophysical research communications*, *351*(3), 602-611.

Arikkath, J. (2012). Molecular mechanisms of dendrite morphogenesis. *Frontiers in Cellular Neuroscience*, *6*, 61.

Arkley, K., Grant, R. A., Mitchinson, B., & Prescott, T. J. (2014). Strategy change in vibrissal active sensing during rat locomotion. *Current Biology*, *24*(13), 1507-1512.

Armada-Moreira, A., Gomes, J. I., Pina, C. C., Savchak, O. K., Gonçalves-Ribeiro, J., Rei, N., Pinto, S., Morais, T. P., Martins, R. S., & Ribeiro, F. F. (2020). Going the extra

(synaptic) mile: excitotoxicity as the road toward neurodegenerative diseases. *Frontiers in Cellular Neuroscience*, *14*, 90.

Aston-Jones, G., & Bloom, F. (1981). Nonrepinephrine-containing locus coeruleus neurons in behaving rats exhibit pronounced responses to non-noxious environmental stimuli. *Journal of Neuroscience*, *1*(8), 887-900.

Aston-Jones, G., Chen, S., Zhu, Y., & Oshinsky, M. L. (2001). A neural circuit for circadian regulation of arousal. *Nature neuroscience*, *4*(7), 732-738.

Aston-Jones, G., & Waterhouse, B. (2016). Locus coeruleus: from global projection system to adaptive regulation of behavior. *Brain research*, *1645*, 75-78.

Au, H. K. E., Isalan, M., & Mielcarek, M. (2021). Gene therapy advances: a meta-analysis of AAV usage in clinical settings. *Frontiers in medicine*, *8*.

Augustine, G. J., Santamaria, F., & Tanaka, K. (2003). Local calcium signaling in neurons. *Neuron*, *40*(2), 331-346.

Awenowicz, P. W., & Porter, L. L. (2002). Local application of dopamine inhibits pyramidal tract neuron activity in the rodent motor cortex. *Journal of neurophysiology*, *88*(6), 3439-3451.

Ayaz, A., Saleem, A. B., Schölvinck, M. L., & Carandini, M. (2013). Locomotion controls spatial integration in mouse visual cortex. *Current Biology*, *23*(10), 890-894.

Ayaz, A., Stäuble, A., Hamada, M., Wulf, M.-A., Saleem, A. B., & Helmchen, F. (2019). Layer-specific integration of locomotion and sensory information in mouse barrel cortex. *Nature communications*, *10*(1), 1-14.

Babu, G. N., Bawari, M., Mathur, V. N., Kalita, J., & Misra, U. K. (1998). Blood glutamate levels in patients with motor neuron disease. *Clin Chim Acta*, *273*(2), 195-200. https://doi.org/10.1016/s0009-8981(98)00039-4

Bae, J. S., Simon, N. G., Menon, P., Vucic, S., & Kiernan, M. C. (2013). The puzzling case of hyperexcitability in amyotrophic lateral sclerosis. *Journal of clinical neurology (Seoul, Korea)*, *9*(2), 65–74. https://doi.org/10.3988/jcn.2013.9.2.65

Baker, A., Kalmbach, B., Morishima, M., Kim, J., Juavinett, A., Li, N., & Dembrow, N. (2018). Specialized subpopulations of deep-layer pyramidal neurons in the neocortex: bridging cellular properties to functional consequences. *Journal of Neuroscience*, *38*(24), 5441-5455.

Ballinger, E. C., Ananth, M., Talmage, D. A., & Role, L. W. (2016). Basal forebrain cholinergic circuits and signaling in cognition and cognitive decline. *Neuron*, *91*(6), 1199-1218.

Barker, H. V., Niblock, M., Lee, Y.-B., Shaw, C. E., & Gallo, J.-M. (2017). RNA misprocessing in C9orf72-linked neurodegeneration. *Frontiers in Cellular Neuroscience*, *11*, 195.

Barry, R. L., Babu, S., Anteraper, S. A., Triantafyllou, C., Keil, B., Rowe, O. E., Rangaprakash, D., Paganoni, S., Lawson, R., & Dheel, C. (2021). Ultra-high field (7T) functional magnetic resonance imaging in amyotrophic lateral sclerosis: a pilot study. *NeuroImage: Clinical*, *30*, 102648.

Bartos, M., & Elgueta, C. (2012). Functional characteristics of parvalbumin- and cholecystokinin-expressing basket cells. *The Journal of physiology*, *590*(4), 669-681. https://doi.org/10.1113/jphysiol.2011.226175

Bataveljic, D., Nikolic, L., Milosevic, M., Todorovic, N., & Andjus, P. R. (2012). Changes in the astrocytic aquaporin-4 and inwardly rectifying potassium channel expression in the brain of the amyotrophic lateral sclerosis SOD1(G93A) rat model. *Glia*, *60*(12), 1991-2003. https://doi.org/10.1002/glia.22414

Batsikadze, G., Paulus, W., Kuo, M.-F., & Nitsche, M. A. (2013). Effect of serotonin on paired associative stimulation-induced plasticity in the human motor cortex. *Neuropsychopharmacology*, *38*(11), 2260-2267.

Beaulieu, C. (1993). Numerical data on neocortical neurons in adult rat, with special reference to the GABA population. *Brain research*, *609*(1-2), 284-292.

Ben Achour, S., & Pascual, O. (2012). Astrocyte-neuron communication: functional consequences. *Neurochem Res*, *37*(11), 2464-2473. https://doi.org/10.1007/s11064-012-0807-0

Bendotti, C., Tortarolo, M., Suchak, S. K., Calvaresi, N., Carvelli, L., Bastone, A., Rizzi, M., Rattray, M., & Mennini, T. (2008). Transgenic SOD1 G93A mice develop reduced GLT-1 in spinal cord without alterations in cerebrospinal fluid glutamate levels. *Journal of neurochemistry*, *79*, 737--746. https://doi.org/10.1046/j.1471-4159.2001.00572.x

Benjaminsen, E., Alstadhaug, K. B., Gulsvik, M., Baloch, F. K., & Odeh, F. (2018). Amyotrophic lateral sclerosis in Nordland county, Norway, 2000–2015: Prevalence, incidence, and clinical features. *Amyotrophic Lateral Sclerosis and Frontotemporal Degeneration*, *19*(7-8), 522-527.

Bennett, E. J., Mead, R. J., Azzouz, M., Shaw, P. J., & Grierson, A. J. (2014). Early detection of motor dysfunction in the SOD1G93A mouse model of Amyotrophic Lateral Sclerosis (ALS) using home cage running wheels. *PloS one*, *9*(9), e107918.

Bensimon, G., Lacomblez, L., & Meininger, V. (1994). A Controlled Trial of Riluzole in Amyotrophic Lateral Sclerosis. *New England Journal of Medicine*, *330*(9), 585-591. https://doi.org/10.1056/NEJM199403033300901

Berdyński, M., Miszta, P., Safranow, K., Andersen, P. M., Morita, M., Filipek, S., Żekanowski, C., & Kuźma-Kozakiewicz, M. (2022). SOD1 mutations associated with amyotrophic lateral sclerosis analysis of variant severity. *Scientific reports*, *12*(1), 1-11.

Bettus, G., Guedj, E., Joyeux, F., Confort-Gouny, S., Soulier, E., Laguitton, V., Cozzone, P. J., Chauvel, P., Ranjeva, J. P., & Bartolomei, F. (2009). Decreased basal fMRI functional connectivity in epileptogenic networks and contralateral compensatory mechanisms. *Human brain mapping*, *30*(5), 1580-1591.

Bilsland, L. G., Sahai, E., Kelly, G., Golding, M., Greensmith, L., & Schiavo, G. (2010). Deficits in axonal transport precede ALS symptoms in vivo. *Proceedings of the National Academy of Sciences*, *107*(47), 20523-20528. https://doi.org/10.1073/pnas.1006869107

Bitetto, G., & Di Fonzo, A. (2020). Nucleo–cytoplasmic transport defects and protein aggregates in neurodegeneration. *Translational neurodegeneration*, *9*(1), 1-16.

Blair, I. P., Williams, K. L., Warraich, S. T., Durnall, J. C., Thoeng, A. D., Manavis, J., Blumbergs, P. C., Vucic, S., Kiernan, M. C., & Nicholson, G. A. (2010). FUS mutations in amyotrophic lateral sclerosis: clinical, pathological, neurophysiological and genetic analysis. *J Neurol Neurosurg Psychiatry*, *81*(6), 639-645. https://doi.org/10.1136/jnnp.2009.194399

Blokhuis, A. M., Groen, E. J., Koppers, M., van den Berg, L. H., & Pasterkamp, R. J. (2013). Protein aggregation in amyotrophic lateral sclerosis. *Acta Neuropathol*, *125*(6), 777-794. https://doi.org/10.1007/s00401-013-1125-6

Bloodgood, B. L., & Sabatini, B. L. (2005). Neuronal activity regulates diffusion across the neck of dendritic spines. *Science*, *310*(5749), 866-869.

Blumenstock, S., Sun, F., Klaus, C., Marinković, P., Sgobio, C., Paeger, L., Liebscher, S., & Herms, J. (2021). Cortical circuit dysfunction in a mouse model of alpha-synucleinopathy in vivo. *Brain communications*, *3*(4), fcab273.

Bonafede, R., & Mariotti, R. (2017). ALS pathogenesis and therapeutic approaches: the role of mesenchymal stem cells and extracellular vesicles. *Frontiers in Cellular Neuroscience*, *11*, 80.

Borasio, G., Linke, R., Schwarz, J., Schlamp, V., Abel, A., Mozley, P., & Tatsch, K. (1998). Dopaminergic deficit in amyotrophic lateral sclerosis assessed with [I-123] IPT single photon emission computed tomography. *Journal of Neurology, Neurosurgery & Psychiatry*, *65*(2), 263-265.

Breton-Provencher, V., & Sur, M. (2019). Active control of arousal by a locus coeruleus GABAergic circuit. *Nature neuroscience*, *22*(2), 218-228.

Bruijn, L. I., Becher, M. W., Lee, M. K., Anderson, K. L., Jenkins, N. A., Copeland, N. G., Sisodia, S. S., Rothstein, J. D., Borchelt, D. R., Price, D. L., & Cleveland, D. W. (1997). ALS-linked SOD1 mutant G85R mediates damage to astrocytes and promotes rapidly progressive disease with SOD1-containing inclusions. *Neuron*, *18*(2), 327-338. https://doi.org/10.1016/s0896-6273(00)80272-x

Brunet, A., Stuart-Lopez, G., Burg, T., Scekic-Zahirovic, J., & Rouaux, C. (2020). Cortical circuit dysfunction as potential driver of Amyotrophic lateral sclerosis. *Frontiers Neuroscience*.

Buratti, E., & Baralle, F. E. (2008). Multiple roles of TDP-43 in gene expression, splicing regulation, and human disease. *Front Biosci*, *13*(8).

Burgold, J., Schulz-Trieglaff, E. K., Voelkl, K., Gutierrez-Angel, S., Bader, J. M., Hosp, F., Mann, M., Arzberger, T., Klein, R., Liebscher, S., & Dudanova, I. (2019). Cortical circuit alterations precede motor impairments in Huntington's disease mice. *Sci Rep*, *9*(1), 6634. https://doi.org/10.1038/s41598-019-43024-w

Burk, K., & Pasterkamp, R. J. (2019). Disrupted neuronal trafficking in amyotrophic lateral sclerosis. *Acta neuropathologica*, *137*(6), 859-877.

Busse, L. (2018). The influence of locomotion on sensory processing and its underlying neuronal circuits. *e-Neuroforum*, *24*(1), A41-A51.

Butler, C. A., Popescu, A. S., Kitchener, E. J., Allendorf, D. H., Puigdellívol, M., & Brown, G. C. (2021). Microglial phagocytosis of neurons in neurodegeneration, and its regulation. *Journal of neurochemistry*, *158*(3), 621-639.

Butti, Z., & Patten, S. A. (2019). RNA dysregulation in amyotrophic lateral sclerosis. *Frontiers in Genetics*, 712.

Carter, M. E., Yizhar, O., Chikahisa, S., Nguyen, H., Adamantidis, A., Nishino, S., Deisseroth, K., & De Lecea, L. (2010). Tuning arousal with optogenetic modulation of locus coeruleus neurons. *Nature neuroscience*, *13*(12), 1526-1533.

Cengiz, B., Fidanci, H., Kiyak Keceli, Y., Baltaci, H., & KuruoGlu, R. (2019). Impaired short- and long-latency afferent inhibition in amyotrophic lateral sclerosis. *Muscle Nerve*, *59*(6), 699-704. https://doi.org/10.1002/mus.26464

Cengiz, B., & Kuruoğlu, R. (2020). A new parameter to discriminate amyotrophic lateral sclerosis patients from healthy participants by motor cortical excitability changes. *Muscle & Nerve*, *61*(3), 354-362.

Chakrabarti, S., Nambiar, J., & Schwarz, C. (2021). Adaptive Whisking in Mice. *Frontiers in Systems Neuroscience*, *15*.

Chen, H., Kankel, M. W., Su, S. C., Han, S. W., & Ofengeim, D. (2018). Exploring the genetics and non-cell autonomous mechanisms underlying ALS/FTLD. *Cell Death & Differentiation*, *25*(4), 648-662.

Chen, J. J. (2020). Overview of current and emerging therapies for amytrophic lateral sclerosis. *The American Journal of Managed Care*, *26*(9 Suppl), S191-S197.

Chen, S. X., Kim, A. N., Peters, A. J., & Komiyama, T. (2015). Subtype-specific plasticity of inhibitory circuits in motor cortex during motor learning. *Nature neuroscience*, *18*(8), 1109-1115.

Chen, T.-W., Wardill, T. J., Sun, Y., Pulver, S. R., Renninger, S. L., Baohan, A., Schreiter, E. R., Kerr, R. A., Orger, M. B., & Jayaraman, V. (2013). Ultrasensitive fluorescent proteins for imaging neuronal activity. *Nature*, *499*(7458), 295-300.

Chen, X., Leischner, U., Rochefort, N. L., Nelken, I., & Konnerth, A. (2011). Functional mapping of single spines in cortical neurons in vivo. *Nature*, *475*(7357), 501-505.

Cheng, L., Xu, C., Wang, L., An, D., Jiang, L., Zheng, Y., Xu, Y., Wang, Y., Wang, Y., & Zhang, K. (2021). Histamine H1 receptor deletion in cholinergic neurons induces

sensorimotor gating ability deficit and social impairments in mice. *Nature communications*, *12*(1), 1-17.

Cho, H., & Shukla, S. (2020). Role of edaravone as a treatment option for patients with amyotrophic lateral sclerosis. *Pharmaceuticals*, *14*(1), 29.

Cho, M. (2013). Oligodendrocyte failure in ALS. *Nature neuroscience*, *16*(5), 525-525.

Citri, A., & Malenka, R. C. (2008). Synaptic plasticity: multiple forms, functions, and mechanisms. *Neuropsychopharmacology*, *33*(1), 18-41.

Clark, R. M., Blizzard, C. A., Young, K. M., King, A. E., & Dickson, T. C. (2017). Calretinin and neuropeptide y interneurons are differentially altered in the motor cortex of the SOD1 G93A mouse model of ALS. *Scientific reports*, *7*, 44461.

Commisso, B., Ding, L., Varadi, K., Gorges, M., Bayer, D., Boeckers, T. M., Ludolph, A. C., Kassubek, J., Müller, O. J., & Roselli, F. (2018). Stage-dependent remodeling of projections to motor cortex in ALS mouse model revealed by a new variant retrograde-AAV9. *Elife*, *7*, e36892. https://doi.org/10.7554/eLife.36892

Coppedè, F. (2011). An overview of DNA repair in amyotrophic lateral sclerosis. *TheScientificWorldJOURNAL*, *11*, 1679-1691.

Corcia, P., Blasco, H., Beltran, S., Piegay, A., & Vourc'h, P. (2022). Treatment of hereditary amyotrophic lateral sclerosis. *Revue Neurologique*.

Corcia, P., & Meininger, V. (2019). Grey Matter 150th anniversary of Charcot's description of amyotrophic lateral sclerosis. *Brain*.

Cozzolino, M., & Carrì, M. T. (2012). Mitochondrial dysfunction in ALS. *Progress in Neurobiology*, *97*(2), 54-66. https://doi.org/https://doi.org/10.1016/j.pneurobio.2011.06.003

Crochemore, C., Pena-Altamira, E., Virgili, M., Monti, B., & Contestabile, A. (2005). Disease-related regressive alterations of forebrain cholinergic system in SOD1 mutant transgenic mice. *Neurochem Int*, *46*(5), 357-368. https://doi.org/10.1016/j.neuint.2004.12.004

Cserép, C., Pósfai, B., & Dénes, Á. (2021). Shaping neuronal fate: functional heterogeneity of direct microglia-neuron interactions. *Neuron*, *109*(2), 222-240.

Cykowski, M. D., Takei, H., Schulz, P. E., Appel, S. H., & Powell, S. Z. (2014). TDP-43 pathology in the basal forebrain and hypothalamus of patients with amyotrophic lateral sclerosis. *Acta neuropathologica communications*, *2*(1), 1-11.

Da Cruz, S., Bui, A., Saberi, S., Lee, S. K., Stauffer, J., McAlonis-Downes, M., Schulte, D., Pizzo, D. P., Parone, P. A., & Cleveland, D. W. (2017). Misfolded SOD1 is not a primary component of sporadic ALS. *Acta neuropathologica*, *134*(1), 97-111.

Dadarlat, M. C., & Stryker, M. P. (2017). Locomotion enhances neural encoding of visual stimuli in mouse V1. *Journal of Neuroscience*, *37*(14), 3764-3775.

Dadon-Nachum, M., Melamed, E., & Offen, D. (2010). The "Dying-Back" Phenomenon of Motor Neurons in ALS. *Journal of Molecular Neuroscience*, *43*(3), 470-477. https://doi.org/10.1007/s12031-010-9467-1

Dai, J., Lin, W., Zheng, M., Liu, Q., He, B., Luo, C., Lu, X., Pei, Z., Su, H., & Yao, X. (2017). Alterations in AQP4 expression and polarization in the course of motor neuron degeneration in SOD1G93A mice. *Molecular Medicine Reports*, *16*(2), 1739-1746.

Dao Duc, K., Lee, C.-Y., Parutto, P., Cohen, D., Segal, M., Rouach, N., & Holcman, D. (2015). Bursting reverberation as a multiscale neuronal network process driven by synaptic depression-facilitation. *PloS one*, *10*(5), e0124694.

Dash, R. P., Babu, R. J., & Srinivas, N. R. (2018). Two decades-long journey from riluzole to edaravone: revisiting the clinical pharmacokinetics of the only two amyotrophic lateral sclerosis therapeutics. *Clinical pharmacokinetics*, *57*(11), 1385-1398.

Deleuze, C., Bhumbra, G. S., Pazienti, A., Lourenço, J., Mailhes, C., Aguirre, A., Beato, M., & Bacci, A. (2019). Strong preference for autaptic self-connectivity of neocortical PV interneurons facilitates their tuning to γ-oscillations. *PLoS biology*, *17*(9), e3000419.

Deng, H.-X., Hentati, A., Tainer, J. A., Iqbal, Z., Cayabyab, A., Hung, W.-Y., Getzoff, E. D., Hu, P., Herzfeldt, B., & Roos, R. P. (1993). Amyotrophic Lateral Ssclerosis and Structural Defects in Cu, Zn Superoxide Dismutase. *Science*, *261*(5124), 1047-1051.

Djukic, B., Casper, K. B., Philpot, B. D., Chin, L. S., & McCarthy, K. D. (2007). Conditional knock-out of Kir4.1 leads to glial membrane depolarization, inhibition of potassium and glutamate uptake, and enhanced short-term synaptic potentiation. *J Neurosci*, *27*(42), 11354-11365. https://doi.org/10.1523/jneurosci.0723-07.2007

Doble, A. (1996). The pharmacology and mechanism of action of riluzole. *Neurology*, *47*(6 Suppl 4), 233S-241S.

Dols-Icardo, O., Montal, V., Sirisi, S., López-Pernas, G., Cervera-Carles, L., Querol-Vilaseca, M., Muñoz, L., Belbin, O., Alcolea, D., & Molina-Porcel, L. (2020). Motor cortex transcriptome reveals microglial key events in amyotrophic lateral sclerosis. *Neurology-Neuroimmunology Neuroinflammation*, *7*(5).

Dombeck, D. A., Graziano, M. S., & Tank, D. W. (2009). Functional clustering of neurons in motor cortex determined by cellular resolution imaging in awake behaving mice. *Journal of Neuroscience*, *29*(44), 13751-13760.

Donnelly, C. J., Zhang, P.-W., Pham, J. T., Haeusler, A. R., Mistry, N. A., Vidensky, S., Daley, E. L., Poth, E. M., Hoover, B., & Fines, D. M. (2013). RNA toxicity from the ALS/FTD C9ORF72 expansion is mitigated by antisense intervention. *Neuron*, *80*(2), 415-428.

Drenan, R. M., Grady, S. R., Steele, A. D., McKinney, S., Patzlaff, N. E., McIntosh, J. M., Marks, M. J., Miwa, J. M., & Lester, H. A. (2010). Cholinergic modulation of locomotion and striatal dopamine release is mediated by α6α4* nicotinic acetylcholine receptors. *Journal of Neuroscience*, *30*(29), 9877-9889.

Dupuis, L., Spreux-Varoquaux, O., Bensimon, G., Jullien, P., Lacomblez, L., Salachas, F., Bruneteau, G., Pradat, P.-F., Loeffler, J.-P., & Meininger, V. (2010). Platelet serotonin level predicts survival in amyotrophic lateral sclerosis. *PloS one*, *5*(10), e13346.

Dyer, M. S., Reale, L. A., Lewis, K. E., Walker, A. K., Dickson, T. C., Woodhouse, A., & Blizzard, C. A. (2021a). Mislocalisation of TDP-43 to the cytoplasm causes cortical hyperexcitability and reduced excitatory neurotransmission in the motor cortex. *J Neurochem*, *157*(4), 1300-1315. https://doi.org/10.1111/jnc.15214

Dyer, M. S., Woodhouse, A., & Blizzard, C. A. (2021b). Cytoplasmic human tdp-43 mislocalization induces widespread dendritic spine loss in mouse upper motor neurons. *Brain Sciences*, *11*(7), 883.

Edwards, L. L., King, E. M., Buetefisch, C. M., & Borich, M. R. (2019). Putting the "sensory" into sensorimotor control: the role of sensorimotor integration in goal-directed hand movements after stroke. *Frontiers in integrative neuroscience*, *13*, 16.

Eichhoff, G., & Garaschuk, O. (2011). Two-photon imaging of neural networks in a mouse model of Alzheimer's disease. *Cold Spring Harbor Protocols*, *2011*(10), pdb. prot065789.

Eisen, A. (2021). The Dying Forward Hypothesis of ALS: Tracing Its History. *Brain Sciences*, *11*(3), 300. https://doi.org/10.3390/brainsci11030300

Eisen, A., Braak, H., Del Tredici, K., Lemon, R., Ludolph, A. C., & Kiernan, M. C. (2017). Cortical influences drive amyotrophic lateral sclerosis. *Journal of Neurology, Neurosurgery & Psychiatry*, *88*(11), 917-924.

Ekestern, E. (2004). Neurotrophic factors and amyotrophic lateral sclerosis. *Neurodegenerative Diseases*, *1*(2-3), 88-100.

Ellender, T. J., Huerta-Ocampo, I., Deisseroth, K., Capogna, M., & Bolam, J. P. (2011). Differential modulation of excitatory and inhibitory striatal synaptic transmission by histamine. *Journal of Neuroscience*, *31*(43), 15340-15351.

Erisken, S., Vaiceliunaite, A., Jurjut, O., Fiorini, M., Katzner, S., & Busse, L. (2014). Effects of locomotion extend throughout the mouse early visual system. *Current Biology*, *24*(24), 2899-2907.

Esposito, Z., Belli, L., Toniolo, S., Sancesario, G., Bianconi, C., & Martorana, A. (2013). Amyloid β, glutamate, excitotoxicity in Alzheimer's disease: are we on the right track? *CNS neuroscience & therapeutics*, *19*(8), 549-555.

Farrugia Wismayer, M., Borg, R., Farrugia Wismayer, A., Bonavia, K., Vella, M., Pace, A., Vassallo, N., & Cauchi, R. J. (2021). Occupation and amyotrophic lateral sclerosis risk: a case-control study in the isolated island population of Malta. *Amyotrophic Lateral Sclerosis and Frontotemporal Degeneration*, *22*(7-8), 528-534.

Fellin, T., Sul, J., D Ascenzo, M., Takano, H., Pascual, O., & Haydon, P. G. (2006). Bidirectional astrocyte-neuron communication: the many roles of glutamate and ATP. Novartis Foundation symposium,

Feng, J., Zhang, C., Lischinsky, J. E., Jing, M., Zhou, J., Wang, H., Zhang, Y., Dong, A., Wu, Z., & Wu, H. (2019). A genetically encoded fluorescent sensor for rapid and specific in vivo detection of norepinephrine. *Neuron*, *102*(4), 745-761. e748.

Fernández-Arjona, M. d. M., Grondona, J. M., Granados-Durán, P., Fernández-Llebrez, P., & López-Ávalos, M. D. (2017). Microglia morphological categorization in a rat model of neuroinflammation by hierarchical cluster and principal components analysis. *Frontiers in Cellular Neuroscience*, *11*, 235.

Ferrari, R., Kapogiannis, D., D Huey, E., & Momeni, P. (2011). FTD and ALS: a tale of two diseases. *Current Alzheimer Research*, *8*(3), 273-294.

Fields, R. D., & Stevens-Graham, B. (2002). New insights into neuron-glia communication. *Science*, *298*(5593), 556-562.

Flik, G., Folgering, J. H., Cremers, T. I., Westerink, B. H., & Dremencov, E. (2015). Interaction between brain histamine and serotonin, norepinephrine, and dopamine systems: in vivo microdialysis and electrophysiology study. *Journal of Molecular Neuroscience*, *56*(2), 320-328.

Fogarty, M. J., Klenowski, P. M., Lee, J. D., Drieberg-Thompson, J. R., Bartlett, S. E., Ngo, S. T., Hilliard, M. A., Bellingham, M. C., & Noakes, P. G. (2016a). Cortical synaptic and dendritic spine abnormalities in a presymptomatic TDP-43 model of amyotrophic lateral sclerosis. *Scientific reports*, *6*, 37968. https://doi.org/10.1038/srep37968

Fogarty, M. J., Mu, E. W., Noakes, P. G., Lavidis, N. A., & Bellingham, M. C. (2016b). Marked changes in dendritic structure and spine density precede significant neuronal death in vulnerable cortical pyramidal neuron populations in the SOD1(G93A) mouse model of amyotrophic lateral sclerosis. *Acta Neuropathol Commun*, *4*(1), 77. https://doi.org/10.1186/s40478-016-0347-y

Fogarty, M. J., Mu, E. W., Noakes, P. G., Lavidis, N. A., & Bellingham, M. C. (2016c). Marked changes in dendritic structure and spine density precede significant neuronal death in vulnerable cortical pyramidal neuron populations in the SOD1G93A mouse model of amyotrophic lateral sclerosis. *Acta neuropathologica communications*, *4*(1), 1-21.

Fogarty, M. J., Noakes, P. G., & Bellingham, M. C. (2015a). Motor cortex layer V pyramidal neurons exhibit dendritic regression, spine loss, and increased synaptic excitation in the presymptomatic hSOD1(G93A) mouse model of amyotrophic lateral sclerosis. *J Neurosci*, *35*(2), 643-647. https://doi.org/10.1523/jneurosci.3483-14.2015

Fogarty, M. J., Noakes, P. G., & Bellingham, M. C. (2015b). Motor cortex layer V pyramidal neurons exhibit dendritic regression, spine loss, and increased synaptic excitation in the presymptomatic hSOD1G93A mouse model of amyotrophic lateral sclerosis. *Journal of Neuroscience*, *35*(2), 643-647.

Forsberg, K., Graffmo, K., Pakkenberg, B., Weber, M., Nielsen, M., Marklund, S., Brännström, T., & Andersen, P. M. (2019). Misfolded SOD1 inclusions in patients with mutations in

C9orf72 and other ALS/FTD-associated genes. *Journal of Neurology, Neurosurgery & Psychiatry*, *90*(8), 861-869.

Forsberg, K., Jonsson, P. A., Andersen, P. M., Bergemalm, D., Graffmo, K. S., Hultdin, M., Jacobsson, J., Rosquist, R., Marklund, S. L., & Brännström, T. (2010). Novel antibodies reveal inclusions containing non-native SOD1 in sporadic ALS patients. *PloS one*, *5*(7), e11552.

Garner, A. R., & Keller, G. B. (2022). A cortical circuit for audio-visual predictions. *Nature neuroscience*, *25*(1), 98-105.

Gautam, M., Jara, J. H., Sekerkova, G., Yasvoina, M. V., Martina, M., & Özdinler, P. H. (2016). Absence of alsin function leads to corticospinal motor neuron vulnerability via novel disease mechanisms. *Human molecular genetics*, *25*(6), 1074-1087.

Geevasinga, N., Menon, P., Ng, K., Van Den Bos, M., Byth, K., Kiernan, M. C., & Vucic, S. (2016). Riluzole exerts transient modulating effects on cortical and axonal hyperexcitability in ALS. *Amyotrophic Lateral Sclerosis and Frontotemporal Degeneration*, *17*(7-8), 580-588.

Geevasinga, N., Menon, P., Nicholson, G. A., Ng, K., Howells, J., Kril, J. J., Yiannikas, C., Kiernan, M. C., & Vucic, S. (2015). Cortical Function in Asymptomatic Carriers and Patients With C9orf72 Amyotrophic Lateral Sclerosis. *JAMA Neurol*, *72*(11), 1268-1274. https://doi.org/10.1001/jamaneurol.2015.1872

Genc, B., Gozutok, O., Kocak, N., & Ozdinler, P. H. (2020). The timing and extent of motor neuron vulnerability in ALS correlates with accumulation of misfolded SOD1 protein in the cortex and in the spinal cord. *Cells*, *9*(2), 502.

Genç, B., Jara, J. H., Lagrimas, A. K., Pytel, P., Roos, R. P., Mesulam, M., Geula, C., Bigio, E. H., & Özdinler, P. H. (2017). Apical dendrite degeneration, a novel cellular pathology for Betz cells in ALS. *Scientific reports*, *7*(1), 1-10.

Geng, H.-Y., Arbuthnott, G., Yung, W.-H., & Ke, Y. (2021). Long-Range Monosynaptic Inputs Targeting Apical and Basal Dendrites of Primary Motor Cortex Deep Output Neurons. *Cerebral cortex*.

Gonchar, Y., Wang, Q., & Burkhalter, A. H. (2008). Multiple distinct subtypes of GABAergic neurons in mouse visual cortex identified by triple immunostaining. *Frontiers in neuroanatomy*, *2*, 3.

Grace, P. M., Loram, L. C., Christianson, J. P., Strand, K. A., Flyer-Adams, J. G., Penzkover, K. R., Forsayeth, J. R., van Dam, A.-M., Mahoney, M. J., & Maier, S. F. (2017). Behavioral assessment of neuropathic pain, fatigue, and anxiety in experimental autoimmune encephalomyelitis (EAE) and attenuation by interleukin-10 gene therapy. *Brain, behavior, and immunity*, *59*, 49-54.

Guareschi, S., Cova, E., Cereda, C., Ceroni, M., Donetti, E., Bosco, D. A., Trotti, D., & Pasinelli, P. (2012). An over-oxidized form of superoxide dismutase found in sporadic amyotrophic lateral sclerosis with bulbar onset shares a toxic mechanism with mutant SOD1. *Proceedings of the National Academy of Sciences*, *109*(13), 5074-5079.

Gunes, Z. I., Kan, V. W., Jiang, S., Logunov, E., Ye, X., & Liebscher, S. (2022). Cortical Hyperexcitability in the Driver's Seat in ALS. *Clinical and Translational Neuroscience*, *6*(1), 5.

Gunes, Z. I., Kan, V. W. Y., Ye, X., & Liebscher, S. (2020). Exciting Complexity: The Role of Motor Circuit Elements in ALS Pathophysiology. *Front Neurosci*, *14*, 573. https://doi.org/10.3389/fnins.2020.00573

Gurney, M. E., Pu, H., Chiu, A. Y., Dal Canto, M. C., Polchow, C. Y., Alexander, D. D., Caliendo, J., Hentati, A., Kwon, Y. W., & Deng, H.-X. (1994). Motor neuron degeneration in mice that express a human Cu, Zn superoxide dismutase mutation. *Science*, *264*(5166), 1772-1775.

Haas, H., & Panula, P. (2003). The role of histamine and the tuberomamillary nucleus in the nervous system. *Nature Reviews Neuroscience*, *4*(2), 121-130.

Haidar, M., Viden, A., Cuic, B., Wang, T., Rosier, M., Tomas, D., Mills, S. A., Govier-Cole, A., Djouma, E., Luikinga, S., Rytova, V., Barton, S. K., Gonsalvez, D. G., Palmer, L. M., McLean, C., Kiernan, M. C., Vucic, S., & Turner, B. J. (2021). Cortical hyperexcitability drives dying forward ALS symptoms and pathology in mice. *biorxiv*, 2021.2008.2013.456320. https://doi.org/10.1101/2021.08.13.456320

Halassa, M. M., & Haydon, P. G. (2010). Integrated brain circuits: astrocytic networks modulate neuronal activity and behavior. *Annual review of physiology*, *72*, 335-355.

Hansson, E., & Rönnbäck, L. (2003). Glial neuronal signaling in the central nervous system. *The FASEB Journal*, *17*(3), 341-348.

Hao, X., Ou, M., Zhang, D., Zhao, W., Yang, Y., Liu, J., Yang, H., Zhu, T., Li, Y., & Zhou, C. (2020). The effects of general anesthetics on synaptic transmission. *Current neuropharmacology*, *18*(10), 936-965.

Harrison, T. C., Ayling, O. G., & Murphy, T. H. (2012). Distinct cortical circuit mechanisms for complex forelimb movement and motor map topography. *Neuron*, *74*(2), 397-409.

Heindl, S., Gesierich, B., Benakis, C., Llovera, G., Duering, M., & Liesz, A. (2018). Automated morphological analysis of microglia after stroke. *Frontiers in Cellular Neuroscience*, *12*, 106.

Heindorf, M., Arber, S., & Keller, G. B. (2018). Mouse motor cortex coordinates the behavioral response to unpredicted sensory feedback. *Neuron*, *99*(5), 1040-1054. e1045.

Heo, Y.-A. (2022). Sodium Phenylbutyrate and Ursodoxicoltaurine: First Approval. *CNS drugs*, 1-7.

Higelin, J., Catanese, A., Semelink-Sedlacek, L. L., Oeztuerk, S., Lutz, A.-K., Bausinger, J., Barbi, G., Speit, G., Andersen, P. M., & Ludolph, A. C. (2018). NEK1 loss-of-function mutation induces DNA damage accumulation in ALS patient-derived motoneurons. *Stem cell research*, *30*, 150-162.

Hinchcliffe, M., & Smith, A. (2017). Riluzole: real-world evidence supports significant extension of median survival times in patients with amyotrophic lateral sclerosis. *Degenerative Neurological and Neuromuscular Disease*, *7*, 61.

Hogg, M. C., Halang, L., Woods, I., Coughlan, K. S., & Prehn, J. H. (2018). Riluzole does not improve lifespan or motor function in three ALS mouse models. *Amyotrophic Lateral Sclerosis and Frontotemporal Degeneration*, *19*(5-6), 438-445.

Homann, J., Koay, S. A., Glidden, A. M., Tank, D. W., & Berry, M. J. (2017). Predictive coding of novel versus familiar stimuli in the primary visual cortex. *biorxiv*, 197608.

Hooks, B. M., Mao, T., Gutnisky, D. A., Yamawaki, N., Svoboda, K., & Shepherd, G. M. G. (2013). Organization of cortical and thalamic input to pyramidal neurons in mouse motor cortex. *The Journal of neuroscience : the official journal of the Society for Neuroscience*, *33*(2), 748-760. https://doi.org/10.1523/JNEUROSCI.4338-12.2013

Hosp, J. A., Pekanovic, A., Rioult-Pedotti, M. S., & Luft, A. R. (2011). Dopaminergic projections from midbrain to primary motor cortex mediate motor skill learning. *Journal of Neuroscience*, *31*(7), 2481-2487.

Howe, M., Ridouh, I., Mascaro, A. L. A., Larios, A., Azcorra, M., & Dombeck, D. A. (2019). Coordination of rapid cholinergic and dopaminergic signaling in striatum during spontaneous movement. *Elife*, *8*, e44903.

Howland, D. S., Liu, J., She, Y., Goad, B., Maragakis, N. J., Kim, B., Erickson, J., Kulik, J., DeVito, L., Psaltis, G., DeGennaro, L. J., Cleveland, D. W., & Rothstein, J. D. (2002). Focal loss of the glutamate transporter EAAT2 in a transgenic rat model of SOD1 mutant-mediated amyotrophic lateral sclerosis (ALS). *Proc Natl Acad Sci U S A*, *99*(3), 1604-1609. https://doi.org/10.1073/pnas.032539299

Hu, M., Ellis, C., Al-Chalabi, A., Leigh, P., & Shaw, C. (1998). Flail arm syndrome: a distinctive variant of amyotrophic lateral sclerosis. *Journal of Neurology, Neurosurgery & Psychiatry*, *65*(6), 950-951.

Huang, S.-L., Wu, L.-S., Lee, M., Chang, C.-W., Cheng, W.-C., Fang, Y.-S., Chen, Y.-R., Cheng, P.-L., & Shen, C.-K. J. (2020). A robust TDP-43 knock-in mouse model of ALS. *Acta neuropathologica communications*, *8*(1), 1-19.

Huber, D., Gutnisky, D. A., Peron, S., O'connor, D. H., Wiegert, J. S., Tian, L., Oertner, T. G., Looger, L. L., & Svoboda, K. (2012). Multiple dynamic representations in the motor cortex during sensorimotor learning. *Nature*, *484*(7395), 473-478.

Huda, K., Salunga, T. L., & Matsunami, K. (2001). Dopaminergic inhibition of excitatory inputs onto pyramidal tract neurons in cat motor cortex. *Neuroscience letters*, *307*(3), 175-178.

Ikawa, M., Okazawa, H., Tsujikawa, T., Matsunaga, A., Yamamura, O., Mori, T., Hamano, T., Kiyono, Y., Nakamoto, Y., & Yoneda, M. (2015). Increased oxidative stress is related to disease severity in the ALS motor cortex: a PET study. *Neurology*, *84*(20), 2033-2039.

Inzunza, O., Serón-Ferré, M. a. J., Bravo, H., & Torrealba, F. (2000). Tuberomammillary nucleus activation anticipates feeding under a restricted schedule in rats. *Neuroscience letters*, *293*(2), 139-142.

Iyer, S., Subramanian, V., & Acharya, K. R. (2018). C9orf72, a protein associated with amyotrophic lateral sclerosis (ALS) is a guanine nucleotide exchange factor. *PeerJ*, *6*, e5815.

Jaber, M., Robinson, S. W., Missale, C., & Caron, M. G. (1996). Dopamine receptors and brain function. *Neuropharmacology*, *35*(11), 1503-1519.

Jacobs, B. L., & Fornal, C. A. (1997). Serotonin and motor activity. *Current opinion in neurobiology*, *7*(6), 820-825.

Jami, M.-S., Salehi-Najafabadi, Z., Ahmadinejad, F., Hoedt, E., Chaleshtori, M. H., Ghatrehsamani, M., Neubert, T. A., Larsen, J. P., & Møller, S. G. (2015). Edaravone leads to proteome changes indicative of neuronal cell protection in response to oxidative stress. *Neurochemistry international*, *90*, 134-141.

Janitzky, K., Lippert, M. T., Engelhorn, A., Tegtmeier, J., Goldschmidt, J., Heinze, H.-J., & Ohl, F. W. (2015). Optogenetic silencing of locus coeruleus activity in mice impairs cognitive flexibility in an attentional set-shifting task. *Frontiers in behavioral neuroscience*, *9*, 286.

Jara, J. H., Sheets, P. L., Nigro, M. J., Perić, M., Brooks, C., Heller, D. B., Martina, M., Andjus, P. R., & Ozdinler, P. H. (2020). The electrophysiological determinants of corticospinal motor neuron vulnerability in ALS. *Frontiers in molecular neuroscience*, *13*, 73.

Jia, H., Rochefort, N. L., Chen, X., & Konnerth, A. (2010). Dendritic organization of sensory input to cortical neurons in vivo. *Nature*, *464*(7293), 1307-1312.

Jing, M., Zhang, P., Wang, G., Feng, J., Mesik, L., Zeng, J., Jiang, H., Wang, S., Looby, J. C., & Guagliardo, N. A. (2018). A genetically encoded fluorescent acetylcholine indicator for in vitro and in vivo studies. *Nature biotechnology*, *36*(8), 726-737.

Joseph, A., & Turrigiano, G. G. (2017). All for One But Not One for All: Excitatory Synaptic Scaling and Intrinsic Excitability Are Coregulated by CaMKIV, Whereas Inhibitory Synaptic Scaling Is Under Independent Control. *J Neurosci*, *37*(28), 6778-6785. https://doi.org/10.1523/jneurosci.0618-17.2017

Julian, T. H., Glascow, N., Barry, A. D. F., Moll, T., Harvey, C., Klimentidis, Y. C., Newell, M., Zhang, S., Snyder, M. P., & Cooper-Knock, J. (2021). Physical exercise is a risk factor for amyotrophic lateral sclerosis: Convergent evidence from Mendelian randomisation, transcriptomics and risk genotypes. *EBioMedicine*, *68*, 103397.

Jun, K. Y., Park, J., Oh, K.-W., Kim, E. M., Bae, J. S., Kim, I., & Kim, S. H. (2019). Epidemiology of ALS in Korea using nationwide big data. *Journal of Neurology, Neurosurgery & Psychiatry*, *90*(4), 395-403.

junior Apicella, A., & Marchionni, I. (2022). VIP-Expressing GABAergic Neurons: Disinhibitory vs. Inhibitory Motif and Its Role in Communication Across Neocortical Areas. *Frontiers in Cellular Neuroscience*, *16*.

Kang, S. H., Li, Y., Fukaya, M., Lorenzini, I., Cleveland, D. W., Ostrow, L. W., Rothstein, J. D., & Bergles, D. E. (2013). Degeneration and impaired regeneration of gray matter oligodendrocytes in amyotrophic lateral sclerosis. *Nature neuroscience*, *16*(5), 571-579.

Keller, G. B., Bonhoeffer, T., & Hübener, M. (2012). Sensorimotor mismatch signals in primary visual cortex of the behaving mouse. *Neuron*, *74*(5), 809-815.

Kelley, K. W., Ben Haim, L., Schirmer, L., Tyzack, G. E., Tolman, M., Miller, J. G., Tsai, H. H., Chang, S. M., Molofsky, A. V., Yang, Y., Patani, R., Lakatos, A., Ullian, E. M., & Rowitch, D. H. (2018). Kir4.1-Dependent Astrocyte-Fast Motor Neuron Interactions Are Required for Peak Strength. *Neuron*, *98*(2), 306-319.e307. https://doi.org/10.1016/j.neuron.2018.03.010

Kerr, J. N., Greenberg, D., & Helmchen, F. (2005). Imaging input and output of neocortical networks in vivo. *Proceedings of the National Academy of Sciences*, *102*(39), 14063-14068.

Khademullah, C. S., Aqrabawi, A. J., Place, K. M., Dargaei, Z., Liang, X., Pressey, J. C., Bedard, S., Yang, J. W., Garand, D., & Keramidis, I. (2020). Cortical interneuron-mediated inhibition delays the onset of amyotrophic lateral sclerosis. *Brain*, *143*(3), 800-810.

Kiernan, M. C., Vucic, S., Talbot, K., McDermott, C. J., Hardiman, O., Shefner, J. M., Al-Chalabi, A., Huynh, W., Cudkowicz, M., & Talman, P. (2021). Improving clinical trial outcomes in amyotrophic lateral sclerosis. *Nature Reviews Neurology*, *17*(2), 104-118.

Kim, J., Hughes, E. G., Shetty, A. S., Arlotta, P., Goff, L. A., Bergles, D. E., & Brown, S. P. (2017). Changes in the Excitability of Neocortical Neurons in a Mouse Model of Amyotrophic Lateral Sclerosis Are Not Specific to Corticospinal Neurons and Are Modulated by Advancing Disease. *J Neurosci*, *37*(37), 9037-9053. https://doi.org/10.1523/jneurosci.0811-17.2017

Kino, Y., Washizu, C., Kurosawa, M., Yamada, M., Miyazaki, H., Akagi, T., Hashikawa, T., Takumi, T., Hicks, G. G., & Hattori, N. (2015). FUS/TLS deficiency causes behavioral and pathological abnormalities distinct from amyotrophic lateral sclerosis. *Acta neuropathologica communications*, *3*(1), 1-11.

Kiritani, T., Wickersham, I. R., Seung, H. S., & Shepherd, G. M. (2012). Hierarchical connectivity and connection-specific dynamics in the corticospinal–corticostriatal microcircuit in mouse motor cortex. *Journal of Neuroscience*, *32*(14), 4992-5001.

Komiyama, T., Sato, T. R., O'Connor, D. H., Zhang, Y.-X., Huber, D., Hooks, B. M., Gabitto, M., & Svoboda, K. (2010). Learning-related fine-scale specificity imaged in motor cortex circuits of behaving mice. *Nature*, *464*(7292), 1182-1186.

Koppers, M., Blokhuis, A. M., Westeneng, H. J., Terpstra, M. L., Zundel, C. A., Vieira de Sá, R., Schellevis, R. D., Waite, A. J., Blake, D. J., & Veldink, J. H. (2015). C 9orf72 ablation in mice does not cause motor neuron degeneration or motor deficits. *Annals of neurology*, *78*(3), 426-438.

Korobeynikov, V. A., Lyashchenko, A. K., Blanco-Redondo, B., Jafar-Nejad, P., & Shneider, N. A. (2022). Antisense oligonucleotide silencing of FUS expression as a therapeutic approach in amyotrophic lateral sclerosis. *Nature Medicine*, 1-13.

Korzhova, V., Marinković, P., Goltstein, P. M., Herms, J., & Liebscher, S. (2019). Long-term dynamics of aberrant neuronal activity in Alzheimer's disease. *biorxiv*, 801902. https://doi.org/10.1101/801902

Kostera-Pruszczyk, A., Niebroj-Dobosz, I., Emeryk-Szajewska, B., Karwanska, A., & Rowinska-Marcinska, K. (2002). Motor unit hyperexcitability in amyotrophic lateral sclerosis vs amino acids acting as neurotransmitters. *Acta Neurol Scand*, *106*(1), 34-38. https://doi.org/10.1034/j.1600-0404.2002.00149.x

Krabbe, S., Paradiso, E., d'Aquin, S., Bitterman, Y., Courtin, J., Xu, C., Yonehara, K., Markovic, M., Müller, C., & Eichlisberger, T. (2019). Adaptive disinhibitory gating by VIP interneurons permits associative learning. *Nature neuroscience*, *22*(11), 1834-1843.

Kreilaus, F., Guerra, S., Masanetz, R., Menne, V., Yerbury, J., & Karl, T. (2020). Novel behavioural characteristics of the superoxide dismutase 1 G93A (SOD1G93A) mouse model of amyotrophic lateral sclerosis include sex-dependent phenotypes. *Genes, Brain and Behavior*, *19*(2), e12604.

Kubota, Y., Karube, F., Nomura, M., & Kawaguchi, Y. (2016). The diversity of cortical inhibitory synapses. *Frontiers in neural circuits*, *10*, 27.

Kumar, D. R., Aslinia, F., Yale, S. H., & Mazza, J. J. (2011). Jean-Martin Charcot: the father of neurology. *Clinical medicine & research*, *9*(1), 46-49.

Kuo, M.-F., Grosch, J., Fregni, F., Paulus, W., & Nitsche, M. A. (2007). Focusing effect of acetylcholine on neuroplasticity in the human motor cortex. *Journal of Neuroscience*, *27*(52), 14442-14447.

Kuo, P.-H., Doudeva, L. G., Wang, Y.-T., Shen, C.-K. J., & Yuan, H. S. (2009). Structural insights into TDP-43 in nucleic-acid binding and domain interactions. *Nucleic acids research*, *37*(6), 1799-1808.

Kwan, A. C., & Dan, Y. (2012). Dissection of cortical microcircuits by single-neuron stimulation in vivo. *Current Biology*, *22*(16), 1459-1467.

Lee, S., Hjerling-Leffler, J., Zagha, E., Fishell, G., & Rudy, B. (2010). The largest group of superficial neocortical GABAergic interneurons expresses ionotropic serotonin receptors. *Journal of Neuroscience*, *30*(50), 16796-16808.

Lee, S., Kruglikov, I., Huang, Z. J., Fishell, G., & Rudy, B. (2013). A disinhibitory circuit mediates motor integration in the somatosensory cortex. *Nature neuroscience*, *16*(11), 1662-1670. https://doi.org/10.1038/nn.3544

Lei, H., Dirren, E., Poitry-Yamate, C., Schneider, B. L., Gruetter, R., & Aebischer, P. (2019). Evolution of the neurochemical profiles in the G93A-SOD1 mouse model of amyotrophic lateral sclerosis. *Journal of cerebral blood flow and metabolism : official journal of the International Society of Cerebral Blood Flow and Metabolism*, *39*(7), 1283–1298. https://doi.org/10.1177/0271678x18756499

Leighton, D. J., Newton, J., Stephenson, L. J., Colville, S., Davenport, R., Gorrie, G., Morrison, I., Swingler, R., Chandran, S., & Pal, S. (2019). Changing epidemiology of motor neurone disease in Scotland. *Journal of neurology*, *266*(4), 817-825.

Leinweber, M., Ward, D. R., Sobczak, J. M., Attinger, A., & Keller, G. B. (2017). A sensorimotor circuit in mouse cortex for visual flow predictions. *Neuron*, *95*(6), 1420-1432. e1425.

Lewerenz, J., & Maher, P. (2015). Chronic glutamate toxicity in neurodegenerative diseases—what is the evidence? *Frontiers in neuroscience*, *9*, 469.

Lian, L., Liu, M., Cui, L., Guan, Y., Liu, T., Cui, B., Zhang, K., Tai, H., & Shen, D. (2019). Environmental risk factors and amyotrophic lateral sclerosis (ALS): a case-control study of ALS in China. *Journal of Clinical Neuroscience*, *66*, 12-18.

Liebscher, S., Keller, G. B., Goltstein, P. M., Bonhoeffer, T., & Hubener, M. (2016). Selective Persistence of Sensorimotor Mismatch Signals in Visual Cortex of Behaving Alzheimer's Disease Mice. *Curr Biol*, *26*(7), 956-964. https://doi.org/10.1016/j.cub.2016.01.070

Limone, F., Mordes, D., Couto, A., Pietiläinen, O., Joseph, B. J., Burberry, A., Ghosh, S. D., Meyer, D., Goldman, M., & Bortolin, L. (2021). Single-nucleus sequencing reveals enriched expression of genetic risk factors sensitises Motor Neurons to degeneration in ALS. *biorxiv*.

Ling, S.-C., Polymenidou, M., & Cleveland, D. W. (2013). Converging mechanisms in ALS and FTD: disrupted RNA and protein homeostasis. *Neuron*, *79*(3), 416-438. https://doi.org/10.1016/j.neuron.2013.07.033

Liu, X., Pimm, M. L., Haarer, B., Brawner, A. T., & Henty-Ridilla, J. L. (2022a). Biochemical characterization of actin assembly mechanisms with ALS-associated profilin variants. *European Journal of Cell Biology*, *101*(2), 151212.

Liu, Y., Andreucci, A., Iwamoto, N., Yin, Y., Yang, H., Liu, F., Bulychev, A., Hu, X. S., Lin, X., & Lamore, S. (2022b). Preclinical evaluation of WVE-004, aninvestigational stereopure oligonucleotide forthe treatment of C9orf72-associated ALS or FTD. *Molecular Therapy-Nucleic Acids*, *28*, 558-570.

Liu, Y., Xin, Y., & Xu, N.-l. (2021). A cortical circuit mechanism for structural knowledge-based flexible sensorimotor decision-making. *Neuron*, *109*(12), 2009-2024. e2006.

Logroscino, G., & Piccininni, M. (2019). Amyotrophic lateral sclerosis descriptive epidemiology: the origin of geographic difference. *Neuroepidemiology*, *52*(1-2), 93-103.

Longinetti, E., & Fang, F. (2019). Epidemiology of amyotrophic lateral sclerosis: an update of recent literature. *Current opinion in neurology*, *32*(5), 771.

Longinetti, E., Regodón Wallin, A., Samuelsson, K., Press, R., Zachau, A., Ronnevi, L.-O., Kierkegaard, M., Andersen, P. M., Hillert, J., & Fang, F. (2018). The Swedish motor neuron disease quality registry. *Amyotrophic Lateral Sclerosis and Frontotemporal Degeneration*, *19*(7-8), 528-537.

Loubinoux, I., Tombari, D., Pariente, J., Gerdelat-Mas, A., Franceries, X., Cassol, E., Rascol, O., Pastor, J., & Chollet, F. (2005). Modulation of behavior and cortical motor activity in healthy subjects by a chronic administration of a serotonin enhancer. *Neuroimage*, *27*(2), 299-313.

Lozeva, V., Valjakka, A., Lecklin, A., Olkkonen, H., Hippeläinen, M., Itkonen, M., Plumed, C., & Tuomisto, L. (2000). Effects of the histamine H1 receptor blocker, pyrilamine, on spontaneous locomotor activity of rats with long-term portacaval anastomosis. *Hepatology*, *31*(2), 336-344.

Luna, J., Diagana, M., Aissa, L. A., Tazir, M., Pacha, L. A., Kacem, I., Gouider, R., Henning, F., Basse, A., & Cisse, O. (2019). Clinical features and prognosis of amyotrophic lateral sclerosis in Africa: the TROPALS study. *Journal of Neurology, Neurosurgery & Psychiatry*, *90*(1), 20-29.

Luo, P., Li, A., Zheng, Y., Han, Y., Tian, J., Xu, Z., Gong, H., & Li, X. (2019). Whole Brain Mapping of Long-Range Direct Input to Glutamatergic and GABAergic Neurons in Motor Cortex. *Front Neuroanat*, *13*, 44. https://doi.org/10.3389/fnana.2019.00044

Lyon, K. A., & Allen, N. J. (2022). From Synapses to Circuits, Astrocytes Regulate Behavior. *Frontiers in neural circuits*, 136.

Mackenzie, I. R., & H. Feldman, H. (2005). Ubiquitin immunohistochemistry suggests classic motor neuron disease, motor neuron disease with dementia, and frontotemporal dementia of the motor neuron disease type represent a clinicopathologic spectrum. *Journal of Neuropathology & Experimental Neurology*, *64*(8), 730-739.

Mahmoud, S., Gharagozloo, M., Simard, C., & Gris, D. (2019). Astrocytes maintain glutamate homeostasis in the CNS by controlling the balance between glutamate uptake and release. *Cells*, *8*(2), 184.

Majumder, V., Gregory, J. M., Barria, M. A., Green, A., & Pal, S. (2018). TDP-43 as a potential biomarker for amyotrophic lateral sclerosis: a systematic review and meta-analysis. *BMC neurology*, *18*(1), 1-7.

Makino, H., Ren, C., Liu, H., Kim, A. N., Kondapaneni, N., Liu, X., Kuzum, D., & Komiyama, T. (2017). Transformation of cortex-wide emergent properties during motor learning. *Neuron*, *94*(4), 880-890. e888.

Marinković, P., Reuter, M. S., Brill, M. S., Godinho, L., Kerschensteiner, M., & Misgeld, T. (2012). Axonal transport deficits and degeneration can evolve independently in mouse models of amyotrophic lateral sclerosis. *Proceedings of the National Academy of Sciences*, *109*(11), 4296-4301. https://doi.org/10.1073/pnas.1200658109

Markram, H., Toledo-Rodriguez, M., Wang, Y., Gupta, A., Silberberg, G., & Wu, C. (2004). Interneurons of the neocortical inhibitory system. *Nat Rev Neurosci*, *5*(10), 793-807. https://doi.org/10.1038/nrn1519

Maurya, S., Sarangi, P., & Jayandharan, G. R. (2022). Safety of Adeno-associated virus-based vector-mediated gene therapy—impact of vector dose. In (pp. 1-2): Nature Publishing Group.

McCombe, P. A., & Henderson, R. D. (2010). Effects of gender in amyotrophic lateral sclerosis. *Gender medicine*, *7*(6), 557-570.

Mejzini, R., Flynn, L. L., Pitout, I. L., Fletcher, S., Wilton, S. D., & Akkari, P. A. (2019). ALS Genetics, Mechanisms, and Therapeutics: Where Are We Now? *Front Neurosci*, *13*, 1310. https://doi.org/10.3389/fnins.2019.01310

Menon, P., Geevasinga, N., van den Bos, M., Yiannikas, C., Kiernan, M. C., & Vucic, S. (2017). Cortical hyperexcitability and disease spread in amyotrophic lateral sclerosis. *Eur J Neurol*, *24*(6), 816-824. https://doi.org/10.1111/ene.13295

Menon, P., Kiernan, M. C., & Vucic, S. (2015). Cortical hyperexcitability precedes lower motor neuron dysfunction in ALS. *Clinical neurophysiology : official journal of the International Federation of Clinical Neurophysiology*, *126*(4), 803–809. https://doi.org/10.1016/j.clinph.2014.04.023

Meyer, H. S., Schwarz, D., Wimmer, V. C., Schmitt, A. C., Kerr, J. N., Sakmann, B., & Helmstaedter, M. (2011). Inhibitory interneurons in a cortical column form hot zones of inhibition in layers 2 and 5A. *Proceedings of the National Academy of Sciences*, *108*(40), 16807-16812.

Migliarini, S., Scaricamazza, S., Valle, C., Ferri, A., Pasqualetti, M., & Ferraro, E. (2021). Microglia morphological changes in the motor cortex of hsod1g93a transgenic als mice. *Brain Sciences*, *11*(6), 807.

Miller, R. G., Jackson, C. E., Kasarskis, E. J., England, J., Forshew, D., Johnston, W., Kalra, S., Katz, J., Mitsumoto, H., & Rosenfeld, J. (2009). Practice parameter update: the care of the patient with amyotrophic lateral sclerosis: drug, nutritional, and respiratory therapies (an evidence-based review): report of the Quality Standards Subcommittee of the American Academy of Neurology. *Neurology*, *73*(15), 1218-1226.

Miller, T. M., Cudkowicz, M. E., Genge, A., Shaw, P. J., Sobue, G., Bucelli, R. C., Chiò, A., Van Damme, P., Ludolph, A. C., & Glass, J. D. (2022). Trial of antisense oligonucleotide Tofersen for SOD1 ALS. *New England Journal of Medicine*, *387*(12), 1099-1110.

Mitchell, H. A., Ahern, T. H., Liles, L. C., Javors, M. A., & Weinshenker, D. (2006). The effects of norepinephrine transporter inactivation on locomotor activity in mice. *Biological psychiatry*, *60*(10), 1046-1052.

Mitchell, J. C., McGoldrick, P., Vance, C., Hortobagyi, T., Sreedharan, J., Rogelj, B., Tudor, E. L., Smith, B. N., Klasen, C., & Miller, C. C. (2013). Overexpression of human wild-type FUS causes progressive motor neuron degeneration in an age-and dose-dependent fashion. *Acta neuropathologica*, *125*(2), 273-288.

Miyazaki, T., Morimoto-Tomita, M., Berthoux, C., Konno, K., Noam, Y., Yamasaki, T., Verhage, M., Castillo, P. E., Watanabe, M., & Tomita, S. (2021). Excitatory and inhibitory receptors utilize distinct post-and trans-synaptic mechanisms in vivo. *Elife*, *10*, e59613.

Mordes, D. A., Morrison, B. M., Ament, X. H., Cantrell, C., Mok, J., Eggan, P., Xue, C., Wang, J.-Y., Eggan, K., & Rothstein, J. D. (2020). Absence of survival and motor deficits in 500 repeat C9ORF72 BAC mice. *Neuron*, *108*(4), 775-783. e774.

Moreno-Delgado, D., Puigdellívol, M., Moreno, E., Rodríguez-Ruiz, M., Botta, J., Gasperini, P., Chiarlone, A., Howell, L. A., Scarselli, M., & Casadó, V. (2020). Modulation of dopamine D1 receptors via histamine H3 receptors is a novel therapeutic target for Huntington's disease. *Elife*, *9*, e51093.

Mori, K., Weng, S.-M., Arzberger, T., May, S., Rentzsch, K., Kremmer, E., Schmid, B., Kretzschmar Hans, A., Cruts, M., Van Broeckhoven, C., Haass, C., & Edbauer, D. (2013). The C9orf72 GGGGCC Repeat Is Translated into Aggregating Dipeptide-Repeat Proteins in FTLD/ALS. *Science*, *339*(6125), 1335-1338. https://doi.org/10.1126/science.1232927

Morin, F., & Beaulieu, C. (1994). Equivalent cell density in three areas of neonatal rat cerebral cortex. *Neuroscience letters*, *176*(1), 85-88.

Mouradian, R. D., Sessler, F. M., & Waterhouse, B. D. (1991). Noradrenergic potentiation of excitatory transmitter action in cerebrocortical slices: evidence for mediation by an α1 receptor-linked second messenger pathway. *Brain research*, *546*(1), 83-95.

Mullard, A. (2021). ALS antisense drug falters in phase III. *Nature reviews. Drug discovery*.

Naka, A., & Adesnik, H. (2016). Inhibitory circuits in cortical layer 5. *Frontiers in neural circuits*, *10*, 35.

Nakai, J., Ohkura, M., & Imoto, K. (2001). A high signal-to-noise Ca2+ probe composed of a single green fluorescent protein. *Nature biotechnology*, *19*(2), 137-141.

Nakken, O., Lindstrøm, J. C., Tysnes, O.-B., & Holmøy, T. (2018). Assessing amyotrophic lateral sclerosis prevalence in Norway from 2009 to 2015 from compulsory nationwide health registers. *Amyotrophic Lateral Sclerosis and Frontotemporal Degeneration*, *19*(3-4), 303-310.

Nashef, A., Cohen, O., Perlmutter, S. I., & Prut, Y. (2022). A cerebellar origin of feedforward inhibition to the motor cortex in non-human primates. *Cell Reports*, *39*(6), 110803.

Naumann, M., Pal, A., Goswami, A., Lojewski, X., Japtok, J., Vehlow, A., Naujock, M., Günther, R., Jin, M., & Stanslowsky, N. (2018). Impaired DNA damage response signaling by FUS-NLS mutations leads to neurodegeneration and FUS aggregate formation. *Nature communications*, *9*(1), 1-17.

Nelson, L. M., Topol, B., Kaye, W., Williamson, D., Horton, D. K., Mehta, P., & Wagner, T. (2018). Estimation of the prevalence of amyotrophic lateral sclerosis in the United States using national administrative healthcare data from 2002 to 2004 and capture-recapture methodology. *Neuroepidemiology*, *51*(3-4), 149-157.

Neumann, M., Sampathu Deepak, M., Kwong Linda, K., Truax Adam, C., Micsenyi Matthew, C., Chou Thomas, T., Bruce, J., Schuck, T., Grossman, M., Clark Christopher, M., McCluskey Leo, F., Miller Bruce, L., Masliah, E., Mackenzie Ian, R., Feldman, H., Feiden, W., Kretzschmar Hans, A., Trojanowski John, Q., & Lee Virginia, M. Y. (2006). Ubiquitinated TDP-43 in Frontotemporal Lobar Degeneration and Amyotrophic Lateral Sclerosis. *Science*, *314*(5796), 130-133. https://doi.org/10.1126/science.1134108

Niblock, M., Smith, B. N., Lee, Y.-B., Sardone, V., Topp, S., Troakes, C., Al-Sarraj, S., Leblond, C. S., Dion, P. A., & Rouleau, G. A. (2016). Retention of hexanucleotide repeat-containing intron in C9orf72 mRNA: implications for the pathogenesis of ALS/FTD. *Acta neuropathologica communications*, *4*(1), 1-12.

Niell, C. M., & Stryker, M. P. (2010). Modulation of visual responses by behavioral state in mouse visual cortex. *Neuron*, *65*(4), 472-479.

Niethard, N., Hasegawa, M., Itokazu, T., Oyanedel, C. N., Born, J., & Sato, T. R. (2016). Sleep-stage-specific regulation of cortical excitation and inhibition. *Current Biology*, *26*(20), 2739-2749.

Nieto-Gonzalez, J. L., Moser, J., Lauritzen, M., Schmitt-John, T., & Jensen, K. (2011). Reduced GABAergic inhibition explains cortical hyperexcitability in the wobbler mouse model of ALS. *Cerebral cortex*, *21*(3), 625-635.

Nigro, M. J., Hashikawa-Yamasaki, Y., & Rudy, B. (2018). Diversity and Connectivity of Layer 5 Somatostatin-Expressing Interneurons in the Mouse Barrel Cortex. *The Journal of Neuroscience*, *38*(7), 1622-1633. https://doi.org/10.1523/JNEUROSCI.2415-17.2017

Nishitoh, H., Kadowaki, H., Nagai, A., Maruyama, T., Yokota, T., Fukutomi, H., Noguchi, T., Matsuzawa, A., Takeda, K., & Ichijo, H. (2008). ALS-linked mutant SOD1 induces ER stress-and ASK1-dependent motor neuron death by targeting Derlin-1. *Genes & development*, *22*(11), 1451-1464.

Nonaka, T., Masuda-Suzukake, M., Hosokawa, M., Shimozawa, A., Hirai, S., Okado, H., & Hasegawa, M. (2018). C9ORF72 dipeptide repeat poly-GA inclusions promote intracellular aggregation of phosphorylated TDP-43. *Human molecular genetics*, *27*(15), 2658-2670.

O'Donovan, S. M., Sullivan, C. R., & McCullumsmith, R. E. (2017). The role of glutamate transporters in the pathophysiology of neuropsychiatric disorders. *npj Schizophrenia*, *3*(1), 32. https://doi.org/10.1038/s41537-017-0037-1

Obrenovitch, T. P. (1998). Amyotrophic lateral sclerosis, excitotoxicity and riluzole. *Trends in pharmacological sciences*, *19*(1), 9.

Oh, J., Lee, C., & Kaang, B.-K. (2019). Imaging and analysis of genetically encoded calcium indicators linking neural circuits and behaviors. *The Korean Journal of Physiology & Pharmacology*, *23*(4), 237-249.

Oliván, S., CAlvO, A. C., RAndO, A., MuñOz, M. J., Zaragoza, P., & Osta, R. (2014). Comparative study of behavioural tests in the SOD1G93A mouse model of amyotrophic lateral sclerosis. *Experimental animals*, 14-0077.

Özdinler, P. H., Benn, S., Yamamoto, T. H., Güzel, M., Brown, R. H., & Macklis, J. D. (2011). Corticospinal motor neurons and related subcerebral projection neurons undergo early and specific neurodegeneration in hSOD1G93A transgenic ALS mice. *Journal of Neuroscience*, *31*(11), 4166-4177.

Pakan, J. M., Lowe, S. C., Dylda, E., Keemink, S. W., Currie, S. P., Coutts, C. A., & Rochefort, N. L. (2016). Behavioral-state modulation of inhibition is context-dependent and cell type specific in mouse visual cortex. *Elife*, *5*.

Palese, F., Sartori, A., Verriello, L., Ros, S., Passadore, P., Manganotti, P., Barbone, F., & Pisa, F. E. (2019). Epidemiology of amyotrophic lateral sclerosis in Friuli-Venezia Giulia, North-Eastern Italy, 2002–2014: a retrospective population-based study. *Amyotrophic Lateral Sclerosis and Frontotemporal Degeneration*, *20*(1-2), 90-99.

Pan, G., Chen, Z., Zheng, H., Zhang, Y., Xu, H., Bu, G., Zheng, H., & Li, Y. (2018). Compensatory mechanisms modulate the neuronal excitability in a kainic acid-induced epilepsy mouse model. *Frontiers in neural circuits*, *12*, 48.

Parkhouse, W. S., Cunningham, L., McFee, I., Litt Miller, J. M., Whitney, D., Pelech, S. L., & Krieger, C. (2008). Neuromuscular dysfunction in the mutant superoxide dismutase mouse model of amyotrophic lateral sclerosis. *Amyotrophic Lateral Sclerosis*, *9*(1), 24-34.

Paul, A., Crow, M., Raudales, R., He, M., Gillis, J., & Huang, Z. J. (2017). Transcriptional architecture of synaptic communication delineates GABAergic neuron identity. *Cell*, *171*(3), 522-539. e520.

Pepper, R. E., Pitman, K. A., Cullen, C. L., & Young, K. M. (2018). How do cells of the oligodendrocyte lineage affect neuronal circuits to influence motor function, memory and mood? *Frontiers in Cellular Neuroscience*, *12*, 399.

Peters, A. J., Lee, J., Hedrick, N. G., O'Neil, K., & Komiyama, T. (2017). Reorganization of corticospinal output during motor learning. *Nature neuroscience*, *20*(8), 1133-1141.

Pieri, M., Carunchio, I., Curcio, L., Mercuri, N. B., & Zona, C. (2009). Increased persistent sodium current determines cortical hyperexcitability in a genetic model of amyotrophic lateral sclerosis. *Exp Neurol*, *215*(2), 368-379. https://doi.org/10.1016/j.expneurol.2008.11.002

Pineda, S. S., Lee, H., Fitzwalter, B. E., Mohammadi, S., Pregent, L. J., Gardashli, M. E., Mantero, J., Engelberg-Cook, E., DeJesus-Hernandez, M., & van Blitterswijk, M. (2021). Single-cell profiling of the human primary motor cortex in ALS and FTLD. *biorxiv*.

Pologruto, T. A., Yasuda, R., & Svoboda, K. (2004). Monitoring neural activity and [Ca2+] with genetically encoded Ca2+ indicators. *Journal of Neuroscience*, *24*(43), 9572-9579.

Polymenidou, M., Lagier-Tourenne, C., Hutt, K. R., Bennett, C. F., Cleveland, D. W., & Yeo, G. W. (2012). Misregulated RNA processing in amyotrophic lateral sclerosis. *Brain research*, *1462*, 3-15. https://doi.org/https://doi.org/10.1016/j.brainres.2012.02.059

Poulet, J. F., & Crochet, S. (2019). The cortical states of wakefulness. *Frontiers in Systems Neuroscience*, *12*, 64.

Prönneke, A., Scheuer, B., Wagener, R. J., Möck, M., Witte, M., & Staiger, J. F. (2015). Characterizing VIP neurons in the barrel cortex of VIPcre/tdTomato mice reveals layer-specific differences. *Cerebral cortex*, *25*(12), 4854-4868.

Prönneke, A., Witte, M., Möck, M., & Staiger, J. F. (2020). Neuromodulation leads to a burst-tonic switch in a subset of VIP neurons in mouse primary somatosensory (barrel) cortex. *Cerebral cortex*, *30*(2), 488-504.

Puig, M. V., Watakabe, A., Ushimaru, M., Yamamori, T., & Kawaguchi, Y. (2010). Serotonin modulates fast-spiking interneuron and synchronous activity in the rat prefrontal cortex through 5-HT1A and 5-HT2A receptors. *Journal of Neuroscience*, *30*(6), 2211-2222.

Rao, S., Chen, R., LaRocca, A. A., Christiansen, M. G., Senko, A. W., Shi, C. H., Chiang, P.-H., Varnavides, G., Xue, J., & Zhou, Y. (2019). Remotely controlled chemomagnetic modulation of targeted neural circuits. *Nature nanotechnology*, *14*(10), 967-973.

Reaume, A., Elliott, J. L., Hoffman, E. K., Kowall, N. W., Ferrante, R. J., Siwek, D. R., Wilcox, H. M., Flood, D. G., Beal, M. F., & Brown, R. H. (1996). Motor neurons in Cu/Zn superoxide dismutase-deficient mice develop normally but exhibit enhanced cell death after axonal injury. *Nature genetics*, *13*(1), 43-47.

Rocha, M. C., Pousinha, P. A., Correia, A. M., Sebastião, A. M., & Ribeiro, J. A. (2013). Early changes of neuromuscular transmission in the SOD1 (G93A) mice model of ALS start long before motor symptoms onset. *PloS one*, *8*(9), e73846.

Roh, M. I., Murakami, Y., Thanos, A., Vavvas, D. G., & Miller, J. W. (2011). Edaravone, an ROS scavenger, ameliorates photoreceptor cell death after experimental retinal detachment. *Investigative ophthalmology & visual science*, *52*(6), 3825-3831.

Rose, L., McKim, D., Leasa, D., Nonoyama, M., Tandon, A., Bai, Y. Q., Amin, R., Katz, S., Goldstein, R., & Gershon, A. (2019). Trends in incidence, prevalence, and mortality of neuromuscular disease in Ontario, Canada: A population-based retrospective cohort study (2003-2014). *PloS one*, *14*(3), e0210574.

Rosen, D. R., Siddique, T., Patterson, D., Figlewicz, D. A., Sapp, P., Hentati, A., Donaldson, D., Goto, J., O'Regan, J. P., Deng, H. X., & et al. (1993). Mutations in Cu/Zn superoxide

dismutase gene are associated with familial amyotrophic lateral sclerosis. *Nature*, *362*(6415), 59-62. https://doi.org/10.1038/362059a0

Ross, C. A., & Poirier, M. A. (2004). Protein aggregation and neurodegenerative disease. *Nature Medicine*, *10*(7), S10-S17.

Roth, B. L. (2016). DREADDs for neuroscientists. *Neuron*, *89*(4), 683-694.

Rothstein, J. D. (1995). Excitotoxicity and neurodegeneration in amyotrophic lateral sclerosis. *Clinical neuroscience (New York, NY)*, *3*(6), 348-359.

Rothstein, J. D., Dykes-Hoberg, M., Pardo, C. A., Bristol, L. A., Jin, L., Kuncl, R. W., Kanai, Y., Hediger, M. A., Wang, Y., Schielke, J. P., & Welty, D. F. (1996). Knockout of glutamate transporters reveals a major role for astroglial transport in excitotoxicity and clearance of glutamate. *Neuron*, *16*(3), 675-686. https://doi.org/10.1016/s0896-6273(00)80086-0

Rothstein, J. D., Tsai, G., Kuncl, R. W., Clawson, L., Cornblath, D. R., Drachman, D. B., Pestronk, A., Stauch, B. L., & Coyle, J. T. (1990). Abnormal excitatory amino acid metabolism in amyotrophic lateral sclerosis. *Ann Neurol*, *28*(1), 18-25. https://doi.org/10.1002/ana.410280106

Rothstein, J. D., Van Kammen, M., Levey, A. I., Martin, L. J., & Kuncl, R. W. (1995). Selective loss of glial glutamate transporter GLT-1 in amyotrophic lateral sclerosis. *Ann Neurol*, *38*(1), 73-84. https://doi.org/10.1002/ana.410380114

Rubio-Garrido, P., Pérez-de-Manzo, F., Porrero, C., Galazo, M. J., & Clascá, F. (2009). Thalamic input to distal apical dendrites in neocortical layer 1 is massive and highly convergent. *Cerebral cortex*, *19*(10), 2380-2395.

Rudy, B., Fishell, G., Lee, S., & Hjerling-Leffler, J. (2011). Three groups of interneurons account for nearly 100% of neocortical GABAergic neurons. *Developmental Neurobiology*, *71*(1), 45-61. https://doi.org/10.1002/dneu.20853

Saba, L., Viscomi, M., Caioli, S., Pignataro, A., Bisicchia, E., Pieri, M., Molinari, M., Ammassari-Teule, M., & Zona, C. (2016). Altered functionality, morphology, and vesicular glutamate transporter expression of cortical motor neurons from a presymptomatic mouse model of amyotrophic lateral sclerosis. *Cerebral cortex*, *26*(4), 1512-1528.

Sábado, J., Casanovas, A., Tarabal, O., Hereu, M., Piedrafita, L., Calderó, J., & Esquerda, J. E. (2014). Accumulation of misfolded SOD1 in dorsal root ganglion degenerating proprioceptive sensory neurons of transgenic mice with amyotrophic lateral sclerosis. *BioMed Research International*, *2014*, 852163-852163. https://doi.org/10.1155/2014/852163

Safari, M.-S., Mirnajafi-Zadeh, J., Hioki, H., & Tsumoto, T. (2017). Parvalbumin-expressing interneurons can act solo while somatostatin-expressing interneurons act in chorus in most cases on cortical pyramidal cells. *Scientific reports*, *7*(1), 12764. https://doi.org/10.1038/s41598-017-12958-4

Sahadevan, S., Hembach, K. M., Tantardini, E., Pérez-Berlanga, M., Hruska-Plochan, M., Megat, S., Weber, J., Schwarz, P., Dupuis, L., & Robinson, M. D. (2021). Synaptic FUS accumulation triggers early misregulation of synaptic RNAs in a mouse model of ALS. *Nature communications*, *12*(1), 1-17.

Salter, M. W., & Beggs, S. (2014). Sublime microglia: expanding roles for the guardians of the CNS. *Cell*, *158*(1), 15-24.

Sasaki, S., & Maruyama, S. (1994). Immunocytochemical and ultrastructural studies of the motor cortex in amyotrophic lateral sclerosis. *Acta neuropathologica*, *87*(6), 578-585.

Sau, D., De Biasi, S., Vitellaro-Zuccarello, L., Riso, P., Guarnieri, S., Porrini, M., Simeoni, S., Crippa, V., Onesto, E., & Palazzolo, I. (2007). Mutation of SOD1 in ALS: a gain of a loss of function. *Human molecular genetics*, *16*(13), 1604-1618.

Savier, E. L., Chen, H., & Cang, J. (2019). Effects of locomotion on visual responses in the mouse superior colliculus. *Journal of Neuroscience*, *39*(47), 9360-9368.

Sawada, H. (2017). Clinical efficacy of edaravone for the treatment of amyotrophic lateral sclerosis. *Expert Opinion on Pharmacotherapy*, *18*(7), 735-738.

Scekic-Zahirovic, J., Oussini, H. E., Mersmann, S., Drenner, K., Wagner, M., Sun, Y., Allmeroth, K., Dieterlé, S., Sinniger, J., Dirrig-Grosch, S., René, F., Dormann, D., Haass, C., Ludolph, A. C., Lagier-Tourenne, C., Storkebaum, E., & Dupuis, L. (2017). Motor neuron intrinsic and extrinsic mechanisms contribute to the pathogenesis of FUS-associated amyotrophic lateral sclerosis. *Acta neuropathologica*, *133*(6), 887-906. https://doi.org/10.1007/s00401-017-1687-9

Scekic-Zahirovic, J., Sanjuan-Ruiz, I., Kan, V., Megat, S., De Rossi, P., Dieterle, S., Cassel, R., Jamet, M., Kessler, P., Wiesner, D., Tzeplaeff, L., Demais, V., Sahadevan, S., Hembach, K. M., Muller, H. P., Picchiarelli, G., Mishra, N., Antonucci, S., Dirrig-Grosch, S., . . . Dupuis, L. (2021). Cytoplasmic FUS triggers early behavioral alterations linked to cortical neuronal hyperactivity and inhibitory synaptic defects. *Nat Commun*, *12*(1), 3028. https://doi.org/10.1038/s41467-021-23187-9

Scekic-Zahirovic, J., Sendscheid, O., El Oussini, H., Jambeau, M., Sun, Y., Mersmann, S., Wagner, M., Dieterle, S., Sinniger, J., Dirrig-Grosch, S., Drenner, K., Birling, M. C., Qiu, J., Zhou, Y., Li, H., Fu, X. D., Rouaux, C., Shelkovnikova, T., Witting, A., . . . Dupuis, L. (2016). Toxic gain of function from mutant FUS protein is crucial to trigger cell autonomous motor neuron loss. *EMBO J*, *35*(10), 1077-1097. https://doi.org/10.15252/embj.201592559

Scekic-Zahirovic, J., Sendscheid, O., El Oussini, H., Jambeau, M., Sun, Y., Mersmann, S., Wagner, M., Dieterlé, S., Sinniger, J., & Dirrig-Grosch, S. (2016). Toxic gain of function from mutant FUS protein is crucial to trigger cell autonomous motor neuron loss. *The EMBO journal*, *35*(10), 1077-1097.

Scheyltjens, I., & Arckens, L. (2016). The Current Status of Somatostatin-Interneurons in Inhibitory Control of Brain Function and Plasticity. *Neural plasticity*, *2016*, 8723623-8723623. https://doi.org/10.1155/2016/8723623

Schneider, D. M., Nelson, A., & Mooney, R. (2014). A synaptic and circuit basis for corollary discharge in the auditory cortex. *Nature*, *513*(7517), 189-194.

Schulthess, I., Gorges, M., Müller, H., Lulé, D., Del Tredici, K., Ludolph, A., & and Kassubek, J. (2016). Functional connectivity changes resemble patterns of pTDP-43 pathology in amyotrophic lateral sclerosis. *Scientific reports*, *6*(1). https://doi.org/10.1038/srep38391

Shang, H., Liu, G., Jiang, Y., Fu, J., Zhang, B., Song, R., & Wang, W. (2015). Pathway analysis of two amyotrophic lateral sclerosis GWAS highlights shared genetic signals with Alzheimer's disease and Parkinson's disease. *Mol Neurobiol*, *51*(1), 361-369. https://doi.org/10.1007/s12035-014-8673-1

Shao, Q., Liang, C., Chang, Q., Zhang, W., Yang, M., & Chen, J.-F. (2019). C9orf72 deficiency promotes motor deficits of a C9ALS/FTD mouse model in a dose-dependent manner. *Acta neuropathologica communications*, *7*(1), 1-3.

Sharma, A., Lyashchenko, A. K., Lu, L., Nasrabady, S. E., Elmaleh, M., Mendelsohn, M., Nemes, A., Tapia, J. C., Mentis, G. Z., & Shneider, N. A. (2016). ALS-associated mutant FUS induces selective motor neuron degeneration through toxic gain of function. *Nature communications*, *7*, 10465-10465. https://doi.org/10.1038/ncomms10465

Shaw, P., Miller, T., Cudkowicz, M., Genge, A., Sobue, G., Nestorov, I., Graham, D.-i., Fanning, L., Fradette, S., & McNeill, M. (2022). Tofersen in adults with SOD1-ALS: phase 3 VALOR trial and open-label extension results. In: BMJ Publishing Group Ltd.

Shellikeri, S., Karthikeyan, V., Martino, R., Black, S., Zinman, L., Keith, J., & Yunusova, Y. (2017). The neuropathological signature of bulbar-onset ALS: a systematic review. *Neuroscience & Biobehavioral Reviews*, *75*, 378-392.

Shepherd, G. M. (2013). Corticostriatal connectivity and its role in disease. *Nature Reviews Neuroscience*, *14*(4), 278-291.

Shibuya, K., Simon, N. G., Geevasinga, N., Menon, P., Howells, J., Park, S. B., Huynh, W., Noto, Y.-i., Vucic, S., & Kiernan, M. C. (2017). The evolution of motor cortical dysfunction in amyotrophic lateral sclerosis. *Clinical Neurophysiology*, *128*(6), 1075-1082.

Siciliano, G., Manca, M. L., Sagliocco, L., Pastorini, E., Pellegrinetti, A., Sartucci, F., Sabatini, A., & Murri, L. (1999). Cortical silent period in patients with amyotrophic lateral sclerosis. *Journal of the neurological sciences*, *169*(1-2), 93-97.

Silberberg, G., & Markram, H. (2007). Disynaptic inhibition between neocortical pyramidal cells mediated by Martinotti cells. *Neuron*, *53*(5), 735-746.

Silva, P. R., Nieva, G. V., & Igaz, L. M. (2019). Suppression of conditional TDP-43 transgene expression differentially affects early cognitive and social phenotypes in TDP-43 Mice. *Frontiers in Genetics*, *10*, 369.

Skouras, S., Falcon, C., Tucholka, A., Rami, L., Sanchez-Valle, R., Lladó, A., Gispert, J. D., & Molinuevo, J. L. (2019). Mechanisms of functional compensation, delineated by eigenvector centrality mapping, across the pathophysiological continuum of Alzheimer's disease. *NeuroImage: Clinical*, *22*, 101777.

Smeyers, J., Banchi, E.-G., & Latouche, M. (2021). C9ORF72: What it is, what it does, and why it matters. *Frontiers in Cellular Neuroscience*, *15*.

Smith, J. A., Das, A., Ray, S. K., & Banik, N. L. (2012). Role of pro-inflammatory cytokines released from microglia in neurodegenerative diseases. *Brain research bulletin*, *87*(1), 10-20.

Sofroniew, N. J., Cohen, J. D., Lee, A. K., & Svoboda, K. (2014). Natural whisker-guided behavior by head-fixed mice in tactile virtual reality. *Journal of Neuroscience*, *34*(29), 9537-9550.

Sohn, J., Okamoto, S., Kataoka, N., Kaneko, T., Nakamura, K., & Hioki, H. (2016). Differential inputs to the perisomatic and distal-dendritic compartments of VIP-positive neurons in layer 2/3 of the mouse barrel cortex. *Frontiers in neuroanatomy*, *10*, 124.

Spruston, N. (2008). Pyramidal neurons: dendritic structure and synaptic integration. *Nature Reviews Neuroscience*, *9*(3), 206-221.

Sreedharan, J., Blair, I. P., Tripathi, V. B., Hu, X., Vance, C., Rogelj, B., Ackerley, S., Durnall, J. C., Williams, K. L., Buratti, E., Baralle, F., de Belleroche, J., Mitchell, J. D., Leigh, P. N., Al-Chalabi, A., Miller, C. C., Nicholson, G., & Shaw, C. E. (2008). TDP-43 mutations in familial and sporadic amyotrophic lateral sclerosis. *Science*, *319*(5870), 1668-1672. https://doi.org/10.1126/science.1154584

Steffens, H., Mott, A. C., Li, S., Wegner, W., Svehla, P., Kan, V. W. Y., Wolf, F., Liebscher, S., & Willig, K. I. (2021). Stable but not rigid: Chronic in vivo STED nanoscopy reveals extensive remodeling of spines, indicating multiple drivers of plasticity. *Sci Adv*, *7*(24). https://doi.org/10.1126/sciadv.abf2806

Stegmann, G. M., Hahn, S., Liss, J., Shefner, J., Rutkove, S., Shelton, K., Duncan, C. J., & Berisha, V. (2020). Early detection and tracking of bulbar changes in ALS via frequent and remote speech analysis. *NPJ digital medicine*, *3*(1), 1-5.

Stenmark, H. (2009). Rab GTPases as coordinators of vesicle traffic. *Nature reviews Molecular cell biology*, *10*(8), 513-525.

Ström, A. L., Gal, J., Shi, P., Kasarskis, E. J., Hayward, L. J., & Zhu, H. (2008). Retrograde axonal transport and motor neuron disease. *Journal of neurochemistry*, *106*(2), 495-505.

Sun, Y., Curle, A. J., Haider, A. M., & Balmus, G. (2020). The role of DNA damage response in amyotrophic lateral sclerosis. *Essays in Biochemistry*, *64*(5), 847-861.

Sundaramoorthy, V., Sultana, J. M., & Atkin, J. D. (2015). Golgi fragmentation in amyotrophic lateral sclerosis, an overview of possible triggers and consequences. *Frontiers in neuroscience*, *9*, 400.

Svoboda, K., & Yasuda, R. (2006). Principles of two-photon excitation microscopy and its applications to neuroscience. *Neuron*, *50*(6), 823-839.

Swanson, O. K., & Maffei, A. (2019). From hiring to firing: activation of inhibitory neurons and their recruitment in behavior. *Frontiers in molecular neuroscience*, *12*, 168.

Szegedi, V., Paizs, M., Baka, J., Barzo, P., Molnar, G., Tamas, G., & Lamsa, K. (2020). Robust perisomatic GABAergic self-innervation inhibits basket cells in the human and mouse supragranular neocortex. *Elife*, *9*.

Takahashi, H., Snow, B., Bhatt, M. H., Peppard, R., Eisen, A., & Calne, D. B. (1993). Evidence for a dopaminergic deficit in sporadic amyotrophic lateral sclerosis on positron emission scanning. *The Lancet*, *342*(8878), 1016-1018.

Takahashi, N., Moberg, S., Zolnik, T. A., Catanese, J., Sachdev, R. N., Larkum, M. E., & Jaeger, D. (2021). Thalamic input to motor cortex facilitates goal-directed action initiation. *Current Biology*, *31*(18), 4148-4155. e4144.

Taylor, J. P., Brown, R. H., Jr., & Cleveland, D. W. (2016). Decoding ALS: from genes to mechanism. *Nature*, *539*(7628), 197-206. https://doi.org/10.1038/nature20413

Teuling, E., Ahmed, S., Haasdijk, E., Demmers, J., Steinmetz, M. O., Akhmanova, A., Jaarsma, D., & Hoogenraad, C. C. (2007). Motor neuron disease-associated mutant vesicle-associated membrane protein-associated protein (VAP) B recruits wild-type VAPs into endoplasmic reticulum-derived tubular aggregates. *Journal of Neuroscience*, *27*(36), 9801-9815.

Tian, L., Hires, S. A., Mao, T., Huber, D., Chiappe, M. E., Chalasani, S. H., Petreanu, L., Akerboom, J., McKinney, S. A., & Schreiter, E. R. (2009). Imaging neural activity in worms, flies and mice with improved GCaMP calcium indicators. *Nature methods*, *6*(12), 875-881.

Tjia, M., Yu, X., Jammu, L. S., Lu, J., & Zuo, Y. (2017). Pyramidal neurons in different cortical layers exhibit distinct dynamics and plasticity of apical dendritic spines. *Frontiers in neural circuits*, *11*, 43.

Tollervey, J. R., Curk, T., Rogelj, B., Briese, M., Cereda, M., Kayikci, M., König, J., Hortobágyi, T., Nishimura, A. L., & Župunski, V. (2011). Characterizing the RNA targets and position-dependent splicing regulation by TDP-43. *Nature neuroscience*, *14*(4), 452-458.

Tovar-y-Romo, L. B., Santa-Cruz, L. D., Zepeda, A., & Tapia, R. (2009). Chronic elevation of extracellular glutamate due to transport blockade is innocuous for spinal motoneurons in vivo. *Neurochemistry international*, *54*(3), 186-191. https://doi.org/https://doi.org/10.1016/j.neuint.2008.09.015

Tremblay, M.-È., Lowery, R. L., & Majewska, A. K. (2010). Microglial interactions with synapses are modulated by visual experience. *PLoS biology*, *8*(11), e1000527.

Tremblay, R., Lee, S., & Rudy, B. (2016). GABAergic Interneurons in the Neocortex: From Cellular Properties to Circuits. *Neuron*, *91*(2), 260-292. https://doi.org/10.1016/j.neuron.2016.06.033

Trotti, D., Rolfs, A., Danbolt, N. C., Brown, R. H., Jr., & Hediger, M. A. (1999). SOD1 mutants linked to amyotrophic lateral sclerosis selectively inactivate a glial glutamate transporter. *Nat Neurosci*, *2*(9), 848. https://doi.org/10.1038/12227

Tu, P.-H., Raju, P., Robinson, K. A., Gurney, M. E., Trojanowski, J. Q., & Lee, V. (1996). Transgenic mice carrying a human mutant superoxide dismutase transgene develop

neuronal cytoskeletal pathology resembling human amyotrophic lateral sclerosis lesions. *Proceedings of the National Academy of Sciences*, *93*(7), 3155-3160.

Turgut, N., Varol SaraÇoglu, G., Kat, S., Balci, K., GÜldiken, B., Birgili, O., & Kabayel, L. (2019). An epidemiologic investigation of amyotrophic lateral sclerosis in Thrace, Turkey, 2006–2010. *Amyotrophic Lateral Sclerosis and Frontotemporal Degeneration*, *20*(1-2), 100-106.

Turner, M., Bakker, M., Sham, P., Shaw, C., Leigh, P., & Al-Chalabi, A. (2002). Prognostic modelling of therapeutic interventions in amyotrophic lateral sclerosis. *Amyotrophic Lateral Sclerosis and Other Motor Neuron Disorders*, *3*(1), 15-21.

Turner, M., Rabiner, E., Hammers, A., Al-Chalabi, A., Grasby, P., Shaw, C., Brooks, D., & Leigh, P. (2005). [11C]-WAY100635 PET demonstrates marked 5-HT1A receptor changes in sporadic ALS. *Brain*, *128*(4), 896-905.

Turner, M. R., Brockington, A., Scaber, J., Hollinger, H., Marsden, R., Shaw, P. J., & Talbot, K. (2010). Pattern of spread and prognosis in lower limb-onset ALS. *Amyotrophic Lateral Sclerosis*, *11*(4), 369-373.

Turrigiano, G. (2011). Too many cooks? Intrinsic and synaptic homeostatic mechanisms in cortical circuit refinement. *Annual review of neuroscience*, *34*, 89-103.

Turrigiano, G. G. (2008). The self-tuning neuron: synaptic scaling of excitatory synapses. *Cell*, *135*(3), 422-435.

Tyzack, G. E., Luisier, R., Taha, D. M., Neeves, J., Modic, M., Mitchell, J. S., Meyer, I., Greensmith, L., Newcombe, J., Ule, J., Luscombe, N. M., & Patani, R. (2019). Widespread FUS mislocalization is a molecular hallmark of amyotrophic lateral sclerosis. *Brain*, *142*(9), 2572-2580. https://doi.org/10.1093/brain/awz217

Usachev, Y. M., & Thayer, S. A. (1997). All-or-none Ca2+ release from intracellular stores triggered by Ca2+ influx through voltage-gated Ca2+ channels in rat sensory neurons. *Journal of Neuroscience*, *17*(19), 7404-7414.

Valle-Bautista, R., Márquez-Valadez, B., Herrera-López, G., Griego, E., Galván, E. J., Díaz, N.-F., Arias-Montaño, J.-A., & Molina-Hernández, A. (2021). Long-Term Functional and Cytoarchitectonic Effects of the Systemic Administration of the Histamine H1 Receptor Antagonist/Inverse Agonist Chlorpheniramine During Gestation in the Rat Offspring Primary Motor Cortex. *Frontiers in neuroscience*, *15*.

Van den Bos, M. A., Higashihara, M., Geevasinga, N., Menon, P., Kiernan, M. C., & Vucic, S. (2018). Imbalance of cortical facilitatory and inhibitory circuits underlies hyperexcitability in ALS. *Neurology*, *91*(18), e1669-e1676.

Van Den Bosch, L., Van Damme, P., Bogaert, E., & Robberecht, W. (2006). The role of excitotoxicity in the pathogenesis of amyotrophic lateral sclerosis. *Biochim Biophys Acta*, *1762*(11-12), 1068-1082. https://doi.org/10.1016/j.bbadis.2006.05.002

van Zundert, B., Peuscher, M. H., Hynynen, M., Chen, A., Neve, R. L., Brown, R. H., Constantine-Paton, M., & Bellingham, M. C. (2008). Neonatal neuronal circuitry shows hyperexcitable disturbance in a mouse model of the adult-onset neurodegenerative disease amyotrophic lateral sclerosis. *The Journal of neuroscience : the official journal of the Society for Neuroscience*, *28*(43), 10864–10874. https://doi.org/10.1523/jneurosci.1340-08.2008

Vance, C., Rogelj, B., Hortobágyi, T., De Vos, K. J., Nishimura, A. L., Sreedharan, J., Hu, X., Smith, B., Ruddy, D., & Wright, P. (2009). Mutations in FUS, an RNA processing protein, cause familial amyotrophic lateral sclerosis type 6. *Science*, *323*(5918), 1208-1211.

Velasques, B., Cagy, M., Piedade, R., & Ribeiro, P. (2013). Sensorimotor integration and attention: An electrophysiological analysis. *Functional brain mapping and the endeavor to understand the working brain*.

Verdone, B. M., Cicardi, M. E., Wen, X., Sriramoji, S., Russell, K., Markandaiah, S. S., Jensen, B. K., Krishnamurthy, K., Haeusler, A. R., & Pasinelli, P. (2022). A mouse model with widespread expression of the C9orf72-linked glycine–arginine dipeptide displays non-lethal ALS/FTD-like phenotypes. *Scientific reports*, *12*(1), 1-17.

Veres, J. M., Nagy, G. A., & Hájos, N. (2017). Perisomatic GABAergic synapses of basket cells effectively control principal neuron activity in amygdala networks. *Elife*, *6*, e20721. https://doi.org/10.7554/eLife.20721

Vitrac, C., & Benoit-Marand, M. (2017). Monoaminergic modulation of motor cortex function. *Frontiers in neural circuits*, *11*, 72.

Vitrac, C., Péron, S., Frappé, I., Fernagut, P.-O., Jaber, M., Gaillard, A., & Benoit-Marand, M. (2014). Dopamine control of pyramidal neuron activity in the primary motor cortex via D2 receptors. *Frontiers in neural circuits*, *8*, 13.

Vogels, O., Veltman, J., Oyen, W., & Horstink, M. (2000). Decreased striatal dopamine D2 receptor binding in amyotrophic lateral sclerosis (ALS) and multiple system atrophy (MSA): D2 receptor down-regulation versus striatal cell degeneration. *Journal of the neurological sciences*, *180*(1-2), 62-65.

Vucic, S., Cheah, B. C., & Kiernan, M. C. (2009). Defining the mechanisms that underlie cortical hyperexcitability in amyotrophic lateral sclerosis. *Experimental neurology*, *220*(1), 177-182.

Vucic, S., Nicholson, G. A., & Kiernan, M. C. (2008). Cortical hyperexcitability may precede the onset of familial amyotrophic lateral sclerosis. *Brain*, *131*(Pt 6), 1540-1550. https://doi.org/10.1093/brain/awn071

Vucic, S., Pavey, N., Haidar, M., Turner, B., & Kiernan, M. (2021). Cortical hyperexcitability: Diagnostic and pathogenic biomarker of ALS. *Neuroscience letters*, *759*, 136039. https://doi.org/ 10.1016/j.neulet.2021.136039

Wake, H., Moorhouse, A. J., Miyamoto, A., & Nabekura, J. (2013). Microglia: actively surveying and shaping neuronal circuit structure and function. *Trends in neurosciences*, *36*(4), 209-217.

Wang, S., Latallo, M. J., Zhang, Z., Huang, B., Bobrovnikov, D. G., Dong, D., Livingston, N. M., Tjoeng, W., Hayes, L. R., & Rothstein, J. D. (2021). Nuclear export and translation of circular repeat-containing intronic RNA in C9ORF72-ALS/FTD. *Nature communications*, *12*(1), 1-14.

Wang, S., Wang, B., Shang, D., Zhang, K., Yan, X., & Zhang, X. (2022). Ion Channel Dysfunction in Astrocytes in Neurodegenerative Diseases. *Frontiers in Physiology*, 11.

Watkins, J. A., Alix, J. J., Shaw, P. J., & Mead, R. J. (2021). Extensive phenotypic characterisation of a human TDP-43Q331K transgenic mouse model of amyotrophic lateral sclerosis (ALS). *Scientific reports*, *11*(1), 1-14.

Webster, C. P., Smith, E. F., Shaw, P. J., & De Vos, K. J. (2017). Protein homeostasis in amyotrophic lateral sclerosis: therapeutic opportunities? *Frontiers in molecular neuroscience*, *10*, 123.

Wilson, J. M. B., Khabazian, I., Pow, D. V., Craig, U. K., & Shaw, C. A. (2003). Decrease in glial glutamate transporter variants and excitatory amino acid receptor down-regulation in a murine model of ALS-PDC [journal article]. *NeuroMolecular Medicine*, *3*(2), 105-117. https://doi.org/10.1385/nmm:3:2:105

Wolpert, D. M., Goodbody, S. J., & Husain, M. (1998). Maintaining internal representations: the role of the human superior parietal lobe. *Nature neuroscience*, *1*(6), 529-533.

Wood, K. C., Blackwell, J. M., & Geffen, M. N. (2017). Cortical inhibitory interneurons control sensory processing. *Current opinion in neurobiology*, *46*, 200-207.

Wooley, C. M., Sher, R. B., Kale, A., Frankel, W. N., Cox, G. A., & Seburn, K. L. (2005). Gait analysis detects early changes in transgenic SOD1 (G93A) mice. *Muscle & Nerve:*

Official Journal of the American Association of Electrodiagnostic Medicine, *32*(1), 43-50.

Wuolikainen, A., Moritz, T., Marklund, S. L., Antti, H., & Andersen, P. M. (2011). Disease-related changes in the cerebrospinal fluid metabolome in amyotrophic lateral sclerosis detected by GC/TOFMS. *PloS one*, *6*(4), e17947-e17947. https://doi.org/10.1371/journal.pone.0017947

Xiao, S., McLean, J., & Robertson, J. (2006). Neuronal intermediate filaments and ALS: A new look at an old question. *Biochimica et Biophysica Acta (BBA) - Molecular Basis of Disease*, *1762*(11), 1001-1012. https://doi.org/https://doi.org/10.1016/j.bbadis.2006.09.003

Xu, X., & Callaway, E. M. (2009). Laminar specificity of functional input to distinct types of inhibitory cortical neurons. *Journal of Neuroscience*, *29*(1), 70-85.

Xu, X., Roby, K. D., & Callaway, E. M. (2010). Immunochemical characterization of inhibitory mouse cortical neurons: three chemically distinct classes of inhibitory cells. *Journal of Comparative Neurology*, *518*(3), 389-404.

Yamashita, S., & Ando, Y. (2015). Genotype-phenotype relationship in hereditary amyotrophic lateral sclerosis. *Translational neurodegeneration*, *4*(1), 1-13.

Yamawaki, N., Tapies, M. G. R., Stults, A., Smith, G. A., & Shepherd, G. M. (2021). Circuit organization of the excitatory sensorimotor loop through hand/forelimb S1 and M1. *Elife*, *10*, e66836.

Yang, C., Qiao, T., Yu, J., Wang, H., Guo, Y., Salameh, J., Metterville, J., Parsi, S., Yusuf, I., & Brown, R. H. (2022). Low-level overexpression of wild type TDP-43 causes late-onset, progressive neurodegeneration and paralysis in mice. *PloS one*, *17*(2), e0255710.

Yu, J., Hu, H., Agmon, A., & Svoboda, K. (2019). Recruitment of GABAergic interneurons in the barrel cortex during active tactile behavior. *Neuron*, *104*(2), 412-427. e414.

Yu, X., Ye, Z., Houston, C. M., Zecharia, A. Y., Ma, Y., Zhang, Z., Uygun, D. S., Parker, S., Vyssotski, A. L., & Yustos, R. (2015). Wakefulness is governed by GABA and histamine cotransmission. *Neuron*, *87*(1), 164-178.

Zanette, G., Tamburin, S., Manganotti, P., Refatti, N., Forgione, A., & Rizzuto, N. (2002a). Changes in motor cortex inhibition over time in patients with amyotrophic lateral sclerosis. *J Neurol*, *249*(12), 1723-1728. https://doi.org/10.1007/s00415-002-0926-7

Zanette, G., Tamburin, S., Manganotti, P., Refatti, N., Forgione, A., & Rizzuto, N. (2002b). Different mechanisms contribute to motor cortex hyperexcitability in amyotrophic lateral sclerosis. *Clinical Neurophysiology*, *113*(11), 1688-1697.

Zang, D. W., & Cheema, S. (2002). Degeneration of corticospinal and bulbospinal systems in the superoxide dismutase 1G93A G1H transgenic mouse model of familial amyotrophic lateral sclerosis. *Neuroscience letters*, *332*(2), 99-102.

Zant, J. C., Rozov, S., Wigren, H.-K., Panula, P., & Porkka-Heiskanen, T. (2012). Histamine release in the basal forebrain mediates cortical activation through cholinergic neurons. *Journal of Neuroscience*, *32*(38), 13244-13254.

Zhang, W., Zhang, L., Liang, B., Schroeder, D., Zhang, Z. W., Cox, G. A., Li, Y., & Lin, D. T. (2016). Hyperactive somatostatin interneurons contribute to excitotoxicity in neurodegenerative disorders. *Nat Neurosci*, *19*(4), 557-559. https://doi.org/10.1038/nn.4257

Zhou, S., Zhou, Y., Qian, S., Chang, W., Wang, L., & Fan, D. (2018). Amyotrophic lateral sclerosis in Beijing: Epidemiologic features and prognosis from 2010 to 2015. *Brain and behavior*, *8*(11), e01131.

Ziemann, U., Winter, M., Reimers, C. D., Reimers, K., Tergau, F., & Paulus, W. (1997). Impaired motor cortex inhibition in patients with amyotrophic lateral sclerosis: evidence from paired transcranial magnetic stimulation. *Neurology*, *49*(5), 1292-1298.

Zimmerman, M. C., Oberley, L. W., & Flanagan, S. W. (2007). Mutant SOD1-induced neuronal toxicity is mediated by increased mitochondrial superoxide levels. *Journal of neurochemistry, 102*(3), 609-618.

Zinszner, H., Sok, J., Immanuel, D., Yin, Y., & Ron, D. (1997). TLS (FUS) binds RNA in vivo and engages in nucleo-cytoplasmic shuttling. *Journal of cell science, 110*(15), 1741-1750.

Zou, Z.-Y., Zhou, Z.-R., Che, C.-H., Liu, C.-Y., He, R.-L., & Huang, H.-P. (2017). Genetic epidemiology of amyotrophic lateral sclerosis: a systematic review and meta-analysis. *Journal of Neurology, Neurosurgery & Psychiatry, 88*(7), 540-549.

Declaration of Author Contributions

All results presented in this thesis, which include experimental design, collection and analysis of experimental data, were performed by the author (see below for exceptions).

For the published manuscript "Cytoplasmic FUS triggers early behavioral alterations linked to cortical neuronal hyperactivity and inhibitory synaptic defects", **the author** contributed to the data acquisition and analysis of neuronal activity under anesthesia in 4 m.o. and 10 m.o. $Fus^{+/+}$ and $Fus^{\Delta NLS/+}$ mice presented in Figure 3.

For the unpublished manuscript "A novel non-cell autonomous mechanism of cortical dysfunction in ALS":

XiaoQian Ye is hereby acknowledged for her contribution to the neural manifold analysis and figure design (Figure 3).

Evgeny Logunov is hereby acknowledged for collecting some of the data used in the comparison of neuronal activity under anesthesia and during wakefulness (Figure 2), neuronal activity under anesthesia (Supplementary Figure 1), and for carrying out the experiments involving the administration of Riluzole (Supplementary Figure 3) and the chemogenetic inhibition of layer II/III neuronal activity in M1 of presymptomatic SOD1^{G93A} mice (Figure 7).

Liliana Ziegler is hereby acknowledged for collecting some of the data used in the chemogenetic inhibition of layer II/III neuronal activity in M1 of presymptomatic SOD1^{G93A} mice (Figure 7).

Shenyi Jiang is hereby acknowledged for providing the immunohistochemistry protocol used for the misfolded-SOD1 staining (Figure 1b).

_____ _____

(Supervisor: Dr. Dr. Sabine Liebscher)　　　　　　(Author: Wing Yin Vanessa Kan)

Acknowledgement

I would like to begin by expressing my deepest appreciation to my supervisor Dr. Dr. Sabine Liebscher for giving me the opportunity to work on this project as well as the opportunity to work on various collaborations. In addition to her patience and guidance for the past five and a half years, I would also like to thank her for the valuable life lessons and mentorship. This journey also would not be possible without the constructive feedback and perspectives from members of my thesis advisory committee, Prof. Dr. Dieter Edbauer and Prof. Dorothee Dormann.

During my time at Liebscher lab, I have also had the opportunity to collaborate with researchers within as well as beyond the walls of our institute, especially PD Dr. Florence Bareyre, Dr. Luc Dupuis and Dr. Katrin Willig. I would also like to thank all the students who have participated in the project, especially Evgeny Logunov and Monica Liliana Ziegler. In addition to people from our lab, I would also like to extend my gratitude to people from the Kerschensteiner and Bareyre labs for showing me around (when it was only me and Pavel at the beginning) and allowing us to use their equipment.

I am also grateful to all the staff at the Graduate School of Systemic Neurosciences (GSN), especially Lena Bittl, Stefanie Bosse and Tanja Schulz-Mirbach, for their prompt and helpful responses, from admitting to the program to all the fun events to applying for financial support to the final stages of the PhD.

Last but not least, I could not get to where I am now without the support of my family, especially my husband Benjamin, my parents, my siblings Jasper and Valerie, as well as friends from inside and outside of the lab. Many thanks go to Samantha Ho, who left snacks and funny sticky notes on my desk, read my thesis and gave constructive comments; XiaoQian Ye, whom I worked with in the lab through days and nights and had great discussions with; and Pavel Švehla, who is the very first person I met in Munich and in the lab. Their moral support helped me push through the challenging hurdles faced during the PhD.

List of Publications

Empl, L., Chovsepian, A., Chahin, M., **Kan, W.Y.V.**, Fourneau, J., Van Steenbergen, V., Weidinger, S., Marcantoni, M., Ghanem, A., Bradley, P. and Conzelmann, K.K., 2022. Selective plasticity of callosal neurons in the adult contralesional cortex following murine traumatic brain injury. Nature Communications.

Gunes, Z.I.; **Kan, V.W.Y.**; Jiang, S.; Logunov, E.; Ye, X.; Liebscher, S. (2022). Cortical Hyperexcitability in the Driver's Seat in ALS. Clinical and Translational Neuroscience.

Steffens H., Mott A. C., Li S., Wegner W., Svehla P., **Kan W.Y.V.**, Wolf F., Liebscher S.# and Willig K.# (2021). Stable but not rigid: Chronic in vivo STED nanoscopy reveals extensive remodeling of spines, indicating multiple drivers of plasticity. Science Advances # equal contribution

Scekic-Zahirovic J., Sanjuan-Ruiz I., **Kan V**, Megat S., De Rossi P., Dieterlé S., Cassel R., Kessler P., Wiesner D., Tzeplaeff L., Demais V., Muller H.P., Picchiarelli G., Mishra N., Grosch S., Kassubek J., Rasche V., Ludolph A., Boutillier A.-L., Roselli F., Polymenidou M., Lagier-Tourenne C., Liebscher S.# and Dupuis L.# (2021). Cytoplasmic accumulation of FUS triggers early behavioral alterations linked to cortical neuronal hyperactivity and inhibitory synaptic defects. Nature communications. # equal contribution

Gunes ZI., **Kan V.**, Ye X. and Liebscher S. (2020). Exciting complexity: the role of motor circuit elements in ALS pathophysiology. Frontiers in Neuroscience.